

https://dspace.org/

Characterization of the electron transport chain in mycobacteria

Cardoso, Nicole Collette

2018
https://hdl.handle.net/10539/27178

Downloaded from a DSpace repository. https://dspace.org/

Characterization of the electron transport chain in mycobacteria



Nicole Collette Cardoso

A thesis submitted to the Faculty of Health Science, University of the Witwatersrand, Johannesburg, in fulfilment of the requirements for the degree of Doctor of Philosophy.

Johannesburg, 2018

"Our deepest fear is not that we are inadequate. Our deepest fear is that we are powerful beyond measure. It is our light, not our darkness that most frightens us. We ask ourselves, 'Who am I to be brilliant, gorgeous, talented, fabulous?' Actually, who are you not to be?"

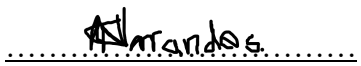
-Marianne Williamson

Dedication

I dedicate this work to my Daddy, Kevin Covidsingh Narrandes (6 October 1960-11 June 2018), who sadly will never get to read this. You were the smartest man I ever knew. Thank you for instilling some of those smarts in me and for your love, pride and belief in me. I will always love you and miss you everyday.

Declaration

I, Nicole Collette Cardoso, declare that this thesis is my own, unaided work. It is being submitted for the degree of Doctor of Philosophy at the University of the Witwatersrand, Johannesburg. It has not been submitted before for any other degree or examination at any other university.



Nicole Collette Cardoso

Signed on 18 day of July 2018 in Johannesburg

Presentations arising from this study

1. Narrandes N, Kana B**.** Characterization of the mycobacterial electron transport chain: Implications for drug efficacy. Oral presentation at the 4th SA TB Conference held at the ICC in Durban, 10th-13th June 2014

2. Narrandes N, Kana B**.** Characterization of the mycobacterial electron transport chain: Implications for drug efficacy. Oral presentation at the Biannual Faculty of Health Science Research Day and Postgraduate Symposium, 17 September 2014

3. Narrandes N, Kana B**.** Characterization of the mycobacterial electron transport chain: Implications for drug efficacy. Oral presentation at the Biannual Faculty of Health Science Research Day and Postgraduate Symposium, 1 September 2016- **First prize for "Best Student Oral Presentation"**

4. Narrandes N, Kana B**.** Characterization of the mycobacterial electron transport chain. Poster presentation at MBRT Postgraduate Research Day. 8 December 2016- **Third prize for "Best Student Poster Presentation"**

5. Cardoso N, Kana B**.** The mycobacterial electron transport chain: How TB breathes? Oral presentation at the NHLS PathRed Congress 2017. 24 June 2017- **Honourable mention for Ora presentation**

Publications arising from this study

1. Cardoso, N., Shee, S., Singh, A and Kana, B.D. “The role of cytochrome *bd* oxidase in the response to oxidative stress in mycobacteria”. In preparation.

2. Cardoso, N., Mizrahi, V.M and Kana, B.D. “Nitrate reduction in *M. smegmatis* is not governed exclusively by *narB* or *narGHJI*.” In preparation.

Abstract

Mycobacterium tuberculosis (Mtb) has a branched electron transport chain (ETC) with two terminal oxidases, the cytochrome *c* oxidase (CcO) and the cytochrome *bd* oxidase (CbdO). The CcO is essential in mycobacteria and is considered the predominantly active terminal oxidase during aerobic respiration. The CbdO on the other hand has been shown to be important under hypoxic conditions in mycobacteria and other organisms. More recently, the mycobacterial CbdO has been implicated in resistance to oxidative stress and in adaptive responses to treatment with ETC-targeting compounds currently being developed for tuberculosis (TB) treatment. The Mtb CbdO has thus been proposed as a promising new drug target. Although mycobacteria are unable to replicate in the absence of oxygen, they are able to survive without it when an alternate electron acceptor is available. This could possibly negate the requirement for either the CcO or the CbdO. An example of this adaptation is the use of nitrate reductase (NR), when nitrate is available as an electron acceptor. The ETC is initiated by the donation of electrons, most commonly by NADH generated during central carbon metabolism (CCM) for the production of energy in the form of ATP. The activity of the ETC is therefore dictated by the available terminal electron acceptors, carbon sources as well as by the available electron donors. Based on these observations we hypothesised that the CbdO contributes to aerobic respiration in mycobacteria. Furthermore, we hypothesised that the availability of different carbon sources or an alternate electron acceptor in the presence of oxygen would affect this activity. We tested our hypotheses using Mtb and *Mycobacterium smegmatis* strains lacking a functional CbdO or disrupted in genes encoding NR enzymes. The growth and energy-producing capabilities of these strains were evaluated under different conditions including in the presence of alternate carbon sources, in the presence of nitrate and in response to different stresses. We demonstrate that the CbdO is required for optimal ATP production under standard aerobic conditions. Furthermore, the enzyme plays a role in protection against toxic intermediates generated during CCM, particularly when grown on propionate or glycerol. The presence of nitrate was able to restore growth and ATP production in a strain lacking a functional CcO, confirming a role for an alternate electron acceptor under aerobic conditions. In addition, we show that the loss of CbdO leads to a decreased tolerance to oxidative stress, enhanced susceptibility to ETC- and cell wall-targeting

drugs and attenuated colonisation of mouse macrophages. Furthermore, we demonstrate that combinatorial loss of both the *narB* and *narGHJI* encoded NRs in *M. smegmatis* does not abrogate NR activity, suggesting that this organism possesses additional NR-encoding genes. Taken together, these data highlight the flexible nature of the mycobacterial electron transport chain and identify the CbdO as an important component of this flexibility, possibly because of its ability to maintain redox homeostasis. Disruption of redox homeostasis as a result of loss of CbdO leads to perturbations in CCM and cell wall biosynthesis and increased oxidative stress, which are collectively detrimental to survival. This supports a case for the development of inhibitors of the mycobacterial CbdO as possible candidates for TB drug development.

Acknowledgments

I would like to thank the organisations through which I received funding; this would not have been possible without the financial support from the Medical Research Council, the University of the Witwatersrand, the National Research Foundation and the Centre of Excellence for Biomedical TB Research.

To Kevin Pethe and all in his lab at Nanyang Technological University, thank you for welcoming me with open arms and helping breathe fresh life into my project. I'll always remember and be grateful for my time spent in Singapore.

Thank you to the past and present members of the CBTBR that were a part of my PhD journey, each of you have contributed to my scientific development and life in some way and you will all always hold a place in my memories.

Thank you to Jules and Chris, who kindly found time to read sections of this thesis and provided helpful recommendations.

Bhav, I can't thank you enough for our random chats that led to you giving me guidance, advice and support for my PhD and more importantly, on how to attain the elusive scientist-family life balance. I believe you've helped me become better in both areas.

To my lab partner-in-crime, Sbu, you have been invaluable through this journey. We got through the trenches together and I couldn't have asked for a better friend to have done it with.

To my supervisor, Bavesh: this was the most difficult thing I've done and I know I would not have been able to do it without you. Your support and unwavering belief in my potential to do good science, to lead and to be a good person means more to me than I could ever explain. Not only am I a better scientist but also a better person because of you and I am eternally grateful.

To my family for their support and understanding, thank you. Dad, thank you for always believing that I am capable of doing anything I choose, and of doing it well. Mummy, thank you for always being excited for anything I accomplish; even the smallest things which seemed insignificant to me at the time. Aunty Annie, thank you for being a perfect example of good work ethic and for always assuring me that struggle is rewarded. To my brother and my sister, I love you guys to bits. You guys constantly telling me I'm a smarty-pants helped me believe it and this helped me persevere.

To my niece and nephews, Skye, Ky and Kree: you three fill my heart with pure joy and love! I did this to hopefully help make the world a better place for you guys and your future cousins one day.

My husband, Darrin: you are the light in my life. Firstly, thank you for all the admin support, including driving me to the lab at odd times and on weekends and not once complaining about it. You've been my biggest supporter and cheerleader. You've always believed I was capable of this and your pride in me and my accomplishments fills my heart with even more love and pride for you, if that's possible. I feel like the luckiest person around to have such a wonderful, supportive partner to have shared this journey with and to share my life with. Thank you for knowing my heart, challenging my mind and helping me be better in every way. I love you infinitely!

Table of Contents

Dedication ..... **iii**

Declaration ..... **iv**

Presentations arising from this study ..... **v**

Publications arising from this study ..... **vi**

Abstract ..... **vii**

Acknowledgments ..... **ix**

Table of Contents ..... **xi**

List of figures ..... **xvii**

List of tables ..... **xix**

List of supplementary figures ..... **xix**

List of supplementary tables ..... **xix**

Abbreviations ..... **xx**

1. Introduction **1**

1.1. History of Tuberculosis 1

1.2. Mtb infection and pathogenesis 2

1.3. The current state of the TB epidemic 4

1.3.1. Latent TB infection 5

1.3.2. Drug resistance 6

1.4. TB treatment and prevention 6

1.5. Future prospects for controlling the TB epidemic 9

2. The mycobacterial electron transport chain and the role of the cytochrome *bd* oxidase **12**

2.1 Background 12

2.2 ATP synthesis 12

2.3 Central carbon metabolism 16
2.3.1 Glycolysis 16
2.3.2 The pyruvate dehydrogenase complex 17
2.3.3 The tricarboxylic acid cycle 19
2.3.4 CCM regulation 21
2.3.5 Mtb CCM 21
2.4 The *E*lectron *T*ransport *C*hain 24
2.4.1 Eukaryotic ETC 25
2.4.2 Prokaryotic ETC 26
2.5 The mycobacterial ETC 28
2.5.1 The mycobacterial electron donors and dehydrogenases 29
2.5.2 The mycobacterial electron carriers 34
2.6 Terminal electron acceptors in mycobacteria 34
2.7 Alternate terminal oxidases 35
2.8 Aerobic terminal oxidases 36
2.9 The respiratory cytochrome *c* proteins 37
2.10 The cytochrome *bd* oxidase 43
2.10.1 Physiological role of CbdO in bacteria 45
2.10.2 The mycobacterial CbdO 46
2.11 Aims and objectives 52
2.12 Methods 53
2.12.1 Mtb Growth curves 53
2.12.2 *M. smegmatis* growth curves 53
2.12.3 Measuring oxygen consumption 54
2.12.4 ATP quantification 55
2.12.5 Biofilm assays 55

2.12.6 Hydrogen peroxide assay 56
2.12.7 Hydroxyl radical detection 57
2.12.8 Acid stress 57
2.12.9 Macrophage culturing 58
2.12.10 Macrophage infections 59
2.12.11 Anaerobic assay 60
2.12.12 Lipid extractions from *M. smegmatis* biofilms. 61
2.12.13 Minimum inhibitory concentration (MIC) determination 61
2.13 Results- Section I 63
2.13.1 Genotypic confirmation of mutant strains 63
2.13.2 Mycobacterial growth dynamics in the absence of the cytochrome *bd* oxidase 65
2.13.3 The Mtb cytochrome *bd* oxidase contributes to aerobic ATP content 67
2.13.4 The reduced ATP content of Δ*cydAB* is attributable to decreased ATP production 68
2.13.5 ATP production in *M. smegmatis* strains 69
2.13.6 Oleic acid affects optical density and ATP production in Mtb 71
2.13.7 The effect of different carbon sources on the growth kinetics of CbdO-deficient *M. smegmatis* 73
2.13.8 The effect of different carbon sources on the growth kinetics of CbdO-deficient Mtb 80
2.14 Results – Section II 85
2.14.1 The effect of nitrate on the growth of *M. smegmatis* respiratory mutants 85
2.14.2 Construction of an *M. smegmatis* unmarked Δ*qcrCAB* mutant 87
2.14.3 The role of nitrate on Mtb growth and energy production 89
2.14.4 A CbdO deficient mutant is defective for biofilm formation 91
2.14.5 Biofilm formation in Mtb 96
2.14.6 Loss of CbdO leads to an altered lipid profile in *M. smegmatis* 100
2.15 Results- Section III 105

2.15.1 The anaerobic survival of Mtb Δ*cydAB* 106
2.15.2 Loss of the CbO leads to increased susceptibility to oxidative stress in Mtb 108
2.15.3 The growth and survival of Mtb in mouse macrophages 110
2.15.4 Loss of CbdO leads to increased susceptibility to drug treatment 111
2.16 Discussion 114
3. Nitrate reduction in *Mycobacterium smegmatis* is not governed exclusively by *narB* or *narGHJI* 129
3.1 Background 129
3.2 Aims and objectives 135
3.3 Methods 136
3.3.1 Nitrate utilisation 136
3.3.2 Anaerobic growth 137
3.3.3 Construction of *narB* complementing vector 137
3.3.4 RNA extractions 138
3.3.5 DNase treatment 138
3.3.6 cDNA conversion 139
3.3.7 Quantitative Real-Time Polymerase Chain Reaction – q(RT)PCR 139
3.4 Results 140
3.4.1 Confirmation of strains used 140
3.4.2 *M. smegmatis* NarGHI is dispensable under anaerobic conditions 140
3.4.3 NarB and NarGHI are not required for biofilm formation 140
3.4.4 Expression of NR-encoding genes in *M. smegmatis* 144
3.4.5 Nitrate utilisation 146
3.4.6 NarB plays a role in oxidative stress response and colony pigmentation 148
3.4.7 Bioinformatics analyses of *M. smegmatis* NR proteins 149
3.5 Discussion 154

3.6 Conclusions 159

A. Appendix A- General materials and methods 160

A1. Strains and culture conditions 160

A1.1. *Escherichia coli* culturing 160

A1.2. *M. smegmatis* culturing 160

A1.3. Mtb culturing 160

A2. Bacterial transformations 161

A2.1. *E. coli* transformations 161

A2.2. *M. smegmatis* electroporations 162

A2.3. Mtb electroporations 162

A3. DNA extractions 163

A3.1. Small scale plasmid extractions 163

A3.2. Large scale plasmid extractions 163

A3.3. Small scale genomic DNA extractions 163

A3.4. Large scale genomic DNA extractions 164

A4. DNA quantification 164

A5. Agarose gel electrophoresis 165

A6. DNA manipulation 165

A6.1. DNA amplification 165

A6.2. Restriction digestion 166

A6.3. Modification of DNA overhangs 167

A6.4. DNA dephosphorylation 167

A6.5. DNA ligation 167

B. Appendix B-Bioinformatics tools 171

B1. BLAST 171

B2. Mycobrowser 171

B3. EcoGene-RefSeq 171
B4. KEGG Pathway Database 171
B5. i-TASSER 172
B6. Sequence alignments 172
B6.1. ClustalW2 172
B6.2. Needle 172
C. Appendix C 174
C1. Media components 174
C2. Media supplement stocks 177
D. Cloning and strain generation 178
D1. Strains used in Chapter 2 178
D2. Strains used in Chapter 3 178
E. Supplementary results for Chapter 3 181
E1. Complementing vector generation 181
E2. PCR confirmation of strains 182
E3. Expression of *sigA* 183
F. Appendix F-Anaerobic model in *M. smegmatis* 190
G. Appendix G- Previously generated, unpublished data on the Mtb CbdO mutant 191
H. Appendix H-CCM entry points for different carbon sources 193
4. References 194

List of figures

Figure 2.1: A schematic diagram of the F_0F_1 ATP synthase in the cytoplasmic membrane.. 14
Figure 2.2: A conventional glycolytic pathway 18
Figure 2.3: The TCA cycle.. 20
Figure 2.4: The GABA shunt. 23
Figure 2.5: The mitochondrial ETC. 25
Figure 2.6: A schematic representation of the electron transport chain in *E. coli* 27
Figure 2.7: A schematic representation of the mycobacterial ETC. 33
Figure 2.8: Architectural arrangement of the cytochrome *bcc* reductase-cytochrome aa_3 oxidase super-complex showing the predicted catalytic cycle of the enzyme. 39
Figure 2.9: A representation of the cytochrome *bd* oxidase showing the predicted catalytic cycle… 44
Figure 2.10: An example of the 384-well plate setup used for *M. smegmatis* growth curves performed in a plate reader. 54
Figure 2.11: An example of the plate setup for the anaerobic growth assay. 60
Figure 2.12: Genotypic confirmation of Mtb Δ*cydAB* mutant by PCR. 63
Figure 2.13: Genotypic confirmation of *M. smegmatis* Δ*cydA::kan* mutant by PCR. 64
Figure 2.14: Growth kinetic analysis of Mtb strains grown under standard laboratory conditions. 65
Figure 2.15: An assessment of the viability of Mtb strains grown in 7H9 supplemented with OADC, glycerol and tyloxapol. 66
Figure 2.16: Cell size comparison of Mtb strains using flow cytometry. 67
Figure 2.17: ATP production of Mtb Δ*cydAB* under standard laboratory conditions. 68
Figure 2.18: Oxygen consumption of Mtb strains grown in the BACTEC MGIT system. 69
Figure 2.19: ATP production of *M. smegmatis* strains grown on 7H10 plates for 7 days. 70
Figure 2.20: Growth curve analysis and ATP production of Mtb Δ*cydAB* grown in 7H9 supplemented with ADS instead of OADC. 72
Figure 2.21: Growth kinetic analysis of *M. smegmatis* strains grown with glycerol and Tween80 as the carbon sources. 73
Figure 2.22: Growth kinetic analysis of *M. smegmatis* strains grown with glycerol and glucose as the carbon sources.. 74
Figure 2.23: Growth curves of *M. smegmatis* in the presence of different carbon sources which do not alter the growth of Δ*cydA::kan* 75
Figure 2.24: Growth kinetic analysis of *M. smegmatis* strains grown with glycerol, glucose and Tween80 as the carbon sources. 76
Figure 2.25: Growth kinetic analysis of *M. smegmatis* strains grown in the presence of bovine serum albumin (BSA). 77
Figure 2.26: A comparison of the growth of *M. smegmatis* strains with acetate as a carbon source. 79
Figure 2.27: A comparison of the slopes of growth curves performed in different media for each *M. smegmatis* strain. 80
Figure 2.28: Growth kinetic analysis of Mtb grown strains grown with single carbon sources. 81
Figure 2.29: A comparison of the growth rate of Mtb strains in media containing different carbon sources. 82
Figure 2.30: Growth curve analysis of *M. smegmatis* strains grown in the presence of 10 mM nitrate and atmospheric oxygen. 85

Figure 2.31: A comparison of ATP content of *M. smegmatis* strains grown under aerobic conditions, in the presence of nitrate. 86
Figure 2.32: Confirmation of the knockout vector, pKOqcrCAB. 87
Figure 2.33: Generation of an unmarked *M. smegmatis qcrCAB* knockout mutant. 88
Figure 2.34: An assessment of the growth dynamics of Mtb strains grown in the presence of nitrate. 90
Figure 2.35: Growth and nitrite accumulation analysis of Mtb strains grown in nitrate minimal medium. 91
Figure 2.36: Starting inoculum for cultures used to setup biofilms.. 92
Figure 2.37: *M. smegmatis* biofilm formation in Sautons media. 93
Figure 2.38: Biofilm formation of *M. smegmatis* strains grown in the presence of 10 mM nitrate. 94
Figure 2.39: The quantification of *M. smegmatis* biofilm biomass in Sautons with and without nitrate. 95
Figure 2.40: Biofilm formation of Mtb strains in Sautons minimal medium, with and without nitrate. 97
Figure 2.41: Quantification of Mtb biofilm biomass with crystal violet. 98
Figure 2.42: A conventional Griess assay performed on samples collected from biofilm cultures reveals that nitrite is produced and secreted in the absence of nitrate. 99
Figure 2.43: Growth kinetic analysis of Mtb strains grown in Sautons minimal media. 100
Figure 2.44: Glycopeptidolipid profile of *M. smegmatis* biofilm cultures. 102
Figure 2.45: The response of Mtb to stresses in vitro. 105
Figure 2.46: Images showing the decolourisation of indicators as oxygen is depleted in the environment and within the cultures. 106
Figure 2.47: The survival of Mtb during an anaerobic growth model. 107
Figure 2.48: The susceptibility of mycobacterial strains to oxidative stress in the form of H_2O_2. 108
Figure 2.49: The measurement of hydroxyl radicals in *M. smegmatis* cultures exposed to oxidative stress. 109
Figure 2.50: Mtb hydroxyl radical measurements with HPF, in the presence of oxidative stress. 110
Figure 2.51: The intracellular growth and survival of Mtb strains in J774 mouse macrophages. 111
Figure 2.52: Additional CCM pathways involved in the use of propionate as a carbon source. 118
Figure 2.53: Proposed mechanisms for the phenotypes observed in a strain lacking a functional CbdO. 127
Figure 3.1: A schematic representation of an example of the Nitrogen cycle in prokaryotes. 130
Figure 3.2: A schematic representation of the electron transfer reactions in the different types of NRs. 133
Figure 3.3: A diagram outlining the Conventional and Modified Griess assays used during this study. 136
Figure 3.4: Survival of *M. smegmatis* under anaerobic conditions in the presence of nitrate. 141
Figure 3.5: Biofilm formation and colony pigmentation of putative NR-deficient strains. 142
Figure 3.6: The development of colony pigmentation in *M. smegmatis* strains over time. 143
Figure 3.7: The expression of *narG* in the presence of nitrate.. 145
Figure 3.8: Nitrate utilisation in MPLN media. 147
Figure 3.9: *M. smegmatis* Δ*narB* and Δ*narB* Δ*narGHJI* mutants are less susceptible to hydrogen peroxide stress. 148
Figure 3.10: Mycobacterial nitrate assimilation pathway. 149
Figure 3.11: NarB domain architecture and predicted 3D structure. 150
Figure 3.12: Genome organization of MSMEI_4108, an additional putative assimilatory NR in *M. smegmatis*. 152
Figure 3.13: A diagram presenting a possible interplay between *sigF* and *narB*. 168

List of tables

Table 1.1: A list of the currently used drugs for the treatment of TB...... 8
Table 1.2: Possible anti-TB drugs currently at different stages of testing and development...... 9
Table 2.1: The different types of respiratory hemes...... 37
Table 2.2: A list of the MIC's of drugs tested against Mtb. 111
Table 2.3: A list of the MICs obtained for drugs tested in *M. smegmatis* 112
Table 3.1: *M. smegmatis* genes encoding proteins with the same domain architecture as NarB.. ... 151

List of supplementary figures

Figure D 1: Genotypic confirmation of Δ*narB*.....179
Figure D 2: Genotypic confirmation of Δ*narGHJI* and Δ*narB* Δ*narGHJI*.....180
Figure E 1: Confirmation of the *narB* complementing vector, pMnarB.....181
Figure E 2: The genotypic confirmation of mutant strains previously generated…….....182
Figure E 3: The expression of *sigA* in strains grown in 7H9 or MPLN.....183
Figure E 4: Sequence alignments of *narG* promoter regions.....185
Figure E 5: Sequence alignments of NarG from different organisms.....189
Figure F 1: An anaerobic shift-down model tested for wild type *M. smegmatis* in the presence and absence of nitrate…….……...……190
Figure G 1: An assessment of the virulence of the Mtb CbdO mutant in a mouse infection model……192
Figure H 1: A schematic representation of the TCA cycle and glycolysis highlighting the point of entry for the different carbon sources used during this study …...…….……...193

List of supplementary tables

Table A 1: Criteria used for the selection of oligonucleotide sequences on Primer3……...165
Table A 2: A list of strains used and generated during this study……..169
Table A 3: A list of the primers used during this study…….....170
Table G 1: A comparison of the NAD^+/NADH ratios in Mtb strains……191

Abbreviations

ADS- Albumin dextrose saline

Mtb- *Mycobacterium tuberculosis*

ETC- Electron transport chain

CbdO- Cytochrome *bd* oxidase

ATP- Adenosine triphosphate

TCA- Tricarboxylic acid

NADH- Nicotinamide adenine dinucleotide (reduced)

NAD^+- Nicotinamide adenine dinucleotide

NDH- NADH dehydrogenase

SDH- Succinate dehydrogenase

FRD- Fumarate reductase

NR- Nitrate reductase

H^+- Proton

PMF- Proton motive force

Pi- Inorganic phosphate

MQ- Menaquinone

Q- Ubiquinone

O_2- Oxygen

NO- Nitric oxide

CO- Carbon monoxide

H_2O_2- Hydrogen peroxide

OH^-- Hydroxyl radical

LB- Lysogeny Broth liquid medium

LA- Lysogeny Broth solid medium

Amp- Ampicillin

Hyg- Hygromycin

Kan- Kanamycin

OADC- Oleic acid-albumin-dextrose-catalase

OD- Optical density

MOI- Multiplicity of infection

CFU- Colony forming units

RLU- Relative fluorescence unit

MIC- Minimum inhibitory concentration

BSL III- Biosafety level three

LPS- Lipopolysaccharide

IFN γ- Interferon gamma

FBS- Fetal bovine serum

PBS- Phosphate buffered saline

HPF- Hydroxyphenyl fluorescein

CCM- Central carbon metabolism

LTBI- latent TB infection

MTBC- Mtb complex

DNA- Deoxyribonucleic acid

TLR- Toll-like receptor

WHO- World Health Organisation

HIV- Human Immuno-deficiency Virus

SDG- Sustainable development goals

TNF- Tumor necrosis factor

IGRA- Interferon gamma release assay

TST- Tuberculin skin test

Rif- Rifampicin

RR- Rif resistant

BCG- Bacille Calmette-Guérin

Eth- Ethambutol

PZA- Pyrazinamide

BDQ- Bedaquiline

CFZ- Clofazimine

OBR- Oral baseline regimen

MOA- Mechanism of action

PDH- Pyruvate dehydrogenase

IDH- Isocitrate dehydrogenase

GS- Glyoxylate shunt

ICL- Isocitrate lyase

CCR- Carbon catabolite repression

PPP- Pentose phosphate pathway

MCC- Methyl citrate cycle

MMP- Methyl malonyl pathway

MCS- Methyl citrate synthase

IMV- Inverted membrane vesicle

NRP- Non-replicating persistence

QH_2- Ubiquinol

MQH_2- Menaquinol

NR- Nitrate reductase

TTP- Time to positivity

GU- Growth unit

MGIT- Mycobacterium growth indicator tube

PCB- Phosphate citrate buffer

DMEM- Dulbecos modified eagle medium

FSC- Forward scatter

SSC- Side scatter

CcR- Cytochrome *c* reductase

CcO- Cytochrome *c* oxidase

GN- Glucose salt

TB- Tuberculosis

MIC- Minimum inhibitory concentration

ROS- Reactive oxygen species

PCR- Polymerase chain reaction

MDR- Multidrug resistant

XDR- Extensively drug resistant

INH- Isoniazid

1. Introduction

1.1. History of Tuberculosis

Tuberculosis (TB) disease, caused by *Mycobacterium tuberculosis* (Mtb), has been and remains a global health threat. Previously known by many names including consumption, phtisis, Pott's disease, scrofula and the White Plague, TB typically manifests in the lungs but is able to affect various organs in the body such as the spleen, stomach, brain and bones. TB was first described by ancient Egyptian doctors according to clinical symptoms and the treatment administered. In addition, the Egyptians were the first to establish a sanatorium which, apart from lung resections, was the only available treatment for TB prior to the discovery of Streptomycin in 1944. Paleopathology has allowed for the diagnosis of TB in historic skeletal samples as a result of the distinct lesions and other skeletal characteristics observed in infected specimens. This has allowed for the identification of TB in skeletons from as early as the Neolithic period (~3000-7000 BC) (Nerlich and Losch, 2009). Paleopathology has also allowed for TB to be identified in skeletal samples from Egypt (~ 3400 BC), Italy (during the first half of the fourth millennium BC), Britain (during the fourth century AD), Jordan (between 3150-3000 BC) and other parts of Europe and South America (between 2000 BC- 1500 AD) (Cave, 1939, Ortner, 1979, Formicola *et al.*, 1987, Daniel, 2006), highlighting the presence of TB disease across the globe during early human civilisation. TB infection has also been diagnosed in a *Homo erectus* fossil discovered in Turkey (Kappelman *et al.*, 2008), supporting the hypothesis that TB is an ancient disease that evolved to infect the *Homo* genus, possibly along with the domestication of animals (Madkour, 2003). It has since been established that TB is more ancient and that animal domestication facilitated the spread of the disease because of the formation of more dense populations but did not give rise to the disease (Weiss and McMichael, 2004, Hershkovitz *et al.*, 2008).

The development of molecular biology tools such as polymerase chain reaction (PCR), have allowed for definitive confirmation of the presence of TB-causing microorganisms in archaeological samples. TB is caused by Mtb and other members of the Mtb complex (MTBC)

made up of *Mycobacterium africanum, Mycobacterium microti, Mycobacterium canetti, Mycobacterium caprae, Mycobacterium pinnipedii* and *Mycobacterium bovis* (Homolka *et al.*, 2012). Molecular techniques not only allow for the confirmation of infection but also for identification of the strain present. Nested PCR of the IS*6110* locus has allowed for the detection of MTBC DNA in individuals from a Neolithic passage grave in Sweden, in lung lesions from a 1000 year old Peruvian mummy (Salo *et al.*, 1994) and in cadavers from ~ 3000 BC in Egypt (Zink *et al.*, 2001). More recently, high performance liquid chromatography (HPLC) has been used to detect MTBC-specific cell wall mycolic acids in historical samples in conjunction with IS*6110* PCR (Hershkovitz *et al.*, 2008, Donoghue *et al.*, 2010). PCRs which allow for differentiation between Mtb and *M. bovis* provide evidence that a strain/s more similar to "modern" Mtb was the causative agent of TB in the Eastern Mediterranean ~ 9000 years ago (Hershkovitz *et al.*, 2008) and during the Iron Age (~ 2200 years ago) in Britain (Taylor *et al.*, 2005). This is substantiated by recent studies of the phylogeny of the MTBC, which provides evidence that Mtb and *M. bovis* evolved from a common ancestor, in contrast to the previously held theory that *M. bovis* was the progenitor of modern Mtb (Sreevatsan *et al.*, 1997, Brosch *et al.*, 2002, Homolka *et al.*, 2012). Considering that TB has afflicted human civilisation for thousands of years, it is not surprising that the disease remains a scourge on global health.

1.2. Mtb infection and pathogenesis

Mtb transmission proceeds via aerosolised droplets containing the infectious bacterial cells. Once breathed in by an individual, the bacterial cells travel to the alveoli of the lungs where they encounter the body's first line of defence, the alveolar macrophages, which are part of the innate immune response. The majority of individuals exposed to Mtb are able to clear the infectious bacterial cells through a strong innate immune response. If the innate immune response fails, as is the case in ~10 % of individuals, an infection is established, which can lead to one of two outcomes: (i) the adaptive immune response contains the spread of the tubercle bacilli, leading to latent TB infection (LTBI) in 90- 95 % of cases or (ii) the adaptive immune response is unable to restrict the growth of Mtb cells leading to active disease in 5-10 % of cases (Koul *et al.*, 2011, Delogu *et al.*, 2013). Individuals harbouring LTBI have a 5 % lifetime risk of developing active

disease, with the risk increasing to 50 % in those who become immune-compromised e.g. HIV infected individuals (Koul *et al.*, 2011).

Mtb primarily resides in professional phagocytic cells including macrophages, neutrophils, monocytes and dendritic cells (DCs) (Ernst, 2012) but has been shown to colonize other nearby cells and organs via the lymphatic system or blood circulatory system (Delogu *et al.*, 2013). The uptake of Mtb by phagocytic cells and the outcomes thereof depend on the interaction of Mtb and Mtb ligands with surface receptors. Interaction of Mtb with complement receptor (CR)3, CR1, CR4 and CD14 has been shown to play a role in phagocytosis (Bhatt and Salgame, 2007). The interaction of Mtb ligands with toll-like receptors (TLRs) promotes the secretion of different cytokines and chemokines, thus recruiting additional immune cells to the site of infection and leading to the formation of a primary granuloma (Bhatt and Salgame, 2007, Ramakrishnan, 2012). Phagocytosis of bacterial pathogens conventionally leads to the formation of a phagolysosome where-in the bacterial cells are subject to various onslaughts from the host, these include reactive oxygen and reactive nitrogen intermediates (ROI and RNI respectively), acidification, reduced oxygen and limited nutrient availability. However, Mtb has evolved various mechanisms to survive these harsh conditions including the ability to arrest phagosome maturation, inhibit host cell apoptosis and autophagy, persist at low oxygen tensions, grow under acidic conditions, utilise alternate carbon sources and repair DNA and protein damage (Ehrt and Schnappinger, 2009, Ernst, 2012, Gengenbacher and Kaufmann, 2012).

TLR-mediated uptake of Mtb by dendritic cells results in the initiation of the adaptive immune response due to the maturation of dendritic cells into efficient antigen presenting cells upon infection with Mtb (Bhatt and Salgame, 2007). DC's carrying Mtb travel to the mediastinal lymph node where $CD4^+$ T cells are activated (Wolf *et al.*, 2008). These specifically activated $CD4^+$ T cells, along with B cells, neutrophils and natural killer (NK) cells are directed to the site of primary granuloma formation and contribute to the development of the granuloma. Granuloma formation was thought to be a host defence mechanism aiding in restricting the spread of the disease; however the process has proved more dynamic with evidence pointing to Mtb being able to manipulate the host immune response to facilitate proliferation and dissemination

(Ramakrishnan, 2012, Orme and Basaraba, 2014). There are different types of granulomas, each with a different structure, possibly possessing Mtb cells with different characteristics (Lenaerts *et al.*, 2007, Ryan *et al.*, 2010). A cellular granuloma is well vascularised and made up of a fibrotic cuff, which surrounds several layers of different immune cells as well as intra- and extracellular bacteria. The caseous/necrotic granuloma is characterised by a central non-vascularized caseum made up of necrotized host cells and some bacterial cells which are surrounded by infected and non-infected immune cells, all of which is contained by a fibrotic cuff. Cavities are an additional type of lesion found in TB-infected lungs. The commonly reported mechanism of cavity formation is as a result of the breakdown of a necrotic granuloma, which has come into contact with an airway and rupture of this cavity leads to the entrance of bacterial cells into the airways (Dartois and Barry, 2013, Orme and Basaraba, 2014). Considering this, cavities are considered to play an important role in transmission

1.3. The current state of the TB epidemic

The latest World Health Organisation (WHO) report, estimates that ~ 6.3 million new cases of TB were reported worldwide in 2016, with 476 774 of these individuals harbouring Human Immune-deficiency Virus (HIV) co-infection (WHO, 2017). South Africa (SA), like India is a high burden country and is one of the seven countries, which account for 64 % of the TB cases globally in addition to Indonesia, China, Nigeria, the Philippines and Pakistan. However, of the six aforementioned countries, SA has the highest HIV co-infection rate (~58 %), which exacerbates the TB burden. Globally, deaths attributable to TB have declined between 2000 and 2016, from 1.7 to 1.3 million respectively. In addition to the 1.3 million deaths in 2016, ~ 0.37 million HIV positive individuals died from TB, thus increasing the total number of deaths caused by TB from 1.3 to 1.74 million in 2016- the highest number of deaths caused by a single pathogen. Although there has been a slight decline in incidence and mortality rates globally, the rates of decline have not been consistent across the different regions e.g. a 6 % decline in mortality was observed in the European region while only a 2.2 % decline was observed in the Eastern Mediterranean region. Furthermore, the rates of decline of incidence and mortality have to increase significantly in order to meet the current Sustainable Development Goals (SDGs) for

TB, which include a 95 % reduction in TB mortality rates and a 90 % reduction in TB incidence rates by 2035 (WHO, 2017).

1.3.1. Latent TB infection

LTBI remains a threat to efforts aim at eradicating the disease and is defined as a persistent immune response to Mtb antigens, without clinical symptoms of active disease (Gideon and Flynn, 2011). It is estimated that 2-3 billion people worldwide harbour LTBI, all of whom carry a 5- 10 % lifetime risk of developing active disease (WHO, 2015). As a result of the high costs, routine testing for LTBI in the general population is not plausible however, the WHO has recommended testing and treatment guidelines for individuals at a higher risk of developing active disease in high and upper mid-income countries. Systematic testing and treatment is strongly recommended for HIV^+ individuals, close adult and child contacts of individuals with active pulmonary disease as well as in patients initiating anti-tumour necrosis factor (TNF) treatment, receiving dialysis, those preparing for organ or blood transplants and patients with silicosis (WHO, 2015). In addition, the WHO suggests that prisoners, healthcare workers, immigrants from high TB burden countries, homeless people and those struggling with substance abuse should also be considered for testing and treatment for LTBI. The testing in these cases is done either by the interferon-gamma release assay (IGRA) or Mantoux tuberculin skin test (TST). The different treatment options for LTBI in these settings include 6 or 9 months of isoniazid (INH) alone, 3 months of weekly rifapentine and INH, 3-4 months of INH and rifampicin (Rif) or 3-4 months of Rif alone (WHO, 2015). The recommendations discussed above primarily apply to countries with a disease burden of less than 100 per 100 000 population, while the previous guidelines still apply in low- and mid-income countries where the disease burden is frequently higher. The previously established guidelines recommend investigation of close and household contacts of an individual with active disease but testing for LTBI was not mandatory (WHO, 2012b). However, it was and still is strongly recommended that HIV^+ individuals and household contacts below the age of 5 are clinically evaluated and treated for LTBI in the absence of active TB disease symptoms (WHO, 2012b). The efficient treatment

of LTBI would significantly contribute to reducing the global burden of TB disease and aid in meeting the SDGs.

1.3.2. Drug resistance

A major hurdle in the fight against TB is the increasing spread of drug resistance. There were an estimated 600 000 new infections with drug resistant TB (DR-TB) in 2016 including 490 000 cases of multi-drug resistant (MDR) TB (defined as resistance to both INH and RIF) and 110 000 rifampicin-resistant (RR) TB cases (WHO, 2017). Drug susceptibility testing (DST) for second line drugs was performed on 39 % of the drug resistant cases and resulted in the identification of 8014 patients with extensively drug-resistant (XDR) TB (defined as MDR with resistance to a fluoroquinolone and one of the second-line injectable drugs) (WHO, 2017). There has been a slow and steady increase in the estimated incidence of DR-TB globally (WHO, 2016). This can be attributed to improved detection and reporting in several countries, however the reported statistics maybe an underestimation because of the low capability of several countries to perform DST, particularly to confirm XDR-TB e.g. Somalia and Papua New Guinea which are both considered to be high burden MDR-TB countries (WHO, 2016). In 2016 MDR/RR-TB was responsible for ~240 000 deaths, an increase from the 190 000 deaths reported in 2014 (WHO, 2016, WHO, 2017). This highlights the high mortality associated with DR-TB. These facts underscore an urgent need for the development of new TB drugs that have novel mechanisms of action and will be active on current DR strains.

1.4. TB treatment and prevention

The Bacille Calmette-Guérin (BCG) vaccine is currently the only available inoculation for the prevention of TB. The vaccine is a live attenuated form of *M. bovis* and the WHO recommends administration to all neonates in high burden countries (WHO, 2012a). Although shown to provide protection against TB meningitis and miliary TB in children (Trunz *et al.*, 2006), the vaccine can lead to complications in HIV-infected and immune-compromised children, such as the development of BCG disease and possibly death (Hesseling *et al.*, 2006). Furthermore, the

BCG vaccine does not protect against reactivation in individuals harbouring LTBI and the protection provided against primary infection in immune-competent individuals is variable and declines over time, with protection lasting up to 10 years (Abubakar *et al.*, 2013, WHO, 2016). This highlights the need for a new, more efficacious vaccine or vaccines that could address the problems described above. There are currently 12 vaccine candidates in different phases of clinical trials which aim to either prevent infection, prevent progression of disease after infection or prevent reactivation of LTBI, however an approved candidate is not expected in the near future (WHO, 2017).

The first recorded treatment of TB with antibiotics was in 1944 with streptomycin. Since then, several drugs have been developed for the treatment of TB, summarised in Table 1.1. The current recommended treatment for new patients with drug-susceptible TB includes a 2 month intensive phase of treatment with INH, Rif, ethambutol (Eth) and pyrazinamide (PZA), followed by a 4 month continuation phase with INH and Rif. A key issue facing the eradication of TB is the treatment of DR-TB, with only a 52 % and 28 % treatment success rate reported for MDR- and XDR- TB respectively, compared to the 83 % for susceptible TB (WHO, 2016). The WHO recommends a stepwise process for developing an MDR/XDR-TB treatment regimen based on DST results when available and patient treatment history. The following steps are recommended when designing a treatment plan: (i) Choose one injectable from Group 2 drugs, (ii) Choose a higher generation fluoroquinolone (Group 3), (iii) Choose two or more Group 4 drugs until there are at least four likely effective second-line drugs, (iv) Choose group 1 drug, usually PZA and (v) Add two or more Group 5 drugs if four second-line drugs are not likely to be effective. The treatment duration can vary in different cases but the WHO recommends an intensive phase of at least 6 months, followed by a minimum of 18 months of treatment after culture conversion. Successful TB treatment is lengthy, costly and in the case of MDR/XDR-TB can have detrimental side effects for patients. It is therefore vital to develop new drugs that could shorten the treatment duration, can target LTBI, that are less toxic and that are able to treat both susceptible and DR-TB cases.

Table 1.1: A list of the currently used drugs for the treatment of TB. The list was compiled from (WHO, 2014)

Drug	Type	Area of metabolism targeted
Isoniazid (INH)	Group 1- First-line oral drugs	Mycolic acid synthesis
Rifampicin (Rif)		Transcription
Ethambutol (Eth)		Arabinogalactan biosynthesis
Pyrazinamide (PZA)		Translation and acidifies cytoplasm
Rifabutin (Rfb)		Transcription
Rifapentine (Rpt)		
Streptomycin (S)	Group 2- Second-line injectable drugs	Protein synthesis
Amikacin (Am)		
Kanamycin (Km)		
Capreomycin (Cm)		
Levofloxacin (Lfx)	Group 3- Second-line fluoroquinolones	DNA supercoiling i.e. DNA gyrase and DNA topoisomerase
Moxifloxacin (Mfx)		
Gatifloxacin (Gfx)		
Ofloxacin (Ofx)		
Ethionamide (Eto)	Group 4- Second-line oral bacteriostatic drugs	Mycolic acid biosynthesis
Cycloserine (Cs)		Peptidoglycan synthesis
Prothionamide (Pto)		Mycolic acid biosynthesis
Terizidone (Trd)		Peptidoglycan biosynthesis
p-aminosalicylic acid (PAS)		Folate biosynthesis
p-aminosalicylate sodium (PAS-Na)		Folate biosynthesis
Bedaquiline (BDQ)	Group 5- Drugs still in development phase, with limited approval for use and drugs with limited data on efficacy and/or long term safety	Respiration i.e. ATP synthase
Delamanid (Dlm)		Cell wall biosynthesis
Linezolid (Lzd)		Initiation of protein synthesis
Clofazimine (CFZ)		Respiration i.e. NADH dehydrogenase
Amoxicillin/Clavulanate (Amx/Clv)		Cell wall biosynthesis
Imipenem/Cilastatin (Ipm/Cln)		
Meropenem (Mpm)		
Thiacetazone (T)		
Clarithromycin (Clr)		Protein synthesis

1.5. Future prospects for controlling the TB epidemic

A drug with a novel mechanism of action has not been approved for the treatment of drug susceptible TB in the past 50 years, which is alarming considering the existence of resistance to all currently-used anti-TB drugs and the steady increase in DR-TB prevalence. There are however several drugs currently in the pipeline undergoing preclinical development and in different phases of clinical trials, Table 1.2.

Table 1.2: Possible anti-TB drugs currently at different stages of testing and development. Adapted from (Pai *et al.*, 2016).

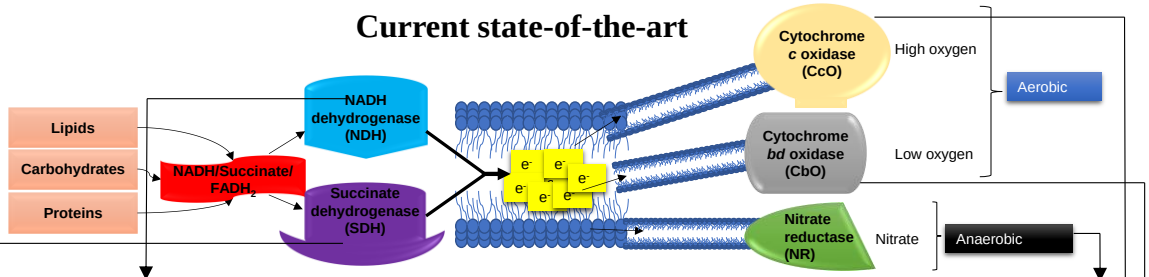
Preclinical development	**Clinical development**		
	Phase I	**Phase II**	**Phase III**
Riminophenazine (Respiration)- TBI-166	Imidazopyridine amide (Respiration)-Q203	Oxazolidinone (Protein synthesis)- Sutezolid	Rifapentine + Moxifloxacin
Caprazene nucleoside (Peptidoglycan biosynthesis)- CPZEN-45	Benzothiazinone (DprE1)-PBTZ169	Oxazolidinone -Linezolid	Delamanid with OBR[¥]
Spectinamide 1599 (Protein synthesis)	3,4-carbostyril derivative - OPC-167832	SQ-109	Pretomanid + Moxifloxacin + Pyrazinamide regimen
Griselimycin Cyclopeptide (DNA polymerase)- SATB-082		High dose rifampicin	Bedaquiline with oral OBR or OBR with injectables
Benzothiazinone (DprE1)-BTZ-043		Diaryquinoline (Respiration)- Bedaquiline + Nitroimidazole - Pretomanid + Pyrazinamide regimen	Bedaquiline + Linezolid with OBR
Benzothiazinone-PBTZ169		Levofloxacin with OBR	
1,4-Azaindole (DprE1)-TBA-7371			
Oxaborole (Protein synthesis)- GSK-070			

[¥]OBR- Oral Baseline Regimen. Bold text indicates chemical class and the drug target is shown in parentheses. Bold text refers to the drug class and text in parentheses refers to the target of the compound.

The majority of the drugs in development belong to new chemical classes and have novel targets in Mtb. Of the drugs currently undergoing Phase II and III clinical trials, linezolid, delamanid and bedaquiline (BDQ) are conditionally approved for MDR/XDR-TB treatment according to the WHO guidelines discussed above. Interestingly, two of the conditionally approved drugs- BDQ and clofazimine (CFZ), target the Mtb respiratory/electron transport chain (ETC). BDQ is a diarylquinoline and targets the complex responsible for producing energy in the form of adenosine triphosphate (ATP), i.e. the ATP synthase enzyme. CFZ has been shown to be reduced by the ETC enzyme NADH dehydrogenase (NDH-II), followed by spontaneous oxidation by oxygen leading to the production of bactericidal ROIs (Yano *et al.*, 2011). An alternate/additional mechanism proposed for the mode of action for CFZ is competition with the electron carrier menaquinone for binding to NDH-II (Lechartier and Cole, 2015). In either case, the activity of CFZ is tied to the mycobacterial ETC. In addition to BDQ and CFZ, the Riminophenazine compound-TBI-166 currently in preclinical development and the Imidazopyrimidine amide compound- Q203 which is in Phase Ib trials, both target Mtb respiration, Table 1.2.

The presence of multiple ETC-targeting drugs currently in clinical trials, the ongoing success of BDQ during MDR-TB treatment and the essentiality of this pathway for mycobacteria during active growth and persistence highlights this area of biology as a promising novel target for drug development. A thorough understanding of this pathway is thus required and warrants in depth research of the mycobacterial ETC. In this thesis we attempt to contribute to the knowledge on the mycobacterial ETC by investigating enzymes involved in the different types of respiration purported to be functional in mycobacteria i.e. aerobic respiration, microaerobic respiration and anaerobic respiration, depicted in the ”Current state-of-the-art” diagram below.Data collected on these complexes from both Mtb and the mycobacterial model organism, *Mycobacterium smegmatis* will be presented in the forthcoming chapters. The diagram summarizes the current relevant literature and highlights the knowledge gaps. Furthermore, the diagram provides an overview of what knowledge gaps are addressed in this thesis, color-coded to each chapter and section. A replica of this diagram is included at the beginning of each new section/chapter highlighting the questions being addressed and the key findings.

Current state-of-the-art



- NDH-I contributes to apoptosis in the host- Miller *et al*. (2010)
- Both Type II NDH enzymes contribute to ETC activity under different conditions and during infection, with Ndh being essential- Shi *et al*. (2005), Yano *et al*., (2006), Awasthy *et al* .(2014)
- NDH-II is involved in activity of CFZ- Weinstein *et al*. (2005), Yano *et al*. (2011)

- Contributes to anaerobic survival of Mtb- Sohaskey (2008)
- Protects against RNI and acid stress under hypoxic coniditions- Tan *et al*. (201)

- Essential for aerobic growth- Matsoso *et al*. (2005
- Inhibited by Q203- Pethe *et al*. (2013)
- Mutants disrupted in CcO maturation are attenuated in mice

- Serves as a terminal oxidase that maintains the PMF under hypoxic condtitions- Eoh and Rhee (2013), Hartman *et al*. (2014), Pecsi *et al*. (2014)

- Important for hypoxic growth – Kana *et al*. (2001)
- Compensates for loss of CcO – Matsoso *et al*. (2005), Small *et al*. (2013), Lamprecht *et al*. (2016), Kalia *at al*. (2017)
- CbdO is induced in response to oxidative stress- Boot *et al*. (2017)
- Loss of CbdO potentiates the activity of BDQ, Q203 and CFZ- Lamprecht *et al*. (2016), Kalia *at al*. (2017), Lu *et al*. (2015), Berney *et al*. (2014)
- Mutants unable to assemble CbdO are attenuated and unable to persist following INH treatment- Dhar and McKinney (2010), Shi *et al* (2005)

Key Knowledge Gaps

Does CbdO play a role in ATP generation?

What is the role of CbdO in growth on different carbon sources?

Chapter 2- Section I

Is there a role for alternate electron acceptors under aerobic conditions?

Are there other previously undescribed roles for CbdO?

Chapter 2- Section II

What is the role of CbdO in response to stress?

What role does CbdO play in drug tolerance?

Chapter 2- Section III

What is the role of respiratory and assimilatory NRs in Msm?

Chapter 3

Key Findings

- Yes for both Msm and Mtb
- Associated with reduced oxygen consumption

- CbdO is important for growth on proprionate in Mtb
- CbdO mutant has increased optical density in oleic acid
- Msm CbdO mutant seems sensitive to glycerol

- Yes, nitrate rescues CcO defect in Msm
- Nitrate reduced growth of CbdO mutant

Deletion of both narGHI and narB-encoded NRs did not affect respiratory NR activity

- Yes, CbdO is involved in biofilm maturation in Msm and Mtb
- Biofilm defects can be rescued by addition of nitrate
- Deletion of CbdO results in an altered lipid profile

- Loss of CbdO gives rise to increased susceptibility to ETC inhibitors and cell wall targeting antibiotics

- CbdO seems to be important for survival under oxidative stress
- Mutant experienced increased hydroxyl radicles
- CbdO important for mac survival.

2. The mycobacterial electron transport chain and the role of the cytochrome *bd* oxidase

2.1 Background

Mtb remains a highly successful pathogen, in part as a result of its metabolic flexibility which allows for adaptations to stressful conditions experienced during pathogenesis. Mtb possesses several mechanisms which allows it to adapt to the harsh conditions experienced including, but not limited to: the ability to arrest phagosome maturation, detoxify ROIs and RNIs, repair damaged DNA and proteins, the ability to utilize various carbon sources, shift from aerobic to anaerobic respiration and achieve a state of clinical latency/dormancy (Ehrt and Schnappinger, 2009). A defining factor of all these adaptations is that Mtb maintains some level of metabolic activity through maintenance of an energized ETC, although activity is severely downregulated in some cases (Rao *et al.*, 2008, Kana, 2009). In order for bacterial cells to remain viable, a sufficient amount of chemical energy in the form of adenosine triphosphate (ATP) is required. The main source of ATP production in the cell is from the membrane-bound ATP synthase complex, the activity of which is driven by the ETC and the associated uptake of protons (H^+) to the periplasm.

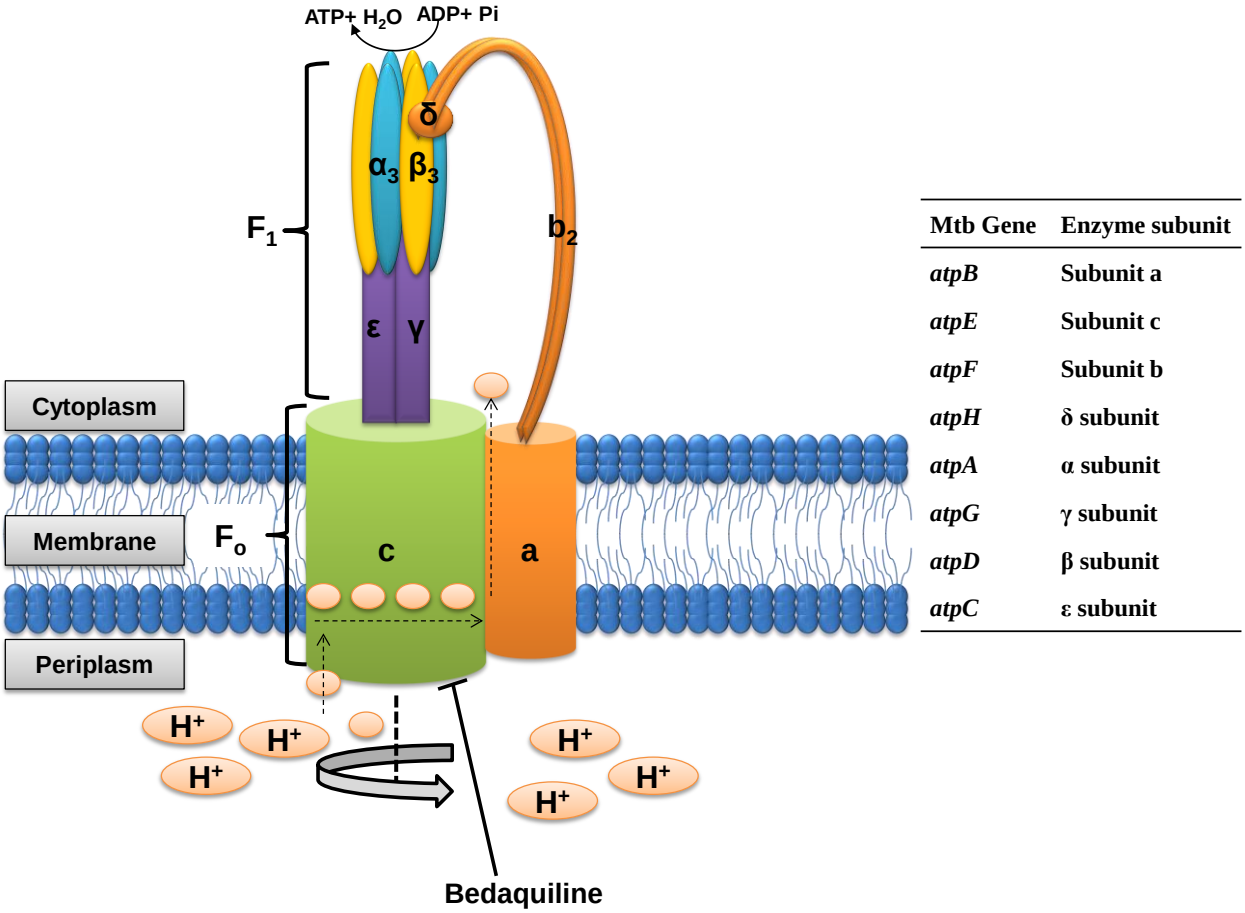
2.2 ATP synthesis

ATP synthesis occurs through substrate level – and oxidative phosphorylation. Whilst catabolism of substrates during glycolysis and the tricarboxylic acid (TCA) cycle yields some ATP (Figure 2.2 and Figure 2.3 respectively), the main source of ATP is the membrane bound F_oF_1 ATP synthase, Figure 2.1 . The ATP synthase is a multi-subunit enzyme made up of two distinct regions - the F_o transmembrane, proton pumping region - and the F_1 cytoplasmic, substrate binding catalytic region, referred to as the rotor and stator respectively (Figure 2.1) (Yoshida *et al.*, 2001). The activity of the ATP synthase is facilitated by the proton motive force (PMF), which is the sum of the electrical and chemical potential across the cytoplasmic membrane. When the PMF is high, protons flow into the cytoplasm via the *c*-ring of the F_o component of ATP synthase. Rotation of the *c*-ring (brought about by proton translocation), together with

rotation of the εγ subunits, results in a conformational change in the β subunits and leads to ATP production from ADP and inorganic phosphate (Pi) in the cytoplasm (Yoshida *et al.*, 2001). As mentioned, the driving force for ATP production is the PMF and consequently the availability of protons in the periplasm is essential for the production of energy. The majority of these protons come from the ETC where electrons move through the cell membrane, via redox reactive respiratory proteins with electron carriers. During this process protons from the cytoplasm are pumped across the membrane, creating a proton gradient. Constant translocation of protons from the cytoplasm to the periplasmic space, where they are taken up by the ATP synthase complex, couples the ETC with energy production. Some respiratory enzymes do not pump protons across the membrane, but consume protons from the cytoplasm during redox reactions, thereby contributing to maintaining the proton gradient between the cytoplasm and the periplasm. In addition to generating ATP, the ATP synthase is also able to catalyse the reverse reaction of ATP hydrolysis in some organisms. ATP synthase forms an essential component of cellular metabolism in virtually all organisms i.e. for ATP production in aerobic organisms and via ATPase activity for PMF maintenance and pH homeostasis in anaerobic organisms (Yoshida *et al.*, 2001, Tran and Cook, 2005).

The Mtb ATP synthase is encoded by the *atpBEFHAGDC* operon (Table insert in Figure 2.1) and with the exception of *atpB*, all the other genes in the operon are considered essential for Mtb growth (Sassetti *et al.*, 2003). In addition, the ATP synthase has been shown to be essential for survival of dormant Mtb cells under hypoxic conditions (Koul *et al.*, 2008, Rao *et al.*, 2008). ATPase activity could not be detected in either *M. smegmatis* or *M. bovis* BCG, suggesting that the essentiality of ATP synthase in mycobacteria is due to the need for ATP synthesis and not for ATP hydrolysis (Haagsma *et al.*, 2010). Nonetheless, the essentiality of the ATP synthase in Mtb highlights the vulnerability of this complex as a drug target for TB. The diarylquinoline, BDQ (previously known as TMC207/R207910) targets this vulnerability. Mtb mutants with resistance to BDQ have been generated and carry point mutations in *atpE*, the *c*-ring- encoding gene (Andries *et al.*, 2005). In addition, it was demonstrated that BDQ binds to the *c*-subunit of the F_o region, thus confirming that the ATP synthase is the target of this drug (Koul *et al.*, 2007). Computational docking studies of BDQ with a predicted structure of the Mtb *c*-ring proposed

that BDQ binds in a pocket formed between two helices of subunit a and four helices of subunit c. In this position, BDQ mimics the conserved Arg-186 residue of subunit a, preventing the transfer of a proton to the acidic Glu-61 of subunit c, thus preventing the rotation of the *c*-ring, proton pumping and ATP synthesis (de Jonge *et al.*, 2007). Segala *et al.* (2012) subsequently provided evidence supporting the theory of BDQ binding to the *c*-ring and interfering with proton translocation. However, based on the inability to detect resistance-conferring mutations in *atpB* and the discovery of additional mutations in *atpE*, Segala *et al.* (2012) propose that the binding pocket is located between two adjacent c subunits and not between subunits a and c.



Mtb Gene	Enzyme subunit
atpB	Subunit a
atpE	Subunit c
atpF	Subunit b
atpH	δ subunit
atpA	α subunit
atpG	γ subunit
atpD	β subunit
atpC	ε subunit

Figure 2.1: A schematic diagram of the F_0F_1 ATP synthase in the cytoplasmic membrane. The direction of proton movement is depicted by black dashed arrows. The solid grey arrow represents the rotation of the c-ring upon proton translocation. Bedaquiline inhibits the activity of the mycobacterial ATP synthase by interfering with c-ring rotation. The table inset lists the Mtb genes encoding each of the enzyme subunits. Figure adapted from Yoshida *et al.* (2001).

Although the precise binding site of BDQ *in vivo* is yet to be demonstrated, it is accepted that the *c*-ring of the ATP synthase is disrupted and this is a determinant of the activity of the drug.

Further investigation into the exact mechanism of action (MOA) of BDQ has generated disparate hypotheses. Koul *et al.* (2014) observed delayed killing of Mtb by BDQ with only a 1 log decrease in CFU after ~7 days. Using transcriptomic and proteomic analyses they demonstrate that Mtb remodels various metabolic pathways in response to BDQ treatment. They specifically observed a decrease in energy-requiring processes e.g. cell wall, protein and DNA synthesis while energy producing pathways were favoured i.e. an increase in expression of ATP synthase-encoding genes and increased expression of certain glycolytic and TCA cycle- encoding genes. Based on these findings the authors propose that the ATP produced during glycolysis is sufficient to sustain survival over a short period of time, which accounts for the delayed onset of killing and this was supported by the enhanced killing of Mtb by BDQ when grown on non-fermentable carbon sources. Taken together, the authors conclude that the primary MOA of BDQ is ATP depletion and that the cell remodels its metabolism accordingly to restore ATP but the alternate pathways are not sufficient, thus leading to death (Koul *et al.*, 2014). Subsequently, Hards *et al.* (2015) demonstrated that BDQ treatment leads to increased oxygen consumption and collapse of the pH gradient but not the membrane potential. They therefore proposed that the bactericidal activity of BDQ is attributable to uncoupling of respiration-driven ATP synthesis and futile proton cycling, possibly through the *c*-ring. They suggest that the delayed onset of killing is due to ATP depletion, while the actual killing can be attributed to the uncoupling which cannot be tolerated by mycobacteria. In the study, the authors observed transcriptional remodelling to suggest an avoidance of producing reducing equivalents in an attempt to reduce proton pumping across the membrane. In contrast to (Koul *et al.*, 2014), Hards *et al.* (2015) observed decreased expression of glycolytic genes. Both studies observed an increase in expression of cytochrome *bd* – encoding genes, which encode an alternate terminal oxidase that transfers electrons to oxygen; however Koul *et al.* (2014) propose that it is a general response to energy metabolism inhibition while Hards *et al.* (2015) propose this as a specific adaptation to avoid proton pumping by the predominant terminal oxidase, cytochrome *c* oxidase (Hards *et al.*,

2015). The findings of these studies provided insight into the MOA of BDQ and highlighted the close interaction of ATP production and central carbon metabolism (CCM) in Mtb.

2.3 Central carbon metabolism

All known life forms on earth are carbon-based and thus possess efficient metabolic pathways which enable the utilisation of various carbon substrates. The most well characterised pathways include glycolysis and the TCA cycle, shown in Figures 2.2 and 2.3 respectively.

2.3.1 Glycolysis

Glycolysis is a multistep pathway, with each reaction catalysed by a specific enzyme. A brief description of each step of glycolysis shown in Figure 2.2: **(1)** The first committed step of glycolysis involves the transfer of a phosphoryl group from ATP to the C_6 carbon of glucose to generate glucose-6-phosphate (G6P) and is catalysed by hexokinase. **(2)** The second step is an isomerization reaction where G6P is rearranged by phosphoglucose isomerase into fructose-6-phosphate (F6P). **(3)** Reaction three of glycolysis requires ATP to donate a phosphoryl group to C_1 of F6P, generating fructose-1,6-bisphosphate (FBP) and is catalysed by phosphofructokinase (PFK). This is a rate-limiting step of glycolysis with the activity of PFK being allosterically regulated by AMP, ATP and citrate. **(4)** In reaction four FBP is cleaved by aldolase generating two triose molecules i.e. glyceraldehyde-3-phosphate (G3P) and dihydroacetone phosphate (DHAP). **(5)** DHAP is then converted to G3P by triose phosphate isomerase, thus two G3P molecules are generated from a single glucose molecule. **(6)** G3P is oxidized and phosphorylated in the sixth step of glycolysis with electrons being donated by NAD+. The reaction is catalysed by glyceraldehyde-3-phosphate dehydrogenase (G3PDH) to produce 1,3-bisphosphoglycerate (BPG) and NADH. **(7)** The first ATP-generating step of glycolysis involves a phosphoryl group from C_1 of BPG being transferred to ADP by phosphoglycerate kinase to generate 3-phosphoglycerate (3PG) and ATP. **(8)** Reaction eight involves the conversion of 3PG to 2PG by the removal of a phosphoryl group from C_3 and addition of a phosphoryl group to C_2. The reaction is catalysed by phosphoglycerate mutase. **(9)** In this reaction 2PG is dehydrated by enolase to generate phosphoenolpyruvate (PEP). **(10)** The final step of glycolysis involves the

generation of pyruvate and ATP from PEP and is catalysed by pyruvate kinase (Berg *et al.*, 2002).

During glycolysis there is a net production of two ATP molecules, with four being produced and two used and two NADH molecules are produced. Several metabolic intermediates produced during glycolysis serve as precursors for the biosynthesis of other compounds including polysaccharides, peptidoglycan, nucleic acids, amino acids, lipids and fatty acids (Kim and Gadd, 2008) The pathway terminates at the production of pyruvate and each glucose molecule produces two pyruvate molecules.

2.3.2 The pyruvate dehydrogenase complex

The final product of glycolysis, pyruvate can either be used aerobically or anaerobically. Under anaerobic conditions pyruvate serves as the first substrate for fermentation to produce lactate or carbon dioxide and ethanol. Under aerobic conditions pyruvate serves as a substrate to produce acetyl-CoA, which then feeds into the TCA cycle. The production of acetyl-CoA involves the oxidative decarboxylation of pyruvate via four steps and is catalysed by the pyruvate dehydrogenase (PDH) complex. The PDH complex is made up of three enzymes i.e. pyruvate dehydrogenase (E1 component), dihydrolipoyl transacetylase (E2 component, DlaT) and dihydrolipoyl dehydrogenase (E3 component, Lpd). In the first step pyruvate is decarboxylated and combined with thiamine pyrophosphate (TPP). Thereafter, the hydroxyethyl group of TPP is oxidized to an acetyl group by the disulfide bridge of lipoamide, consequently converting the disulfide bridge to a sulfhydryl group. This reaction yields acetyllipoamide and TPP. Both the first and second steps are catalysed by the E1 component of PDH. During the third step, the

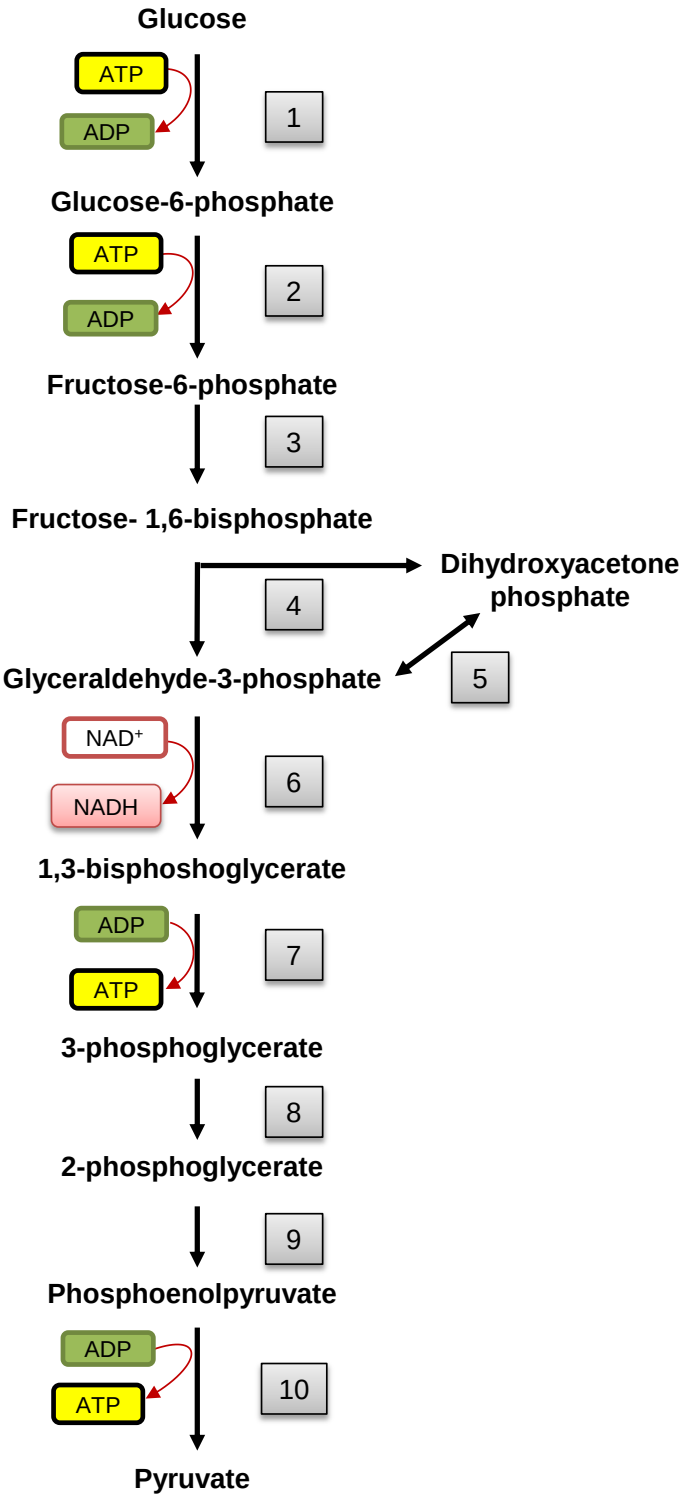


Figure 2.2: A conventional glycolytic pathway. Each reaction is described in the text and the enzymes for each step are: (1) hexokinase, (2) phosphoglucose isomerase, (3) phosphofructokinase, (4) aldolase, (5) triose phosphate isomerase, (6) glyceraldehyde-3-phospahet dehydrogenase, (7) phosphoglycerate kinase, (8) phosphoglycerate mutase, (9) enolase, (10) pyruvate kinase. Figure adapted from Berg *et al.* (2002).

acetyl group of acetyllipoamide is transferred to CoA by the E2 component, generating acetyl-CoA and dihydrolipoamide. In the final step, the oxidized form of lipoamide is regenerated by the PDH E3 component via the transfer of two electrons from dihydrolipoamide to NAD+, thus generating NADH and oxidized lipoamide (Berg *et al.*, 2002).

2.3.3 The tricarboxylic acid cycle

The TCA cycle is also a multistep pathway and produces three NADH molecules, one $FADH_2$ and one GTP, depicted in Figure 2.3. In addition to producing essential reducing equivalents, the TCA cycle also generates precursors for the biosynthesis of amino acids, purine and pyrimidine nucleotides and porphyrins (Berg *et al.*, 2002). A description of the reactions in Figure 2.3: **(1)** In the first reaction of the TCA cycle, acetyl-CoA and oxaloacetate are condensed to produce citrate and CoA is released. The reaction is catalysed by citrate synthase and is important as it allows for the introduction of carbohydrate, lipid and protein products into the TCA cycle for complete oxidation. **(2)** Citrate is converted to isocitrate by aconitase, which involves the re-positioning of an OH group from C3 to C4. **(3)** The third reaction of the TCA cycle is catalysed by isocitrate dehydrogenase (IDH) and involves two steps. Firstly, the OH group at C4 of isocitrate is oxidized producing NADH, followed by the release of CO_2 from the intermediate to yield α-ketoglutarate. **(4)** The fourth reaction of the TCA cycle is the oxidative decarboxylation of α-ketoglutarate to generate succinyl-CoA, CO_2 and NADH. The reaction is similar to the oxidative decarboxylation of pyruvate, involves the same cofactors and is catalysed by the α-ketoglutarate dehydrogenase (α-KDH) complex, which is made up of enzymes similar to those of the PDH complex. The KDH complex is made up of an α-ketoglutarate complex (E'1), a transsuccinylase (E'2) and a dihydrolipoyl dehydrogenase (E3) which is the same as the enzyme in the PDH complex. **(5)** The production of succinate in the TCA cycle is the only step to generate a high energy nucleotide molecule. The reaction is catalysed by succinyl-CoA synthetase and involves the cleavage of CoA from succinyl-CoA by free phosphate, which is then transferred to GDP to form GTP. **(6)** During the sixth step of the TCA cycle succinate dehydrogenase (SDH) catalyses the removal of two protons from succinate which are transferred to FAD, generating fumarate and $FADH_2$. This step of the TCA cycle directly links CCM and the ETC as succinate can serve

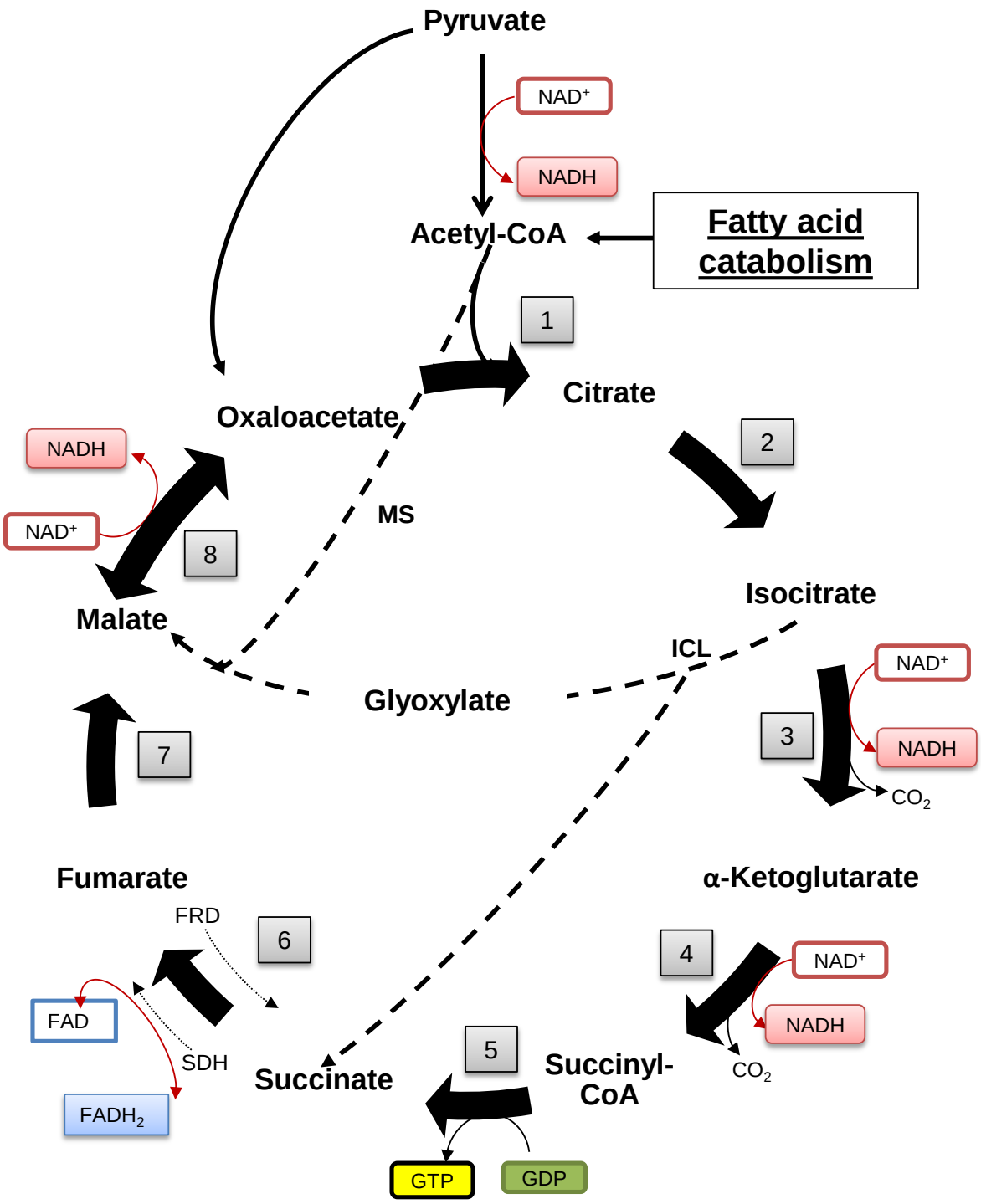


Figure 2.3: The TCA cycle. Each numbered step and the associated enzyme is described in the text. The dashed lines represent modifications possible in the TCA cycle, specifically the glyoxylate shunt. During the glyoxylate shunt isocitrate serves as the substrate for ICL to produce succinate and glyoxylate. MS catalyses the condensation of glyoxylate with acetyl-CoA to produce malate. MS: malate synthase, ICL, isocitrate lyase, FRD: fumarate reductase, SDH: succinate dehydrogenase. Figure adapted from Berg *et al.* (2002).

as an electron donor for the initiation of the ETC via SDH. **(7)** The generation of malate in the TCA cycle involves the addition of a water molecule to fumarate and is catalysed by fumarase. **(8)** Oxaloacetate is regenerated in the final step of the TCA cycle by malate dehydrogenase which catalyses the oxidation of malate and transfer of electrons to NAD, generating NADH. The TCA cycle is adaptable with several points at which it can be modified. One such modification is the glyoxylate shunt (GS), where isocitrate is converted to succinate and glyoxylate by isocitrate lyase (ICL), thus bypassing α-ketoglutarate and fumarate.

2.3.4 CCM regulation

Central carbon metabolism and its regulation has been well characterised in the model organisms *Escherichia coli* and *Bacillus subtilis*. *E. coli*, like many other bacteria, preferentially uses glucose as the foremost carbon source and displays diauxic growth i.e. the sequential use of different available carbon sources, starting with the source that supports the fastest growth. One of the main regulatory mechanisms of diauxic growth, and thus central carbon metabolism, is referred to as carbon catabolite repression (CCR) (Gorke and Stulke, 2008). CCR is facilitated by different pathways/mechanisms in different organisms, however the ultimate goal of each is the same: to enable the use of the most efficient carbon source to facilitate robust growth (Gorke and Stulke, 2008). However, mycobacteria and other actinomycetes are unique in that they do not display diauxic growth and have no detectable CCR system. Unlike *E coli* and *B. subtilis*, Mtb is an intracellular pathogen whose only known natural host and reservoir are humans and specifically macrophages. Mtb has therefore evolved to use the available nutrients in this restrictive environment and considering this, it is not surprising that CCM and regulation are unconventional in this organism.

2.3.5 Mtb CCM

The Mtb genome contains a full repertoire of genes encoding enzymes for complete pathways of glycolysis, the pentose phosphate pathway (PPP), the TCA cycle, the glyoxylate shunt (GS), the GABA shunt, the methylcitrate cycle (MCC) and the methymalonyl pathway (MMP) (Rhee *et al*., 2011). However, bioinformatic analysis is not sufficient to conclude activity or preference

for any of these pathways. A difference in CCM of Mtb was detected as early as the 1950's with Segal and Bloch demonstrating that Mtb from mouse lungs preferentially grew on fatty acids compared to in the presence of carbohydrates (Bloch and Segal, 1956). As a result of advances in molecular biological techniques and metabolomics, which allowed for more in depth analyses of CCM in mycobacteria, the overall importance of CCM for the viability, virulence and pathogenesis of Mtb has been demonstrated in several innovative studies. These are described further below.

A significant discovery on CCM in Mtb was the identification of the importance of the GS enzyme ICL for *in vivo* growth and survival; supporting the hypothesis that fatty acids are the preferred carbon source for Mtb *in vivo* (McKinney et al., 2000, Munoz-Elias and McKinney, 2005). Mtb retains two ICL-encoding genes, *icl1* and *icl2* (Kapopoulou et al., 2011), both of which are required for optimal ICL activity (Munoz-Elias and McKinney, 2005). An ICL-deficient strain (Δ*icl1* Δ*icl2*) displayed several unusual characteristics i.e. it was unable to grow on odd- and even-chain fatty acids, was attenuated in resting and activated human and mouse macrophages and was unable to survive during infections of immune-competent and immune-compromised mice. These observations proved the essentiality of this enzyme for virulence and pathogenesis of Mtb (Munoz-Elias and McKinney, 2005). It was subsequently shown that ICL1 is both an isocitrate lyase and methylcitrate lyase (MCL) (Gould *et al.*, 2006), with the activity of the latter being required for growth on propionate via the MCC (Munoz-Elias *et al.*, 2006). Interestingly it was shown that while essential for growth on propionate *in vitro*, other enzymes of the MCC i.e. methycitrate synthase (MCS) and methylcitrate dehydratase (MCD), were dispensable during mouse infections (Munoz-Elias *et al.*, 2006). This resulted in the identification of a functional MMP in Mtb which, in the presence of vitamin B_{12}, can fulfil anaplerotic functions and substitute for the MCC (Savvi *et al.*, 2008). These data highlight the flexibility of CCM in Mtb, which is further enhanced by the presence of multiple copies of genes for several enzymes in the different pathways.

Another unique characteristic of the TCA cycle identified in Mtb is the lack of α-KDH activity in cell lysates, despite the presence of genes encoding each protein of the complex in the Mtb

genome (Tian *et al.*, 2005b). Two of the putative α-KDH complex proteins, DlaT (*Rv2215*) and LpdC (Rv0462), together with component E1/AceE (*Rv2241*), were shown to form a functional PDH complex (Tian *et al.*, 2005b). Furthermore, DlaT and LpdC form a complex with AhpC and AhpD, constituting an NADH-dependent peroxidase and peroxynitrite reductase. This provided the first evidence for a role of CCM enzymes in alternate cellular processes, in this case antioxidant defence (Bryk *et al.*, 2002). Further investigation of the lack of α-KDH activity led to the identification of an alternate pathway to generate succinate in the TCA cycle via the activity of an α-ketoglutarate decarboxylase (Kgd), together with a succinic semialdehyde dehydrogenase (SSADH), thus highlighting another distinctive feature of CCM in mycobacteria. (Tian *et al.*, 2005a). This alternative pathway, referred to as the GABA shunt is shown in Figure 2.4.

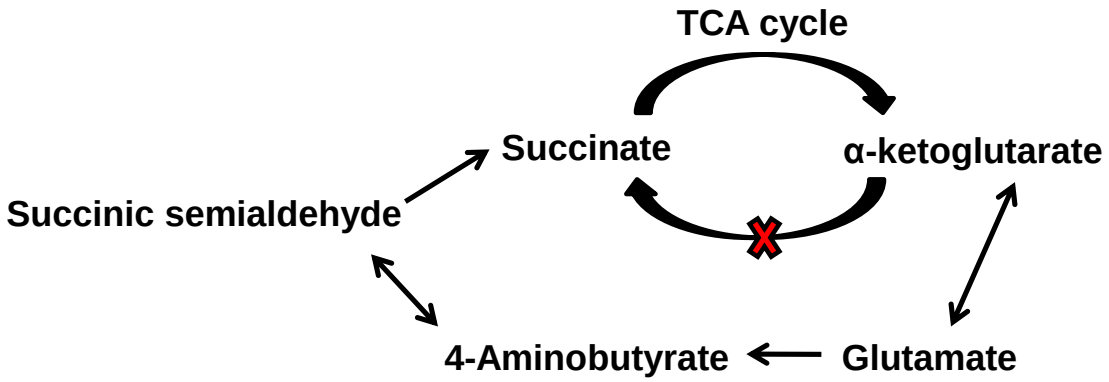


Figure 2.4: The GABA shunt. In Mtb this is the proposed pathway for the production of succinate in the TCA cycle due to the lack of an α-ketoglutarate dehydrogenase enzyme in this organism. Figure adapted from Berg *et al.* (2002)

In addition to the unique characteristics and adaptations of CCM highlighted above, growing evidence suggests that several conventional CCM-enzymes play a role in other cellular processes in Mtb. As mentioned, two enzymes of the PDH complex are also involved in an antioxidant defence system (Bryk *et al.*, 2002). Recently it was shown that the E1 component of the PDH complex has 2-hydroxy-3-adipate synthase (HOAS) activity (de Carvalho *et al.*, 2010b), which was subsequently shown to protect against toxic aldehydes generated during glutamate anaplerosis. Together with DlaT, AhpC and AhpD is able to protect against nitrosative stress

with either α-ketoglutarate or pyruvate providing reducing power by serving as the electron donors (Maksymiuk *et al.*, 2015). Pyruvate kinase catalyses the final step of glycolysis, thus playing an essential role in CCM. However, in addition to this role it has recently been demonstrated that the activity of pyruvate kinase is required for regulation in preventing metabolic block during carbon co-catabolism (Noy *et al.*, 2016). Furthermore, the essentiality of malate synthase, the second enzyme of the GS, is as a result of its requirement for glyoxylate detoxification when Mtb is grown in the presence of fatty acids, as is the case *in vivo* (Puckett et al., 2017).

CCM is essential as it provides the precursors for the synthesis of all the required biomolecules in the cell and importantly, generates the reducing equivalents required to initiate the ETC to provide energy for all cellular processes. This is particularly significant in Mtb, which relies solely on ATP generated by oxidative phosphorylation for growth (Koul *et al.*, 2008, Rao *et al.*, 2008). Taking into account the uniqueness and adaptability of CCM in Mtb, it therefore stands to reason that the ETC of Mtb may behave in an analogously flexible manner and that perturbations of the ETC may have consequences for CCM.

2.4 The *E*lectron *T*ransport *C*hain

The main purpose of the ETC is to produce a PMF that drives the activity of the ATP synthase, thus generating energy in the form of ATP. The ETC is made up of several enzymes and enzyme complexes and is located in the inner mitochondrial membrane of eukaryotes and the cytoplasmic membrane in prokaryotes. The ETC involves the movement of electrons from donors such as NADH or succinate to electron carriers such as ubiquinone (Q) or menaquinone (MQ). This is followed by a number of reduction-oxidation (redox) reactions where electrons are transferred to carriers with successively higher reduction potentials eventually terminating with oxygen as the terminal oxidant in the majority of cases (Richardson, 2000). This process has been studied extensively in mitochondria, which serve as the energy powerhouses for eukaryotic cells.

2.4.1 Eukaryotic ETC

In eukaryotes, specifically mammalian mitochondria, the ETC is made up of four distinct complexes, Complex I to IV depicted in Figure 2.5. Complex I is the NADH dehydrogenase (NDH) which oxidises NADH derived from glycolysis and the TCA cycle to NAD^+. The electrons are then transferred to the electron carrier Q and the reaction is coupled with the extrusion of protons, thus initiating the ETC. Alternatively, the ETC can be initiated by electrons derived from succinate via SDH, known as Complex II. During this reaction, succinate is oxidised to fumarate and electrons are transferred to Q with no coupled extrusion of protons. Complex III is a cytochrome *c* reductase which oxidises ubiquinol (QH_2), reduces cytochrome *c* and pumps protons into the intermembrane space. Complex IV of the eukaryotic ETC is a cytochrome *c* oxidase, which oxidises cytochrome *c* and reduces molecular oxygen to water, coupled with the extrusion of protons. The pumping of protons by Complex I, III and IV generates a PMF, which is then consumed by the ATP synthase complex, referred to as Complex V, to generate ATP (Richardson, 2000, Rich and Marechal, 2010, Sazanov, 2015). The overall arrangement of the mitochondrial ETC and the movement of electrons is shown in Figure 2.5.

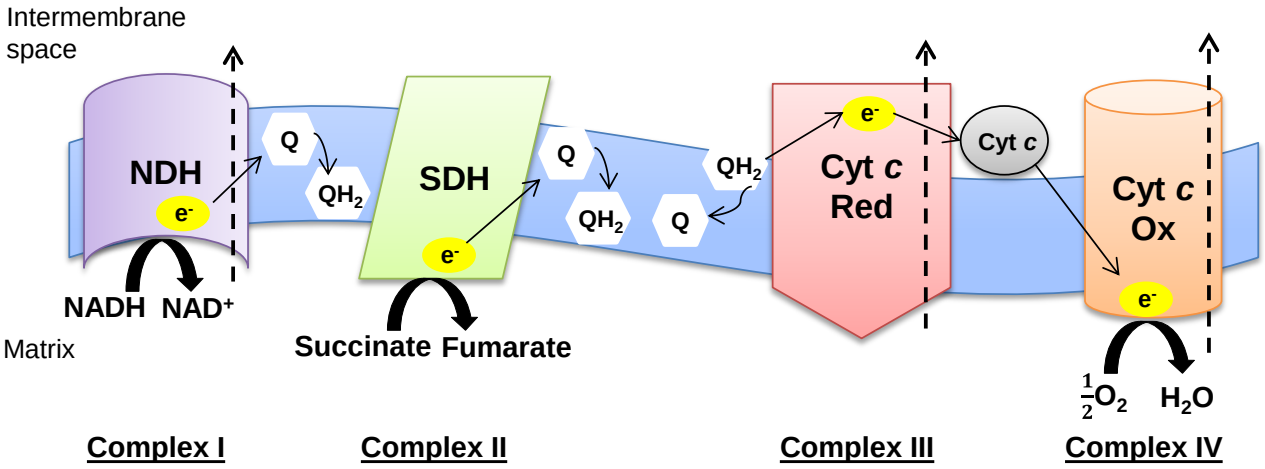


Figure 2.5: The mitochondrial ETC. Shown is a representation of the mammalian mitochondrial electron transport chain depicting the complexes involved in aerobic respiration. NDH: NADH dehydrogenase, SDH: Succinate dehydrogenase, Cyt c Red: Cytochrome c reductase, Cyt c Ox: Cytochrome c oxidase, Ubiquinone, QH_2: Ubiquinol. Figure adapted from Berg *et al.* (2002).

The ETC of mitochondria is known to be highly conserved, however some degree of flexibility has been observed at the level of electron input (Rich and Marechal, 2010). The Electron transfer flavoprotein (ETF), which is reduced by dehydrogenases that oxidise fatty acids and different types of amino acids, is able to donate electrons to the ETC via the membrane-attached ETF-ubiquinol oxidoreductase (ETF-QO) (Rich and Marechal, 2010), providing a third point of entry for electrons. In addition, electrons for the ETC can be obtained from dihydroorotate, glycerol-3-phosphate and choline directly; however, none of the enzymes involved in these reactions are able to translocate protons (Rich and Marechal, 2010). Although ETC flexibility is observed in eukaryotes, the level is in stark contrast to the amount of plasticity observed in prokaryotes where the flexibility is observed throughout the chain and not only at the point of electron entry.

2.4.2 Prokaryotic ETC

The ETC of bacteria is distinguished from that found in mitochondria by extreme flexibility and branching, allowing for the use of several different electron donors and terminal electron acceptors, as well as a variety of enzymes which catalyse the redox reactions (Richardson, 2000). The pathway in bacteria is similar to that in mitochondria, with the donation of electrons into the quinone pool via dehydrogenases and subsequent oxidation of the reduced quinones by terminal oxidases that transfer the electrons to a terminal oxidant. The first level of flexibility observed in the bacterial respiratory chain is the presence of multiple dehydrogenases which feed electrons into the pathway (Richardson, 2000, Borisov and Verkhovsky, 2009), highlighted for *E. coli* in Figure 2.6. In contrast to mitochondria, bacteria are able to utilise electron carriers other than Q under different conditions, with the use dependent on the available terminal electron acceptor/s (Borisov and Verkhovsky, 2009). MQ and demethylmenaquinone (DMQ) are examples of alternate electron carriers in *E. coli* (Richardson, 2000, Borisov and Verkhovsky, 2009). ETCs are commonly referred to as branched when more than one terminal oxidase is available in the presence of oxygen; however, using *E. coli* as an example it can be seen that some bacterial ETCs are not only branched but also extremely adaptable with the ability to utilise various terminal electron acceptors other than oxygen (Richardson, 2000). Further complicating the ETC of *E. coli* is the presence of multiple copies of enzymes e.g. two NDH's, two formate

dehydrogenases, two hydrogenases, two lactate dehydrogenases, two DMSO oxidases, two cytochrome *bd* oxidases and three nitrate reductases (Richardson, 2000).

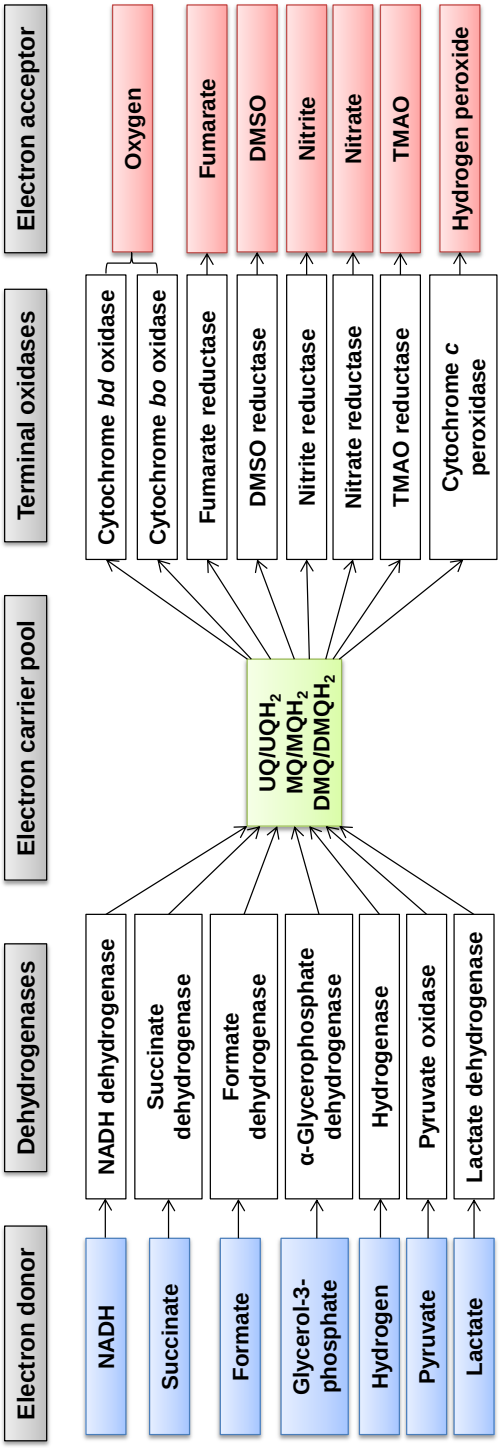


Figure 2.6: A schematic representation of the electron transport chain in *E. coli*. The multiple electron donors, dehydrogenases, terminal oxidases and electron acceptors available for respiration are shown. Figure adapted from Richardson (2000).

As a result of the variety of environments that bacteria and archaea can occupy, a large degree of diversity is observed between prokaryotic ETCs (Kim and Gadd, 2008). The flexibility of the prokaryotic ETC is hypothesised to be an evolutionary adaptation, allowing the prokaryote to respond to the various environmental conditions encountered which can vary from complete aerobiosis to complete anaerobiosis (Borisov and Verkhovsky, 2009, Kana, 2009). This adaptable nature is further beneficial for pathogens such as Mtb, which are exposed to various conditions during infection and pathogenesis, including a range of oxygen tensions and the availability of alternate electron acceptors.

2.5 The mycobacterial ETC

Mtb and other members of the *Mycobacterium* genus are considered obligate aerobes and thus rely on the availability of oxygen for growth. However, much like other bacteria, mycobacteria possess a flexible, branched ETC which facilitates growth aerobically as well as survival under hypoxic and anaerobic conditions (Wayne, 1996, Kana *et al.*, 2001, Matsoso *et al.*, 2005, Kana, 2009). The ability of Mtb to persist under reduced oxygen tensions was demonstrated by Wayne and Hayes (Wayne, 1996). In the model presented, the authors show that Mtb transitions through two stages of non-replicating persistence (NRP) in response to depleting oxygen levels (Wayne, 1996). The first stage, NRP-1 is observed at ~1 % dissolved oxygen (DO) and is characterised by an increase in optical density (OD) but a stagnation of CFUs, DNA synthesis and ATP content. NRP-2 begins at DO levels below 0.06 % where no increase in OD, CFUs or ATP is observed (Wayne, 1996). The authors propose that the ability of Mtb to attain NRP facilitates the pathogen achieving a state of clinical latency for prolonged periods in the host (Wayne, 1996). Interestingly, of the many different types of granulomas, it is predicted that caseous necrotic granulomas in humans are hypoxic (Barry *et al.*, 2009). This was supported by the detection of hypoxic granulomas in guinea pigs, rabbits and non-human primates (Via *et al.*, 2008). Whether the Mtb bacilli in these lesions are fully metabolically active or in a persistent state is yet to be confirmed, however their susceptibility to the anaerobically-active compound metronidazole suggests that they may exhibit a physiology similar to NRP-2 cells in the Wayne model (Wayne, 1996, Via *et al.*, 2008). Regardless of the physiological state of the Mtb cells in granulomas, a

flexible ETC that is able to adapt to the varying oxygen tensions experienced in different granulomas in order to grow and/or persist is essential. The forthcoming section will describe the flexibility of the mycobacterial ETC.

2.5.1 The mycobacterial electron donors and dehydrogenases

The mycobacterial ETC can be initiated by number of electron donors, either by directly contributing to the menaquinol pool or via the production of NADH. The most well characterized mycobacterial electron donor is NADH. In the first step of the ETC, NADH is oxidized by NDH which, in mycobacteria, is a NAD/NADH: menaquinone oxidoreductase that catalyses the formation of NAD^+- the main oxidant in bacterial cells (Kana, 2009). NDH highlights the flexibility of the ETC in mycobacteria as Mtb possesses two types of NDH's: NDH-I which is similar to the mitochondrial Complex I and NDH-II, the single subunit enzyme (Weinstein *et al.*, 2005). NDH-I is a fourteen subunit, proton-translocating enzyme and is encoded by the *nuoABCDEFGHIJKLMN* operon (Weinstein *et al.*, 2005). Weinstein *et al* (2005) observed no reduction in NDH activity when the Mtb NDH-I was inhibited, this together with the ability to obtain transposon mutants with insertions in genes of the operon, and the lack of a complete *nuoA-N* operon in *M. leprae*, suggests that NDH-I is dispensable for respiratory activity in mycobacteria (Sassetti *et al.*, 2003, Weinstein *et al.*, 2005, Griffin *et al.*, 2011). However, *nuoB* transcript was detected in aerobic Mtb cultures, and transcript levels decreased with reducing oxygen tensions, providing evidence of a role for NDH-I under aerobic conditions (Shi *et al.*, 2005). It has subsequently been shown that NDH-I, specifically the molybdopterin cofactor (MoCo)-dependent subunit NuoG, has anti-apoptotic function and in the absence of *nuoG* Mtb virulence is decreased in mice (Velmurugan *et al.*, 2007). The molecular mechanism of this anti-apoptotic function has been attributed to neutralisation of NADPH-oxidase (NOX2)-derived ROS to inhibit TNF α- mediated macrophage apoptosis (Miller *et al.*, 2010). These data provide compelling evidence that respiratory activity may not be the primary role of NDH-I in Mtb, thus pointing to NDH-II as the main NDH.

NDH-II is a non-proton-translocating, single subunit enzyme and two copies are present in Mtb, encoded by *ndh* (*Rv1854c*) and *ndhA* (*Rv0392c*) (Weinstein *et al.*, 2005). Unlike *nuoB*, the

expression of *ndh* during mouse infections increased transiently and was detected throughout the chronic infection, highlighting a role for NDH-II during pathogenesis (Shi *et al.*, 2005). Interestingly, of the two NDH-II-encoding homologues, only *ndh* has been shown to be essential in Mtb, and while *ndhA* is transcribed, a physiological role is yet to be assigned to NDH-IIA (Awasthy *et al.*, 2014). Unlike Mtb, the model organism *M. smegmatis* contains a single *ndh* homologue, *MSMEG_3621* (Kapopoulou *et al.*, 2011). NDH-II is essential for *M. smegmatis* viability and mutations in the *ndh* gene lead to an array of phenotypes including temperature sensitivity, auxotrophy and most notably, resistance to INH and Eth (Miesel *et al.*, 1998). A role for NDH-II in resistance to INH and Eth was later confirmed in Mtb with the mechanism being ascribed to competitive inhibition of binding of INH-NAD/ETH-NAD adducts to InhA because of increased NADH levels (Vilcheze *et al.*, 2005). Furthermore, NDH-II has been implicated in the susceptibility of Mtb to CFZ (Yano *et al.*, 2011), phenothiazines (Yano *et al.*, 2006), quinolinequinones (Heikal *et al.*, 2016) and quinolinyl pyrimidines (Shirude *et al.*, 2012). With regards to CFZ, NDH-II is implicated in the mechanism of action whereby NDH-II reduces CFZ and the reduced CFZ is subsequently spontaneously oxidised by oxygen, generating high levels of ROS, which damages various cellular components thus leading to death (Yano *et al.*, 2011). The authors hypothesised that CFZ competes with MQ which was supported by a study that demonstrated supplementation of Mtb cultures with increasing concentrations of MQ leads to a reduction in CFZ mycobactericidal activity (Lechartier and Cole, 2015). Quinolinequinones have been shown to exert activity in a similar manner to CFZ (Heikal *et al.*, 2016). Phenothiazines on the other hand are predicted to directly target NDH-II however, the exact mechanism of action is not known. It is predicted that the analogue trifluoperazine binds to intermediates formed during NADH oxidation and MQ reduction, thus disrupting product release and substrate binding (Yano *et al.*, 2006). The essentiality of NDH-II and its role in susceptibility to drugs highlights this enzyme as a promising drug target and the recent resolution of the catalytic mechanism (Yano *et al.*, 2014) will aid in the development of novel compounds to target this component of the mycobacterial ETC.

The next well-characterized electron donor is succinate, which is an integral part of the TCA cycle where it is oxidized to fumarate by SDH (Berg *et al.*, 2002, Kana, 2009). SDH therefore

plays an important role in both the ETC and in substrate utilization. The bacterial SDH, like Complex II in mitochondria, is able to catalyse the reversible reaction of succinate oxidation to fumarate, coupled with quinone reduction to quinol. Complex II enzymes are named according to the direction of the reaction which is kinetically favoured. Succinate: quinone oxidoreductases favour the oxidation of succinate, while quinol: fumarate reductases (FRDs) favour the oxidation of quinol and reduction of fumarate (Iverson, 2013). The crystal structures of several SDH/FRD enzymes have been resolved and are all similar. The enzymes are composed of at least 3 subunits, arranged into two domains i.e. the soluble domain, which is responsible for succinate oxidation/fumarate reduction and the membrane-bound domain, which catalyses the oxidation and reduction of quinol and quinone respectively (Iverson, 2013, Maklashina *et al.*, 2013).

In keeping with the flexibility of the mycobacterial ETC, Mtb retains an *sdhCDAB* (*Rv3316-Rv3319*)-encoded SDH (SDH-2), as well as a second putative *Rv0247c-Rv0249c*-encoded enzyme (SDH-1) predicted to be essential for *in vitro* growth by Griffin *et al*. (2011). SDH activity is required for the adaptation of mycobacteria to reduced levels of oxygen (Eoh and Rhee, 2013, Hartman *et al.*, 2014, Pecsi *et al.*, 2014). Under hypoxic conditions, in the presence of a fatty acid or glucose as the carbon source, Mtb increases the expression of the glyoxylate shunt enzyme ICL for increased production of succinate, which is used to maintain the membrane potential and ATP production in the absence of nitrate as the terminal electron acceptor (Eoh and Rhee, 2013). This was the second demonstrated mechanism of adaptation to hypoxia via succinate, after Watanabe *et al*. (2011) demonstrated that Mtb could operate the reductive arm of the TCA cycle for the production of succinate to maintain the membrane potential under hypoxia (Watanabe *et al.*, 2011).

The role of SDH activity in the adaptation to hypoxia was demonstrated using the inhibitor 3-Nitropropionate (3NP), however which of the SDH enzymes is responsible for this adaptation was not confirmed (Eoh and Rhee, 2013). Hartman *et al.* (2014) subsequently attempted to resolve this by generating single knock-out mutants of *sdh1* and *sdh2* (Hartman *et al.*, 2014). The authors established that SDH-1 is the predominant enzyme in Mtb and they propose a model in which SDH mediates respiration during the adaptation to hypoxia by reducing the MKH_2 pool,

thereby reducing oxygen consumption while still providing a mechanism for the maintenance of the membrane potential and ATP production (Hartman *et al.*, 2014). Interestingly, both *sdh1* and *sdh2* could be individually knocked out in Mtb without severe consequences, suggesting that the FRD-encoded by *Rv1552-Rv1555*, could catalyse the oxidation of succinate to fumarate (Hartman *et al.*, 2014). While not essential in Mtb, *sdh2* could not be knocked out in *M. smegmatis*, which does not harbour an FRD-encoding operon (Pecsi *et al.*, 2014). This would suggest that *sdh1* and/or *sdh2* have both SDH and FRD activity in *M. smegmatis*, however no FRD activity could be detected from inverted membrane vesicles (IMVs) (Pecsi *et al.*, 2014), suggesting that differences in essentiality could point to differences in succinate/fumarate metabolism between the two organisms.

In addition to NDH and SDH, mycobacteria carry several additional dehydrogenases able to utilise alternate substrates to initiate the ETC, reviewed in (Kana, 2009, Cook *et al.*, 2014a, Cook *et al.*, 2014b, Cook *et al.*, 2017) and depicted in Figure 2.7. The alternate enzymes present in mycobacteria include proline dehydrogenase, carbon monoxide dehydrogenase, alanine dehydrogenase, lactate dehydrogenase (LDH), glycerol-3-phosphate dehydrogenase (G3PDH), malate dehydrogenase/quinone oxidoreductase, hydrogenases and F_{420}-dependent glucose-6-phosphate dehydrogenase (Cook *et al.*, 2014b, Cook *et al.*, 2017). A number of these enzymes are predicted to play a role in adaptation to stress as observed by up-regulation of the genes encoding hydrogenases, alanine dehydrogenase, proline dehydrogenase, G3PDH, CO dehydrogenase and malate quinone oxidoreductase in response to starvation and/or oxygen limitation in *M. smegmatis* (Berney and Cook, 2010). In recent years, progress has been made in assigning functions to alternate primary dehydrogenases; however, the precise contribution of each enzyme to ETC activity under different conditions remains to be elucidated. The presence of a large repertoire of enzymes able to donate electrons to the ETC further highlights the flexibility of Mtb and possibly ensures that the pathogen is always poised to initiate the ETC for energy production and redox balance. This flexibility is further augmented by the presence of multiple homologues for several genes encoding primary dehydrogenases e.g. two LDH-encoding genes (*Rv1872c* and *Rv0694*) in Mtb (Billig *et al.*, 2017), three hydrogenase genes in

M. smegmatis (Berney *et al.*, 2014b) and four putative G3PDH-encoding genes in Mtb and *M. smegmatis* (Kapopoulou *et al.*, 2011).

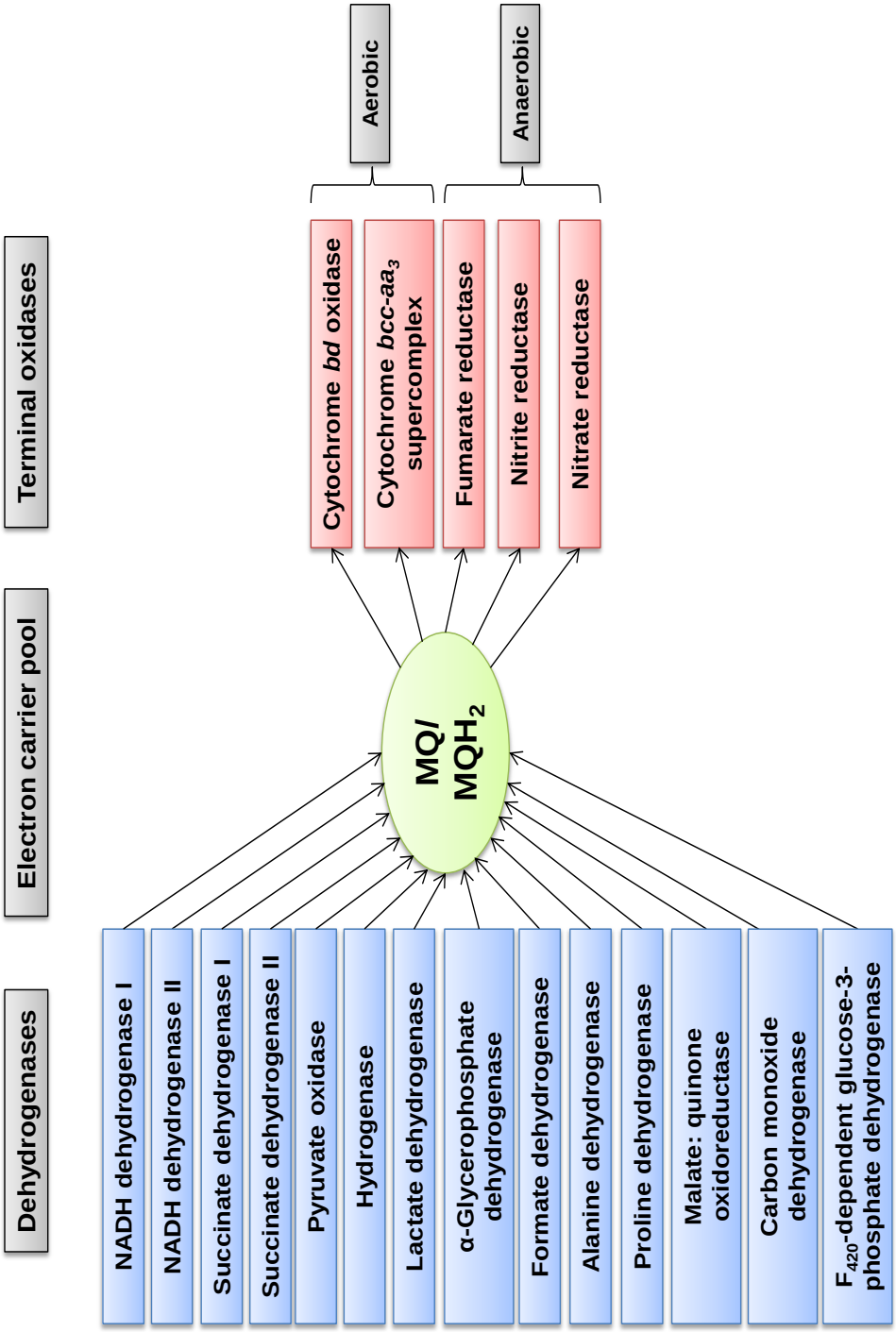


Figure 2.7: A schematic representation of the mycobacterial ETC. The numerous probable dehydrogenases able to donate electrons to the menaquinone pool are shown on the left in blue. The multiple terminal oxidases predicted to transfer electrons to terminal electron acceptors under aerobic and anaerobic conditions are shown on the right in red. The diagram was constructed based on existing data and current genome annotations.

2.5.2 The mycobacterial electron carriers

Lipophilic electron carriers are an essential component of the ETC as they are required for the Q cycle in various membrane-bound respiratory complexes that facilitate the movement of protons across the membrane thus maintaining the PMF. Gram-negative prokaryotes such as *E. coli* retain, and are able to, utilise three electron carriers i.e. Q, MQ and DMQ (Richardson, 2000, Borisov and Verkhovsky, 2009). In contrast, mycobacteria like many Gram-positive bacteria have been known to possess a single electron carrier: MQ-9 (Dhiman *et al.*, 2009). The biosynthesis of MQ-9 is a multi-step pathway, requiring the action of several enzymes encoded by *menABCDEG* operon and has become a subject of investigation for drug development as result of all the genes being identified as essential for growth in multiple high-throughput screens (Sassetti *et al.*, 2003, Dhiman *et al.*, 2009, Kana, 2009, Griffin *et al.*, 2011, Sukheja *et al.*, 2017). However, it has recently been shown that *M. smegmatis* synthesises an alternate polyketide quinone electron carrier, which is induced in oxygen-deficient environments such as biofilms (Anand *et al.*, 2015). Although no functional or biochemical evidence was provided, the presence of these alternate electron carriers in Mtb was inferred from homology, transcript analysis and detection of the polyketide quinone in Mtb biofilm extracts (Anand *et al.*, 2015). Given that mycobacteria are able to utilise several electron donors under different conditions, particularly hypoxia, it is not surprising that an alternate electron carrier would be available under these conditions and once again highlights the flexibility of the mycobacterial ETC.

2.6 Terminal electron acceptors in mycobacteria

It is intriguing that the genome of Mtb harbours genes which encode terminal oxidase enzymes that are able to transfer electrons to numerous alternate terminal electron acceptors such as nitrate, nitrite and fumarate (Cole *et al.*, 1998). To date no evidence has been presented to show that these alternate electron acceptors are able to support the growth of mycobacteria in the absence of oxygen. Rather, the main role of these alternate terminal electron acceptors in mycobacteria is thought to be the disposal of reducing equivalents for redox homeostasis as well as generating a PMF while the cells adapt to surviving in the absence of oxygen (Kana, 2009, Cook *et al.*, 2014b).

2.7 Alternate terminal oxidases

Nitrate reductase (NR), which catalyses the reduction of nitrate to nitrite, is the most well characterised alternate terminal oxidase in mycobacteria. Mtb possesses two NR enzymes, the multi-subunit, membrane-bound NarGHI and the fused NarX which appears to be dispensable for NR activity in Mtb (Sohaskey and Wayne, 2003). Unlike other organisms, Mtb relies solely on NarGHI for both the respiratory and assimilatory functions of NR (Malm *et al.*, 2009). Furthermore, it has been shown that *narGHJI* expression is constitutive in Mtb with NR activity being regulated by the nitrate transporter, NarK2 which is upregulated under hypoxic conditions and in response to NO (Sohaskey and Wayne, 2003, Sohaskey, 2005). NR activity of Mtb is dispensable under standard laboratory conditions and during mouse infections, however it has been demonstrated that NR activity is important for Mtb under reduced oxygen tensions and in response to INH treatment during human macrophage infections (Aly *et al.*, 2006, Sohaskey, 2008, Cunningham-Bussel *et al.*, 2013a). In addition nitrate respiration has been shown (i) to protect hypoxic cells from acid stress and RNS (Tan *et al.*, 2010), (ii) to facilitate the intracellular growth of Mtb in NO-producing human macrophages (Jung *et al.*, 2013) and (iii) to facilitate the endogenous production of nitrite which slows down Mtb growth, increases ATP and regulates a number of genes involved in adaptation to various stresses including NO, oxidative stress and iron deprivation (Cunningham-Bussel *et al.*, 2013b). These data taken together with the reduced virulence of a Δ*narGHJI M. bovis* BCG strain in immune-deficient mice (Weber *et al.*, 2000), provide compelling evidence that this alternate terminal oxidase is important in mycobacterial physiology and metabolism in response to stress. In contrast to Mtb and other pathogenic mycobacteria, *M. smegmatis* is predicted to possess distinct NR enzymes for assimilation and respiration, which will be discussed further in Chapter 3 of this thesis.

The genome of Mtb encodes a single nitrite reductase enzyme, NirBD which is essential for the assimilation of both nitrate and nitrite (Malm *et al.*, 2009). In addition, *nirBD* was shown to be important for the survival of Mtb during the Wayne model of dormancy and during a human-macrophage dormancy model, both of which are characteristically hypoxic (Akhtar *et al.*, 2013). Thus, it is hypothesised that NirBD may serve as a terminal oxidase in the absence of oxygen when nitrite is available (Akhtar *et al.*, 2013).

An additional mechanism of maintaining a PMF across the membrane of Mtb in the absence of oxygen is proposed to be facilitated by FRD. In the presence of glucose and under reduced oxygen levels, FRD is up-regulated to produce succinate via the reductive arm of the TCA cycle (Watanabe *et al.*, 2011). The succinate is then pumped across the membrane to maintain a PMF by this fermentative process (Watanabe *et al.*, 2011). The role of succinate in maintaining an energised membrane was later confirmed by (Eoh and Rhee, 2013, Hartman *et al.*, 2014), however the mechanism in this case was independent of FRD activity.

In addition to NR and nitrite reductase the mycobacterial model organism *M. smegmatis* also encodes three hydrogenases as mentioned above. Hyd1 and Hyd2, encoded by *MSMEG_2262-2263* and *MSMEG_2719-2720* respectively, have been shown to act as dehydrogenases which oxidise H_2 and donate electrons to the ETC (Berney *et al.*, 2014a, Berney *et al.*, 2014b). Hyd3 on the other hand has been shown to serve as a terminal oxidase which generates H_2 in the absence of oxygen (Berney *et al.*, 2014a). Interestingly, *hyd2* and *hyd3* are both regulated by the *dos* regulon in *M. smegmatis*, which is the collection of genes that are induced during adaptation to hypoxia and in response to NO (Voskuil *et al.*, 2003).

The availability of several terminal oxidases that can maintain the PMF in the absence of oxygen once again highlights the metabolic flexibility of mycobacteria. However, mycobacteria are traditionally classified as obligate aerobes and thus possess efficient terminal oxidases able to utilise oxygen as the final electron acceptor during respiration.

2.8 Aerobic terminal oxidases

Mycobacteria, like many prokaryotes possess a branched aerobic respiratory chain with two terminal oxidases available that are able to reduce oxygen to water, referred to as cytochrome oxidases. Cytochromes are heme-containing proteins that were first discovered in the 1800's and are involved in various biological electron transfer processes, most commonly respiration (Thony-Meyer, 1997, Liu *et al.*, 2014). Cytochromes are classified according to the type/s of heme they contain and the environment of the heme-binding site. The different types of hemes present in respiratory cytochromes include heme *a, b* (protoheme), *c, d, d_1* and *o* (Liu *et al.*,

2014). When in a reduced state, each heme displays three peaks in the UV-Vis spectrum referred to as the α, β and γ peaks; therefore different cytochromes have distinct spectra. Cytochrome proteins are categorised according to the absorbance maximum of the α peak of its associated heme when in a reduced state (Thony-Meyer, 1997, Liu *et al.*, 2014). Examples of the different types of respiratory cytochromes and absorbance maxima of their associated hemes are shown in Table 2.1. The two cytochrome oxidases present in mycobacteria are of the aa_3 and *bd* type.

Table 2.1: The different types of respiratory hemes. A list of examples of the different types of hemes present in respiratory enzymes and their associated diagnostic wavelengths when in a reduced state.

	α peak (nm)	Example
Heme *a*	587-611	Cytochrome aa_3 oxidase
Heme *b*	557-563	Cytochrome b_6f complex
Heme *c*	549-561	Cytochrome c
Heme *d*	630-635	Cytochrome *bd* oxidase
Heme d_1	625	Cytochrome cd_1 nitrite reductase
Heme *o*	560	Cytochrome bo_3 oxidase

2.9 The respiratory cytochrome *c* proteins

The reduction potential between quinol and oxygen is not sufficient for the reaction to be energetically favourable. Therefore, an intermediate electron carrier is required which also contributes to the PMF when oxidised and reduced. Cytochrome *c* is able to perform this function and in order for the ETC to proceed to completion, cytochrome *c* needs to be reduced with electrons from the quinol pool and oxidised by oxygen. These reactions are catalysed by cytochrome *c* reductase (CcR) and cytochrome *c* oxidase (CcO) respectively. In mitochondria, the cytochrome *c* reductase (Complex III), cytochrome *c* and cytochrome *c* oxidase (Complex IV) are separate components with cytochrome *c* being a mobile element, while the reductase and oxidase are membrane bound, Figure 2.5. The cytochrome *c* reductase or cytochrome bc_1 reductase is an integral membrane protein made up of 11 subunits in mitochondria but can be as

few as three subunits in bacteria. The functional core of the enzyme contains cytochrome *b*, a Rieske iron-sulfur protein and cytochrome *c*, with different types of cytochrome *b* and *c* present in different organisms (Sone *et al.*, 2001, Crofts, 2004). A representation of the catalytic cycle of CcR with a non-mobile cytochrome c_1 is shown in Figure 2.8 as the blue subunits. The reaction catalysed by this enzyme proceeds via a process called the Q-cycle. The process can be separated into two steps with reactions that are spatially divided into the Q_0 and Q_i sites. Briefly, two electrons are extracted from a bound quinol with one electron being transferred to the 2Fe-2S cluster in the Rieske iron sulphur protein (Q_0 site) and the second being transferred to a low potential *b* heme (b_L), at the Q_i site. During this process, two protons are pumped into the intermembrane space. The electron from the 2Fe-2S cluster is then transferred to the first cytochrome *c*, which then transfers the electron to a second cytochrome *c* (c_1) that is mobile in mitochondria. Cytochrome c_1 is then oxidised by cytochrome *c* oxidase. The electron from b_L is transferred to a high potential *b* heme (b_H), which reduces a quinone at a separate site to produce a partially reduced intermediate referred to as semiquinone. The initial quinol which was oxidised is released while the semiquinone remains bound. Thereafter, a second quinol is oxidised and electrons are transferred in the same manner. During the reduction of the semiquinone by b_H in the second step, two protons are consumed from the matrix. Overall, the process results in the production of two reduced cytochrome c_1 , pumping of four protons into the intermembrane space, consumption of two protons from the matrix, the oxidation of two quinols and reduction of one quinone (Gao *et al.*, 2003, Crofts, 2004).

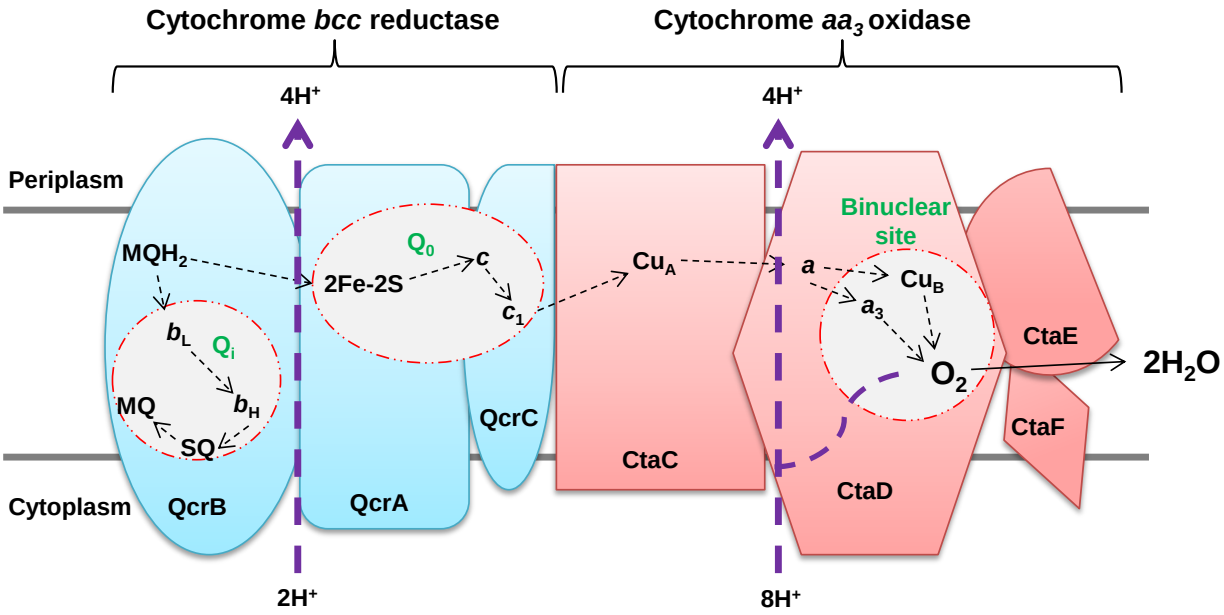


Figure 2.8: Architectural arrangement of the cytochrome *bcc* reductase-cytochrome *aa*$_3$ oxidase super-complex showing the predicted catalytic cycle of the enzyme. The blue subunits make up the CcR and the reds subunits constitute the CcO. Black dashed lines show the movement of electrons while the purple dashed lines depict the movement of protons. The red-bordered grey areas highlight distinct catalytic centers in the enzyme complex. MQH_2: menaquinol, MQ: menaquinone, SQ: semiquinone. Figure adapted from Gao *et al.* (2003), Wikstrom (2004), Kadenbach and Huttemann (2015), Yoshikawa and Shimada (2015) .

Cytochrome *c* oxidase belongs to the heme-copper superfamily of oxidases and has been well characterised in eukaryotes, specifically the bovine enzyme (Garcia-Horsman *et al.*, 1994, Ferguson-Miller and Babcock, 1996). The enzyme catalyses the four-electron reduction of dioxygen to water and pumps four protons. Similar to the cytochrome *c* reductase, the CcO is a membrane bound protein made up of 13 subunits in eukaryotes (cytochrome *aa*$_3$ oxidase in mitochondria) and 3 to 4 subunits in bacteria. The catalytic core of the CcO is made up of a copper atom (Cu_A), heme *a* and a binuclear site made up of a second copper atom (Cu_B) and heme a_3 (Wikstrom, 2004). The catalytic mechanism of CcO has long been debated, particularly with regards to proton-pumping. However, it is commonly accepted that the reaction proceeds via two phases i.e. an oxidative phase where the enzyme is oxidised by oxygen and the reductive phase where the enzyme is reduced before another oxygen molecule binds (Bloch *et al.*, 2004, Yoshikawa and Shimada, 2015). During catalysis several intermediates of the different substrates and prosthetic groups are formed but for simplicity the overall catalytic cycle is shown within the red subunits of Figure 2.8 and can be summarized as follows: Oxygen binds to and is reduced by

the CcO when the a_3-Cu_B binuclear site is in a fully reduced state. The reduced state is achieved by the successive donation of four electrons from four separate reduced cytochrome *c* molecules to the Cu_A site and then to the heme *a,* from which electrons are transferred to the heme a_3 and Cu_B. Four protons are consumed and two pumped during the reduction of the a_3-Cu_B binuclear site. During the oxidative phase, molecular oxygen is reduced to water at the binuclear site with three electrons donated from heme a_3 and Cu_B and a fourth from a tyrosine residue, all of which is coupled with consumption of four protons and pumping of two protons (Bloch *et al.*, 2004, Wikstrom, 2004, Kadenbach and Huttemann, 2015, Yoshikawa and Shimada, 2015).

The catalytic mechanisms of the CcR and CcO appear to be conserved in both mitochondria and aerobic bacteria with homologous protein complexes. However, mycobacteria and other actinomycetes are distinguished in that they do not possess a soluble cytochrome *c* but rather a di-heme cytochrome *c* protein as the third subunit of the CcR (Sone *et al.*, 2001, Matsoso *et al.*, 2005). It has since been shown that the CcR and CcO form a stable super-complex in the actinomycete *Corynebacterium glutamicum*, referred to as the cytochrome *bcc-*aa_3 complex (Niebisch and Bott, 2003, Graf *et al*., 2016). Based on the lack of a gene encoding a soluble cytochrome *c* in mycobacteria and the high sequence similarity shared between the CcR- and CcO- encoding homologues in Mtb and *C. glutamicum,* it is hypothesised that mycobacteria also harbour a cytochrome *bcc-*aa_3 super-complex (Sone *et al.*, 2001, Matsoso *et al.*, 2005). Indeed, evidence has been presented showing a strong interaction between the *bcc* and aa_3 complexes in *M. smegmatis* which are based mainly on hydrophobic forces (Megehee *et al.*, 2006). More recently a stable hybrid super-complex made up of the Mtb *bcc* and *M. smegmatis* aa_3 was isolated, providing further evidence that mycobacteria synthesise a super-complex of CcR and CcO (Kim *et al.*, 2015).

In mycobacteria the genes encoding the CcR i.e. *qcrC, qcrA* and *qcrB* are arranged in an operon, while those encoding the CcO (*ctaE, ctaD, ctaC* and *ctaF*) are not all operonic i.e. *ctaC* and *ctaF* appear operonic, *ctaE* is immediately upstream of the *qcrCAB* operon and *ctaD* is located in a different region of the chromosome (Matsoso *et al.*, 2005). Apart from *ctaF* whose role is yet to be determined, all the super-complex-encoding genes are annotated as essential for growth in

Mtb, highlighting the importance of this branch of the aerobic ETC in mycobacterial physiology (Sassetti *et al.*, 2003, Griffin *et al.*, 2011). The ability to delete *qcrCAB* and *ctaC* in *M. smegmatis* was therefore fascinating but explained by the presence of an alternate terminal oxidase, cytochrome *bd* oxidase, which facilitated the growth of these mutants, albeit to a lesser extent than the wild type strain (Matsoso *et al.*, 2005). It was demonstrated that the *qcrCAB* operon could not be knocked-out in Mtb (Matsoso *et al*., 2005). However, this does not necessarily indicate the essentiality of this operon in the pathogen but may rather be due to diminished growth of a mutant lacking *qcrCAB*, which would not have formed easily visible colonies during the incubation period employed (Matsoso *et al.*, 2005).

Over the past five years, increasing attention has been paid to the mycobacterial *bcc-aa*$_3$ complex following the discovery of Q203, a novel imidazopyridine amide (IPA) compound which inhibits the growth of Mtb by disrupting the *bcc* complex (Pethe *et al.*, 2013). Pethe *et al.* (2013) discovered Q203 in a high-throughput screen of novel compounds in a macrophage infection model and showed that it was active against DS-, MDR- and XDR-TB. The compound was shown to be non-toxic in human cell lines, displayed delayed killing at levels comparable to INH treatment in mouse infection models, was associated with reduced lung pathology in mice and was proposed to target QcrB because of the isolation of resistant strains carrying mutations with an amino acid change at Thr313 in QcrB (Pethe *et al.*, 2013). In addition, Q203 treatment was shown to reduce intracellular ATP levels, pointing to a mechanism of action for the drug (Pethe *et al.*, 2013). These data highlighted Q203 as a promising compound for the treatment of DR-TB, emphasising this area of Mtb metabolism as promising for drug development. These studies laid the foundation for the phase I clinical trials that are currently underway with Q203 (Pethe *et al.*, 2013, Kang *et al.*, 2014). In addition to Q203, another group developed a set of novel IPA's which were evaluated in *M. bovis* BCG and were also shown to target QcrB, further validating this class of compounds as promising anti-tubecular drugs and highlighting QcrB as a vulnerable target (Abrahams *et al.*, 2012).

The proton pump inhibitor, lansoprazole (LPZ) has been identified as a potent inhibitor of Mtb in a cell-based high-throughput screen of drugs approved for conditions other than TB (Rybniker *et*

al., 2015). The authors found that LPZ is a prodrug, which when reduced to lansoprazole sulfide inhibits Mtb growth in a manner similar to Q203 (Rybniker *et al.*, 2015). The mutation of leucine to proline at position 176 in QcrB leads to resistance to LPZ but interestingly the Q203 resistance-conferring mutation does not lead to LPZ resistance, pointing to distinct binding sites of the two compounds in the same protein (Rybniker *et al.*, 2015).

Q203 and BDQ both target the ETC and both led to a reduction in intracellular ATP levels (Koul *et al.*, 2007, Pethe *et al.*, 2013). It has previously been shown that the efflux pump inhibitor (EPI), verapamil potentiates the activity of BDQ and when recently investigated for Q203, it was observed that EPI's play a role in the tolerance of Mtb to Q203 (Jang *et al.*, 2017). This finding is both clinically promising and worrying. The findings provide evidence that co-administration of an EPI would potentiate the activity of Q203. However, clinical samples have been isolated that carry a mutation in the efflux pump transcriptional regulator, Rv0678 which leads to an upregulation of the MmpS5-MmpL5 efflux pump and results in resistance to BDQ and CFZ (Andries *et al.*, 2014). Although the efflux pump/s involved in tolerance to Q203 is/are yet to be identified, this does provide proof that an additional mechanism of resistance to Q203 does exist (Jang *et al.*, 2017).

In addition to overcoming IPA susceptibility as a result of the development of resistance mutations, it has been reported that Mtb is able to overcome growth inhibition independently of mutations in *qcrB* (Arora *et al.*, 2014). This phenomenon has been attributed to the presence of the second aerobic respiratory branch in Mtb, facilitated by the *cydAB*-encoded cytochrome *bd* oxidase (CbdO) (Arora *et al.*, 2014). This has recently been confirmed by Lamprecht *et al.* (2016) who show that the CbdO can maintain the aerobic respiratory activity when the *bcc-aa*$_3$ complex is inhibited by Q203 and by Kalia *et al.* (2017) who highlighted the synthetic lethality when both Mtb terminal oxidases are inhibited. Although the *bcc-aa*$_3$ complex is regarded as essential in mycobacteria and represents a promising drug target, the findings described above highlight an important role for this alternate aerobic respiratory pathway in Mtb.

2.10 The cytochrome *bd* oxidase

CbdO enzymes are uniquely prokaryotic terminal oxygen reductases that are distributed among several phyla. The CbdO is distinct from cytochrome *c* oxidoreductases in that no Fe-S clusters or copper ions are present in the enzyme. The enzyme has been shown to catalyse the two-electron oxidation of quinol and the four-electron reduction of oxygen to water. Although no protons are pumped by the CbdO, it still contributes to the PMF by the uptake of protons from the cytoplasm. The CbdO is an integral membrane protein commonly made up of two subunits-CydA and CydB of ~ 58 and 43 kDa respectively in *E. coli*, the organism wherein the CbdO has been extensively studied (Miller *et al.*, 1988), shown in Figure 2.9. In proteobacteria, a third subunit is present and has been shown to be important for activity via its involvement in assembly or stability of the active site and is referred to as CydX (VanOrsdel *et al.*, 2013, Hoeser *et al.*, 2014). The enzyme has two subunits (CydA and CydB) and three heme-containing redox centres, which are required for catalysis i.e. heme b_{558}, heme b_{595} and heme *d* (Borisov *et al*., 2011a). CydA is predicted to have nine transmembrane helices while CydB is predicted to have eight (Osborne and Gennis, 1999). In addition, the Q-loop is found in the hydrophilic region connecting helices 6 and 7 of CydA and forms part of the quinol binding site (Osborne and Gennis, 1999). Two types of CbdO's have been identified which differ in the length of their Q-loop; the *E. coli* protein has a long Q-loop because of an insertion in the C-terminal portion while a short Q-loop is present in the Mtb protein (Osborne and Gennis, 1999).

Based on kinetic analysis, a catalytic mechanism for CbdO was proposed to be made up of six steps: (i) Ubiquinol binds to the one-electron reduced enzyme, (ii) reduction of heme *b* leads to the immediate binding of molecular O_2, (iii) release of ubiquinone and reduction of oxygen to peroxide, (iv) scission of the O-O bond results in the release of a water molecule and production of an oxoferryl form of the enzyme, (v) a second ubiquinol then binds and transfers electrons to the heme centres and finally (vi) a second water molecule is released and the enzyme reverts to its one-electron reduced state for the beginning of another catalytic cycle (Junemann *et al.*, 1995). This catalytic mechanism has since been revised by Matsumoto *et al*. (2006). They provide evidence that ubiquinol binds to and is reduced by CbdO that is in an oxygenated one-electron reduced state, which is a stable intermediate regularly isolated, much the same as the

stable oxoferryl intermediate (Matsumoto *et al.*, 2006). The catalytic mechanism presented by Matsumoto *et al.* (2006) better accounts for the rapid O_2 binding capacity of the CbdO. Worth noting is that both mechanisms are based on the linear movement of electrons from heme b_{558} to the putative binuclear centre of heme b_{595} and heme *d* (Borisov *et al.*, 2011a). The recent resolution of the CbdO crystal structure from *Geobacillus thermodenitrificans* refutes the presence of a binuclear centre and presents a triangular conformation of the three hemes, with the proposed electron transfer reaction proceeding from heme b_{558} directly to heme *d*, followed by equilibration between heme b_{595} and heme *d* (Safarian *et al.*, 2016). Furthermore, the authors show that both CydA and CydB have nine transmembrane helices each, with all three hemes located in CydA. They present two possible proton channels and demonstrate that a third subunit forms part of the complex and is referred to as CydS, with a predicted role analogous to CydX (Safarian *et al.*, 2016). Although the authors did not provide a definitive catalytic mechanism, the presentation of the first crystal structure of CbdO provides a foundation for future investigations on this intriguing enzyme. Based on the newly resolved crystal structure and on previous analyses, a schematic of the mycobacterial CbdO and movement of electrons is depicted in Figure 2.9.

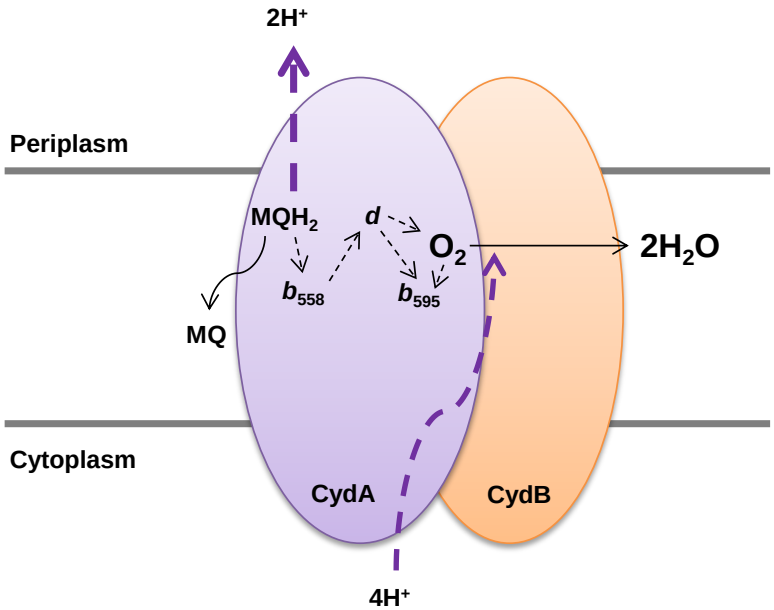


Figure 2.9: A representation of the cytochrome *bd* oxidase showing the predicted catalytic cycle. Black dashed lines show the movement of electrons while the purple dashed lines depict the movement of protons. MQH_2: menaquinol, MQ: menaquinone. Figure adapted from Safarian *et al.* (2016)

2.10.1 Physiological role of CbdO in bacteria

The CbdO was traditionally thought to be necessary only at reduced oxygen concentrations due to its higher affinity for oxygen and associated oxygen scavenging abilities. It has since been well established that the CbdO is indeed important under hypoxic conditions but also plays an essential role in the resistance and adaptation to several unfavourable conditions encountered by bacteria. CbdO in *E. coli* has been implicated in resistance to oxidative and nitrosative stress, the ability to exit from stationary phase, adaptation to high temperatures and exposure to low levels of cyanide (Wall *et al.*, 1992, Siegele and Kolter, 1993, Siegele *et al.*, 1996, Borisov *et al.*, 2015). In addition, the CbdO has been shown to protect against respiratory inhibition by hydrogen sulphide (Forte *et al.*, 2016, Korshunov *et al.*, 2016). The *E. coli* CbdO was also shown to play a role in heme biosynthesis and protein folding in the periplasm by providing oxidative power (Bader *et al.*, 1999, Mobius *et al.*, 2010). In the nitrogen-fixing Gram-negative bacterium A*zotobacter vinelandii* loss of CbdO lead to reduced stationary phase survival, iron deficiency and increased sensitivity to metal ions, iron chelators and oxidative stress- all presumably due do to an increase in oxygen poisoning of the nitrogenase enzymes (Edwards *et al.*, 2000). CbdO was also shown to be important in an anaerobic bacterium involved in human periodontal disease, *Porphyromonas gingivalis* which is surprisingly able to consume oxygen because of the CbdO and in its absence, is more susceptible to oxidative stress (Leclerc *et al.*, 2015). Furthermore, the CbdO has been shown to be important for several bacterial pathogens: in *Shigella flexneri* (Way *et al*., 1999) and *Brucella abortus* (Endley *et al.*, 2001) the enzyme was highlighted as important for intracellular survival and virulence, in *Salmonella* the CbdO contributes to nitrosative stress resistance during pathogenesis (Jones-Carson *et al.*, 2016) and in uropathogenic *E. coli* CbdO has been shown to facilitate host colonisation due its contribution to NO tolerance (Shepherd *et al.*, 2016). These data highlight a central role for CbdO in various metabolic processes in a diversity of bacterial species including aerobic, anaerobic, pathogenic and non-pathogenic organisms.

2.10.2 The mycobacterial CbdO

In mycobacteria, CbdO is encoded by the *cydAB* operon, specifically *Rv1623c-Rv1622c* in Mtb and *MSMEG_3233-MSMEG_3232* in *M. smegmatis* (Kana *et al.*, 2001). The *cydAB* operon is part of a gene cluster in mycobacteria made up of an additional two genes, *cydD* (*Rv1621c*) and *cydC* (*Rv1620c*), which are predicted to encode the ABC transporter CydDC. According to the Mycobrowser (Appendix B) database *cydC* is a pseudogene in *M. smegmatis*, however (Aung *et al.*, 2014) recently showed that *cydD* and *cydC* are part of an operon which is hypoxically induced. In addition, recent work in our laboratory has shown that loss of the *cydDC* operon in *M. smegmatis* leads to phenotypes generally associated with loss of a functional CbdO in *E. coli*, thus providing evidence that a functional CydDC is encoded in *M. smegmatis* which performs an analogous function to the *E. coli* enzyme (Moseki, 2017). Furthermore, using heterologous complementation, Moseki (2017) showed that the Mtb *cydDC* is able to restore CbdO function in an *E. coli* mutant thus providing evidence that the Mtb enzyme is able to function as an ABC-type transporter. In contrast to proteobacteria, no *cydX* or *cydS* homologue has been identified in mycobacteria.

In Mtb the *dos* regulon is a well characterised operon which responds to hypoxia and NO, two of the conditions under which the CbdO is responsive in other organisms. However, the *cydABDC* gene cluster does not form part of the *dos* regulon (Voskuil *et al.*, 2003) and was not upregulated during the model wherein the *dos* regulon was characterised (Sherman *et al.*, 2001, Park *et al.*, 2003). This may have been due to the model used, which was different to the NRP-1 Wayne model that is conventionally used to investigate hypoxia. Kana *et al.* (2001) show that *cydAB* is upregulated upon reducing dissolved oxygen content in *M. smegmatis* cultures from 21 to 0.5 %. This oxygen-dependent regulation of *cydAB* was confirmed by Berney and Cook (2010) who demonstrated that the operon was upregulated more than 50 fold in cultures with an oxygen saturation of 2.5 %. Furthermore, Matsoso *et al*. (2005) revealed that the loss of *qcrCAB* results in the upregulation of *cydAB* under normoxic conditions in *M. smegmatis*. In Mtb, Shi *et al.* (2005) showed a transient increase in *cydA* expression during a chronic mouse infection while Small *et al.* (2013) showed that the CbdO content of Mtb increases when cytochrome *c* maturation is disrupted. A large scale analysis of the transcriptional response of Mtb to inhibitors

of metabolism identified *cydA* to be upregulated upon treatment with a variety of compounds including cyanide, chlorpromazine (CPZ), thioridazine (TRZ), CCCP, nigericin, CFZ, DNP, sodium azide, dicyclohexylcarboxiimide, PZA and also during NRP-1 of the Wayne model and when grown on palmitate (Boshoff *et al.*, 2004). Interestingly β-lactam treatment was also shown to upregulate *cydA* ~2-fold (Sala *et al.*, 2009). These data demonstrated that *cydAB* is regulated aerobically, hypoxically and in response to drug treatment; however the mechanism/facilitators of the regulation were not yet identified.

In *M. smegmatis cydAB* expression was shown to be cyclic AMP receptor protein (CRP)-dependent during hypoxia (Aung *et al.*, 2014). A CRP binding site was identified ~65 bp upstream of the transcription start site which was required for the maximal expression of *cydA* during hypoxia, thus CRP is an activator under these conditions (Aung *et al.*, 2014). The authors further demonstrated that *cydAB* and *cydDC* form independent operons and that *cydDC* is not CRP-dependent, although a 10 bp inverted repeat was shown to be required for its expression (Aung *et al.*, 2014). In support of CRP-dependent *cydA* regulation in mycobacteria, it was demonstrated that Mtb *cydA* is upregulated ~ 2.5-fold under aerobic conditions in a mutant strain lacking CRP, suggesting that CRP negatively regulates *cydA* under aerobic conditions (Rickman *et al.*, 2005). Under normoxic conditions, in the absence of CRP, *cydA* expression was unaltered in *M. smegmatis*, pointing to a possible additional regulator of this operon under different conditions (Rickman *et al.*, 2005, Aung *et al.*, 2014). This is supported by the presence of a 10 bp inverted repeat 40 bp upstream of Mtb *cydA* that is a binding site for BlaI, which is specifically responsive to β-lactam exposure (Sala *et al.*, 2009). In addition, *cydB* was recently shown to be part of the two component SenX3-RegX3 regulatory network which is also made up of *rpfA* and *ald*, genes involved in cell wall synthesis and CCM respectively (Roberts *et al.*, 2011). These data suggest that the mycobacterial CbdO plays a role in multiple physiological processes including adaptation to reduced oxygen tensions, responding to metabolic inhibitors, changes in CCM and cell wall perturbations. A role for the CbdO in cell wall and redox biology was also recently presented by (Mishra *et al.*, 2017) who showed that *cydAB* was significantly upregulated in response to treatment with the cell wall-targeting combination augmentin.

The first data on CbdO functionality in mycobacteria was presented by Kana *et al.* (2001) who demonstrated that loss of a functional CbdO, by deletion of *cydA*, leads to a reduction in the ability of *M. smegmatis* to survive at low oxygen tensions (1% and 0.5% dissolved O_2). In contrast to the *E. coli* strain, no stationary phase exit defect was observed for the *M. smegmatis* mutant but it did display reduced growth in the presence of cyanide when co-cultured with the wild type strain, suggesting that the enzyme contributes to cyanide resistance in mycobacteria (Kana *et al.*, 2001). Transcriptomic analysis of respiratory genes during mouse infections revealed that *cydA* expression transiently increased during chronic infection and a strain disrupted in a putative CbdO assembly-encoding gene, *cydC*, displayed a reduced cell number in the lungs of mice during chronic infection (Shi *et al.*, 2005). These important findings highlight a role for the CbdO in the virulence of Mtb, particularly in acclimatising to the host adaptive immune response (Shi *et al.*, 2005). In contrast to Shi *et al.* (2005), Dhar and McKinney (2010) later showed that a strain disrupted in *cydC* was able to grow and survive just as well as wild type in untreated mice but were cleared from the lungs and spleens of infected mice more rapidly than wild type upon INH treatment (Dhar and McKinney, 2010). The discrepancy in survival of a *cydC* mutant between the two studies was attributed to the difference in parental strains in which the mutants were generated i.e. H37Rv in the Shi study and Erdman in the Dhar study (Shi *et al.*, 2005, Dhar and McKinney, 2010). However the different doses, method of infection and mouse ages could also account for the inconsistency i.e. in the Shi study a low dose (~ 2 x 10^2 CFU) aerosol infection of 8-10 week old mice was performed whereas in the Dhar study a higher dose (~1x 10^6 CFU) was administered intravenously into 5-6 week old mice. Regardless of the incongruent survival result, both studies point to an important role for the CbdO in Mtb virulence and pathogenesis, with Dhar and McKinney highlighting the increased susceptibility of a strain lacking a functional CbdO to the first-line drug INH. It is worth noting however that neither study provided evidence that only the CbdO is non-functional in the mutant strain used, therefore the phenotypes observed could be attributable to the loss of an independent, unidentified function of the *cydDC*– encoded transporter and not as a result of the specific loss of CbdO itself.

The evidence presented by (Kana *et al.*, 2001, Matsoso *et al.*, 2005, Shi *et al.*, 2005, Dhar and McKinney, 2010) formed part of the ground-breaking studies which sparked an interest in the

aerobic terminal oxidases of mycobacteria and presented them as possible vulnerable targets for novel drug development. Since then and during the compilation of this thesis, numerous studies have been presented on the mycobacterial aerobic terminal oxidases (Forte *et al.*, 2013, Lu *et al.*, 2015, Lamprecht *et al.*, 2016, Kalia *et al.*, 2017), many of which were in line with our initial hypotheses. Forte *et al.* (2013) proposed that the Mtb CbdO may be involved in resistance to H_2O_2 via a catalase activity- based on the identification of this activity in *E. coli* (Borisov *et al.*, 2013) and the observation that an Mtb strain in which cytochrome *c* maturation was disrupted displayed an increased resistance to H_2O_2 concomitant with an increased production of CbdO (Small *et al.*, 2013). The involvement of the mycobacterial CbdO in resistance to H_2O_2 stress was later confirmed by Lu *et al.* (2015), who showed that the *M. smegmatis* Δ*cydA* strain was more susceptible than wild type to H_2O_2, CFZ and BDQ. They further confirmed this by showing that the Δ*qcrCAB M. smegmatis* strain, which was previously shown to have increased *cydA* expression (Matsoso *et al.*, 2005), behaved the same as or was more resistant than wild type to the treatments (Lu *et al.*, 2015). The involvement of the Mtb enzyme in resistance to oxidative stress is yet to be presented. Recent investigations on the Mtb CbdO were in the context of drug discovery and validating the terminal aerobic oxidases as prominent targets for novel drug development. Lamprecht *et al.* (2016) showed that CbdO is able to maintain aerobic respiration when the main aerobic branch is inhibited by Q203. In addition, they showed that the strain referred to as *cydKO*, which is a *cydC* mutant, is unable to respire upon Q203 treatment (Lamprecht *et al.*, 2016). Furthermore the authors demonstrated synergistic killing of Mtb with different combinations of ETC inhibitors and propose that this combination therapy would be most successful in eradicating Mtb via two predominant mechanisms: (i) the reduction in energy production and (ii) the production of damaging agents during the response to energy depletion (Lamprecht *et al.*, 2016). However, the drug treatment experiments in the Lamprecht study used extremely high concentrations of compounds (between 30 and 300 x MIC), which would be physiologically questionable, furthermore no kill kinetic data for the *cydKO* strain was presented to support the oxygen consumption data for Q203 and BDQ treatment. Rather, based on the oxygen consumption of the mutant strain in the presence of BDQ, they suggest that the mutant is not hyper-susceptible to BDQ in contrast to previous observations in both *M. smegmatis* (Lu *et al.*, 2015) and Mtb (Berney *et al.*, 2014c). Nonetheless, the data presented by Lamprecht *et al.*

(2016) highlight the flexibility of the Mtb ETC which can be exploited for more efficient killing of the pathogen.

The hypothesis that simultaneous targeting of multiple respiratory complexes would result in complete sterilisation of Mtb was further supported by another recent study (Kalia *et al.*, 2017). Consistent with Lamprecht *et al.* (2016), Kalia and colleagues demonstrate that Q203 treatment results in complete inhibition of oxygen consumption in a Δ*cydA* mutant, while BDQ inhibited respiration equally in the wild type and mutant. In addition the authors demonstrated that Q203 treatment resulted in enhanced killing of Δ*cydA* under aerobic replicating conditions and further show that this killing is enhanced in nutrient starved, persistent cultures of the mutant (Kalia *et al.*, 2017). Further investigation of the Δ*cydA* mutant *in vivo* and *ex vivo* revealed no differences in growth and survival during THP-1 macrophage infections and during mouse infections compared to the wild type when no treatment was administered (Kalia *et al.*, 2017). This was in-line with the data for a *cydC* mutant presented by Dhar and McKinney (2010) but contradictory to that presented by Shi *et al*. (2005). However, increased clearance of the Δ*cydA* mutant was observed in mice and macrophages upon Q203 treatment (Kalia *et al.*, 2017). Interestingly, treatment with BDQ during macrophage infections did not result in increased killing of Δ*cydA* but increased killing was observed at the later time points during mouse infections- a result which was unexpected in light of the *in vitro* data presented (Kalia *et al.*, 2017). As a result of the enhanced killing of the Δ*cydA* mutant by both Q203 and BDQ, the authors thus proposed that all three of the respiratory complexes involved (CbdO, the Cytochrome *bcc-aa*$_3$ complex and ATP synthase) should be targeted to obtain complete sterilization in the clinical setting during MDR and XDR treatment, consistent with previous suggestions (Berney *et al.*, 2014c, Lamprecht *et al.*, 2016, Kalia *et al.*, 2017).

The literature evaluated thus far points to the highly adaptable nature of Mtb. This flexibility was observed in several different areas of physiology and metabolic processes, notably CCM and respiration. Our laboratory and others hypothesise that this flexibility is crucial to the success of Mtb as a pathogen and that an adaptable and responsive ETC is central to this flexibility. Furthermore, based on the long-standing literature suggesting that the CbdO plays a role in the

adaptation to various stress conditions, we further purport that the mycobacterial CbdO is involved in adaptations to the varying, oftentimes harsh environmental conditions experienced during the life cycle of Mtb and is thus important for the virulence and/or pathogenesis. We therefore set out to further characterise the mycobacterial CbdO.

2.11 Aims and objectives

The worked described in this chapter had the primary aim of determining how the CbdO contributes to the growth, survival and energy production in mycobacteria under different conditions.

The specific objectives include:

- To determine if the Δ*cydAB* mutant in Mtb displays different growth dynamics compared to the wild type, H37Rv, and if this is affected by the available carbon source
- To determine if Δ*cydAB* behaves differently to H37Rv in the presence of an alternate terminal electron acceptor
- To determine if the Δ*cydAB* mutant has perturbed ETC activity
- To evaluate how Δ*cydAB* survives under reduced oxygen tensions
- To investigate how Δ*cydAB* survives under physiologically relevant stressful conditions including oxidative, acid and nitrosative stress
- To evaluate the susceptibility of Δ*cydAB* to different antibiotics and
- To measure the intracellular survival of Δ*cydAB* in mouse macrophages

For clarity, the results of this chapter will be split into three sections.

- Section I will describe growth dynamics and energy production under standard laboratory conditions and in the presence of different carbon sources.
- Section II will address the effect of an anaerobic terminal acceptor on aerobic growth and energy production as well as in two alternate models of growth i.e. an anaerobic model and biofilm model.
- Section III will evaluate the effects of different stresses on growth dynamics.

2.12 Methods

2.12.1 Mtb Growth curves

A description of the media components and supplements used can be found in Appendix C. Growth curves to compare the growth dynamics of Δ*cydAB* to H37Rv were setup in 50 ml 7H9 liquid medium supplemented with OADC and tyloxapol for each strain. Cultures were incubated at 37 ˚C with 5 % CO_2 and no agitation. Optical density at 600 nm (OD_{600}) was recorded daily for seven days. Similarly, growth curves were carried out with strains grown in 7H9 supplemented with ADS and in addition to recording OD_{600} readings, samples were also collected for CFU determination at the different time points. In addition to the growth curves in 7H9 with two different supplementations, growth curves were also performed in MB media which contains nitrate as the sole nitrogen source to determine if the availability of an additional electron acceptor affected Mtb growth and/or energy production. For the growth curves described above, samples were collected at each time point to determine ATP content as outlined in section 2.11. The growth curves performed to evaluate the role of individual carbon sources were carried out as described above except the individual carbon sources acetate, glycerol, glucose, succinate or propionate were included in 7H9 at 0.2 % and only OD readings were recorded.

2.12.2 *M. smegmatis* growth curves

Growth curves were performed for the *M .smegmatis* strains in different media. The growth curves were setup in 384-well plates in 50 µl of media in quadruplicate as shown in Figure 2.10 below. A 10 ml pre-culture was grown to mid-log phase (OD 0.3-0.5) in 7H9 supplemented with ADS, glycerol and Tween80. The cells were collected by centrifugation at 1731 x *g* for 10 mins and re-suspended in 10 ml PBS. A second round of centrifugation was performed and pellets were re-suspended in 1 ml PBS. A final wash step was carried out and cells were re-suspended in 0.5- 1 ml PBS. The cells were then diluted to an OD of 0.01 in PBS plus the appropriate antibiotics. To setup the 384-well plate 100 µl of sdH_2O was added to the grey wells in Figure 2.10. Forty five microliters of each medium was added to the appropriate wells. This was followed by the addition of 5 µl of the diluted cells (OD 0.01) to each media-containing well.

The plate was then incubated at 37 ˚C in the SpectraMax plate reader (Molecular Devices) which was setup to record the optical density of each well every 2 hours for 80- 90 hours, with a single shaking step included before each recording.

2.12.3 Measuring oxygen consumption

Measuring the oxygen consumption of cells gives an indication of respiratory capacity and may reveal insight into observed growth and ATP content differences between wild type and the Δ*cydAB* mutant. The BACTEC MGIT system relies on the dye Tris 4, 7-diphenyl-1, 10-phenanthroline ruthenium chloride, which is quenched in the presence of oxygen and fluoresces when oxygen is being consumed thus indicating growth. This system is conventionally used in a diagnostic setting and provides a result as the time to positivity (TTP), which is the time at which a minimal fluorescent signal is detected indicating growth. In addition to TTP, the growth unit (GU) is another readout generated by the MGIT system and represents the last fluorescence

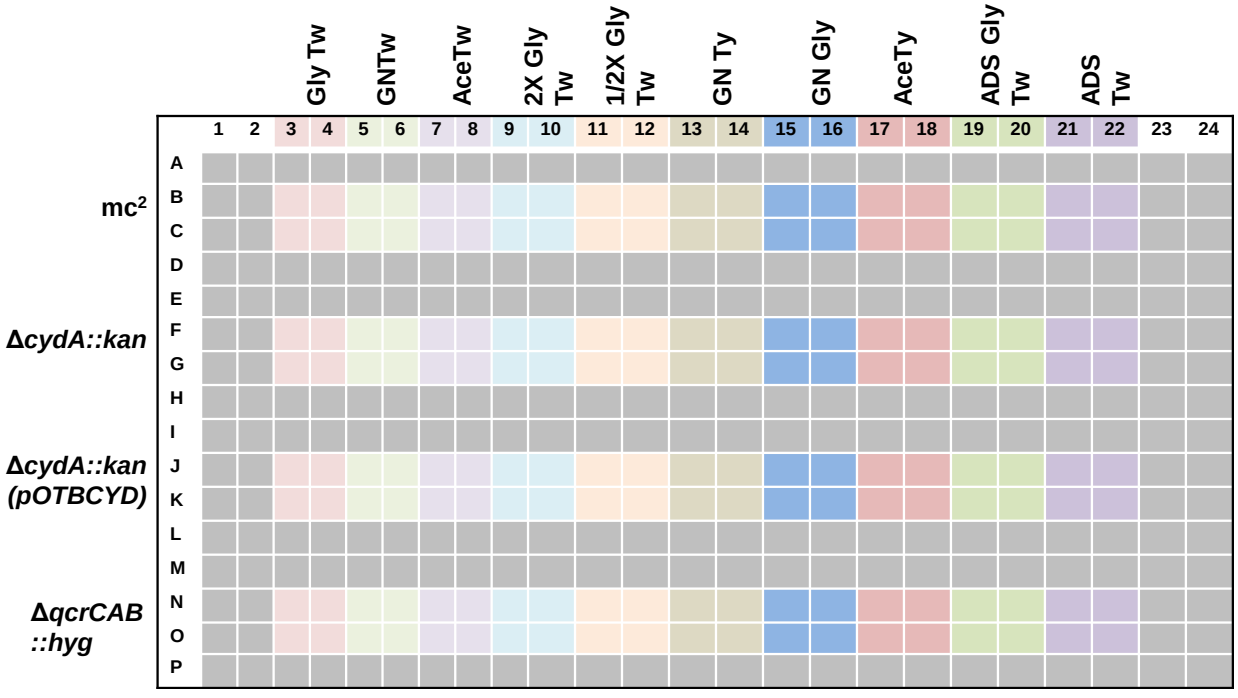


Figure 2.10: An example of the 384-well plate setup used for *M. smegmatis* growth curves performed in a plate reader. The grey wells contained water while the different colours represent the different media used. The basal medium in each case was 7H9 which was then supplemented with different carbon sources and/or detergents. Gly: glycerol, Tw: Tween80, GN: glucose, Ace: acetate, Ty: tyloxapol, ADS: albumin dextrose salt.

signal recorded before removal of the MGIT tube. Because this system relies on an O_2 responsive dye and allows for the simultaneous testing of multiple strains at once, we decided to utilise it to compare oxygen consumption between different Mtb strains. Commercially available MGIT tubes contain 7 ml 7H9 and were supplemented with 800 µl of an OADC/PANTA mixture prior to being inoculated. Cultures were grown in 7H9 OADC to an OD ~1.5, diluted to 0.05 and 10-fold serial dilutions were prepared. Two hundred microliters of the 10^{-2}-10^{-5} dilutions were used to inoculate the MGIT tubes yielding a further 40x dilution of each starting inoculum. The tubes were then placed into the BACTEC MGIT 960, incubated at 37 ˚C and were removed when flagged positive. Negative control tubes, which were inoculated with 200 µl fresh 7H9 were also incubated to rule out contaminations and were removed after 42 days.

2.12.4 ATP quantification

The intracellular ATP levels of different strains were assessed with the BacTitre Glo Microbial Cell Viability Assay Kit (Promega). Two different protocols were used for cells from liquid and solid media. Tominimize the effect of different growth rates in liquid medium on ATP production, one protocol used *M. smegmatis* cells collected from agar plates in the assay. Briefly, cells were spread on solid media and incubated at 37 ºC. After 7 days 100 mg of cells were scraped of each plate and re-suspended in 1 ml fresh liquid media. Each suspension was frozen for 30 min at - 80º C, followed by boiling at 95º C for 5 min. For each sample, 100 µl was added in triplicate to a 96-well opaque white plate. An equal volume of the BacTitre Glo reagent was then added to two of the three wells for each sample and incubated in the dark at 37 ºC for 10 min. Luminescence was recorded on the SpectraMax plate reader and presented as relative luminescence units (RLUs). For liquid samples, the protocol described by (Rao *et al.*, 2008) was followed with the modification where samples were frozen at -80 ˚C until all samples were collected for processing.

2.12.5 Biofilm assays

Biofilms in this study were defined as the distinctive ruffled structure formed at the liquid-air interface of stationary cultures. To generate biofilms, the cultures were grown to stationary phase

in 7H9 medium. An aliquot of the culture was washed twice with modified Sautons minimal medium (SM) (without Tween80) by centrifugation at 2360 ×*g*. The cell suspension was adjusted to an OD_{600} of 2 and ten- fold serial dilutions were prepared (10^{-1}- 10^{-8}) in SM. Biofilms were grown in 6-well tissue culture plates with 10 ml SM in each well. One hundred microliters of cell suspensions 10^{0}-10^{-5} were added to individual wells. The 6-well plates were sealed with labelling tape (Sigma) and incubated at 37 ºC for Mtb and 30 ˚C for *M. smegmatis,* with no shaking for 5-7 weeks or 3-7 days respectively. The 10^{-5}-10^{-8} dilutions were used to determine CFU counts. The biomass of biofilms was quantified using crystal violet staining as previously described (Recht and Kolter, 2001). Briefly, biofilms were grown to maturation in 24-well tissue culture plates. Thereafter, 1 ml of a 0.1% solution of crystal violet was added to each biofilm to be quantified and incubated at room temperature for 10 mins to allow for staining. This was followed by the removal of the planktonic cells and liquid below the biofilm, which was then allowed to dry for 15 mins at room temperature. A 99 % solution of ethanol was then added to each sample in 1 ml aliquots and mixed by pipetting. This was followed by a 100x dilution of the sample, a brief centrifugation to pellet cell debris and then addition of 100 µl aliquots to a 96-well microtitre plate. The absorbance of each sample was then recorded on the BioTek ELx800 plate reader at 570 nm using the Gen5 software.

2.12.6 Hydrogen peroxide assay

The CbdO has been implicated in resistance to oxidative stress in several other organisms (Edwards *et al.*, 2000, Leclerc *et al.*, 2015) and it has been hypothesised that the same could be true in Mtb (Forte *et al.*, 2013). Totest this, different Mtb strains were exposed to oxidative stress in the form of hydrogen peroxide (H_2O_2) and assessed for survival. Cultures were grown to exponential phase in 7H9 ADS and then sub-cultured into fresh 7H9 ADS medium to an OD= 0.01. An aliquot was taken for each strain, serially diluted and dilutions inoculated onto 7H11 solid media for CFU determination. H_2O_2 was then added to each culture at a final concentration of 5 mM and incubated at 37 ˚C with samples taken for CFU determination after 2, 4 and 24 hrs.

2.12.7 Hydroxyl radical detection

The *E. coli* CbdO has been shown to possess both catalase and low peroxidase activity, which could contribute to detoxification of hydrogen peroxide. If this catalase/peroxidase activity is one of the functions of the CbdO, its absence could lead to decreased H_2O_2 detoxification and thus increased accumulation of hydroxyl radicals ($OH^{\cdot}$). The dye, hydroxyphenyl fluorescein (HPF) reacts with hydroxyl radicals and was used to measure $OH^{\cdot}$ in Mtb. We hypothesized that there would be an accumulation of $OH^{\cdot}$ in the Mtb Δ*cydAB* mutant as a result of endogenous production, which would be exacerbated upon exposure to oxidative stress. Multiple aliquots of exponential phase cultures were therefore setup and treated with HPF alone or with HPF and H_2O_2. The experiment was setup in a 96-well black, clear bottom plate and incubated at 37 ˚C in the SpectraMax fluorescent plate reader for 24 hrs, with fluorescence readings recorded every hour. A set of the treated samples was also incubated in Eppendorf tubes at 37 ˚C for 4 hrs, followed by two washes in PBS. The cell pellets were re-suspended in 250 µl PBS and run on the Cytoflex flow cytometer. The following settings were used on the Cytoflex: slow flow rate (10 µl/min), E00 (FSC), 360 (SSC) and 825 (FL1).

2.12.8 Acid stress

In *E. coli* the CbdO has been implicated in resistance to various stress conditions, including acid stress. Toassess if the CbdO may play a similar role in Mtb, an acid stress assay was performed as previously described (Vandal *et al.*, 2008). Briefly, exponential phase cultures of Mtb grown in 7H9 were pelleted by centrifugation at 2360 x *g* and washed twice in phosphate citrate buffer (PCB) containing tyloxapol. The washed cells were then used to inoculate 8 ml fresh PCB at an OD_{600} = 0.05. An aliquot from each culture was taken for CFU determination as T_0 at this time point. The cultures were then incubated at 37 ˚C and 5 % CO_2 with no agitation for six days. Samples were taken on day three and day six for CFU determination to compare the survival of the different Mtb strains under acidic conditions.

2.12.9 Macrophage culturing

J774 mouse macrophages were used to perform infections with Mtb cells. An aliquot of the macrophage cell line was generously provided by the Stellenbosch node of the CBTBR. Macrophage cells were grown in Dulbecco's Modified Eagles Medium (DMEM) with high glucose and $_{L}$-glutamine and without pyruvate. DMEM was supplemented with fetal bovine serum (FBS) at a final concentration of 1 % and the DMEM+FBS mixture was made up fresh and warmed at 37 ˚C prior to use. To start a culture, a frozen aliquot of cells was thawed by sequentially adding 500 µl warm medium to the frozen cells and dispensing into a sterile 50 ml falcon tube until all the contents of the cryo-tube was thawed. The macrophage cells were then pelleted by centrifugation at 1000 rpm for 10 mins. This was followed by discarding the supernatant and re-suspending the cells in ~ 500 µl fresh medium by flicking of the tube. The cell suspension was then used to inoculate 10 ml of fresh medium in a 50 ml tissue culture flask which was then incubated at 37 ˚C and 5 % CO_2 for 4 hrs to allow for cells to adhere to the surface of the flask. Thereafter, the supernatant in the flask was discarded, 10 ml of fresh medium was added and the culture was returned to the incubator. The medium in the culture was changed daily and the culture was evaluated for growth by viewing the cells under an inverted microscope. Once the culture had expanded sufficiently to adhere to the entire bottom surface of the flask, the cells were dislodged and used to seed larger cultures. To do this, the culture was washed twice with cold PBS with gentle swirling. This was followed by the addition of ~ 4 ml Accutase, gentle swirling and incubation at 37 ˚C for 5 mins. Following the incubation and brief swirling, the cells were mechanically dislodged by striking the flask against the palm of the hand, while in a horizontal position. Cells were washed once by centrifugation with fresh DMEM to remove the Accutase and the cell pellet was re-suspended and used to inoculate 2-4 flasks containing 50 ml fresh DMEM, which were then incubated as before, with the medium being replaced daily. Once these cultures had grown sufficiently (~3-4 days), the cells were dislodged as described above, pooled together, washed and used to prepare plates for infections with Mtb. Following the wash step with fresh media, the cells were re-suspended in 1 ml DMEM. Two 5 µl aliquots were taken from the cell suspension to count and assess for viability. One of the aliquots was added to 95 µl Türk and the other to 95 µl Trypan blue (0.4 %), for a 50 x dilution factor. The cells were then counted by adding 10 µl of each mixture to a

haemocytometer, and viewing under an inverted microscope. Türk solution stains the nuclei of cells and allows for a total cell count to be determined. Trypan blue is only permeable through damaged membranes and stains dead or dying cells; therefore unstained Trypan blue-treated cells were counted as viable cells. The number of viable cells in the suspension was determined using the following equation:

$$Total\ \#\ viable\ cells = Avg\ of\ viable\ cell\ counts\ \times Dilution\ factor\ \times 10^4$$

Depending on the multiplicity of infection (MOI) used and the number of Mtb strains being used for infections, an appropriate dilution of the macrophage cell suspension was prepared accordingly. Twenty-four well tissue culture plates were then prepared with 1 ml of the macrophage suspension aliquoted into each well. These plates were then incubated overnight at 37 ˚C and 5 % CO_2 to allow for the macrophage cells to adhere to the plate surface.

2.12.10 Macrophage infections

The Mtb strains used for macrophage infections were grown in 7H9 to an OD ~ 0.5 and diluted appropriately in fresh DMEM, depending on the chosen MOI. The macrophage-seeded plates that were incubated overnight were used for infections by replacing the media with 1 ml of the prepared bacterial suspension in DMEM. Duplicate wells were setup for each strain tested and the infection plates were incubated for ~ 4 hrs to allow for the bacterial cells to be phagocytosed by the macrophages. Thereafter, the supernatant was replaced with 1 ml fresh DMEM to remove extracellular bacterial cells. At this time point (T_0), a set of infections was sacrificed to determine the intracellular CFU count. Macrophages were lysed with 0.1 % SDS, ten-fold serial dilutions of the suspension were prepared in PBS and spread onto 7H11 solid media. Activated macrophage infections were performed as described above, with the exception that 1 U IFN γ and 1 µg/ml LPS were added to the bacterial cell suspension immediately before being added to the plates containing macrophage cells. Infections were carried out for three days, with CFU counts being performed each day.

2.12.11 Anaerobic assay

Mtb cultures between 0.3 and 0.4 were diluted to 0.1 and aliquoted into 24-well plates. Methylene blue was added at a final concentration of 1.5 µg/ml. A single plate was setup for each time point at which CFU's would be determined. Each plate was incubated individually in a sealed container that had an Anaerogen pouch (Oxoid) and a pink indicator strip. The indicator strip decolourises as oxygen is depleted and therefore reports on the oxygen status of the environment. Samples from each culture were plated on Day 0, Day 7, Day 14 and Day 21 to monitor CFU's over time under anaerobic conditions.

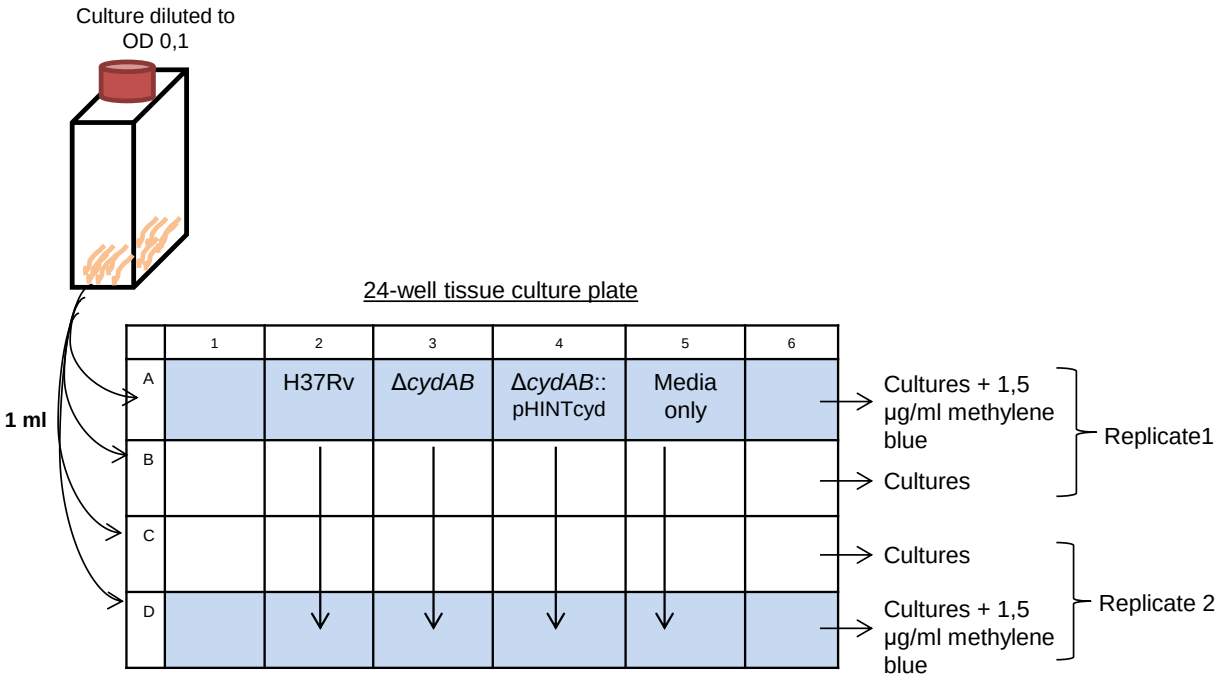


Figure 2.11: An example of the plate setup for the anaerobic growth assay. 24-well tissue culture plates were used. Rows A1-D1 and A1-D6 were empty. A single plate was used to perform two replicates and 1 ml of culture at OD 0.1 was used for each strain. Methylene blue was added to a set of wells for each strain to indicate oxygen depletion.

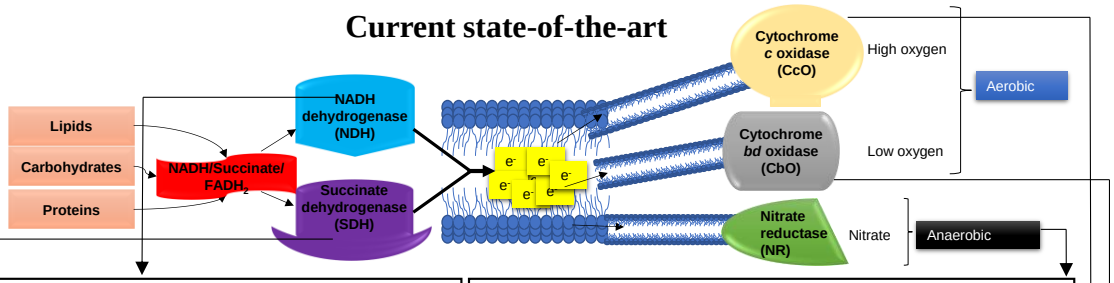
2.12.12 Lipid extractions from *M. smegmatis* biofilms.

Biofilms formed on 10 ml of medium in 6-well tissue culture plates were harvested from two replicate wells and pooled by centrifugation at 3900 x g for 30 mins. Cell pellets were washed with 10 ml PBS three times. This was followed by re-suspension of cells in 2:1 Chloroform:Methanol solution at 20 µl/mg of cells. Cell suspensions were then incubated overnight with constant agitation. Following the overnight incubation, cell debris was collected by centrifugation at 3900 x g for 30 mins and the supernatant was transferred to a fresh tube and another round of centrifugation was performed. The supernatant was collected and 0.2 volumes of 0.9% NaCl was added and the solution mixed. The organic layer was separated by centrifugation at 1150 x g for 10 mins and split into multiple 2 ml Eppendorf tubes to be desiccated in the SpeedVac (Eppendorf) at 65 °C. Pellets were re-suspended in ~ 100 µl 2:1 Chloroform:Methanol. For each sample, ~ 10 µl was spotted onto Silica Gel 60 F_{254} plates (Merck). TLC plates were run in chloroform:methanol solution (100:7) until the solvent from was ~ 2 cm from the end of the plate. Lipids were viewed by spraying plates with a 40 % sulphuric acid solution containing 0.1 % Orcinol and charred at 140 °C for 2 to 3 minutes.

2.12.13 Minimum inhibitory concentration (MIC) determination

The susceptibility of Mtb and *M. smegmatis* to various drugs was determined using the broth microdilution assay (Collins and Franzblau, 1997). Ninety six-well microtitre plates were prepared with two-fold serial dilutions of the different drugs in a volume of 50 µl. Cultures were grown to an OD_{600} = 0.3, diluted 500 fold and 50 µl of the diluted cells were dispensed into each well of the plate. MIC plates setup with Mtb were incubated at 37 ˚C and 5 % CO_2 for 7-14 days, after which they were scored for visible growth. *M. smegmatis* plates were incubated at 37 ˚C in sealed containers with wet paper to prevent evaporation for 3-5 days, after which they were scored by measuring the OD_{600} of each well in a Biotek plate reader.

Current state-of-the-art



- NDH-I contributes to apoptosis in the host- Miller *et al.* (2010)
- Both Type II NDH enzymes contribute to ETC activity under different conditions and during infection, with Ndh being essential- Shi *et al.* (2005), Yano *et al*., (2006), Awasthy *et al* .(2014)
- NDH-II is involved in activity of CFZ- Weinstein *et al*. (2005), Yano *et al.* (2011)

- Contributes to anaerobic survival of Mtb- Sohaskey (2008)
- Protects against RNI and acid stress under hypoxic coniditions- Tan *et al*. (201)

- Essential for aerobic growth- Matsoso *et al*. (2005
- Inhibited by Q203- Pethe *et al*. (2013)
- Mutants disrupted in CcO maturation are attenuated in mice

- Serves as a terminal oxidase that maintains the PMF under hypoxic condtitions- Eoh and Rhee (2013), Hartman *et al*. (2014), Pecsi *et al*. (2014)

- Important for hypoxic growth – Kana *et al*. (2001)
- Compensates for loss of CcO – Matsoso *et al*. (2005), Small *et al*. (2013), Lamprecht *et al*. (2016), Kalia *at al*. (2017)
- CbdO is induced in response to oxidative stress- Boot *et al*. (2017)
- Loss of CbdO potentiates the activity of BDQ, Q203 and CFZ- Lamprecht *et al*. (2016), Kalia *at al*. (2017), Lu *et al*. (2015), Berney *et al*. (2014)
- Mutants unable to assemble CbdO are attenuated and unable to persist following INH treatment- Dhar and McKinney (2010), Shi *et al* (2005)

Key Knowledge Gaps

Does CbdO play a role in ATP generation?

What is the role of CbdO in growth on different carbon sources?

Is there a role for alternate electron acceptors under aerobic conditions?

What is the role of CbdO in response to stress?

Are there other previously undescribed roles for CbdO?

What role does CbdO play in drug tolerance?

Chapter 2- Section I

Chapter 2- Section II

Chapter 2- Section III

What is the role of respiratory and assimilatory NRs in Msm?

Chapter 3

Key Findings

- Yes for both Msm and Mtb
- Associated with reduced oxygen consumption

- Yes, nitrate rescues CcO defect in Msm
- Nitrate reduced growth of CbdO mutant

- Yes, CbdO is involved in biofilm maturation in Msm and Mtb
- Biofilm defects can be rescued by addition of nitrate
- Deletion of CbdO results in an altered lipid profile

- Loss of CbdO gives rise to increased susceptibility to ETC inhibitors and cell wall targeting antibiotics

- CbdO is important for growth on proprionate in Mtb
- CbdO mutant has increased optical density in oleic acid
- Msm CbdO mutant seems sensitive to glycerol

Deletion of both narGHI and narB-encoded NRs did not affect respiratory NR activity

- CbdO seems to be important for survival under oxidative stress
- Mutant experienced increased hydroxyl radicles
- CbdO important for mac survival.

2.13 Results- Section I

2.13.1 Genotypic confirmation of mutant strains

The Mtb mutant strains used in this study were previously generated at the CBTBR and are listed in Table A2. A description on how they were constructed can be found in Appendix D1. Toensure that the correct strains were being used during experiments, a PCR screen was performed to confirm the genotype of each strain. The primers used for the genotypic confirmation of Mtb Δ*cydAB* are listed in Table A3 and a schematic representation of the PCR strategy is shown in Figure 2.12A. The 805 bp band would be amplified in the wild type strain, while the 468 bp band would be generated in the mutant strain. A 2586 bp band could be generated in the wild type strain; however the PCR parameters used do not favour the amplification of products larger than 1 kb. The appropriate bands were detected in the wild type and mutant strains, as shown in Figure 2.12B. In addition, both the wild type 805 bp band and mutant 468 bp band were detected in the complemented strains as expected.

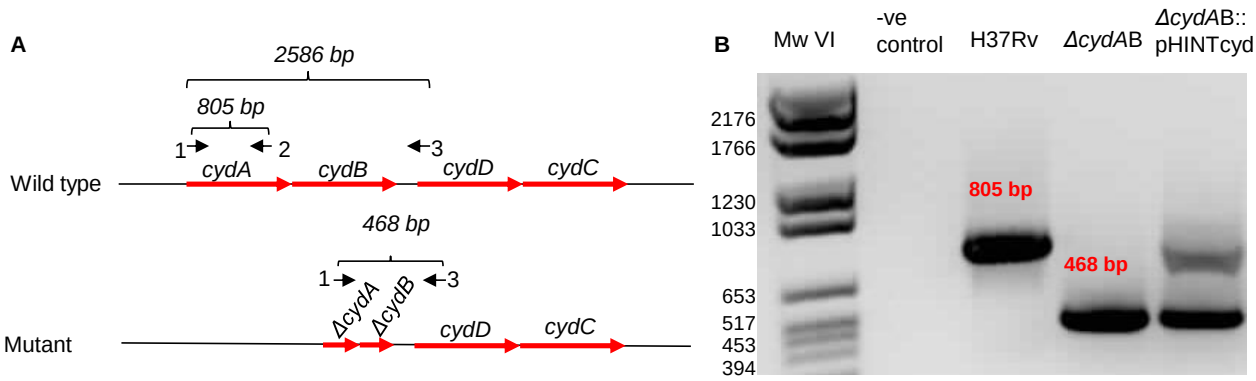


Figure 2.12: Genotypic confirmation of Mtb Δ*cydAB* mutant by PCR. (A) Schematic representation of the genomic region of the wild type Mtb strain (H37Rv) and the Δ*cydAB* mutant showing the primer positions and expected amplicons. Primers are represented as black arrows and numbered 1, 2 and 3 corresponding to the primers cydR, cydI and cydF respectively. **(B)** Gel image of amplicons generated during the PCR reactions, confirming the genotype of each strain.

The PCR strategy used for the confirmation of the *M. smegmatis* Δ*cydA::kan* strain, along with the expected amplicon sizes are shown in Figure 2.13A. Two sets of primers were used i.e. one set (1 and 2 in Figure 2.13A) that binds in *cydA* and a second set (3 and 4 in Figure 2.13A) which

binds to and amplifies the kanamycin resistance gene, *aph*. The amplicons obtained for all strains assessed with primers 1 and 2 are shown in Figure 2.13B and were as expected. The lack of the 157 bp wild type band in the complemented strain, Δ*cydA::kan* (pOTBCYD) was attributed to the complementation vector which carries the Mtb *cydAB* homologues, to which the *M. smegmatis* primers do not bind. Primers 3 and 4 would not anneal in the wild type and thus no amplicon was expected for that reaction, as seen in Figure 2.13C. The correct band, corresponding to the *aph* gene was observed in both the mutant and complemented strains, Figure 2.13C.

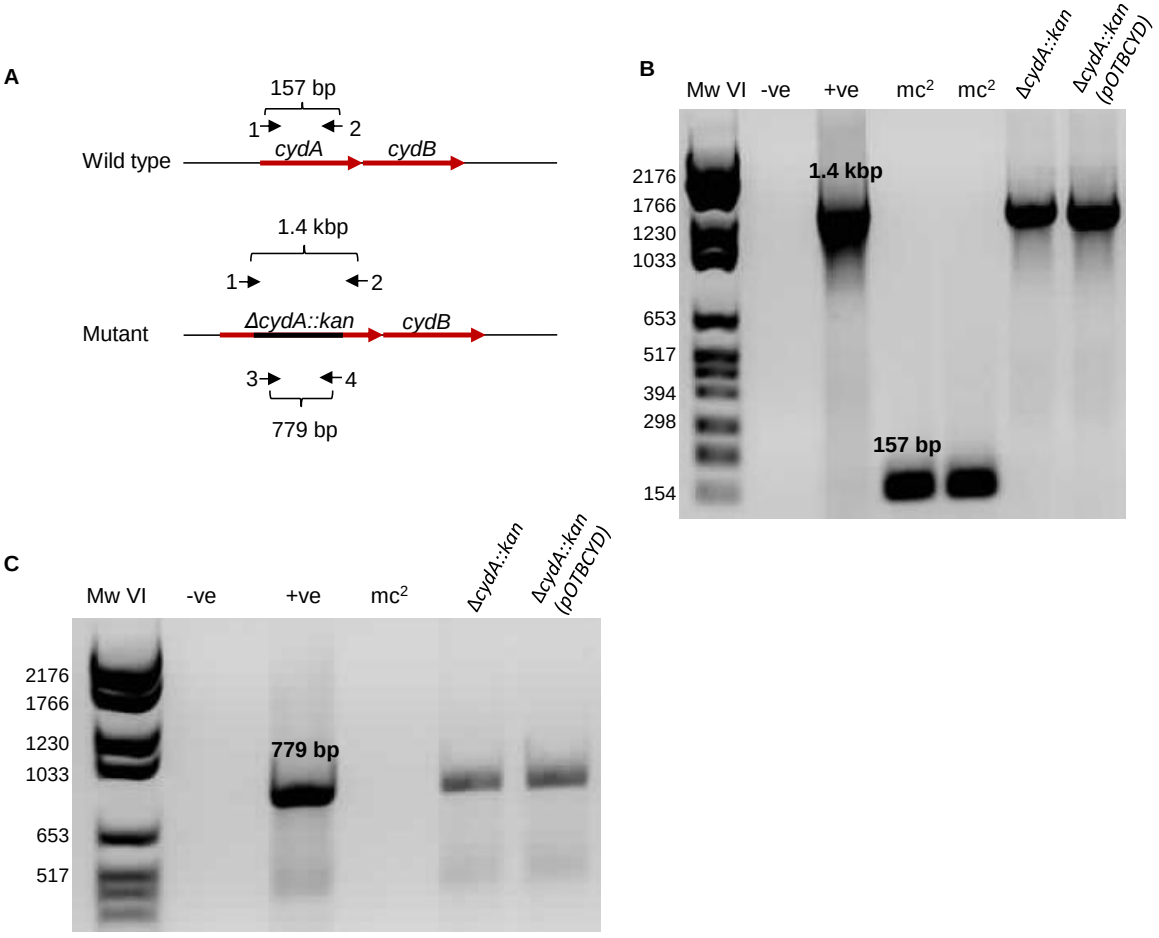


Figure 2.13: Genotypic confirmation of *M. smegmatis* Δ*cydA::kan* mutant by PCR. (A) Schematic representation of the genomic region of the wild type (mc^2) and mutant (Δ*cydA::kan*) strains showing the primer positions and expected amplicons. Primers are numbered and represented as black arrows. **(B)** Gel image of the amplicons obtained for PCR reactions with primers 1 and 2. **(C)** Gel image of PCR products obtained for the reactions with primers 3 and 4. The primer sequences and annealing temperatures are shown in Table S2 with the numbers in (A) corresponding to: 1- cydUSF, 2- cydDSR, 3- KanF and 4:- KanR.

2.13.2 Mycobacterial growth dynamics in the absence of the cytochrome *bd* oxidase

Mycobacteria possess two cytochrome oxidase enzymes which have been studied in *M. smegmatis* i.e. CcO which forms part of the *bcc-aa*$_3$ super complex and the CbdO. The *bcc-aa*$_3$ super complex is catalytically more efficient and predominantly active under normoxic conditions (Matsoso *et al.*, 2005). The CbdO has a higher affinity for oxygen and is required for growth under microaerobic conditions (Kana *et al.*, 2001). In addition, the CbdO is able to compensate for the loss of the CcO (Matsoso *et al.*, 2005) demonstrating the capacity of the CbdO to also function under normoxic conditions. The *M. smegmatis* CbdO was previously shown to be dispensable for growth (Kana *et al.*, 2001). Herein we confirm that as observed in *M. smegmatis*, the Mtb CbdO is also dispensable for growth under standard laboratory conditions (Figure 2.14). However, based on optical density, the Δ*cydAB* mutant appears to have a growth advantage at later time points.

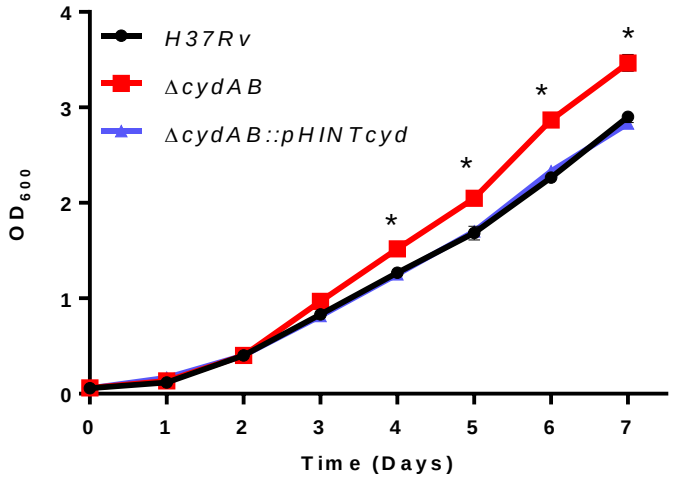


Figure 2.14: Growth kinetic analysis of Mtb strains grown under standard laboratory conditions. Strains were grown in complete 7H9 medium supplemented with OADC, glycerol and tyloxapol. Cultures were incubated at 37 ˚C with optical density readings recorded daily. The averages of at least three independent experiments are plotted and standard errors for each time point are included. Statistical significance was determined using the Students t-test. *P< 0.0001.

To investigate this further additional growth curves were setup and aliquots were plated onto solid media to quantify the colony forming units (CFU's) for each strain. No differences were observed by CFU assessment (Figure 2.15). Alternatively, the increased OD_{600} observed for Δ*cydAB* could be because of an increased cell size and to investigate this cell sizes of the wild type and mutant strains were compared using flow cytometry. Flow cytometry is a laser-based technology that relies on light scatter and can be used for cell size determination. The forward scatter (FSC) of light is generally indicative of cell size while the side light scatter (SSC) represents the granularity or complexity of the cell. One of the advantages of flow cytometry is the sensitivity, thus small changes in size can be detected and quantified. We hypothesised that a shift in either the FSC or SSC would be observed in cells of different sizes. As shown in Figure 2.16, no difference in FSC or SSC was observed between the wild type and mutant strains suggesting that they were approximately the same size. However, this would need to be confirmed by scanning electron microscopy (SEM). As such, the reason for an increased optical density of a Δ*cydAB* liquid culture is yet to be determined.

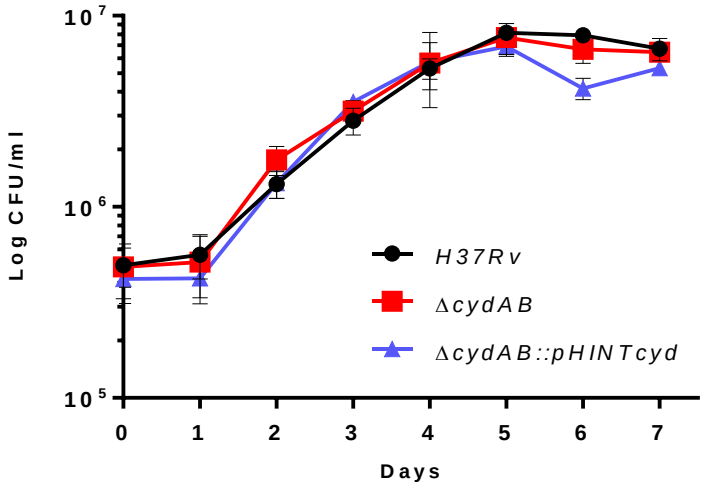


Figure 2.15: An assessment of the viability of Mtb strains grown in 7H9 supplemented with OADC, glycerol and tyloxapol. Cultures were incubated at 37 ˚C with aliquots collected at the time points plotted for CFU determination. The average of three independent experiments is plotted for each time point and standard error bars are included.

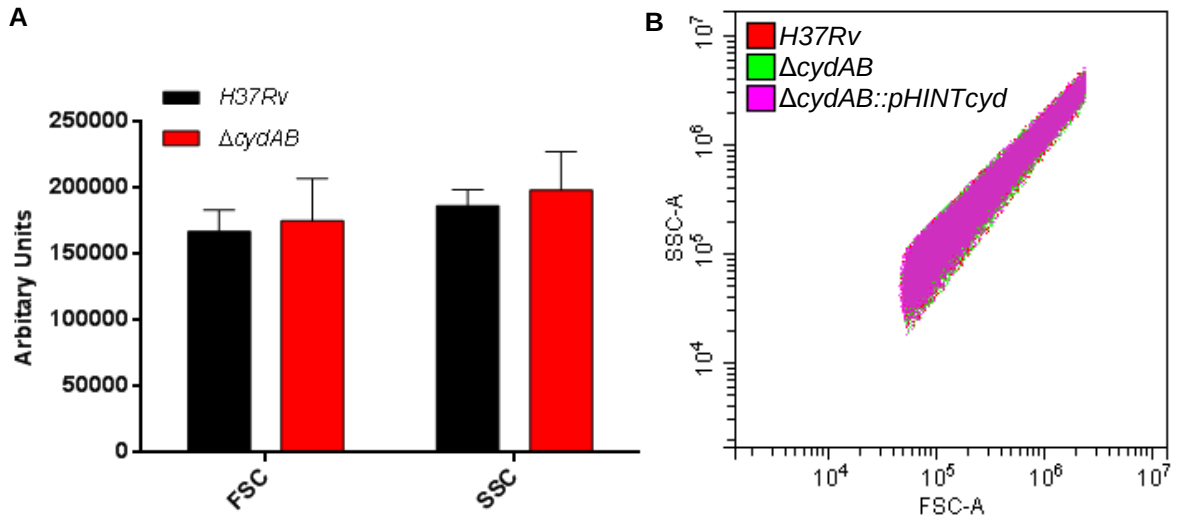


Figure 2.16: Cell size comparison of Mtb strains using flow cytometry. (A) A comparison of the FSC and SSC of wild type Mtb and the Δ*cydAB* mutant grown in 7H9 OADC. **(B)** An example of a dot plot overlay for FSC vs SSC obtained on the Cytoflex flow cytometer and analysed using the CytExpert software.

2.13.3 The Mtb cytochrome *bd* oxidase contributes to aerobic ATP content

As discussed above, Δ*cydAB* did not display any growth defects under normoxic conditions, however this does not rule out the possibility that loss of the CbdO could disrupt ETC activity. The main objective of the ETC is to produce energy in the form of ATP. Measuring the ATP content of the cell provides a readout of ETC activity, thus allowing for the assessment of ETC perturbations, such as the inhibition or removal of proteins/protein complexes. When assessed for ATP content, the Mtb CbdO-deficient strain had significantly less ATP than the wild type strain (Figure 2.17). This provides evidence that the mycobacterial CbdO contributes to ETC activity under normoxic conditions. Interestingly, the time points at which the most significant differences were observed are the time points at which differences in OD_{600} were observed between the wild type and mutant strain (Figure 2.14). However, the two results appear to contradict each other. On Days 5, 6 and 7 the OD of Δ*cydAB* is higher than the wild type strain, shown in Figure 2.14, whereas at these same time points the ATP content of the mutant is ~2 fold lower than the wild type (Figure 2.14). The reduced ATP content was further investigated.

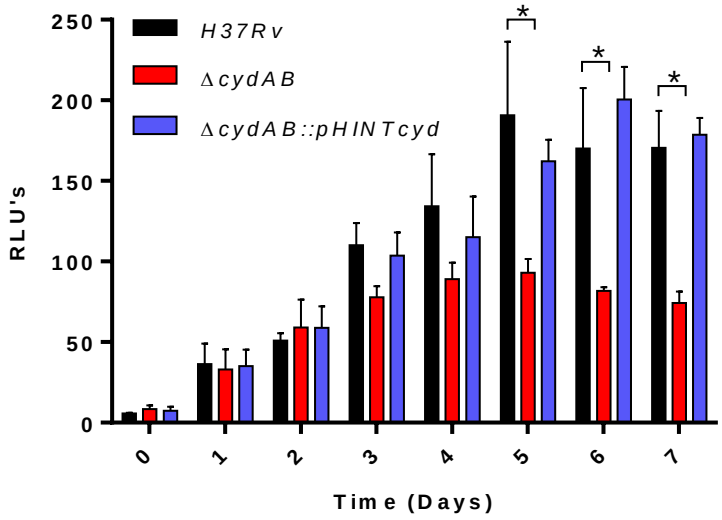


Figure 2.17: ATP production of Mtb Δ*cydAB* under standard laboratory conditions. Cultures were grown in 7H9 supplemented with OADC, glycerol and tyloxapol. Mean values and standard errors of at least three independent experiments are plotted. The Students t-test was used for statistical analysis. *P < 0.006

2.13.4 The reduced ATP content of Δ*cydAB* is attributable to decreased ATP production

A reduced ATP content could either be attributed to a reduction in ATP production or an increase in ATP consumption. An increase in ATP utilisation would lead to an increase in oxygen consumption in order to meet the escalating energy requirements of the cell to achieve the high levels of growth observed. Therefore, measuring oxygen consumption could provide insight into the reduced ATP content of cells lacking a functional CbdO. Oxygen consumption was measured using the Bactec MGIT system which contains a dye that is quenched in the presence of oxygen but fluoresces once oxygen levels decrease. The standard readout of this system in a diagnostic setting is TTP, which is the time at which a minimal fluorescent signal is detected. We hypothesized that a strain with increased oxygen consumption would have a faster TTP. An increase in ATP consumption in Δ*cydAB* would support the result of a slightly faster growth rate which could require more ATP. Alternatively, the reduced amount of ATP in the mutant cells could have been due to a decreased level of ATP production. No differences in TTP were observed between H37Rv and Δ*cydAB* (Figure 2.18A), suggesting no differences in early growth rate between the two strains, which was consistent with the growth curve results observed in Figure 2.14 where a similar growth pattern was observed over the first three days.

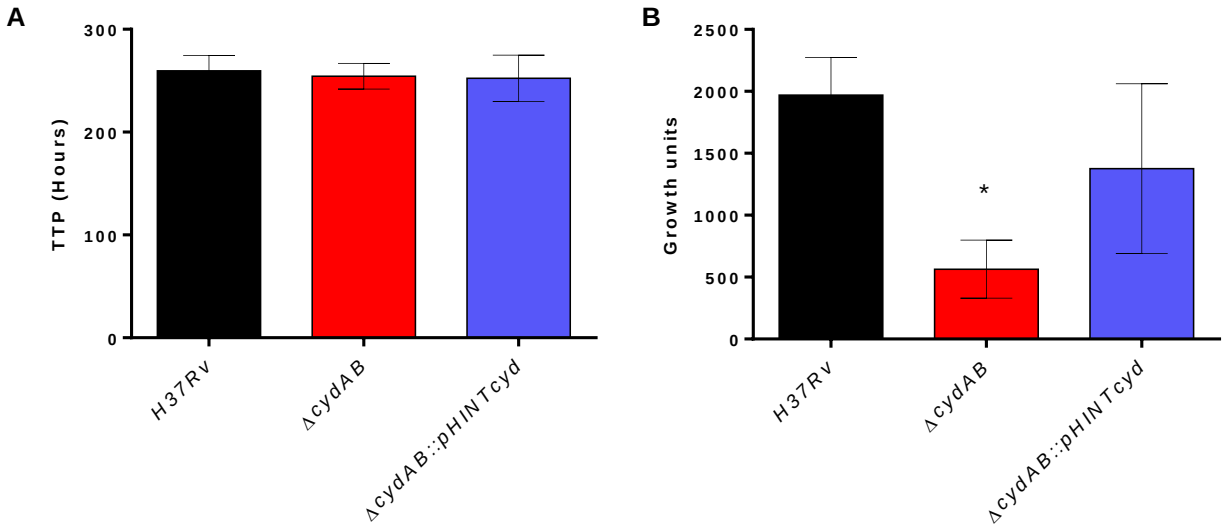


Figure 2.18: Oxygen consumption of Mtb strains grown in the BACTEC MGIT system. (A) The time to positivity of Mtb strains grown in MGIT tubes. **(B)** A comparison of the growth units, indicative of oxygen consumption of wild type and mutant Mtb at the time of removal from the BACTEC MGIT system. The Students t-test was used for statistical analysis. *P<0.002

The growth unit (GU) is another reading provided by the MGIT system and represents the fluorescence reading at the time of tube removal. This would be a more accurate measurement of oxygen consumption as it represents the most current fluorescence reading in the tube, which correlates with the amount of oxygen present. Analysis of this result shows that the Δ*cydAB* mutant has a significantly lower GU than the wild type (Figure 2.18B). A lower GU suggests a higher level of oxygen present in the tube and thus a lower oxygen consumption rate. Taking this result together with the reduced ATP content of the Δ*cydAB* mutant provides evidence in support of the hypothesis that this strain produces less ATP than the wild type. The data obtained for oxygen consumption and ATP content suggests that the Mtb CbdO is required for optimal respiration and inhibition of this enzyme leads to reduced activity of the ETC under normoxic conditions.

2.13.5 ATP production in *M. smegmatis* strains

The finding that the Mtb Δ*cydAB* produced lower levels of ATP when compared to the wild type under normoxic conditions, prompted us to assess whether a similar situation prevailed in the corresponding *M. smegmatis* mutant, which displayed growth defects under hypoxic conditions (Kana *et al.*, 2001). The *M. smegmatis* respiratory mutant strains, Δ*cydA::kan* and Δ*qcrCAB::hyg* used during this study were previously assessed for growth under standard

conditions but not for energy production (Kana *et al.*, 2001, Matsoso *et al.*, 2005). We therefore compared the ATP production in these strains with that of the wild type strain. As a control for reduced ATP production, we used a previously reported Δ*qcrCAB::hyg* mutant, defective for CcO. Matsoso *et al.* (2005) demonstrated that the Δ*qcrCAB::hyg* had a growth defect in 7H9 liquid medium which could interfere with ATP measurements. Tocircumvent this, the samples used to measure ATP were obtained by scraping 1 mg of cells from 7 day old 7H10 plates supplemented with glucose and glycerol. This allowed for the measurement of ATP from a consistent wet weight of cells for all the strains, thereby reducing inconsistencies as a result of differing growth rates. The data shown in Figure 2.19 confirm that the mycobacterial CbdO contributes to ATP production under aerobic conditions. As expected, Δ*qcrCAB::hyg* displayed

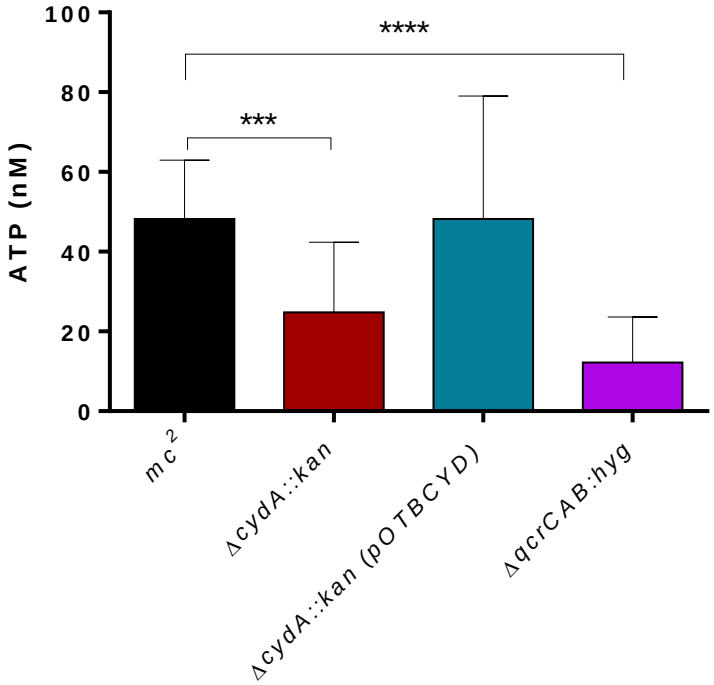


Figure 2.19: ATP production of *M. smegmatis* strains grown on 7H10 plates for 7 days. ATP assays were performed for cultures grown on 7H10 supplemented with glucose and glycerol for 7 days. The averages of at least three replicates, each performed with technical duplicates is plotted with standard errors. Statistical analysis was performed using the Students t-test. ***P=0.0001, ****P<0.0001

significantly reduced ATP levels, as a result of the loss of the main aerobic respiratory branch.

2.13.6 Oleic acid affects optical density and ATP production in Mtb

Considering that Kana *et al*. (2001) demonstrated that *M. smegmatis* displayed no growth phenotype in 7H9 supplemented with GN (Glucose, NaCl-Appendix C) and glycerol, we hypothesised that the media supplementation my affect the outcome of growth and ATP analysis in Mtb. An alternative supplementation for 7H9 is ADS (Albumin dextrose salt, Appendix C) and we next sought to assess the effect of this supplementation on the growth and energy production in CbdO-deficient Mtb. The OD, CFU's and ATP production of the different Mtb strains were assessed in this medium and results are shown in Figure 2.20A, B and C respectively. In contrast to the initial growth curves carried out in 7H9 supplemented with OADC (Figure 2.14), no difference in growth was observed between wild type and Δ*cydAB*, Figure 2.20A and Figure 2.20B. Furthermore, the difference in ATP content between the wild type and mutant was not statistically significant when grown in 7H9 supplemented with ADS, although the ATP levels did appear reduced in Δ*cydAB*. These data, along with the data presented for growth in 7H9 supplemented with OADC (Figure 2.14), demonstrated that CbdO plays a role in CCM in Mtb. More specifically, the presence of oleic acid leads to an increased optical density and decreased ATP content of Δ*cydAB*. However, it cannot be ruled out that the presence of catalase may play a role in the phenotype observed in Figure 2.14.

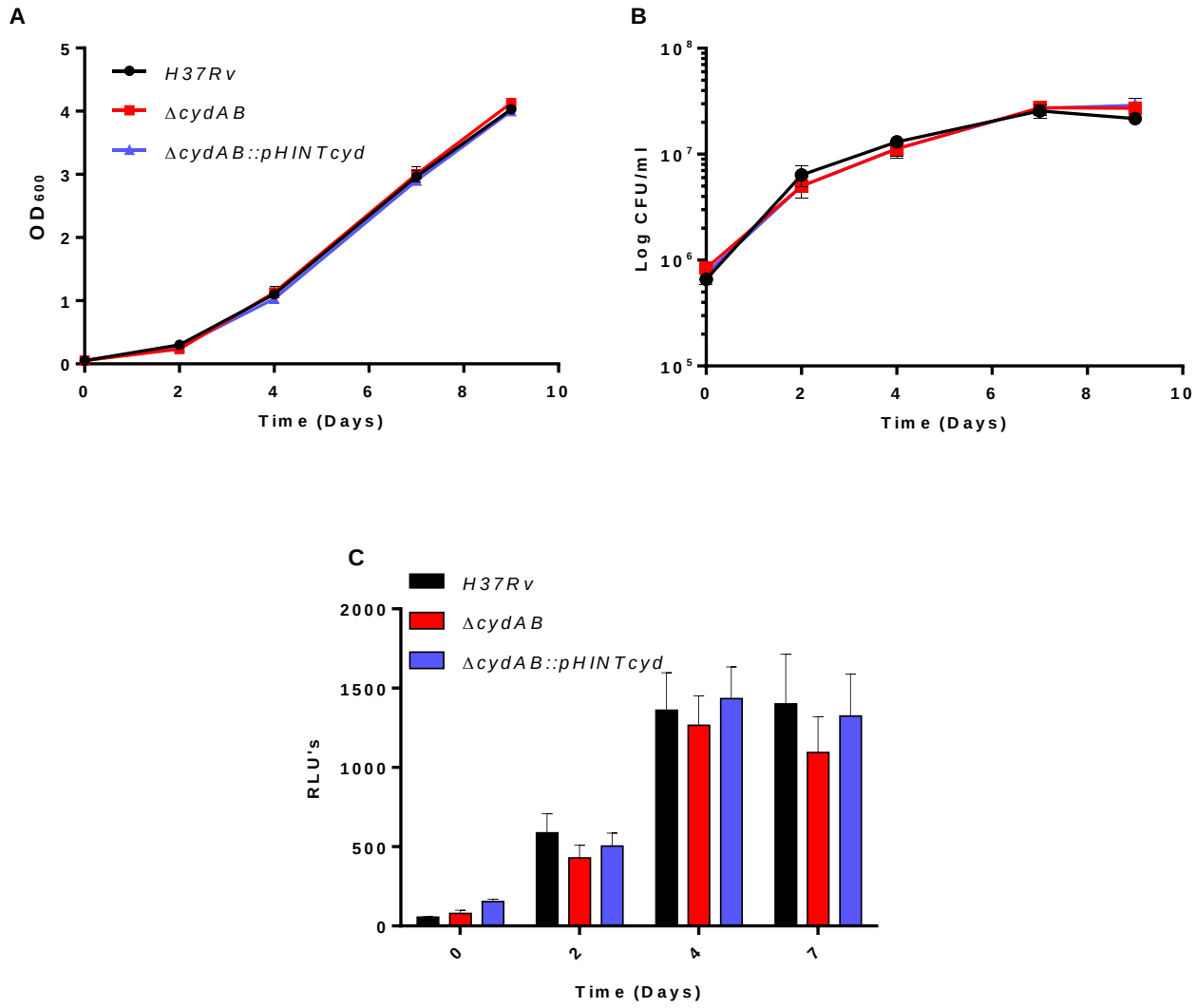


Figure 2.20: Growth curve analysis and ATP production of Mtb Δ*cydAB* grown in 7H9 supplemented with ADS instead of OADC. Cultures were grown in 7H9 supplemented with ADS, glycerol and tyloxapol, incubated at 37 ˚C and aliquots were collected at the indicated time points for **(A)** Optical density readings, **(B)** CFU determination and **(C)** ATP measurements. Each time point represents the average of three independent experiments with standard error bars included.

2.13.7 The effect of different carbon sources on the growth kinetics of CbdO-deficient *M. smegmatis*

The data presented demonstrates that the CbdO plays a role in ETC transport during growth under standard aerobic conditions *in vitro*. Furthermore, Chapter 1 highlighted an important role for CCM in the operation of an efficient ETC. We therefore sought to evaluate the effect of CCM variations on the growth of CbdO-deficient mycobacterial strains. To this end, 7H9 was used as the basal medium and supplemented with different carbon sources. The growth curves for *M. smegmatis* were performed in a 384-well plate format as described in section 2.8.2 and shown in Figure 2.10. The carbon sources assessed in *M. smegmatis* included glucose, glycerol, Tween80, albumin and acetate in different combinations. Glucose, glycerol and Tween80 are conventionally used for the culturing of *M. smegmatis.* Each of the carbon sources was selected based on their respective entry points into CCM, shown in Appendix H-Figure H2. Of the ten different combinations evaluated, six showed statistically significant differences in growth between Δ*cydA::kan* and wild type, shown in Figure 2.21, Figue 2.22, Figure 2.24, Figure 2.25B and Figure 2.26B.

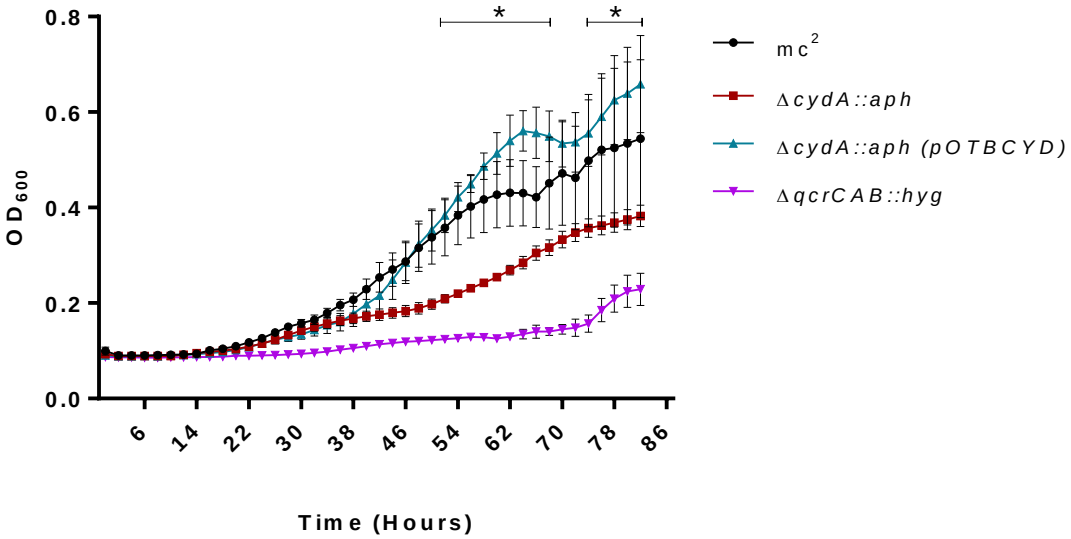


Figure 2.21: Growth kinetic analysis of *M. smegmatis* strains grown with glycerol and Tween80 as the carbon sources. Cultures were grown in 7H9 supplemented with 0,2% glycerol and 0,05% Tween80, incubated at 37 ˚C with OD readings recorded every two hours for 82 hrs. Each time point represents at least four independent experiments and the corresponding standard errors. A Students t-test was used to compare each time point for mc^2 and Δ*cydA::kan.* *P< 0,05.

The remaining four media combinations showed no growth differences between the CbdO-deficient and wild type strains, Figure 2.23, Figure 2.25A and Figure 2.26A.

In contrast, the Δ*qcrCAB::hyg* mutant was severely attenuated in all the different media combinations. When grown in the presence of carbon sources glycerol and Tween80, Δ*cydA::kan* appeared to have a longer lag phase. Over the course of the experiment the mutant did not reach optical densities as high as the wild type (Figure 2.21). When complemented with the Mtb CbdO-encoding genes in Δ*cydA::kan* (pOTBCYD), the phenotype is reversed, confirming a role for this enzyme for optimal growth under these conditions. When the ratio of glucose:glycerol was equal, Δ*cydA::kan* again exhibited an extended lag phase, Figure 2.22. However, after ~62 hrs, the mutant is able to reach levels similar to wild type and appeared to maintain exponential growth until the growth curve was terminated. Although the complemented strain displayed reduced growth compared to wild type, the growth between 44 and 56 hrs was higher than the mutant and overall the growth pattern resembles that of the wild type.

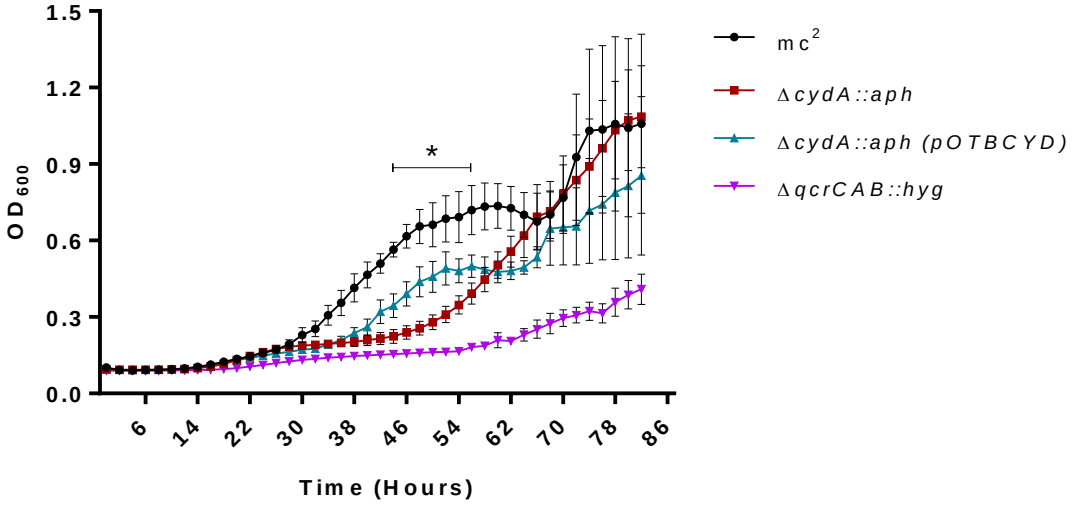


Figure 2.22: Growth kinetic analysis of *M. smegmatis* strains grown with glycerol and glucose as the carbon sources. Cultures were grown in 7H9 supplemented with 0,2% glycerol, 0,2% glucose and 0,05 % tyloxapol, incubated at 37 ˚C with OD readings recorded every two hours for 82 hrs. Each time point represents at least four independent experiments and the corresponding standard errors. A Students t-test was used to compare each time point for mc^2 and Δ*cydA::kan.* *P< 0,04.

The growth of Δ*cydA::kan* in the presence of glucose and Tween80 or glucose alone was not different to wild type as seen in Figure 2.23A and Figure 2.23B respectively. This suggests that the reduced growth of Δ*cydA::kan* observed in Figure 2.21 and Figure 2.22 were due to a role of the CbdO in growth on glycerol. To explore this further the strains were assessed in media containing different amounts of glycerol. The greatest difference in growth between wild type and Δ*cydA::kan* was 2.5 fold and observed at 46 hrs in Figure 2.22. At the same time point, with half the amount of glycerol, a 2-fold difference was observed between the two strains, Figure 2.24A. This suggests that a lower amount of glycerol was more permissive for growth of Δ*cydA::kan*. However, unlike with 0.2 % glycerol, seen in Figure 2.22, the mutant did not reach wild type growth levels in the presence of 0.1 % glycerol, shown in Figure 2.24A. It is possible that the mutant may have achieved a similar biomass when compared to the wild type if the experiment was extended further.

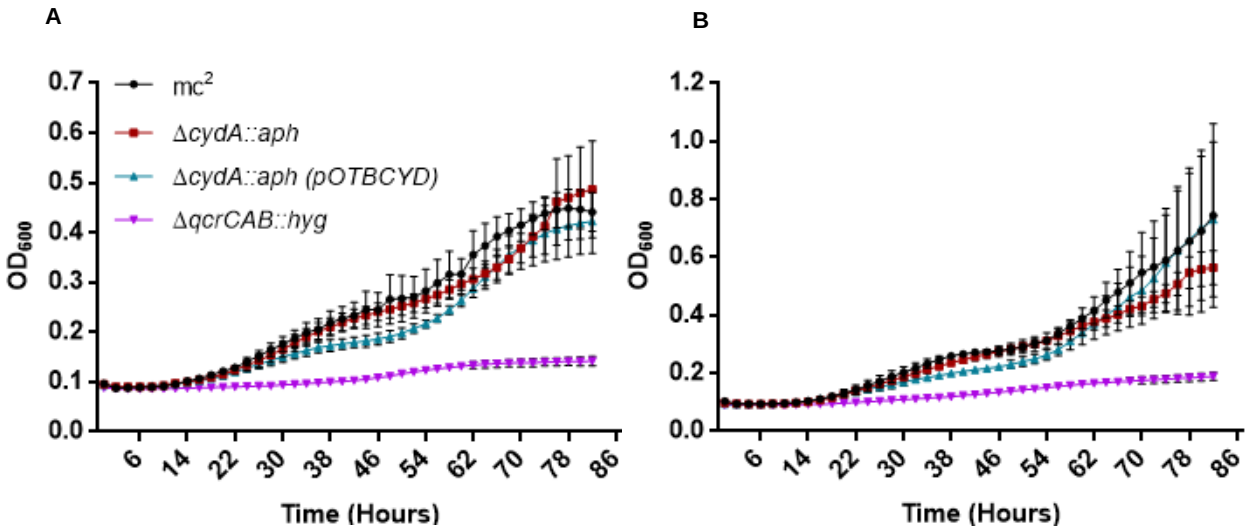


Figure 2.23: Growth curves of *M. smegmatis* in the presence of different carbon sources which do not alter the growth of Δ*cydA::kan*. (A) glucose and Tween80, **(B)** Glucose. Cultures were grown in 7H9 supplemented with 0,2% glucose and 0,05% Tween80, incubated at 37 ˚C with OD readings recorded every two hours for 82 hrs. Each time point represents at least three independent experiments and the corresponding standard errors.

In the presence of 0.4 % glycerol, a 2.5-fold growth difference was observed between wild type and Δ*cydA::kan* at 46 hrs, Figure 2.24B. The Δ*cydA::kan* reached a maximum OD of ~ 0.7 and

appeared to be in stationary phase at the termination of the growth curve. This is in contrast to the growth observed in the presence of 0.2 % and 0.1 % glycerol respectively and suggested that an increased concentration of glycerol attenuates the growth of Δ*cydA::kan*.

The pattern of growth observed for wild type and Δ*cydA::kan* (pOTBCYD) in the presence of glycerol and an additional carbon source is reminiscent of diauxic growth conventionally observed in *E. coli*. A brief description of this pattern observed in Figure 2.24A: between 0-22 hrs a lag phase is seen, from 26-44 hrs is an exponential phase, between 46-54 hrs the culture appears stationary, thereafter a second exponential phase is seen between 56-68 hrs. This is in contrast to the commonly observed method of carbon co-catabolism in mycobacteria when mixed carbon sources are available (de Carvalho *et al.*, 2010a). Interestingly, Δ*cydA::kan* did not display this pattern of growth, pointing to a disruption of CCM regulation in the absence of a functional CbdO. However, in order for this phenomenon to be confirmed in *M. smegmatis* the kinetics of carbon source utilisation would need to be determined.

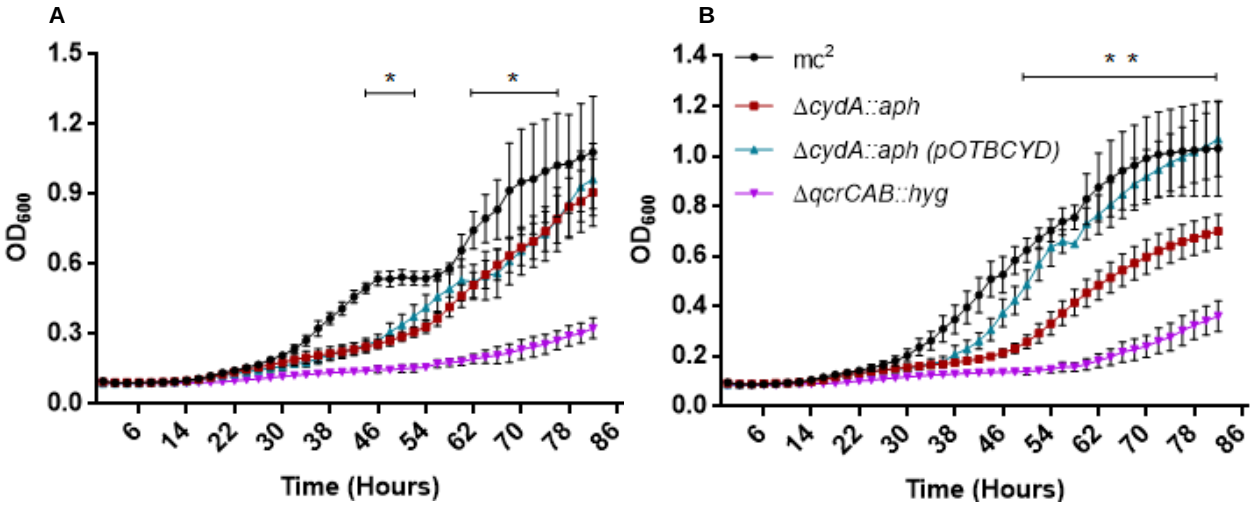


Figure 2.24: Growth kinetic analysis of *M. smegmatis* strains grown with glycerol, glucose and Tween80 as the carbon sources. Cultures were grown in 7H9 supplemented with 0,2% glucose, 0,05% Tween80 and 0,1% glycerol **(A)** or 0,4 % glycerol **(B).** Each time point represents at least three independent experiments and the corresponding standard errors. *P< 0,05. **P< 0,002.

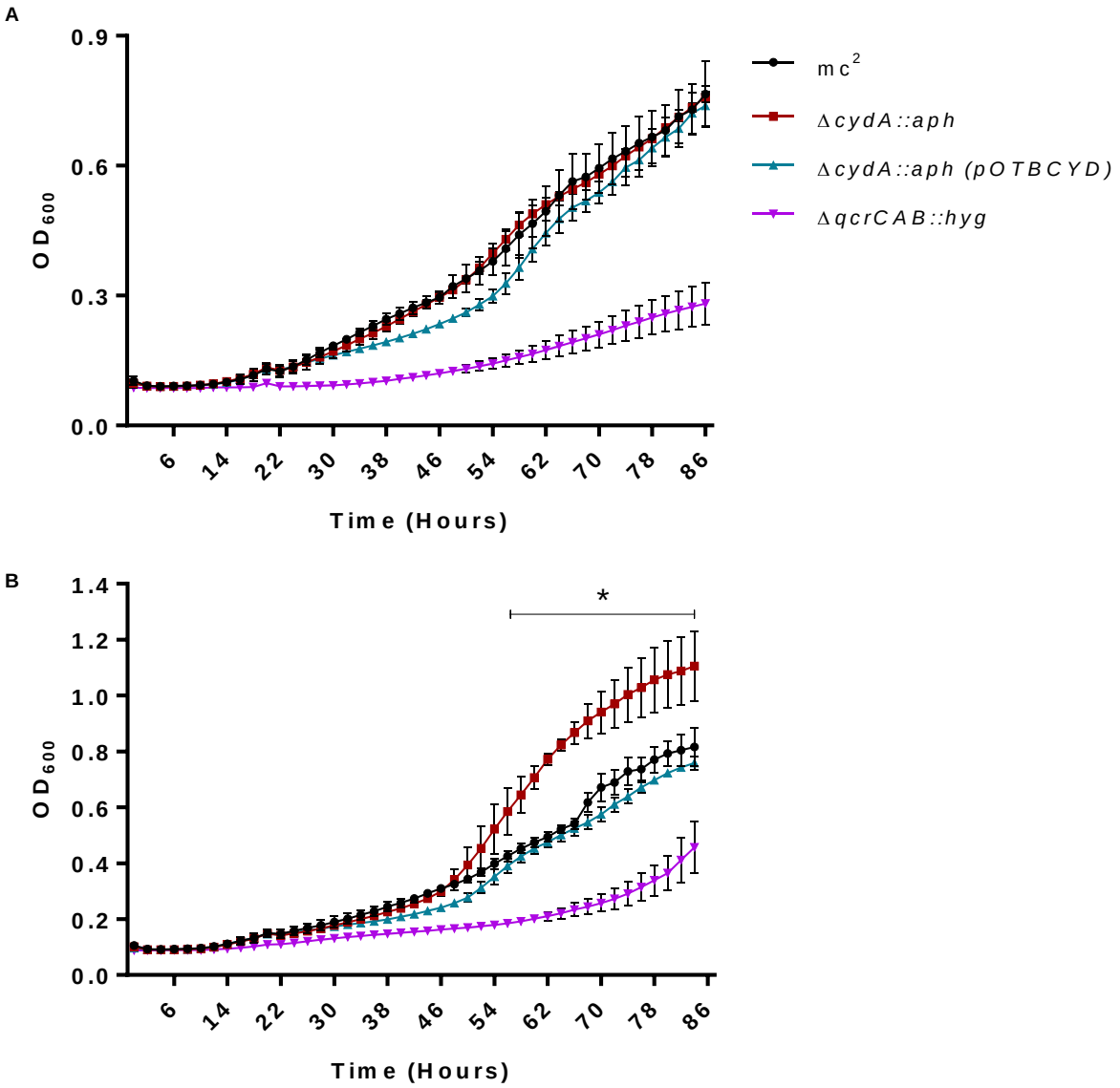


Figure 2.25: Growth kinetic analysis of *M. smegmatis* strains grown in the presence of bovine serum albumin (BSA). Cultures were grown in 7H9 supplemented with 0,2% glucose, 0.5% BSA, 0,05% Tween80 and in the absence **(A)** or presence **(B)** of 0,2 % glycerol. Growth curves were performed at 37 ˚C with OD readings recorded every two hours for 82 hrs. Each time point represents at least three independent experiments and the corresponding standard errors.

Mtb is commonly cultured in rich medium that contains bovine serum albumin (BSA) which serves as a carbon source as well as a protectant against toxic levels of fatty acids (Lynn *et al.*, 1979). We therefore assessed the effect of BSA on the growth of *M. smegmatis* in the presence

and absence of glycerol. In the absence of glycerol, no difference in growth was observed for Δ*cydA::kan* and wild type, shown in Figure 2.25A. Consistent with the previous growth kinetics, Δ*qcrCAB::hyg* was also attenuated when BSA was available. In contrast to the growth observed for Δ*cydA::kan* in the previous growth kinetics, the presence of BSA and glycerol stimulated the growth of Δ*cydA::kan* significantly more than wild type as seen in Figure 2.25B.

Fatty acids have been shown to be the preferred carbon source for Mtb *in vivo* (McKinney *et al.*, 2000). We therefore evaluated the effect of the two-carbon fatty acid acetate on the growth of *M. smegmatis*, with and without Tween80. Compared to glucose and glycerol, acetate did not appear to support robust growth of *M. smegmatis* under the conditions tested. Nonetheless, no difference in growth was observed between wild type and Δ*cydA::kan* when grown in the presence of both acetate and Tween80, shown in Figure 2.26A. In the absence of Tween80, acetate was restrictive for the growth of Δ*cydA::kan*, as seen in Figure 2.26B. This result suggested that CbdO was important for the optimal growth of *M. smegmatis* on fatty acids. To summarise: it can be seen that wild type had a growth advantage over Δ*cydA::kan* in glycerol+Tween80 (Figure 2.21), glycerol+glucose (Figure 2.22), glucose+glycerol+Tween80 (Figure 2.22) and in acetate alone (Figure 2.26B). Similar growth dynamics were observed between the mutant and wild type when grown in acetate+Tween80 (Figure 2.26A), glucose+BSA+Tween80 (Figure 2.25A) and in glucose with or without Tween80 (Figure 2.23). The only medium in which the mutant displayed a growth advantage was in the presence of glucose+glycerol+BSA+Tween80 shown in Figure 2.25B. The growth curves discussed above allowed for the comparison of growth between strains and showed that Δ*cydA::kan* was disadvantaged in many cases.

Todetermine the best carbon source/s for an individual strain, a comparison of that strains growth in each medium was performed using the slopes of each growth curve. The slopes were determined by fitting a linear equation to the exponential phase of each graph in GraphPad and were plotted on a single axis for each strain, Figure 2.27. The exponential phase was determined based on the carbon source/s which showed the earliest onset of logarithmic growth in a strain and was then kept constant for the strain in the different media. The slope of a curve is indicative of the growth rate and thus serves as a surrogate to determine the preferred carbon source/s. The

graphs in Figure 2.27 show that media containing multiple carbon sources made up of glucose, glycerol and Tween80 facilitated the best growth of all the strains tested. It can also be seen that each strain had different preferences i.e. wild type and Δ*cydA::kan* (pOTBCYD) grew best in media containing 0.4 % glycerol, 0.2 % glucose and 0.05 % Tween80 while the most robust growth for Δ*cydA::kan* was observed in the presence of BSA, 0.2 % glucose, 0.2 % glycerol and 0.05 % Tween80.

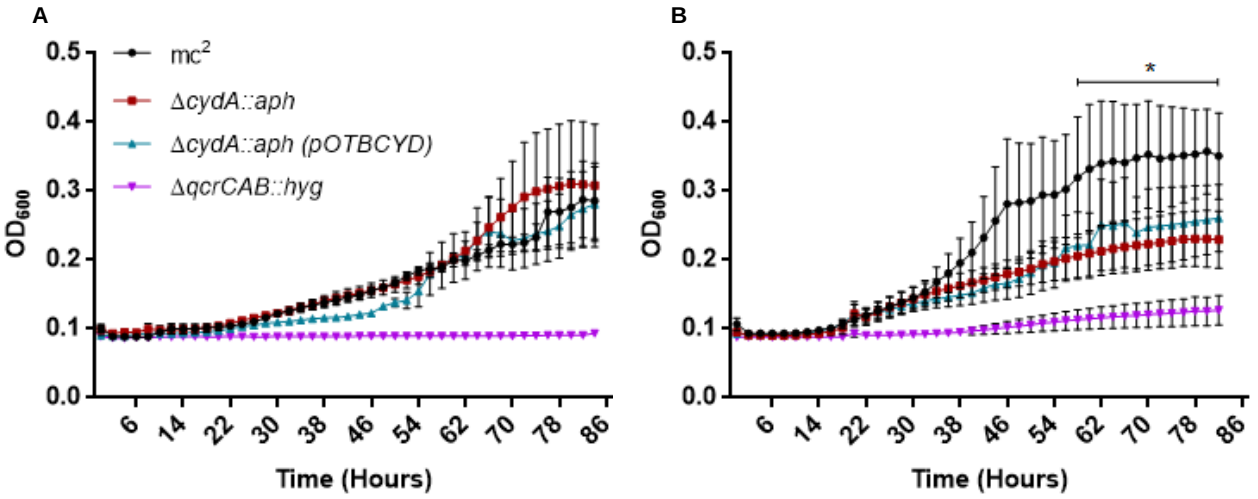


Figure 2.26: A comparison of the growth of *M. smegmatis* strains with acetate as a carbon source. Cultures were grown in 7H9 supplemented with 0,2% acetate and **(A)** with or **(B)** without 0,05% Tween80, incubated at 37˚C.OD readings were recorded every two hours for 82 hrs. Each time point represents at least three independent experiments and the corresponding standard errors. *P< 0,05.

Slope values were obtained for Δ*qcrCAB::hyg* and indicate that the best medium for growth of this strain contained 0.2 % glucose and glycerol. However, this may not be an accurate representation as the exponential phase of growth had not been reached for this strain in most instances when the growth curves were terminated. Although prolonged lag phases were observed for Δ*cydA::kan* in some instances in the growth curve graphs, slope analysis demonstrates that during the respective exponential phases for wild type and Δ*cydA::kan*, significant differences in growth rate were only observed in four different media i.e. glycerol+Tween80, glucose+glycerol+Tween80, ADS+glycerol+glucose+Tween80 and in acetate alone. Taken together, these data demonstrate that loss of CbdO results in perturbations of CCM in *M. smegmatis*.

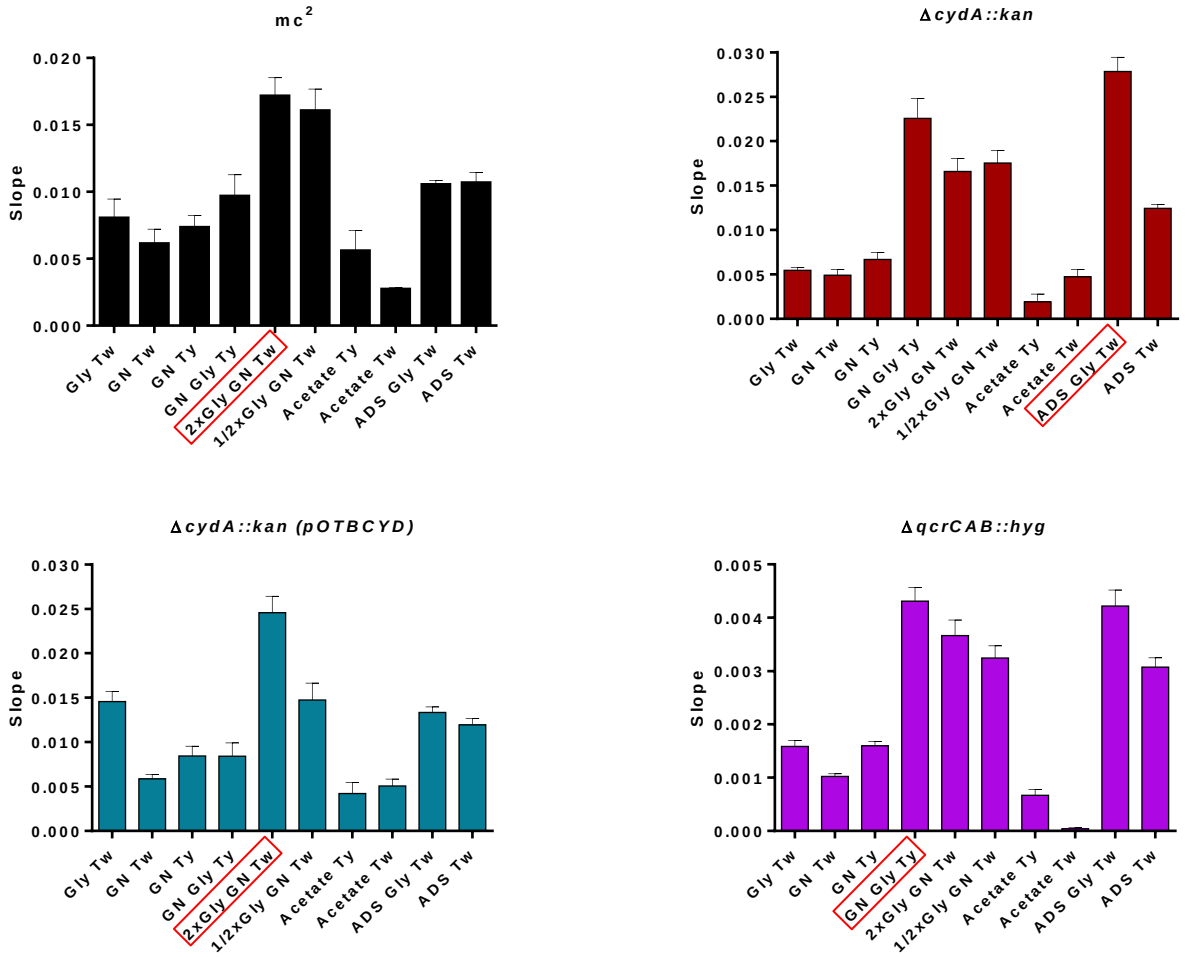


Figure 2.27: A comparison of the slopes of growth curves performed in different media for each *M. smegmatis* strain. The slope allows for the determination of the preferred growth medium for each strain, highlighted in by a red box. Gly: glycerol, Tw: Tween80, GN: glucose, Ty: tyloxapol, ADS: BSA+ glucose.

2.13.8 The effect of different carbon sources on the growth kinetics of CbdO-deficient Mtb

To further evaluate the effect of different carbon sources on the growth of a CbdO-deficient strain, growth curves were performed for Mtb with single carbon sources. The carbon sources assessed were succinate, glucose, glycerol, acetate and propionate, all of which feed into CCM metabolism at different points (Figure H2). The graphs in Figure 2.28A-D showed that there was no difference in growth between the wild type, mutant and complemented strain when grown on glucose, glycerol, succinate or acetate individually. However, when grown on propionate as the

sole carbon source, Δ*cydAB* displayed a growth defect at later time points that was not reversed in the complemented strain, Figure 2.28E.

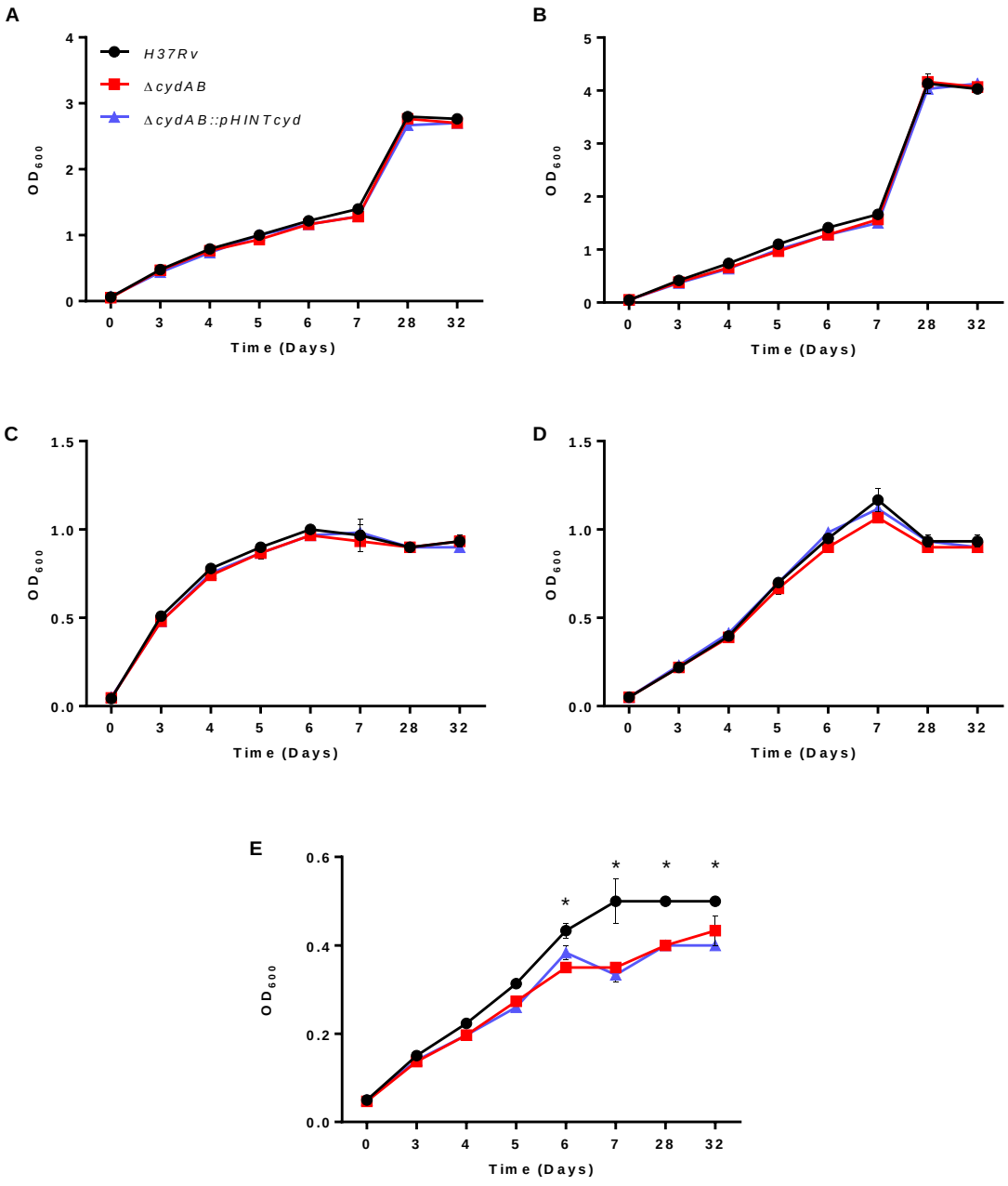


Figure 2.28: Growth kinetic analysis of Mtb grown strains grown with single carbon sources. (A) Glucose, **(B)** Glycerol, **(C)** Succinate , **(D)** Acetate, **(E)** Propionate. Cultures were grown in 7H9 supplemented with 0.2% of the carbon source and 0.05 % tyloxapol, incubated at 37˚C and OD readings were recorded at the time points shown on the graph. Each time point represents three independent experiments and the corresponding standard errors. Statistical significance was determined using the Students t-test. *P<0.006

Consistent with the observations in *M. smegmatis*, Mtb exhibited a preference for different carbon sources. To analyse this further the slopes of each Mtb graph was determined as described for *M. smegmatis* and was plotted in a graph, Figure 2.29. Mtb is able to co-catabolize different carbon substrates (de Carvalho *et al.*, 2010a), therefore it was expected that the most robust growth would be observed in the presence of multiple carbon sources. This was confirmed in Figure 2.29 where it can be seen that Mtb obtained the highest growth rate in media containing multiple carbon sources i.e. 7H9 OADC and 7H9 ADS. With the exception of Δ*cydAB*, which had a higher growth rate than wild type in 7H9 OADC, no other differences in carbon source preference were observed between the strains tested. A comparison of the growth rates achieved in different carbon sources by individual strains revealed no difference between the following pairs: glucose-glycerol, glucose-acetate, glucose-succinate, succinate-acetate or OADC-ADS. Significant differences were observed when the remaining growth rates were compared in each strain. In the wild type, mutant and complement strains the growth rates could be ranked according to carbon source in descending order as: OADC, ADS, glycerol, glucose, acetate,

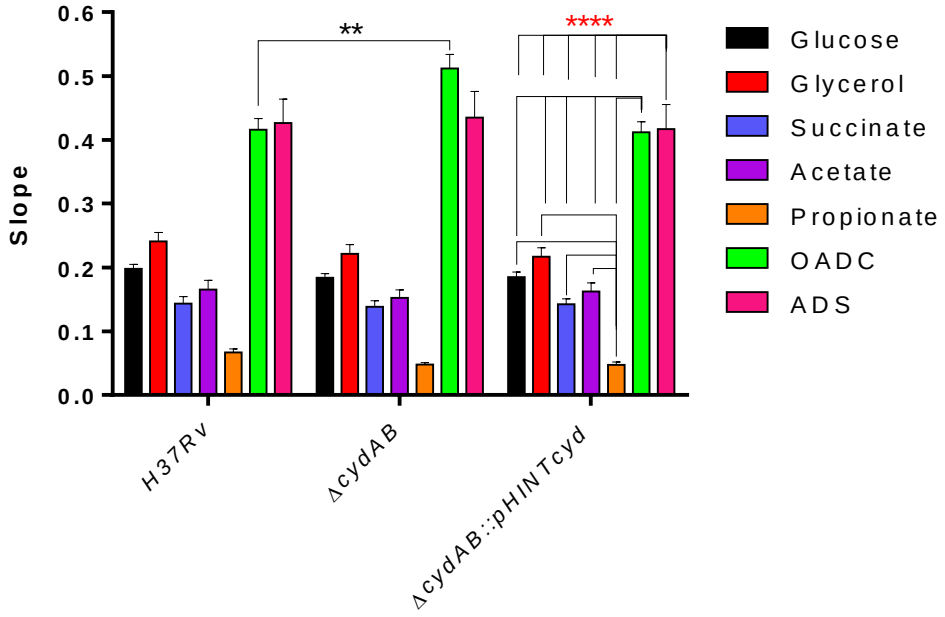


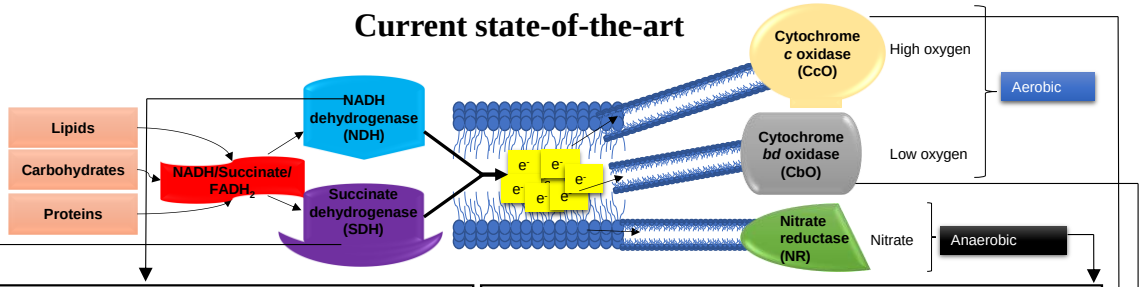
Figure 2.29: A comparison of the growth rate of Mtb strains in media containing different carbon sources. Statistical analysis was performed in GraphPad using 2way ANOVA comparison. For each test α was set at 0.05. **Statistically significant result determined by 2way ANOVA comparison of strains. ****Statistical significance determined by 2way ANOVA comparison of different carbon sources within a strain.

succinate and propionate. For clarity, the statistically significant results for comparisons between different carbon sources is only shown for the genetically complemented strain in Figure 2.29, however the same statistical significance was observed for the wild type and Δ*cydAB*.

Section I conclusions:

- The mycobacterial CbdO has a role in CCM as loss of this enzyme leads to defective growth in the presence of certain carbon sources
- *M. smegmatis* may exhibit diauxic growth
- The most robust growth for mycobacteria was observed with mixed carbon sources, particularly in the presence of glucose and glycerol
- Oleic acid led to an increase in optical density of the CbdO mutant and reduction in ATP content by an unknown mechanism
- Loss of CbdO leads to a growth defect during stationary when propionate is the sole carbon source

Current state-of-the-art



- NDH-I contributes to apoptosis in the host- Miller *et al.* (2010)
- Both Type II NDH enzymes contribute to ETC activity under different conditions and during infection, with Ndh being essential- Shi *et al.* (2005), Yano *et al.*, (2006), Awasthy *et al* .(2014)
- NDH-II is involved in activity of CFZ- Weinstein *et al.* (2005), Yano *et al.* (2011)

- Contributes to anaerobic survival of Mtb- Sohaskey (2008)
- Protects against RNI and acid stress under hypoxic coniditions- Tan *et al.* (201)

- Essential for aerobic growth- Matsoso *et al.* (2005
- Inhibited by Q203- Pethe *et al.* (2013)
- Mutants disrupted in CcO maturation are attenuated in mice

- Serves as a terminal oxidase that maintains the PMF under hypoxic condtitions- Eoh and Rhee (2013), Hartman *et al.* (2014), Pecsi *et al.* (2014)

- Important for hypoxic growth – Kana *et al.* (2001)
- Compensates for loss of CcO – Matsoso *et al.* (2005), Small *et al.* (2013), Lamprecht *et al.* (2016), Kalia *at al.* (2017)
- CbdO is induced in response to oxidative stress- Boot *et al.* (2017)
- Loss of CbdO potentiates the activity of BDQ, Q203 and CFZ- Lamprecht *et al.* (2016), Kalia *at al.* (2017), Lu *et al.* (2015), Berney *et al.* (2014)
- Mutants unable to assemble CbdO are attenuated and unable to persist following INH treatment- Dhar and McKinney (2010), Shi *et al* (2005)

Key Knowledge Gaps

Is there a role for alternate electron acceptors under aerobic conditions?

Are there other previously undescribed roles for CbdO?

Does CbdO play a role in ATP generation?

What is the role of CbdO in growth on different carbon sources?

What is the role of CbdO in response to stress?

What role does CbdO play in drug tolerance?

Chapter 2- Section I

What is the role of respiratory and assimilatory NRs in Msm?

Chapter 3

Chapter 2- Section III

Chapter 2- Section II

Key Findings

- Yes, nitrate rescues CcO defect in Msm
- Nitrate reduced growth of CbdO mutant

- Yes, CbdO is involved in biofilm maturation in Msm and Mtb
- Biofilm defects can be rescued by addition of nitrate
- Deletion of CbdO results in an altered lipid profile

- Yes for both Msm and Mtb
- Associated with reduced oxygen consumption

- Loss of CbdO gives rise to increased susceptibility to ETC inhibitors and cell wall targeting antibiotics

- CbdO is important for growth on proprionate in Mtb
- CbdO mutant has increased optical density in oleic acid
- Msm CbdO mutant seems sensitive to glycerol

Deletion of both narGHI and narB-encoded NRs did not affect respiratory NR activity

- CbdO seems to be important for survival under oxidative stress
- Mutant experienced increased hydroxyl radicles
- CbdO important for mac survival.

2.14 Results – Section II

2.14.1 The effect of nitrate on the growth of *M. smegmatis* respiratory mutants

Mycobacteria possess several enzymes able to utilise terminal electron acceptors other than oxygen, shown in Figure 2.7. As described in section 2.5.4, nitrate is the most well characterised alternate terminal electron acceptor in mycobacteria. Given that mycobacteria are able to simultaneously co-catabolise different carbon sources (de Carvalho *et al.*, 2010a), which provide the reducing equivalents to initiate the ETC, we sought to evaluate to role of an alternate terminal electron acceptor on mycobacterial growth and energy production in the presence of oxygen. To assess the role of nitrate in *M. smegmatis*, growth kinetics were assessed in minimal medium containing 10 mM nitrate (MPLN- Appendix C) as previously described (Narrandes *et al.*, 2015). From the growth curve shown in Figure 2.30, it can be seen that Δ*cydA::kan* displayed a growth defect in this minimal medium. The growth defect was reversed in the complemented strain, Δ*cydA::kan* (pOTBCYD), confirming that it was a phenotype specific to the loss of CbdO. The growth analysis also revealed that the availability of nitrate was able to rescue the growth defect of Δ*qcrCAB:hyg*, Figure 2.30.

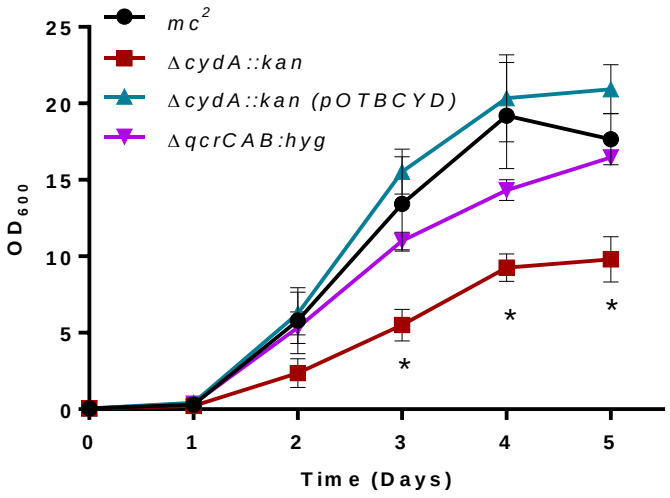


Figure 2.30: Growth curve analysis of *M. smegmatis* strains grown in the presence of 10 mM nitrate and atmospheric oxygen. Cultures were grown at 37 ˚C, with shaking at 115 rpm for 5 days and OD readings were recorded daily. The averages of three independent experiments are plotted for each time point, with standard errors depicted. The Student t-test was used for statistical analysis. *P < 0.003.

This was a fascinating result as it suggests that *M. smegmatis* is able to concurrently utilise two terminal electron acceptors and that in the absence of the CcO, a crippled ETC can use nitrate to maintain the energy requirements of the cell. ATP content was then measured in Δ*cydA::kan* and Δ*qcrCAB::hyg* to determine if the growth defect and rescue, respectively, had an effect on energy production. ATP levels were measured in cultures grown on solid media and liquid media, as described in section 2.9.4, shown in Figure 2.31A and B respectively. The Δ*cydA::kan* mutant contained lower levels of ATP than wild type when grown in MPLN, although the result was not statistically significant for samples from solid media (Figure 2.31A). Over the course of the growth curve performed in MPLN, it was seen that Δ*cydA::kan* consistently contained less ATP than wild type, Figure 2.31B. Supporting the observations in Figure 2.30, the availability of nitrate restored ATP production in Δ*qcrCAB::hyg* in both solid (Figure 2.31A) and liquid (Figure 2.31B) media. These data confirm that nitrate plays a role in ETC activity under aerobic conditions and importantly, that the availability of nitrate is able to rescue the growth and energy production defect of Δ*qcrCAB::hyg*. This suggests that the *M. smegmatis* CcO is dispensable under aerobic conditions when nitrate is available and this was investigated further.

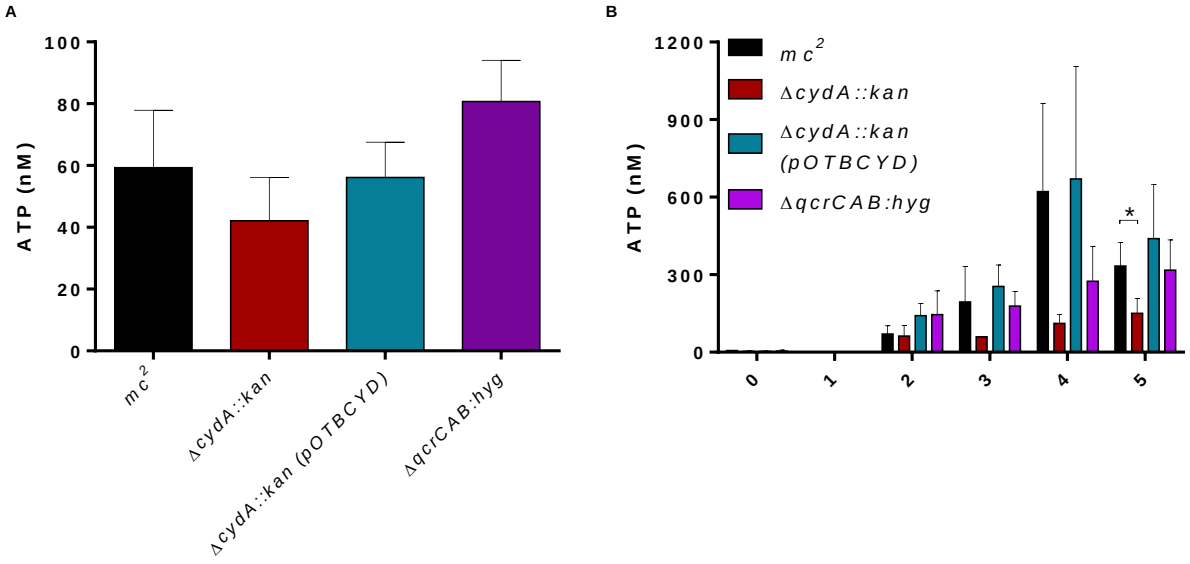
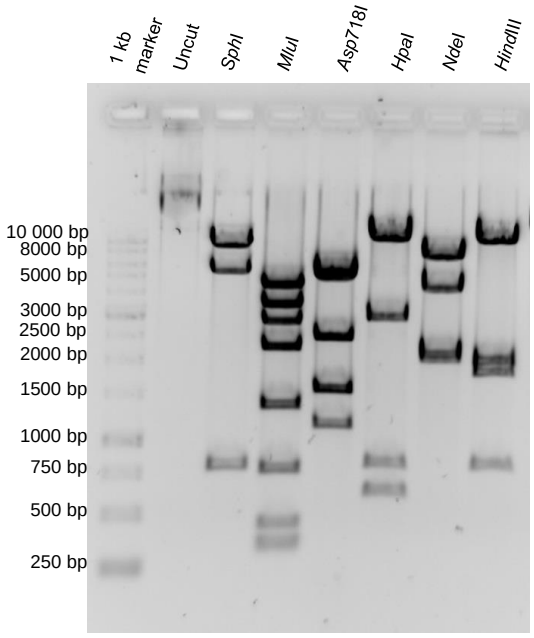


Figure 2.31: A comparison of ATP content of *M. smegmatis* strains grown under aerobic conditions, in the presence of nitrate. ATP production was measured from cultures grown on solid MPLN **(A)** or from aliquots taken from growth curves performed in MPLN **(B)** The students t-test was used to compare strains. *P<0.015

2.14.2 Construction of an *M. smegmatis* unmarked Δ*qcrCAB* mutant

The Δ*qcrCAB::hyg* mutant used in this study was generated by Matsoso *et al*. (2005), who described difficulty in obtaining the mutant. Based on the ability of nitrate to rescue the growth of, and restore ATP production in Δ*qcrCAB::hyg*, shown in Figure 2.30 and Figure 2.31, we hypothesised that the inclusion of nitrate in the selection medium would allow for the mutant to be more readily attainable. To this end, a knockout vector was designed and used to generate an unmarked deletion in *qcrCAB* by two-step allelic exchange (Parish and Stoker, 2000). The vector, pKOqcr, was generated as described in Appendix B. The p2nil intermediate construct (p2nilqcrKO) was sequenced to confirm that no mutations had been introduced during the PCR amplification of the upstream and downstream regions and the final suicide vector was confirmed by restriction mapping, Figure 2.32. The DNA fragments observed during restriction analysis corresponded to the expected sizes of this vector and it was subsequently used for the generation of the mutant.



Enzyme	Expected size (bp)
*Sph*I	816, 5592, 9816
*Mlu*I	315, 425, 780, 2292, 3567, 4281, 4564
*Asp*718I	30, 1132, 1580, 2457, 5197, 5738
*Hpa*I	624, 822, 3112, 11666
*Nde*I	697, 3559, 4377, 7591
*Hind*III	27, 739, 1876, 2092, 11490

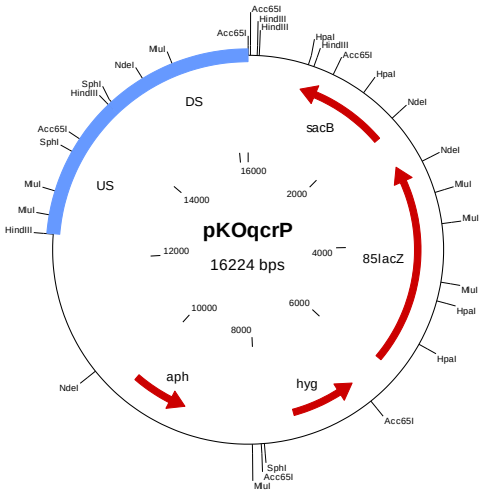


Figure 2.32: Confirmation of the knockout vector, pKOqcrCAB. The gel image of the restriction mapping is shown, along with the expected fragment sizes in the table. The vector map shows the positions of the restriction enzyme sites and selectable marker positions.

The suicide vector was electroporated into wild type *M. smegmatis* and single crossovers (SCOs) were selected for by culturing on conventional 7H10 supplemented with kanamycin, hygromycin and X-gal. A single blue colony was picked from this plate and grown overnight in the presence of nitrate and absence of antibiotics to allow for a second cross over even to occur. Serial dilutions were prepared and plated onto 7H10 plates containing X-gal, nitrate and sucrose for selection of cells which had lost the vector backbone in the second cross over event. After ~ 5 days of incubation, multiple colonies emerged (Figure 2.33A), of which twenty white colonies

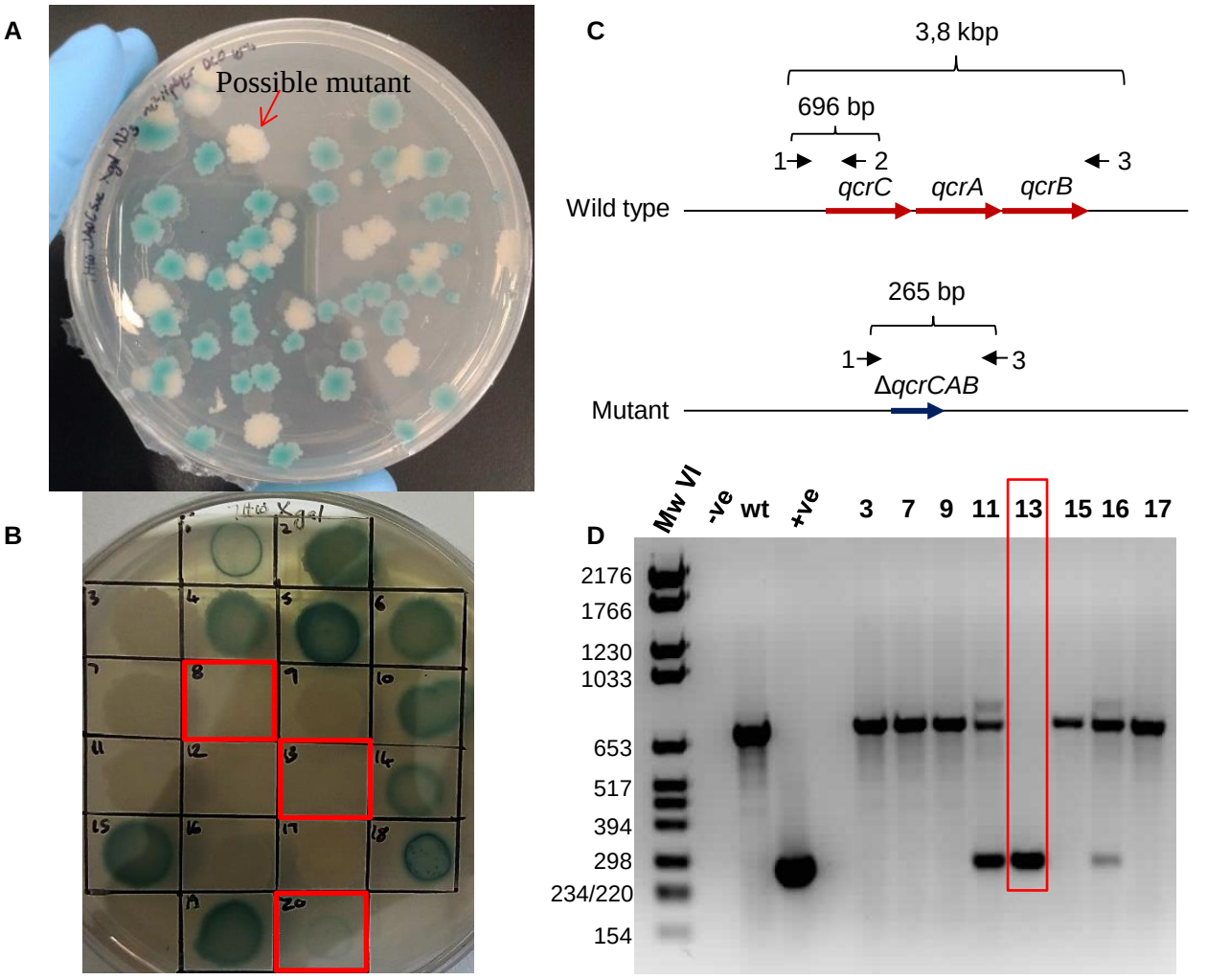


Figure 2.33: Generation of an unmarked *M. smegmatis qcrCAB* knockout mutant. (A) An image of one of the plates showing colonies that arose after a second recombination even in the presence of nitrate. **(B)** A second round of screening of white colonies picked from (A) in the absence of nitrate, photographed after 5 days. **(C)** A schematic of the PCR strategy designed to identify mutants. **(D)** An example of a PCR screening gel, highlighting the clone selected as Δ*qcrCABKO*. The well numbers correspond to colony numbers in B.

were picked for sub-culturing on 7H10 plates with X-gal, with and without antibiotic to confirm loss of the vector. Ten of the colonies selected remained white and unable to grow in the presence of the suicide vector selective antibiotics, hygromycin and kanamycin shown in Figure 2.33B. DNA was extracted from colonies and screened by PCR, Figure 2.33C. An initial PCR screen of eight colonies (7 white and 1 blue) revealed that one was a mutant (13 in Figure 2.33B and 2.33C), as evidenced by the production of the 265 bp DNA fragment corresponding to the mutant allele during the PCR reaction. A subsequent PCR screen of the remaining white colonies shown in Figure 2.33B revealed two more mutants (Colony 8 and colony 20, highlighted in red boxes in the figure). Interestingly, none of the white colonies picked appeared to have an altered morphology as was described by Matsoso *et al*. (2005). However, when those colonies were spotted onto 7H10 medium without nitrate, they took much longer to emerge, thus confirming the growth defect of an *M. smegmatis* strain lacking CcO, Figure 2.33B. The number of Δ*qcrCABKO* mutants identified during the PCR screen suggested that a CcO deficient mutant of *M. smegmatis* was readily obtainable in the presence of nitrate. In addition, this mutant was unmarked and did not require antibiotic selection, suggesting that the inclusion of nitrate bypasses the need for a functional CcO. To confirm this, the mutant generation procedure would need to be carried out in the absence of nitrate but we predict that fewer mutants would be generated, as was observed by Matsoso *et al*. (2005) who detected only five mutants even though a higher level of selection stringency was employed by the inclusion of an antibiotic resistance marker in the mutant allele. As a result of time limitations, these experiments were not conducted.

2.14.3 The role of nitrate on Mtb growth and energy production

To assess dependency on nitrate for growth in Mtb, growth curves were performed in MB media (Appendix C), which was described as a nitrogen-limiting medium for nitrate assimilation (Williams *et al.*, 2011). A comparison of the components of MB with that of 7H9 reveals that the two are very similar, the main difference being the presence of 10 mM nitrate in the former (Appendx C). MB is supplemented with ADS and is thus more similar to 7H9 supplemented with ADS. There were no differences in growth between wild type and Δ*cydAB*, Figure 2.34A. Furthermore, no differences in ATP production were observed between the strains either, Figure

2.34B. These data suggest that the availability of nitrate does not significantly affect the growth or energy production of Mtb strains.

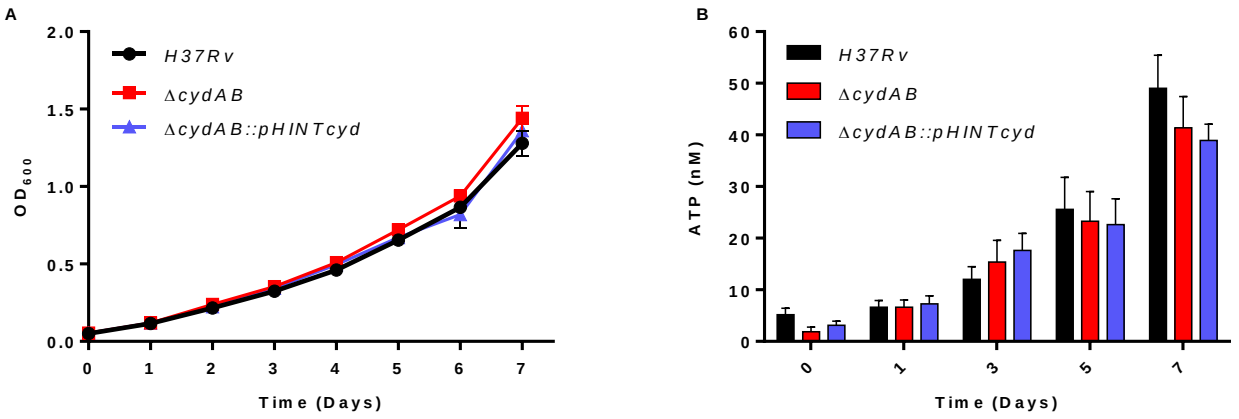


Figure 2.34: An assessment of the growth dynamics of Mtb strains grown in the presence of nitrate. (A) Mtb cultures were grown in MB media supplemented with ADS, 0.2 % glycerol and 0.05 % tyloxapol. **(B)** Aliquots from the the growth curve were analysed for ATP production. An average of three independent experiments is plotted for each time point and standard error values are included

The results observed in Figure 2.34 are contradictory to what was observed for the *M. smegmatis* strains grown in the presence of nitrate. However, as mentioned above MB is comparable to complete 7H9 while the MPLN medium used for *M. smegmatis* was a minimal medium. We therefore assessed the Mtb strains in MPLN (Figure 2.35) to determine if this media type will produce a result similar to that observed in *M. smegmatis*. To serve as a control, the double mutant Mtb strain, Δ*cydAB* Δ*nar*, which lacks *cydAB* and *narGHJI* was also included as it was expected that this strain would not be able to utilise nitrate. No growth defect was observed for the Mtb CbdO-deficient strain when grown in nitrate minimal medium, in contrast to what was observed for the equivalent *M. smegmatis* strain (Figure 2.30). From the growth curve it can be seen that the double mutant is attenuated but it does display some cryptic growth over the course of the experiment. To investigate this further, a conventional Griess assay (described in section 3.3.1 and Figure 3.3) was performed to measure nitrite accumulation. All the strains, except for Δ*cydAB* Δ*nar* were able to secrete nitrite, confirming that nitrate reductase activity was abolished in this strain, Figure2.35B. This also suggested that the cryptic growth observed for this strain

was most likely due to internal stores of a nitrogen source that were able to sustain growth of the strain until ~ day 17.

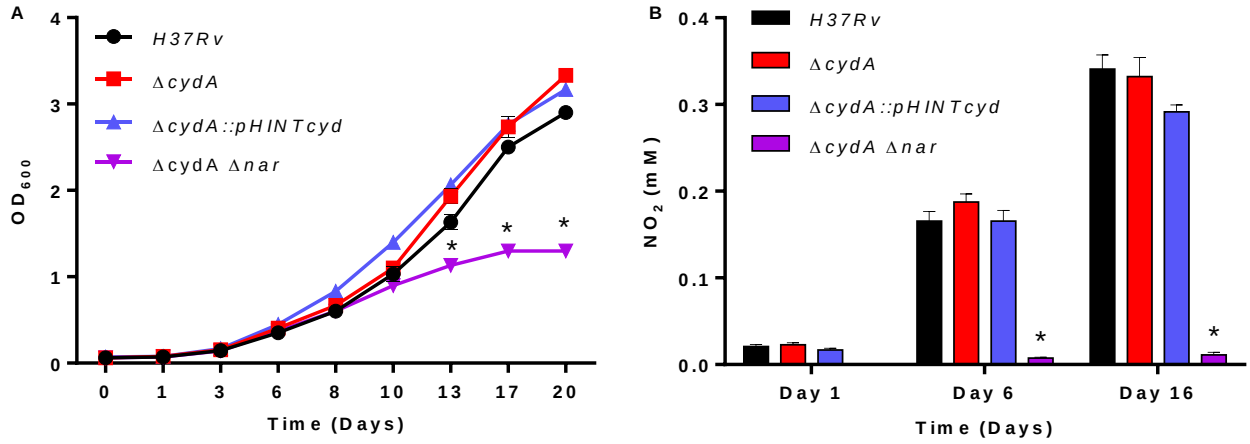


Figure 2.35: Growth and nitrite accumulation analysis of Mtb strains grown in nitrate minimal medium. (A) Cultures were grown in MPLN containing 10 mM nitrate as the nitrogen source. **(B)** Extracellular accumulation of nitrite over time. The mean of three independent experiments is plotted, along with standard error bars.

2.14.4 A CbdO deficient mutant is defective for biofilm formation

A biofilm is a complex bacterial community commonly found in nature. The biofilm structure has been implicated in pathogenesis, most notably in *Pseudomonas* and *Staphylococci* species (Gupta *et al.*, 2016). Biofilms are also known to be tolerant to stresses such as antibiotics and limited oxygen and nutrients, which allows for the persistent survival of the organisms within the structure (Gupta *et al.*, 2016). Although a role for biofilms during infection is yet to be confirmed, it has been shown that pathogenic and non-pathogenic mycobacteria are able to form robust biofilms *in vitro* (Ojha and Hatfull, 2007, Ojha *et al*., 2008). A recent study investigating biofilm formation in mycobacteria revealed that a pellicle biofilm formed on the liquid-air interface displays a gradient of oxygen tensions, with the least amount of oxygen being observed closer to the liquid interface (Anand *et al.*, 2015). In addition, it has been demonstrated that *Pseudomonas aeruginosa* biofilms are largely oxygen-limited (Borriello *et al.*, 2004). We therefore hypothesised that a biofilm would serve as a good model of hypoxic/reduced oxygen

growth. Biofilms for *M. smegmatis* were setup as described in section 2.12.5. The CFUs of the starting inoculum used to initiate biofilm formation for each strain were determined. This was done to ensure that any possible defects observed were not as a result of discrepancies in the amount of cells used for each strain, and this was confirmed in Figure 2.36. As seen in Figure 2.37A, Δ*cydA::kan* is unable to form mature biofilms in SM medium (Appendix C) and the phenotype is reversed in the heterologously complement strain. As a control, methylene blue was included in a set of wells for each strain to obtain an indication of the oxygen content in the wells. Over the incubation period methylene blue did not completely decolourise (Figure 2.37B), providing evidence that oxygen was still available for biofilms grown in this model. This also suggests that the inability of Δ*cydA::kan* to form a biofilm was not due to a reduction in oxygen availability. Furthermore, analyses of colonies grown on solid media, which are types of biofilms that are fully exposed to oxygen, revealed that Δ*cydA::kan* had an altered colony morphology (Figure 2.37C). From the images depicted in Figure 2.37C, it can be seen that the wild type and complemented strains form typical irregularly shaped colonies, with surface ruffling. In contrast, Δ*cydA::kan* colonies appeared smooth, more round and shiny. These data suggest that loss of CbdO leads to an inability of *M. smegmatis* to form a structured, complex bacterial community typical for different types of biofilms.

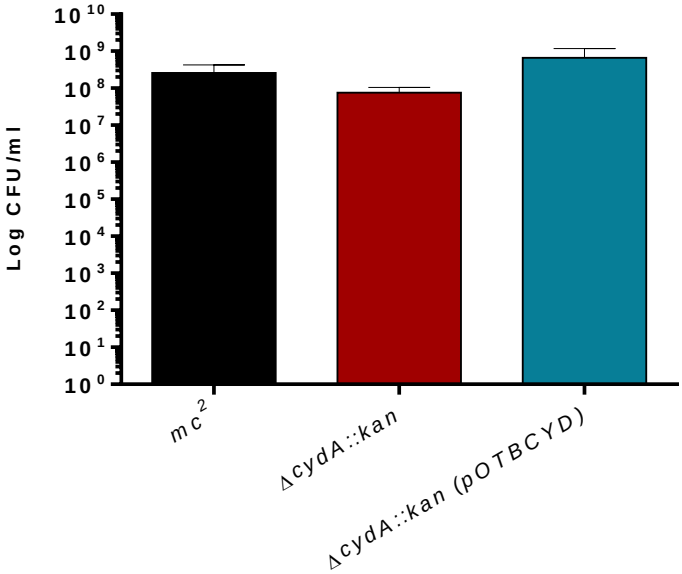


Figure 2.36: Starting inoculum for cultures used to setup biofilms. The average of three independent experiments is plotted for each strain, with standard error bars included.

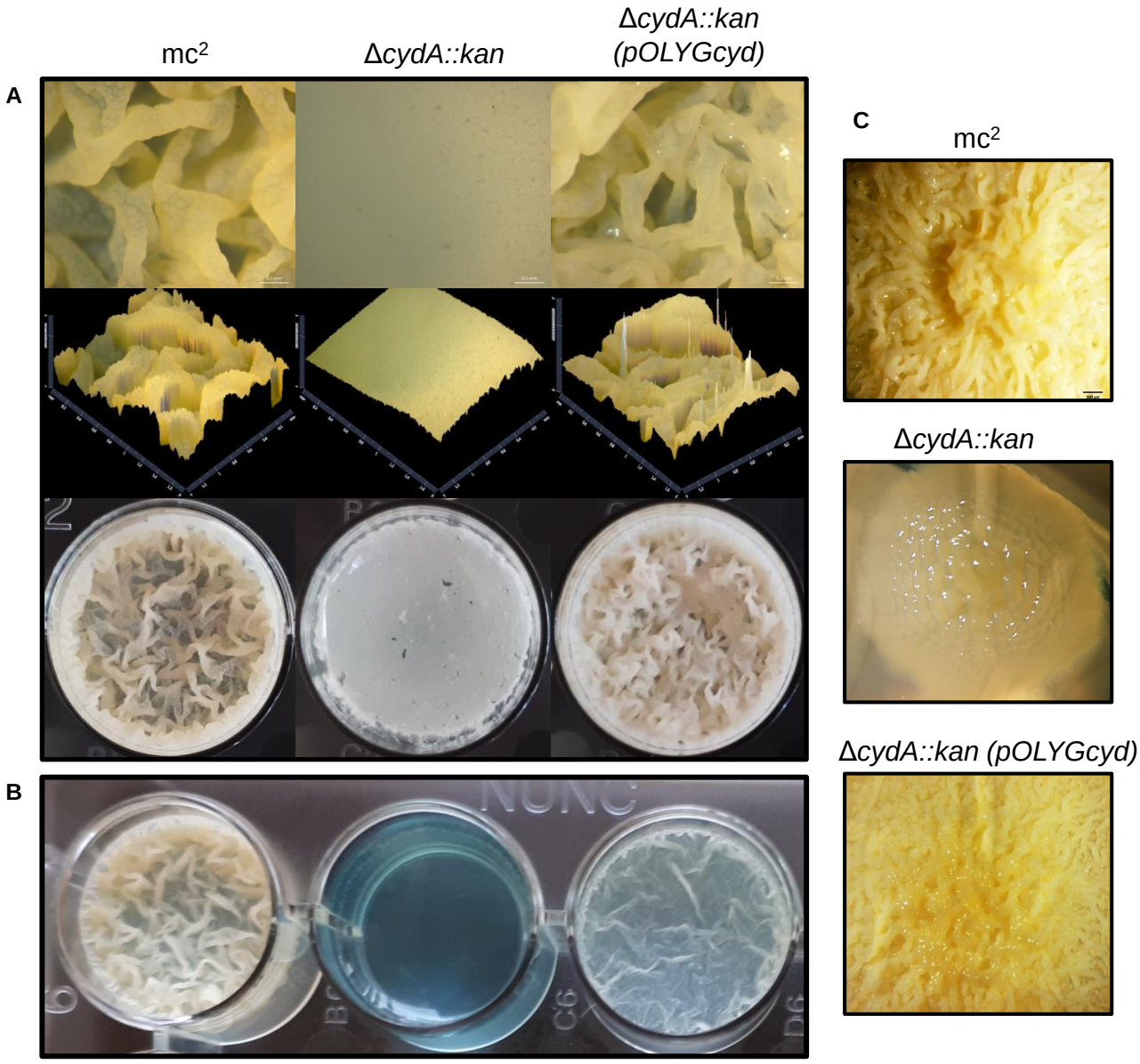


Figure 2.37: *M. smegmatis* biofilm formation in Sautons media. Biofilms were incubated at 30 ˚C for 5-7 days without agitation. **(A)** Images of biofilms formed in Sautons. The top two panels were captured on a dissecting microscope and viewed in the ZEN software package. The top panel is at 5X magnification. The second panel is a 2.5 dimensional plot highlighting the surface depth and ruffling of the biofilm. Images in the bottom panel were captured on a standard digital camera. **(B)** Images of biofilms formed in the presence of 1.5 μg/ml methylene blue. **(C)** Images of colonies formed on solid 7H10 media after incubation at 37 ˚C for 7 days

Based on the observation of Anand *et al*. (2015), who showed that the addition of nitrate was able to rescue the phenotype of a strain unable to form biofilms, we tested if the same phenomenon would be observed for Δ*cydA::kan*. Biofilms were setup with the same inoculum as was used for the experiments in Figure 2.37, except that 10 mM NO_3 (the same as was used during planktonic growth curves in Figure 2.30) was included in the Sautons medium that was inoculated. The inclusion of nitrate was able to rescue the biofilm defect of Δ*cydA::kan* to a certain extent, shown in Figure 2.38. However, the biofilms of wild type and the complemented strain grown in Sautons with nitrate appear to be denser than those in Sautons alone, suggesting that the improved growth observed for Δ*cydA::kan* was a general response.

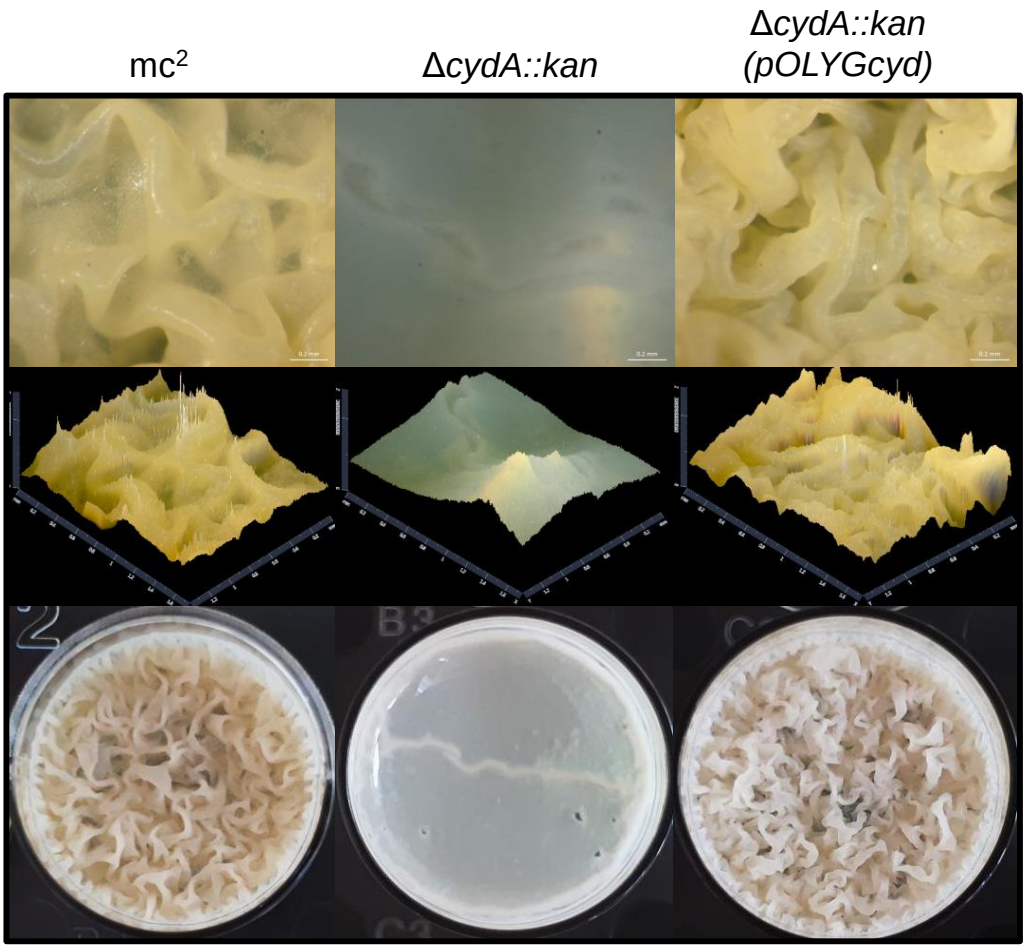


Figure 2.38: Biofilm formation of *M. smegmatis* strains grown in the presence of 10 mM nitrate. Biofilms were incubated at 30 ˚C for 5-7 days without agitation. The top two panels were captured on a dissecting microscope and viewed in the ZEN software package. The top panel is at 5X magnification. The second panel is a 2.5 dimensional plot highlighting the surface depth and ruffling of the biofilm. Images in the bottom panel were captured on a standard digital camera.

Supporting this is the fact that the biofilm formed for Δ*cydA::kan* in the presence of nitrate does not exhibit the characteristic ruffled surface as seen in the wild type and complemented strain in Figure 2.37 and Figure 2.38. This suggests that the mechanism responsible for the biofilm deficiency in Δ*cydA::kan* is different to that of the polyketide quinone-deficient strain (Δ*pks10*), wherein the biofilm-formation deficiency was attributed to loss of the polyketide quinone electron carrier that was essential for growth under reduced oxygen tensions (Anand *et al.*, 2015). Tofurther investigate the biofilm phenotype, the biofilm biomass was determined by crystal violet staining for each strain in the presence and absence of nitrate, as outlined in section 2.15.5. The graph in Figure 2.39 shows that Δ*cydA::kan* had a significantly lower biofilm biomass, compared to the wild type strain in the presence and absence of nitrate. However, the biomass of the mutant grown in nitrate was significantly more than without it.

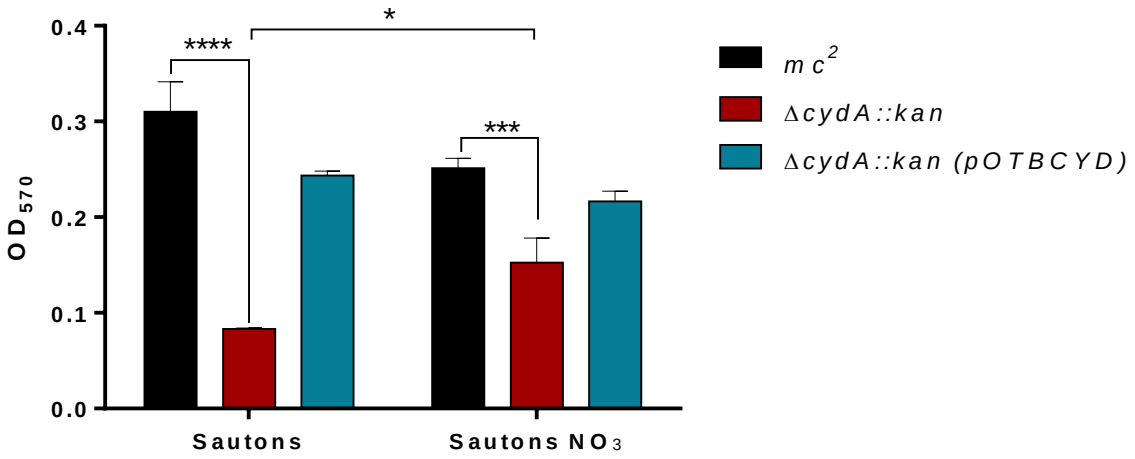


Figure 2.39: The quantification of *M. smegmatis* biofilm biomass in Sautons with and without nitrate. The average of three independent experiments is plotted for each strain with standard errors included. 2way ANOVA was used for statistical analysis with α set at 0.05.

In contrast to what was expected based on the images in Figure 2.38, it appeared as though the inclusion of nitrate did not increase the biomass of the wild type or complemented strain. Based on these data, it appeared as though nitrate was able to promote biofilm formation of Δ*cydA::kan*, however it was not sufficient to promote the full maturation of the biofilm in this strain, as was observed for Δ*pks10* (Anand *et al.*, 2015). However, the concentration of nitrate at

which full restoration of biofilm formation was observed by Anand *et al*. (2015), was significantly higher than used during this study (235 mM vs 10 mM), suggesting that nitrate may fully restore biofilm formation in Δ*cydA::kan* at higher concentrations. However, because of the reduced growth of the Δ*cydA::kan* in nitrate, this is unlikely.

2.14.5 Biofilm formation in Mtb

The biofilm phenotype observed for the *M. smegmatis* CbdO-deficient strain prompted an investigation into biofilm formation of the Mtb strain. The experiments were setup as described for *M. smegmatis*, with and without nitrate. Consistent with the phenotype observed in *M. smegmatis*, the Mtb CbdO-deficient strain was unable to form mature biofilms in Sautons, Figure 2.40A. In contrast to *M. smegmatis*, exaggerated colony morphology was not observed for the Mtb mutant, shown in Figure 2.40C, although it does appear to have decreased surface ruffling. The wild type and complemented strain were able to form biofilms equally as well. Furthermore, the presence of nitrate was able to rescue the observed defect of Δ*cydAB*, consistent with the observation in *M. smegmatis*. The space below was left blank to fit Figure 2.40 on a full page.

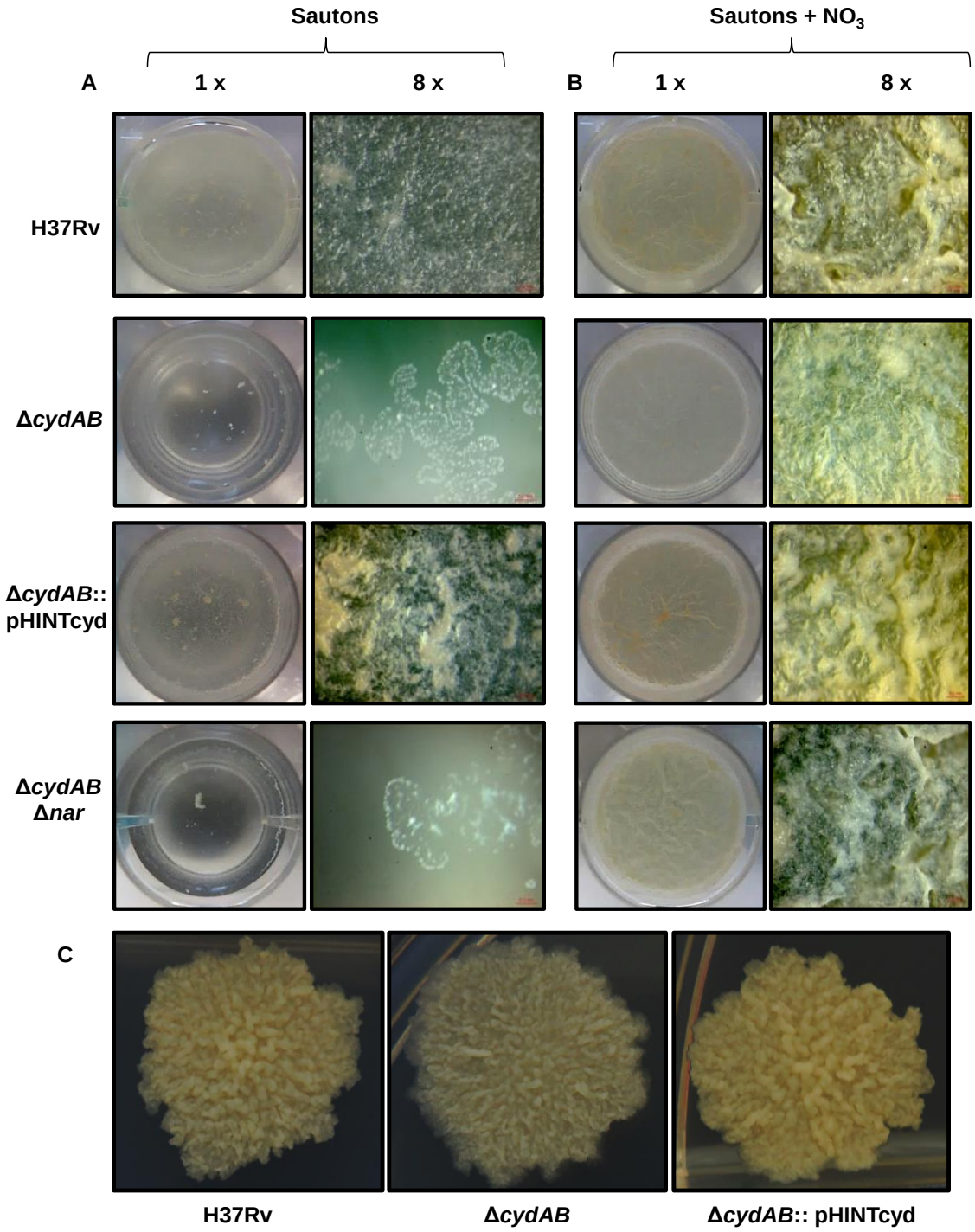


Figure 2.40: Biofilm formation of Mtb strains in Sautons minimal medium, with and without nitrate. (A) Images of biofilms generated in Sautons media alone. **(B)** Images of biofilms formed in Sautons containing 10 mM nitrate. The 1x magnification images were captured with a camera, while the 1.6x images were recorded using a dissecting microscope and the ZEN software. **(C)** The colony morphology of Mtb strains grown on 7H11 solid media

Interestingly, the presence of nitrate appeared to stimulate biofilm formation in Mtb. Quantification of the biofilm biomass confirmed that the presence of nitrate resulted in the production of thicker biofilms for all the strains tested, shown in Figure 2.41. The double mutant, Δ*cydAB* Δ*nar*, which was shown to be incapable of nitrate reduction in Figure 2.35, was included as a control during the biofilm experiments. As expected, the mutant was unable to form a biofilm, presumably as a result of the loss of *cydAB*. However, because a mutant lacking only *narGHJI* was not assessed, it cannot be ruled out that loss of NR activity could contribute to the observed phenotype in Δ*cydAB* Δ*nar*. The double mutant was included as a control for biofilm formation in nitrate as we expected that loss of NR activity in the Δ*cydAB* background would lead to the inability of nitrate to rescue the biofilm phenotype of a CbdO mutant. Contrary to what was expected, it can be seen that the presence of nitrate was also able to rescue the phenotype of a strain that could not form biofilms and lacked NR activity. This suggested that the double mutant may retain NR activity in this biofilm model. A Griess assay was therefore performed on biofilm cultures to investigate this further. The graph presented in Figure 2.42 shows that nitrite was present in the supernatant of biofilms formed in the absence and presence of nitrate. A higher amount of nitrite was detected for the wild type, Δ*cydAB* and Δ*cydAB::pHINTcyd* when nitrate was available, although the differences were not statistically

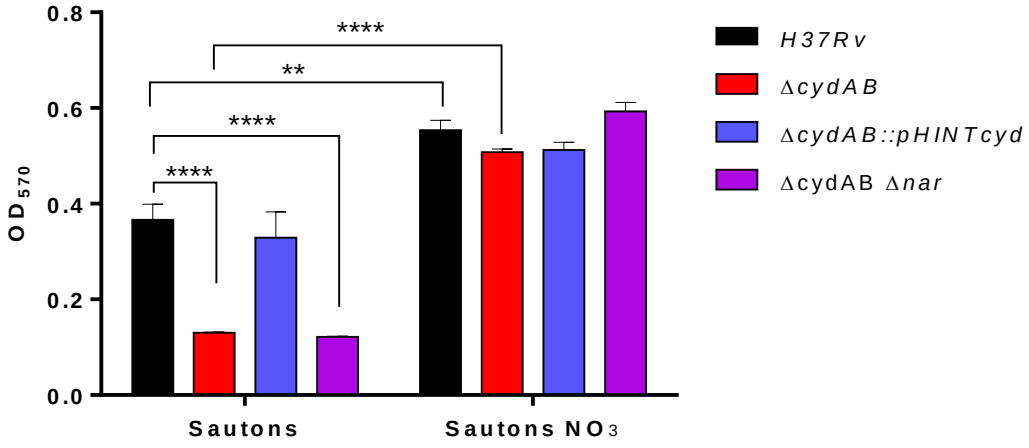


Figure 2.41: Quantification of Mtb biofilm biomass with crystal violet. The average of three independent experiments is plotted for each strain with standard errors included. 2way ANOVA was used for statistical analysis with α set at 0.05.

significant.

The double mutant on the other hand, showed no increase in extracellular nitrite in the presence of nitrate, confirming the loss of NR activity in this strain. For each Griess assay performed, fresh medium was used as the blank and no colour change was observed when the Griess reagents were added to the medium sample, confirming that the nitrite detected in the samples was not due to traces of nitrite in the medium. The presence of nitrite in the supernatant of biofilm samples formed without nitrate suggests that during the formation of a biofilm, Mtb is able to produce and secrete nitrite. Furthermore, the observed rescue of biofilm defects with nitrate, even in the absence of a functional NR, suggests that the mechanism of biofilm restoration with nitrate is independent of NR activity. This mechanism is yet to be elucidated.

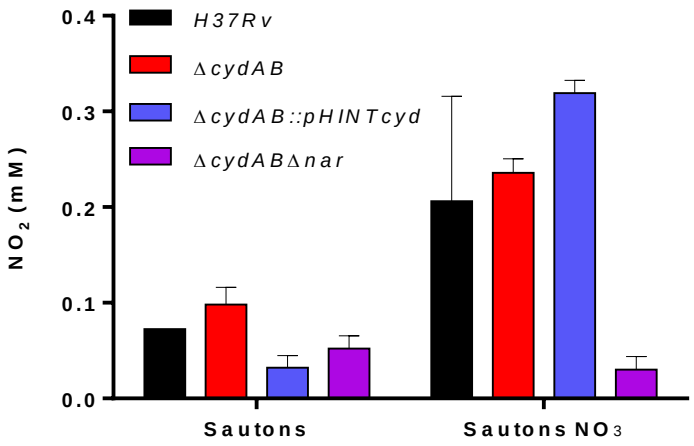


Figure 2.42: A conventional Griess assay performed on samples collected from biofilm cultures reveals that nitrite is produced and secreted in the absence of nitrate. The assay was performed as described in section3.3.1. Each bar represents the average of three independent experiments and standard errors are included.

In order to confirm that the observed biofilm defect of Δ*cydAB* and Δ*cydAB* Δ*nar* was specifically as a result of the inability to form biofilms and not because of an inability to grow in Sautons, a growth curve was performed in Sautons containing tyloxapol as a detergent to prevent clumping. The graph in Figure 2.43 confirms that neither Δ*cydAB* nor Δ*cydAB* Δ*nar* were defective for growth in Sautons under standard conditions. The growth curve was carried out for

a longer period than the previous growth curves to confirm that the mutant strains had no stationary-phase growth defect.

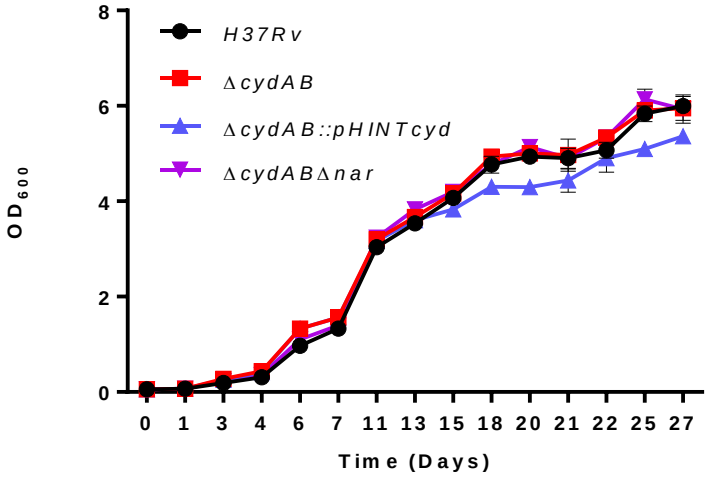


Figure 2.43: Growth kinetic analysis of Mtb strains grown in Sautons minimal media. Cultures were incubated at 37 ˚C and OD readings were recorded at the indicated time points. Each data point represents the average of three independent experiments and standard error bars are included.

2.14.6 Loss of CbdO leads to an altered lipid profile in *M. smegmatis*

Mycobacterial biofilms have received increasing attention towing to the presence of conditions akin to those predicted to be experienced in the granuloma being identified within mycobacterial biofilms e.g. varying oxygen tensions, reduced nutrients etc. However, it remains to be established whether Mtb forms biofilms during infection and at this point, biofilms represent a good model to study bacterial persistence in the laboratory only. An investigation in *M. smegmatis* revealed the essentiality of glycopeptidolipid (GPL) acetylation for pellicle biofilm formation and sliding motility (Recht and Kolter, 2001). We therefore assessed the GPL profile of *M. smegmatis* strains from biofilms to determine if an altered GPL profile could be the reason for the biofilm defect of Δ*cydA:kan*. Using TLC, we observed an altered lipid profile in Δ*cydA:kan*, highlighted by red boxes in Figure 2.44. There appeared to be an accumulation of ~ 4 lipids closer to the loading front and one that is the third from the top. Interestingly, the

presence of nitrate appeared to alter the lipid profile of the mutant further, highlighted by yellow boxes in Figure 2.44. The profile observed was similar to that observed by Ojha *et al*. (2002), an example of which is shown in the insert in Figure 2.44. Worth nothing though was the difference in extraction methods used and the media in which the samples were grown. The Ojha study performed a deacetylation on the extracted lipids, which was not carried out during this study. In addition, the lipid profile shown in Figure 2.44 was from biofilm cultures, as opposed to planktonic cultures that were the sample source in the Ojha study (Ojha *et al.*, 2002). Interestingly, the profile shown in the insert is from cultures that were starved of glucose, which is consistent with the biofilm extracts that were grown in SM with no glucose and glycerol as the carbon source. These data provide evidence that loss of the *M. smegmatis* CbdO leads to cell wall lipid alterations and in addition, the presence of nitrate is able to affect the lipid profile of the mutant. A comparison of the lipid profile obtained for the wild type and complemented strains from the different media, suggests that the presence of nitrate did not alter the lipid profile. The bands for the profile of the complemented strain in nitrate appear more intense, but this was most likely due to an increased amount of lipids in that extract, seeing as all the bands are darker in that sample. The differences observed between the wild type and mutant are not likely as a result of sample loading discrepancies, as at least two sets of bands appear to be of the same intensity and serve as loading controls. However, ideally the specific lipid content of each sample should be quantified by radioactive labelling and the lipids should be identified by liquid chromatography-light spectrometry (LC-MS). As a basis, this experiment provides the first evidence of a role for CbdO in lipid/cell wall biosynthesis in mycobacteria and reveals a promising area to identify the possible mechanism for the biofilm defect observed.

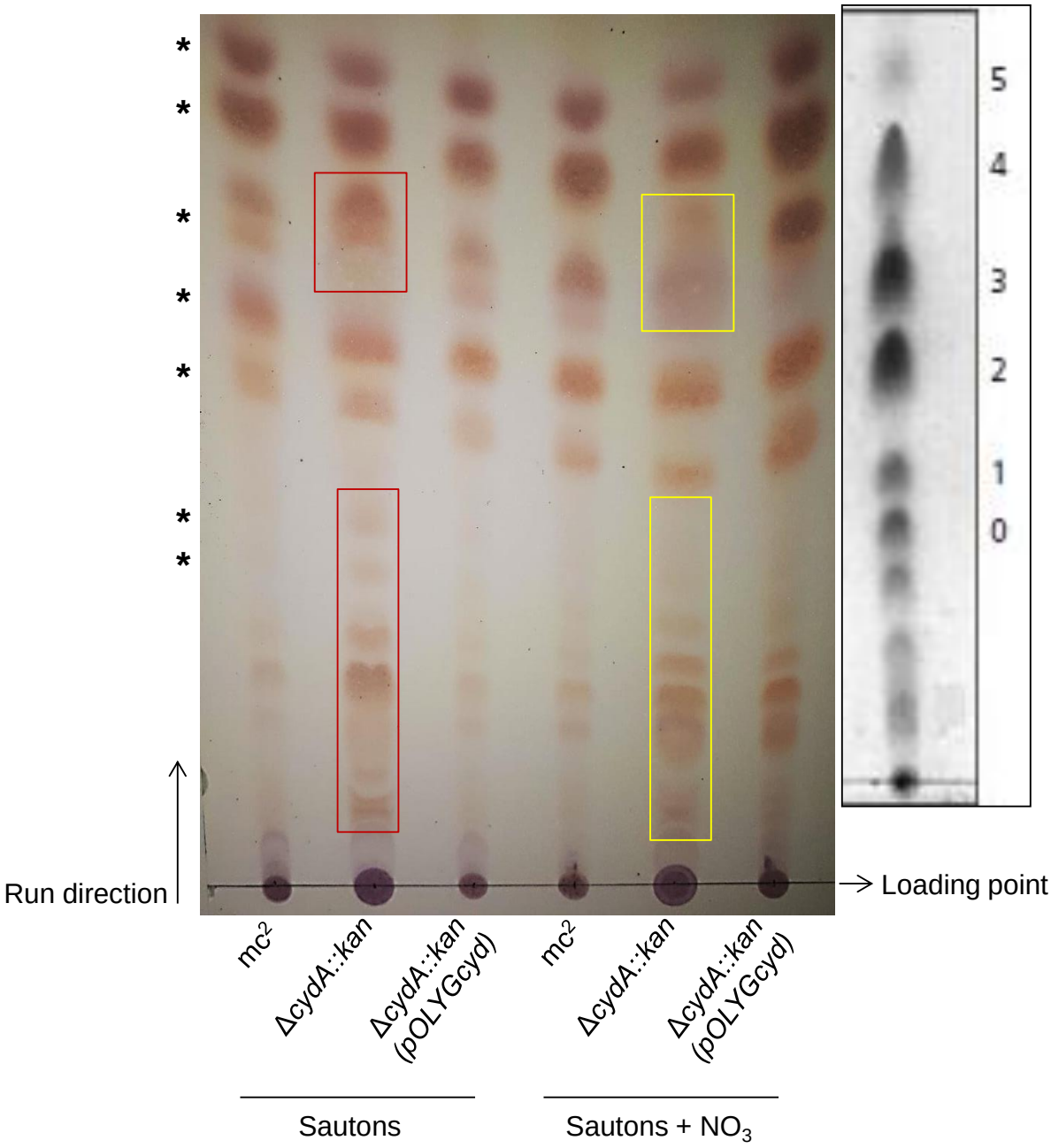
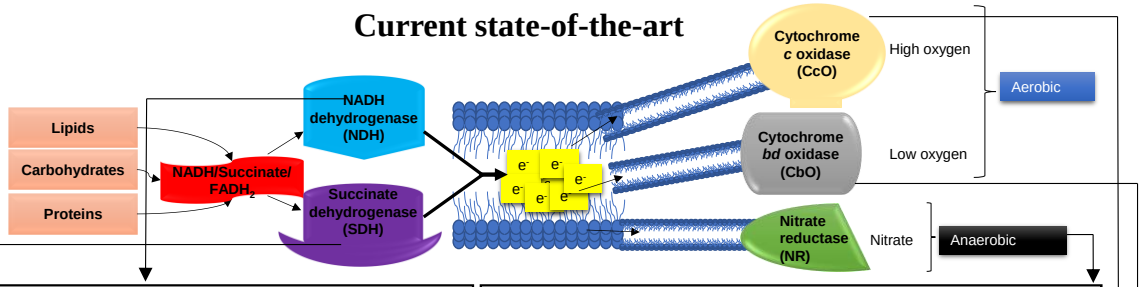


Figure 2.44: Glycopeptidolipid profile of *M. smegmatis* biofilm cultures. Total lipids were extracted from biofilm-derived cultures with chloroform:methanol (2:1). The lipid profile for biofilms formed in the presence and absence of nitrate were compared. TLC plates were developed with 0.1 % orcinol in 40 % sulphuric acid and charred at 140˚C for ~3 mins. The GPLs are labeled with *, based on labeling presented by Ojha *et al*. (2002) shown in the insert.

Section II conclusions:

- Nitrate is able rescue the growth and ATP production deficiency in the *M. smegmatis* CcO mutant
- Nitrate appears to be toxic to *M. smegmatis* in the absence of CbdO
- Loss of CbdO leads to an inability to form biofilms in both Mtb and *M. smegmatis*
- Nitrate is able to rescue the biofilm phenotype of CbdO-deficient strains, independently of NR activity
- The biofilm defect, as a result of CbdO loss, is associated with alterations in the GPL profile

Current state-of-the-art



- NDH-I contributes to apoptosis in the host- Miller *et al.* (2010)
- Both Type II NDH enzymes contribute to ETC activity under different conditions and during infection, with Ndh being essential- Shi *et al.* (2005), Yano *et al.*, (2006), Awasthy *et al* .(2014)
- NDH-II is involved in activity of CFZ- Weinstein *et al.* (2005), Yano *et al.* (2011)

- Contributes to anaerobic survival of Mtb- Sohaskey (2008)
- Protects against RNI and acid stress under hypoxic coniditions- Tan *et al.* (201)

- Essential for aerobic growth- Matsoso *et al.* (2005
- Inhibited by Q203- Pethe *et al.* (2013)
- Mutants disrupted in CcO maturation are attenuated in mice

- Serves as a terminal oxidase that maintains the PMF under hypoxic condtitions- Eoh and Rhee (2013), Hartman *et al.* (2014), Pecsi *et al.* (2014)

- Important for hypoxic growth – Kana *et al.* (2001)
- Compensates for loss of CcO – Matsoso *et al.* (2005), Small *et al.* (2013), Lamprecht *et al.* (2016), Kalia *at al.* (2017)
- CbdO is induced in response to oxidative stress- Boot *et al.* (2017)
- Loss of CbdO potentiates the activity of BDQ, Q203 and CFZ- Lamprecht *et al.* (2016), Kalia *at al.* (2017), Lu *et al.* (2015), Berney *et al.* (2014)
- Mutants unable to assemble CbdO are attenuated and unable to persist following INH treatment- Dhar and McKinney (2010), Shi *et al* (2005)

Key Knowledge Gaps

Does CbdO play a role in ATP generation?

Is there a role for alternate electron acceptors under aerobic conditions?

What is the role of CbdO in growth on different carbon sources?

Are there other previously undescribed roles for CbdO?

What is the role of CbdO in response to stress?

What role does CbdO play in drug tolerance?

Chapter 2- Section I

Chapter 2- Section II

What is the role of respiratory and assimilatory NRs in Msm?

Chapter 2- Section III

Key Findings

Chapter 3

- Yes for both Msm and Mtb
- Associated with reduced oxygen consumption

- Yes, nitrate rescues CcO defect in Msm
- Nitrate reduced growth of CbdO mutant

- Yes, CbdO is involved in biofilm maturation in Msm and Mtb
- Biofilm defects can be rescued by addition of nitrate
- Deletion of CbdO results in an altered lipid profile

- Loss of CbdO gives rise to increased susceptibility to ETC inhibitors and cell wall targeting antibiotics

- CbdO is important for growth on proprionate in Mtb
- CbdO mutant has increased optical density in oleic acid
- Msm CbdO mutant seems sensitive to glycerol

Deletion of both narGHI and narB-encoded NRs did not affect respiratory NR activity

- CbdO seems to be important for survival under oxidative stress
- Mutant experienced increased hydroxyl radicles
- CbdO important for mac survival.

2.15 Results- Section III

Mtb is predicted to encounter numerous stresses within the granuloma, including ROS, RNS, acid stress and reduced nutrient availability. CbdO has been implicated in resistance to some of these harsh conditions in other bacterial organisms, reviewed in section 2.10.1 of this thesis. We therefore assessed the *in vitro* susceptibility of CbdO-deficient mycobacterial strains to the following stresses: oxidative, acid, antibiotic, hypoxic and NO stress via acidified nitrite. No statistically significant differences were observed between Δ*cydAB* and wild type in response to acid or NO stress respectively, Figure 2.45A and Figure 2.45B respectively.

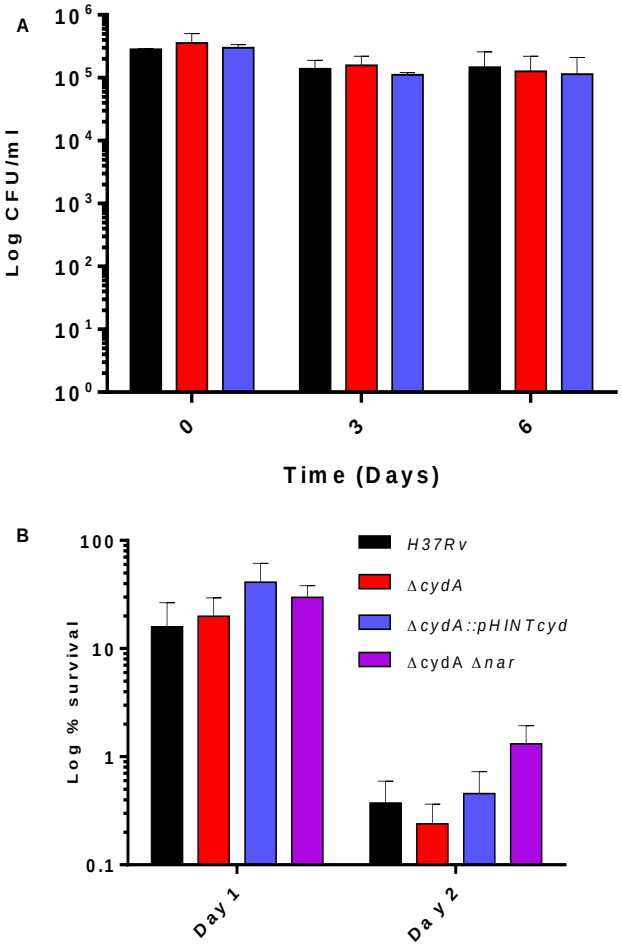


Figure 2.45: The response of Mtb to stresses *in vitro*. (A) Acid stress assay in phosphate citrate buffer. **(B)** A comparison of the survival of Mtb strains exposed to 12 mM acidified nitrite. The average of at least two (A) or three (B) independent experiments is plotted with standard errors included.

2.15.1 The anaerobic survival of Mtb Δ*cydAB*

The *M. smegmatis* CbdO has been shown to be important for adaptation to reduced oxygen tensions (Kana *et al.*, 2001). Toassess this in Mtb, an anaerobic model described by Tan *et al*. (2010) was used; with the modification that 7H9 liquid medium was used instead of Dubos. The duration of this model is significantly shorter than the Wayne model and allows for the simultaneous assessment of multiple strains (Wayne, 1996, Tan *et al.*, 2010). As a proof-of-concept, the model was first assessed in wild type *M. smegmatis* with and without nitrate. Consistent with reports for this model in Mtb (Tan *et al.*, 2010), there was a decrease in viability over time and nitrate did not appear to have a significant effect on survival (Appendix F, Figure F1), as was previously reported for Mtb when oxygen was gradually depleted (Sohaskey, 2008,

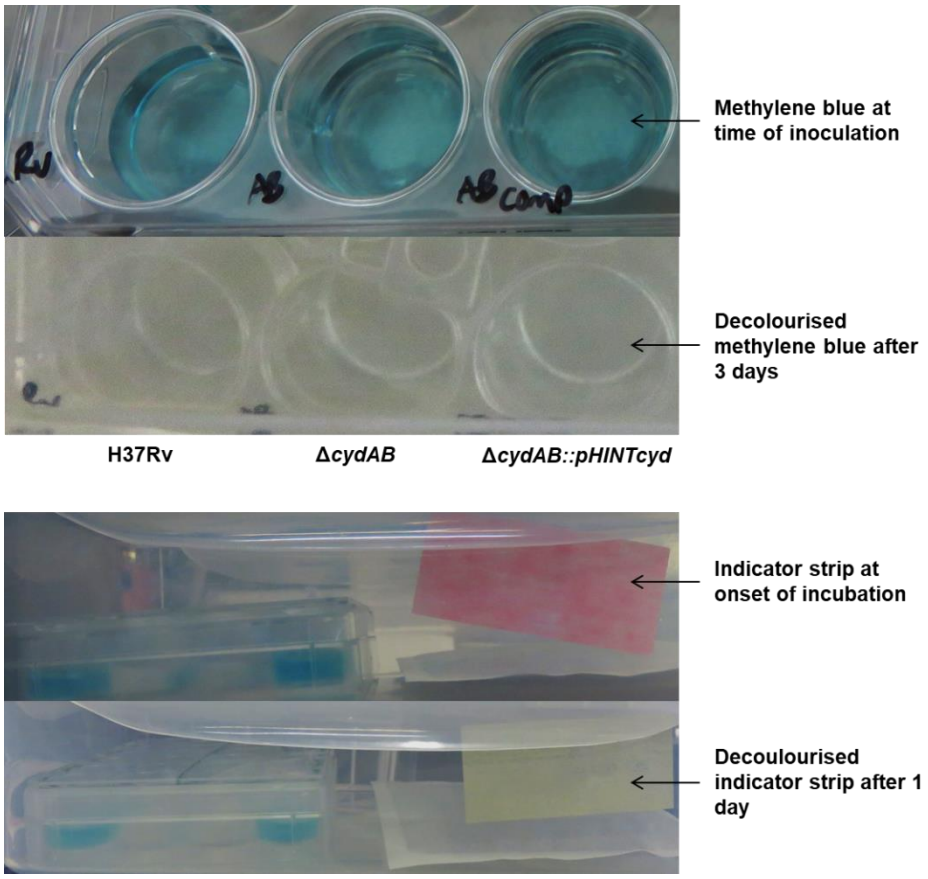


Figure 2.46: Images showing the decolourisation of indicators as oxygen is depleted in the environment and within the cultures. Decolourisation of the pink strip indicates that oxygen has been removed from the environment while decolourisation of methylene blue in control culture wells demonstrates that the available oxygen has been consumed in the culture.

Tan *et al.*, 2010). Based on this result and the previous observations, the model for Mtb was setup without nitrate. The pink indicator strip decolourises when oxygen is removed and indicates that the atmosphere in the container is anaerobic after one day of incubation, shown in Figure 2.46. However, as shown by Tan *et al*. (2010), this model allows for the gradual depletion of oxygen in a culture, evidenced by the discolouration of the methylene blue only after 3 days of incubation, Figure 2.46. We hypothesised that the CbdO-deficient Mtb strain would display a growth defect over time. As such, the experiment was setup to determine the viability of each strain over three weeks. Unexpectedly, Δ*cydAB* did not display a growth defect under the reduced oxygen tensions generated using this model, Figure 2.47. However, in order to make direct comparisons to the result observed in *M. smegmatis* (Kana *et al*., 2001), a better model would be growth in a bioreactor wherein the oxygen levels can be measured and carefully controlled. In addition, based on the results presented in section 2.10.7, the carbon source used for an experiment comparing growth dynamics would need to be carefully determined or, alternatively, multiple carbon sources would need to be tested.

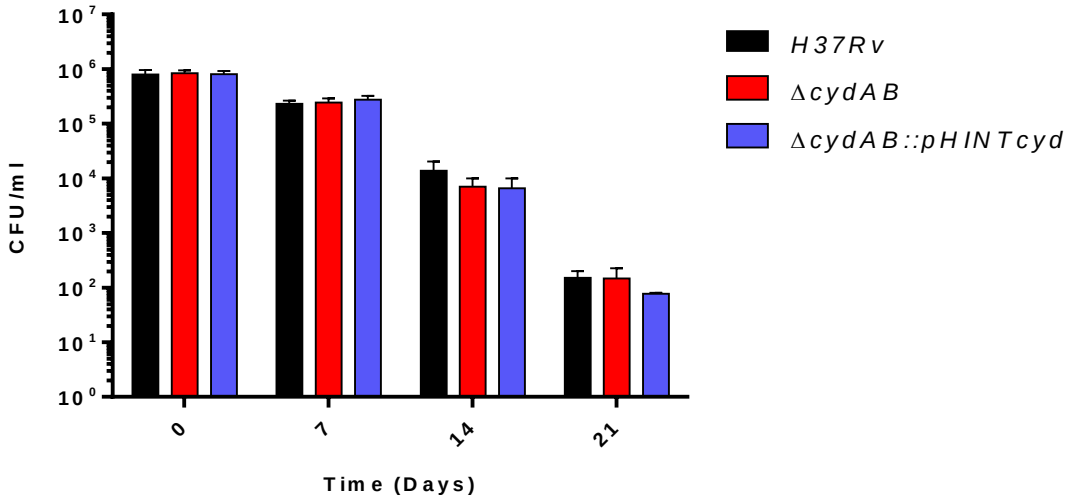


Figure 2.47: The survival of Mtb during an anaerobic growth model. Cultures were grown in 7H9 and incubated in individual sealed boxes containing an Anaerogen pouch which makes the environment anaerobic over ~ 24 hrs. The averages of four independent experiments are plotted with standard error bars.

2.15.2 Loss of the CbO leads to increased susceptibility to oxidative stress in Mtb

It has been demonstrated, in *E. coli* that CbdO plays a role in resistance to oxidative and nitrosative stress. The *E. coli* CbdO was shown to have both catalase and peroxidase activity and the ability to decompose peroxynitrite (Borisov *et al.*, 2010, Borisov *et al.*, 2013). We therefore hypothesized that the mycobacterial strains lacking a CbdO would be more susceptible to oxidative stress. In addition, Small *et al.* (2013), demonstrated that a strain over-expressing *cydAB* displayed hyper-resistance to hydrogen peroxide and this led to Forte *et al.* (2013), hypothesizing that the mycobacterial CbdO is involved in resistance to hydrogen peroxide. We confirmed this hypothesis in both *M. smegmatis* and Mtb, shown in Figure 2.48A and B respectively. A reduction in survival for both the Mtb and *M. smegmatis* CbdO-deficient strains compared to the wild type strains was observed, however the results were only statistically significant for *M. smegmatis*. For unknown reasons in both Mtb and *M. smegmatis*, reintroduction of the genes encoding a functional CbdO did not reverse the phenotype.

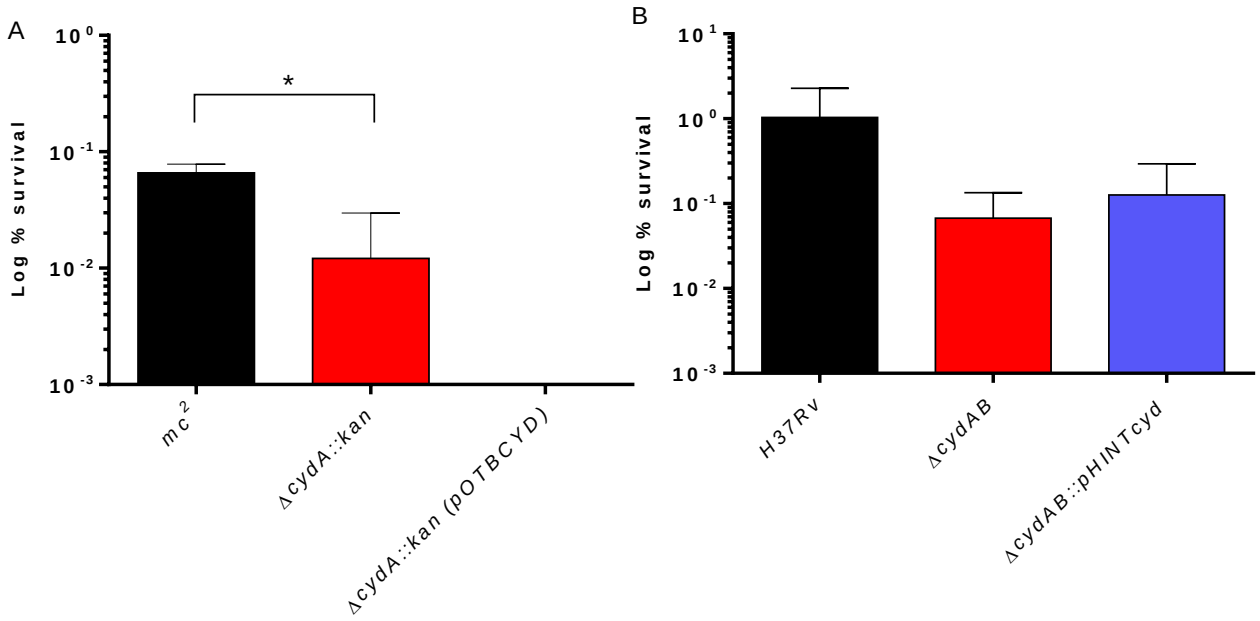


Figure 2.48: The susceptibility of mycobacterial strains to oxidative stress in the form of H_2O_2. (A) *M. smegmatis* strains were exposed to 5 mM H202 and the percent survival after 45 mins was calculated form the CFUs obtained. **(B)** Mtb cultures were exposed to 5 mM H2O2 for 24 hrs, at which point CFUs were determined and percent survival relative to the starting inoculum was calculated. The average of at least three independent experiments is plotted for each strain along with standard error bars. The Student t-test was used for statistical analysis. *P<0.02

To further explore the response to oxidative stress, the production of hydroxyl radicals in these strains was evaluated. Hydroxyphenyl fluorescein (HPF) which fluoresces in the presence of hydroxyl radicals was used to assess oxidative stress in the Δ*cydAB* mutant. In Figure 2.49A it appeared as though the mutant contained higher levels of hydroxyl radicals than wild type in the absence of any stress, however the difference was not statistically significant. The $OH^{\cdot}$ content of Δ*cydAB* was observed to be higher than the wild type and complemented strains in response to H_2O_2 (Figure 2.49B). Thiourea (TU) was included as a control in these experiments for its oxidative stress-quenching properties. Interestingly, the addition of TU significantly reduces the fluorescent signal in Δ*cydA::kan* under normal conditions (Figure 2.49A), implying that oxidative stress is being quenched in this strain to a greater level than in wild type. The results presented in Figure 2.49B demonstrate that TU is able to quench oxidative stress, as observed by a reduction in fluorescent signal in samples containing TU. These results support the increased susceptibility of Δ*cydA::kan* to oxidative stress. When investigated in Mtb, the same observations were made (Figure 2.52), confirming the hypothesis that CbdO is important for resistance to oxidative stress in mycobacteria.

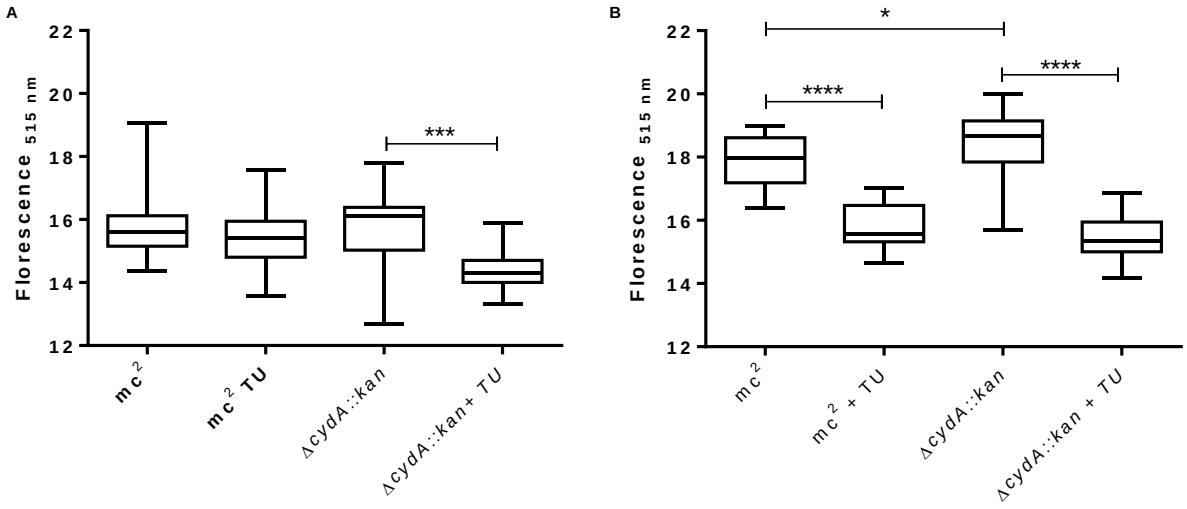


Figure 2.49: The measurement of hydroxyl radicals in *M. smegmatis* cultures exposed to oxidative stress. (A) The production of OD radicals under normal conditions. **(B)** The producton of OG radicals in response to 5 mM hydrogen peroxide treatment. Graphs represent the average of two independent experiments, performed in duplicate. One-way ANOVA was used for statistical analysis. TU- thiourea

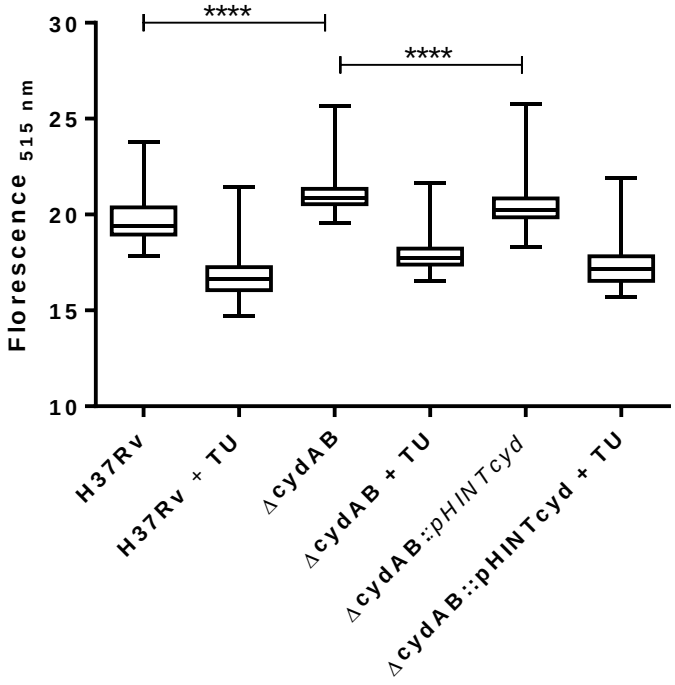


Figure 2.50: Mtb hydroxyl radical measurements with HPF, in the presence of oxidative stress. Graphs represent the average of three independent experiments. One-way ANOVA was used for statistical analysis. TU- thiourea

2.15.3 The growth and survival of Mtb in mouse macrophages

The *in vitro* data presented above indicated that the Mtb CbdO mutant is defective in responding to oxidative stress. To investigate this further, an *ex vivo* infection model with J774 mouse macrophages, where oxidative stress is expected to occur, was setup to evaluate growth and survival. The first set of infection experiments were performed in resting macrophages and no significant difference in growth was observed between Δ*cydAB* and wild type (Figure 2.51A). This suggests that the Mtb CbdOis not required for infection of, and replication within, resting mouse macrophages. A previous study suggested that a functional CbdO is required for survival of Mtb upon activation of the adaptive immune response (Shi *et al.*, 2005). We therefore, assessed the survival of Δ*cydAB* in mouse macrophages that were activated with IFN γ and LPS. It was observed that Δ*cydAB* was attenuated for growth in activated mouse macrophages, although only the Day 2 result was considered statistically significant. These data highlight an important role for the Mtb CbdO during pathogenesis.

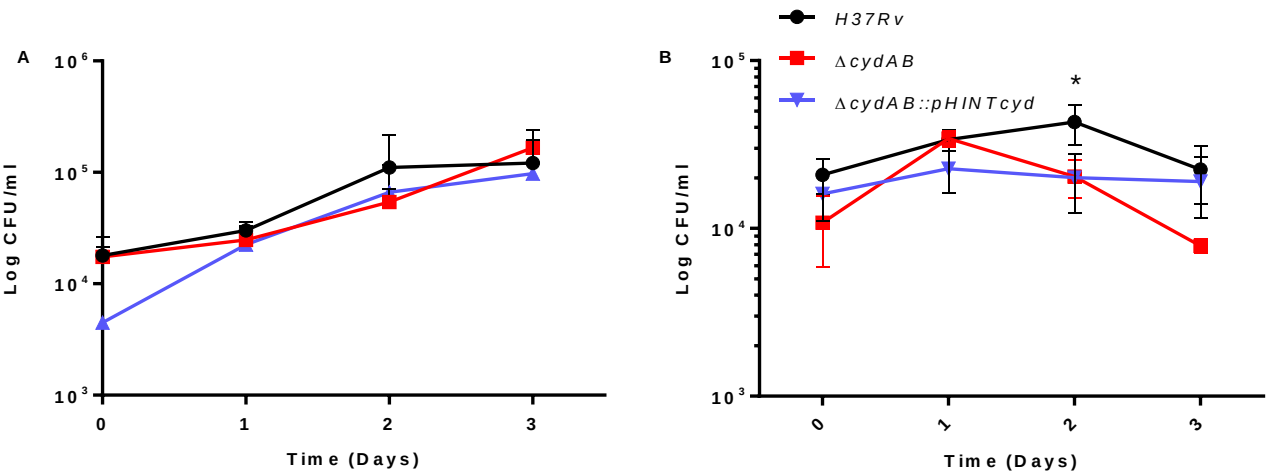


Figure 2.51: The intracellular growth and survival of Mtb strains in J774 mouse macrophages. The average of three independent experiments, each done in duplicate was plotted for each point and standard errors are included. The Student t-test was performed for statistical analysis. *P< 0.03

2.15.4 Loss of CbdO leads to increased susceptibility to drug treatment

Thus far Δ*cydAB* has displayed a range of phenotypes, involved in multiple cellular processes. We therefore sought to determine if the changes in cell metabolism of Δ*cydAB* would have an effect on the susceptibility to drugs. To this end, MIC's were setup with multiple clinically-relevant drugs and compounds known to target energy metabolism. The results listed in Table 2.2 show that loss of CbdO enhanced the susceptibility of Mtb to antibiotics with varying modes

Table 2.2: A list of the MIC's of drugs tested against Mtb.

	H37Rv	Δ*cydAB*	Δ*cydA:B:pHINTcyd*	Fold change (H37Rv/Δ*cydAB*)
Clofazimine (µg/ml)	0,4-0,8	0,2-0,4	0,4-0,8	**2**
Ethionamide (µg/ml)	0,8-1,6	0,2-0,4	0,4-1,6	**2-4**
Rifampicin (µg/ml)	0,0025-0,01250	0,0025-0,025	0,00125-0,025	**2**
Isoniazid (µg/ml)	0,003-0,025	0,003-0,025	0,003-0,05	**-**
Meropenem (µg/ml)	4,0-8,0	2,0-4,0	4,0-8,0	**2**
Bedaquiline (µg/ml)	0,25-0,5	0,125-0,25	0,25-0,5	**2**
Q203 (nM)	~80	<0,039	~80	**>2000**

of action and targets. This result was confirmed by analysis of drug susceptibility in *M. smegmatis*, shown in Table 2.3. Not surprisingly, the greatest increase in susceptibility was observed for Q203 which targets the CcO. The data presented in Figure 2.44, highlighting the alterations in cell wall lipid content of Δ*cydA::kan* may provide an explanation for the decrease in MIC for the cell wall-targeting antibiotics. Furthermore, in Mtb, the increased sensitivity of Δ*cydAB* to ethionamide was not observed for INH, although the drugs share a common target-*inhA*. In contrast, an increased susceptibility to INH was observed for the *M. smegmatis* mutant which may point to additional roles for the CbdO in the non-pathogenic mycobacterium. An increased susceptibility to BDQ was observed in both Mtb and *M. smegmatis*, as previously reported (Berney *et al.*, 2014c). Taken together, the increased susceptibility of Δ*cydAB* to antibiotics with multiple different targets suggests that inhibition of CbdO in Mtb would potentiate the activity of some current clinical drugs. In order to confirm this, drug combination treatment in an infection model with Δ*cydAB* would be useful.

Table 2.3: A list of the MICs obtained for drugs tested in *M. smegmatis*

	mc²	**Δ*cydA::kan***	**Δ*cydA::kan* (*pOTBCYD*)**	***Fold change* (mc² /Δ*cydA::kan***
INH (mM)	0,07686	0,02917	0,04431	**2,6**
BDQ (uM)	0,09313	~ 0,05858	0,07025	**1,6**
CFZ (uM)	0,9511	~ 0,2343	0,2825	**4,1**

* INH- isoniazid, BDQ- bedaquiline and CFZ- clofazimine

Section III conclusion:

- Loss of CbdO leads to increased susceptibility to oxidative stress
- Mtb lacking CbdO is attenuated for growth in mouse macrophages
- CbdO contributes to resistance to different antimicrobial agents

2.16 Discussion

Mtb remains one of the most deadly pathogens, in part as a result of its metabolic flexibility, which allows the bacterium to adapt to and survive under various unfavourable conditions. The most devastating consequence of adaptation is the development of drug resistance, which renders current treatment strategies inadequate in eliminating the disease. Tocombat this, there has been a surge in drug discovery programs with the goal of identifying and developing new drugs, with novel targets that would augment current treatment programs to aid in meeting the global sustainable development goals. To this end, a novel ETC-targeting drug has been developed and conditionally approved for the treatment of DR-TB, BDQ. BDQ targets the ATP synthase enzyme, which in mycobacteria is essential and forms an integral part of the ETC. Furthermore, several other novel compounds targeting different components of the ETC have been identified and shown to be lethal to Mtb. This has highlighted the mycobacterial ETC as a rich area for the discovery of novel drug targets which, when inhibited leads to the efficient killing of mycobacterial cells. As discussed in section 2.4.2, the prokaryotic ETC is inherently flexible. Therefore, a thorough understanding of this area of biology in Mtb would aid in the quest for the discovery of novel drug targets and provide insight into ETC adaptations as a result of inhibition with current and prospective treatment compounds. We therefore aimed to further characterise the mycobacterial ETC by investigating the role of terminal respiratory enzymes of Mtb and *M. smegmatis* in growth and adaptation to different conditions.

The loss of CbdO was shown to have no effect on the growth of *M. smegmatis* under standard laboratory conditions i.e. aerobically in 7H9 supplemented with glucose, glycerol and Tween80 (Kana *et al.*, 2001). In contrast, when assessing the Mtb CbdO mutant under standard laboratory conditions for this strain, we observed that the mutant displayed an increased OD at later time points of the growth curve but no difference in CFUs were noted when compared to wild type. Furthermore, no cell size difference was observed between the mutant and wild type, ruling this out as contributor to the increased OD observed. The standard culturing medium for Mtb is 7H9 supplemented with OADC, glycerol and Tween80. However, during this study tyloxapol was used as a detergent as it was observed to reduce clumping to a greater extent than Tween80 and is also not metabolised as a carbon source. The available carbon sources in this medium were therefore oleic acid, BSA, dextrose

(glucose) and glycerol. As shown in Figure 2.53, the carbon source being metabolised effects the amount of reducing equivalents being produced. Therefore, the availability of additional carbon sources (BSA and oleic acid) could account for the difference in growth dynamics observed between the Mtb and *M. smegmatis* mutant strains. However, a lack of increase in CFUs or cell size in the Mtb mutant suggests that the additional carbon sources do not enhance the growth of Δ*cydAB* and that the increased OD achieved in this strain is attributable to an alternate phenomenon. That the phenotype is specific to the loss of CbdO is not in doubt, as the genetic complementation of this strain results in a growth pattern similar to wild type. Interestingly, early investigations into the effect of oleic acid on mycobacterial growth revealed that the presence of the fatty acid leads to an increase in turbidity of cells as a result of increased intracellular vacuoles, presumably containing readily available stores of the preferred carbon source (Schaefer and Lewis, 1965). If there is an increase in production of these vacuoles in Δ*cydAB* in the presence of oleic acid, this mechanism could explain the observed phenotype. Performing transmission electron microscopy and lipid staining of cultures grown in this medium would provide insight in this regard. Nevertheless, these data do demonstrate an interplay between CbdO and CCM.

The interplay was further confirmed by the decrease in ATP content of Δ*cydAB* when grown in 7H9 containing OADC. The reduction in ATP was also observed in the CbdO mutant of *M. smegmatis*, which contradicts a previous study that showed no difference in ATP content between Δ*cydA::kan* and wild type, even though the mutant displayed a slightly longer lag phase (Lu *et al.*, 2015). However, the measurement of ATP in that study was performed in media containing albumin, glucose and Tween80, which we show in this study to provide a growth advantage to the CbdO mutant. Furthermore, different methods of ATP measurement were used i.e. ATP concentrations were determined based on a standard curve during this study, while Lu *et al*. (2015) presented relative ATP levels based on overall luminescence. Nonetheless, the data presented here demonstrate that loss of the CbdO results in the reduced ability of the ETC to facilitate ATP production. This was supported by the reduced oxygen consumption of Δ*cydAB* when grown in the MGIT system. However, this particular observation was in contrast to the result recently presented by Kalia *et al*. (2017) who demonstrated no difference in oxygen consumption between the wild type and CbdO mutant. However, once again different methods of oxygen consumption were used and the 7H9 growth medium used in that study was supplemented with ADS and Tween80, as opposed to

OADC and tyloxapol used for the experiments mentioned above during this study. This may explain the contradictory results and is further supported by data presented in this thesis where no difference in growth or ATP production between wild type and Δ*cydAB* was noted when grown in 7H9 supplemented with ADS. In the method, used by Lamprecht *et al*. (2016) which measured oxygen consumption in 7H9 supplemented with OADC for ~ 22 mins, no difference was seen between the wild type and mutant strain. However, it cannot be ruled out that a difference would be seen with longer incubation times and furthermore, it was later reported that the strain used was a mutant disrupted in *cydC* and not *cydAB* (Arora *et al.*, 2017), which could account for the disparate results observed between this dissertation study and that of Lamprecht *et al*. (2016).

A connection between CbdO activity and CCM was further demonstrated by the growth curves performed for *M .smegmatis* with different carbon sources. The data from these experiments suggest that the loss of CbdO leads to an increased sensitivity to glycerol, evidenced by the reduced level of growth of the mutant in media containing glycerol, compared to the wild type. This effect is abrogated when BSA is present, due to the presence of albumin, which has been shown to bind methylglyoxal and is generally included in mycobacterial cultivation media for its toxicity-reducing properties (Lynn *et al.*, 1979, Lo *et al.*, 1994). The unregulated metabolism of glycerol leads to an increase in the production of toxic methylglyoxal in *E. coli*, the detoxification of which relies on glutathione-dependent enzymes (Freedberg *et al.*, 1971). Methylglyoxal toxicity has also been observed in Mtb and has been implicated in the MOA of novel pyrimidine-imidazole (PI) compounds, which inhibit bacterial growth only in the presence of glycerol (Pethe *et al.*, 2010, Berney *et al.*, 2012). Interestingly, the mechanism of Mtb growth inhibition by PIs was shown to involve ATP depletion, presumably as a result of the diversion of ATP for glycerol phosphorylation (Pethe *et al.*, 2010). It is therefore reasonable to predict that in a strain which contains reduced ATP levels (Δ*cydA::kan*), the presence of glycerol may be inhibitory due to increased methylglyoxal toxicity and/or diversion of ATP stores for glycerol metabolism thus further lowering ATP levels. In contrast to *M. smegmatis*, the Mtb CbdO mutant does not appear to be sensitive to glycerol. However, only a single concentration of glycerol was tested in Mtb and toxicity may be observed when higher levels of glycerol are present. Tovalidate the glycerol growth inhibition hypothesis and further investigate methylglyoxal toxicity in CbdO-deficient strains, experiments should be performed to determine the MIC of

methylglyoxal and also to evaluate the role of increasing concentrations of glycerol on growth and ATP production in Mtb.

Evaluation of different carbon sources in Mtb revealed attenuation for Δ*cydAB* only in the presence of propionate at later time points. Propionyl-CoA, the oxidation product of propionate has been shown to be toxic to cells as a result of inhibition of CoA-dependent enzymes including PDH (Brock and Buckel, 2004). The toxicity of propionyl-CoA is alleviated by either the methylcitrate or methylmalonyl pathway in mycobacteria (Figure 2.52A and Figure 2.52B respectively), with the latter requiring Vitamin B_{12} supplementation (Munoz-Elias *et al.*, 2006, Upton and McKinney, 2007, Savvi *et al.*, 2008). The reduced ability of Δ*cydAB* to persist with propionate as the sole carbon source therefore suggests that one of these pathways may be disrupted in the mutant. Vitamin B_{12} was not included in the culture medium for these experiments, suggesting that the phenotype can most likely be attributed to the MCC. Metabolomic flux analysis of an ICL–deficient mutant which is unable to grow on propionate, revealed that propionate leads to an increase in 2-methylcitrate and alterations of NAD^+/NADH ratios in that strain (Eoh and Rhee, 2014), thus directly implicating propionate metabolism with respiratory activity. A similar mechanism may prevail in Δ*cydAB,* but to a lesser extent than the ICL mutant. It would therefore be interesting to see if the inclusion of vitamin B_{12} could rescue the observed phenotype.

Overall, the effect of different carbon sources on the CbdO-deficient mycobacterial strains appeared more prominent in *M. smegmatis,* pointing to differences in carbon metabolism between Mtb and *M. smegmatis*. It is worth noting however, that the growth analysis experiments were performed differently between these strains i.e. in a small volume (50 μl) and microtitre plate format for *M. smegmatis,* as opposed to larger volumes (25- 50 ml) in culture flasks for Mtb. The differences in experimental setup could account for the more dramatic phenotypes observed for the CbdO mutant of *M. smegmatis*. Although the experiments were all performed under aerobic conditions, the relative amount of gas available was different for the two experimental setups, and it is possible that the *M. smegmatis* cultures had a reduced oxygen tension. The inclusion of the oxygen indicator methylene blue would have been more insightful for this experimental setup. Nonetheless, the data presented herein do highlight the interplay between CCM and perturbations of the ETC, particularly as a result of removal of CbdO. Further investigation is required to elucidate the

mechanism/s responsible for the observed phenotypes; however the data presented here provide a basis for future experiments.

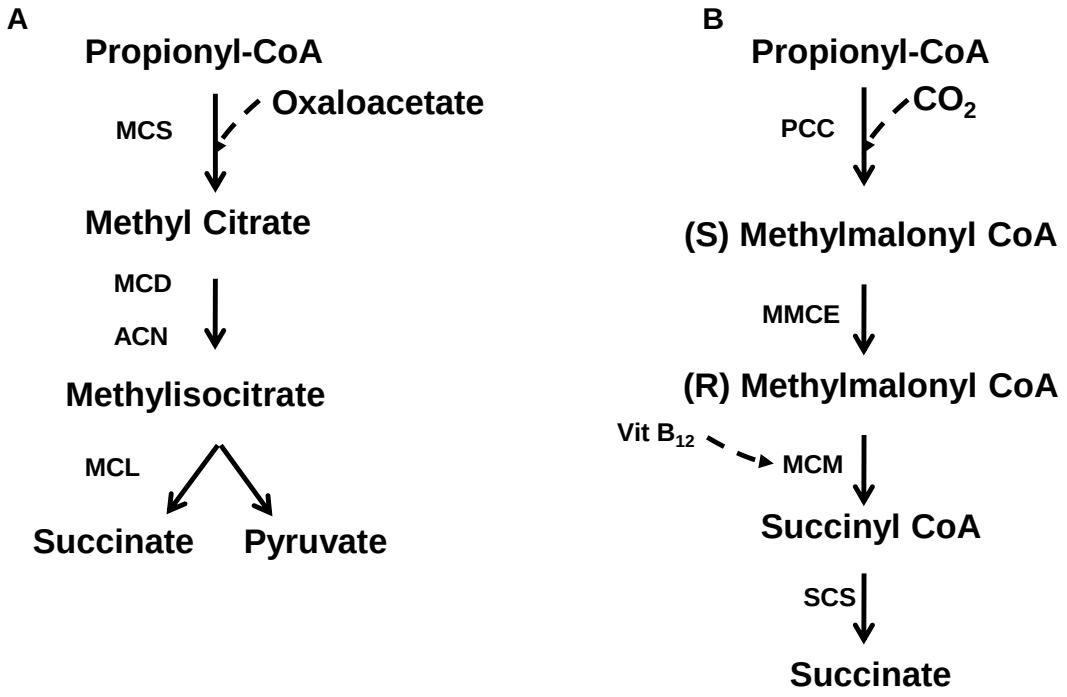


Figure 2.52: Additional CCM pathways involved in the use of propionate as a carbon source. **(A)** The methyl citrate cycle commonly used for propionate metabolism and for anaplerotic functions. **(B)** The methyl malonyl pathway that can compensate for inhibition of the MCC only in the presence of Vitamin B_{12}. MCS- methylcitrate synthase, MCD- methylcitrate dehydratase, ACN- aconitase, MCL- methylisocitrate lyase, PCC- propionyl-CoA carboxylase, MMCE- methylmalonyl-CoA epimerase, MCM- methylmalonyl-CoA mutase, SCS- succinate synthase. Figure adapted from Savvi *et al* (2008).

One of the most intriguing results presented in this thesis was the ability of nitrate to rescue the growth defect and restore ATP production in the *M. smegmatis* strain lacking a functional CcO. Mtb has been shown to respire using nitrate in the presence of oxygen in human macrophages (Cunningham-Bussel *et al.*, 2013b); however, to our knowledge this is the first evidence of nitrate being able to rescue the *in vitro* growth of a mutant defective in aerobic respiratory capacity. In the case of the Δ*qcrCAB*::*hyg* mutant, the strain still retains a fully functional CbdO, which was shown to sustain the growth of this mutant, albeit to a much lower extent than the wild type (Matsoso *et al.*, 2005). An alternative possibility is that reduced viability of the CcO mutant could be due, not only to reduced oxygen utilisation but also to disruption of other metabolic pathways in the cell, which the CbdO cannot

compensate for. In that scenario, perhaps the presence of nitrate is able to rescue the phenotype via an unknown function other than serving as the substrate for nitrate reduction. The ability to utilise nitrate as an electron acceptor for growth suggests that *M. smegmatis* would be able to grow anaerobically in the presence of nitrate; however this was not observed when tested, suggesting that the rescue observed requires at least one functional aerobic respiratory branch. Regardless of the mechanism involved, the ability of nitrate to compensate for the loss of CcO has implications for drug treatment with compounds targeting this complex e.g. Q203. Until now, other researchers have proposed that the presence of CbdO could interfere with the potency of CcO-targeting compounds in Mtb (Arora *et al.*, 2014, Lamprecht *et al.*, 2016, Kalia *et al.*, 2017, Moosa *et al.*, 2017, Berube and Parish, 2018); however we propose that this should be extended to take into account the presence of nitrate when evaluating such compounds. This is particularly important when taking into account the ability of Mtb to utilise the product of host-derived NO as a substrate for NR *in vivo* which facilitates resistance to INH, acid and RNI stress (Tan *et al.*, 2010, Cunningham-Bussel *et al.*, 2013b).

As discussed further below, the medium used for this experiment contained high concentrations of glycerol and therefore it cannot be ruled out that the growth rescue was attributed to this. However, preliminary data wherein 7H9 supplemented with nitrate was used also enhanced the growth of the CcO mutant. In addition, growth curves performed with an increased concentration of glycerol did not significantly enhance the growth of this mutant strain and the reduced growth was observed on 7H10 solid medium, which contains 2.5 x the glycerol used in liquid 7H9. Furthermore, we demonstrated the ability to readily obtain a Δ*qcrCAB* mutant when nitrate was included in the counter-selection medium, thus supporting our hypothesis that nitrate is able to compensate for the loss of a functional CcO in *M. smegmatis*.

In contrast to the stimulation of growth in the *M. smegmatis* CcO mutant, the presence of nitrate appears to be inhibitory for the growth of the *M. smegmatis* CbdO mutant. The role of CbdO oxidase in protection against RNI has been described in other organisms (Borisov *et al.*, 2015, Jones-Carson *et al.*, 2016); therefore, we hypothesised that the observed phenotype could be due to an increase in the production of these toxic intermediates in the presence of nitrate as the sole nitrogen source. Further analysis of the components of the medium used for

this experiment revealed the high concentration of glycerol (10 x more than in conventional medium). Given the results discussed above for different carbon sources, it is also plausible that the reduced growth and ATP content of Δ*cydA::kan* when grown in MPLN could be attributed to the increased glycerol concentration and not the presence of nitrate. To further clarify this phenotype and that of the Δ*qcrCAB::hyg* mutant, growth analysis in the presence of varying amounts of both glycerol and nitrate should be performed, as well as in the presence of an antioxidant which has RNI-quenching properties. In contrast to *M. smegmatis*, the presence of nitrate did not have an effect on the planktonic growth of the Mtb mutant, even in the presence of increased glycerol concentrations, pointing to differences in carbon and nitrate metabolism between the two organisms. Furthermore, the availability of nitrate had no effect on ATP production suggesting that nitrate reduction does not contribute to the PMF under aerobic conditions. However, in the absence of ATP production data from a single *narGHJI* mutant and the Δ*cydAB* Δ*nar* double mutant under the same conditions, these conclusions are largely speculative.

Another striking result presented in this study was the inability of CbdO mutants to form mature biofilms. Biofilm formation in mycobacteria has been relatively well characterised with mutations in several genes being associated with an inability to form biofilms. Including: *groEL1, alf1, pknG, lsr2, pks10* and *pks1* (Recht and Kolter, 2001, Ojha *et al.*, 2005, Chen *et al.*, 2006, Anand *et al.*, 2015, Wolff *et al.*, 2015). The mechanism of biofilm disruption in the majority of these mutants was due to an effect on cell wall lipids. The defective biofilm development of a *groEL1* mutant was attributed to disruptions in mycolic acid synthesis and was supported by the inability of an InhA mutant to form biofilms also (Ojha *et al.*, 2005). An insertion mutant of *alf1* in *M. smegmatis* produced only deacetylated GPLs (Recht and Kolter, 2001), with a GPL TLC profile that looked very similar to that obtained for Δ*cydA::kan*, suggesting that reduced acetylation in Δ*cydA::kan* could be responsible for the biofilm defect. However, the *alf1* mutant did not exhibit the smooth colony phenotype observed for Δ*cydA::kan*, suggesting that other mechanisms may be responsible in a CbdO deficient strain. Performing TLC analysis on GPL samples from Δ*cydA::kan* that have been deacetylated would be useful to explore this further.

The *lsr2* mutant mutant strain displayed reduced biofilm formation and altered colony morphology similar to that obtained for Δ*cydA::kan* (Chen *et al.*, 2006). The phenotypes

observed for the *lsr2* mutant strain were attributed to the inability to synthesise mycolyl-diacylglycerols, which are a type of mycolic acid found in the mycobacterial cell wall (Chen *et al.*, 2006). Lsr2 has since been identified as a global transcriptional regulator that is involved in adapting to reduced oxygen levels in Mtb (Bartek *et al.*, 2014). Interestingly, during a model of rapid anaerobiosis used in that study, it was observed that the loss of *lsr2* leads to a 25- fold upregulation of *cydA*, suggesting that Lsr2 represses CbdO in that model of growth, confirmed by the detection of an Lsr2 binding site in the gene (Bartek *et al.*, 2014). However, a role for Lsr2 in the defective biofilm formation of CbdO mutant strains cannot be deduced from the existing data as *cydAB* forms part of the Lsr2 regulatory network but it is not known if CbdO activity may regulate Lsr2. Although it is plausible that Lsr2 may detect and respond to oxygen levels via the activity of CbdO. In this scenario, the loss of CbdO may impair Lsr2 activity and thus have an effect on the genes controlled by this regulator, such as those genes encoding mycolyl-diacylglycerols, which are required for biofilm formation. However, this is speculative and would require further investigation.

Another area of metabolism implicated in biofilm formation is redox balance. PknG is a serine/threonine kinase, the activity of which is induced by NADH and thus responds to the redox state of the cell (Wolff *et al.*, 2015). Wolff *et al*. (2015) showed that the Mtb *pknG* mutant was unable to form biofilms, had an increased sensitivity to oxidative stress and had reduced survival in macrophages, all reminiscent of the phenotypes observed for Δ*cydAB* mutant in this study. The mechanism proposed was attributed to an inability to regulate redox homeostasis by the hydrolysis of excess NADH via a cascade which is initiated by the kinase activity of PknG (Wolff *et al.*, 2015). As shown in Appendix G, redox balance in Δ*cydAB* is altered with this strain containing high levels of NAD^+. It is possible that this imbalance leads to dysregulation of PknG and could therefore account for the observed biofilm defect. Interestingly, PknG is also involved in regulation of the TCA cycle and specifically induces the activity of α-ketoglutarate decarboxylase and glutamate dehydrogenase via phosphorylation of the inhibitor of these enzymes, GarA (Wolff *et al.*, 2015). An interplay between CbdO and PknG could therefore explain the phenotypes observed on different carbon sources.

An alternate electron carrier, polyketide quinone (PkQ), has been identified and shown to be specifically expressed under hypoxic conditions and in biofilms (Anand *et al.*, 2015).

Disruption of PkQ lead to defective biofilm formation, which was rescued by nitrate (Anand *et al.*, 2015), once again reminiscent of the phenotypes observed for the CbdO mutants. Anand *et al*. (2015) propose that nitrate is able to rescue the biofilm defect by serving as an electron sink, however whether NR was required for this was not determined. The requirement of NR for this rescue can be inferred from the detection of nitrite in biofilm cultures of strains carrying a functional NR but not in a Δ*cydAB* Δ*nar* double mutant. However, the presence of nitrate appeared to stimulate biofilm formation in the double mutant suggesting that an alternate NR-independent mechanism that promotes biofilm maturation exists. In addition, the PkQ mutant was also shown to be more susceptible to antibiotics (Anand *et al.*, 2015). Consistent with the MIC data for planktonic cells, we expect the same to be true for the CbdO oxidase mutants.

Biofilms have increased tolerance to drug treatment and are commonly thought to be similar in characteristic to persistent bacterial infections, as such the activity of drugs in biofilms may provide insight into their activity in the host (Richards and Ojha, 2014). Based on the increased susceptibility to certain drugs of planktonic cultures of CbdO mutants and the associated predicted susceptibility in biofilms, we hypothesised that this mutant would be more susceptible to treatment *in vivo*. This hypothesis was supported by Kalia *et al*. (2017) who show that a CbdO mutant is more susceptible to Q203 and BDQ, as expected based on *in vitro* data obtained during this study and others performed with *M. smegmatis*, Mtb and *M. marinum* (Berney *et al.*, 2014c, Hards *et al.*, 2015, Lu *et al.*, 2015, Lamprecht *et al.*, 2016). In addition to an increased susceptibility to the ETC-targeting drugs BDQ and Q203, the Mtb CbdO mutant was also more susceptible to CFZ, Rif, Eth, D-cycloserine and meropenem. The MIC results obtained during this study for BDQ, Q203 and CFZ are consistent with the current literature in that an increased susceptibility was observed with CbdO mutants. However, variation was observed in the absolute MIC concentrations. The H37Rv MIC obtained for BDQ during this study was between 0.25-0.5 μg/ml, which was comparable to that reported by Berney *et al*. (2014) but significantly higher than 0.03 μg/ml reported by Moosa *et al.* (2017). This discrepancy could be due to the method of scoring utilised i.e. by observation of the presence or absence of a cell pellet during this study vs by the use of Alamar blue by Moosa *et al.* (2017). Taking into account the concentration differences, the fold change in susceptibility observed between the wild type and CbdO mutant was consistent at 2-fold for both studies, confirming a role for CbdO in susceptibility to BDQ as

previously reported (Berney *et al.*, 2014c). A similar pattern was observed for Q203 (Moosa *et al.*, 2017) and CFZ (Lu *et al.*, 2015).

The increased susceptibility of a CbdO mutant to Q203 has been reported before and attributed to complete inhibition of aerobic respiration in this strain (Lamprecht *et al.*, 2016, Kalia *et al.*, 2017). We show that the availability of an alternate electron acceptor restores growth and ATP production in a strain lacking a functional CcO. This suggests that the potency of Q203 may be decreased in the presence of an alternate electron acceptor such as nitrate. This is of particular importance during treatment in the host, as it has been demonstrated that nitrate is available to and important for Mtb during pathogenesis. The results of the Phase II clinical trials with Q203 would shed light on whether the occurrence of this phenomenon is a strong possibility. Until those results are available, it would be interesting to test the susceptibility of the Mtb strains evaluated during this study to Q203 treatment *in vitro* and in a macrophage infection model in the presence of nitrate.

Consistent with the current literature in *M. smegmatis*, we showed that loss of CbdO leads to an increased susceptibility to CFZ (Lu *et al.*, 2015). In addition, we show that this phenotype is also observed in the Mtb mutant. The MOA of CFZ is based on the production of ROS via the activity of NDH (Yano *et al.*, 2011). The increased susceptibility of the CbdO mutant could therefore be as a result of an increased susceptibility to oxidative stress. Supporting this, we observed a reduction in survival of CbdO mutants when exposed to H_2O_2 and an increased amount of hydroxyl radicals present in the mutant strains as a result of H_2O_2 exposure. The role of CbdO in protection against oxidative stress has been well documented in other bacteria (Edwards *et al.*, 2000, Borisov *et al.*, 2013, Leclerc *et al.*, 2015). Notably, in *E. coli* it has been demonstrated that CbdO has both peroxidase and catalase activity, which facilitate protection against oxidative stress (Borisov *et al.*, 2010, Borisov *et al.*, 2013). Whether the mycobacterial enzymes have any of these activities is yet to be determined.

In contrast, we did not observe an increased sensitivity to NO in the Mtb CbdO mutant as has been reported for the *E. coli* mutant (Mason *et al.*, 2009). This could be because of the method used to generate nitrosative stress. During this study, a previously described model based on the predicted production of NO from sodium nitrite in acidified media was used (Firmani and Riley, 2002, Mowa *et al.*, 2009). Whereas for the *E. coli* studies, specific NO-

releasing compounds were used (Mason *et al.*, 2009). Therefore, it cannot be ruled out that CbdO contributes to the susceptibility of mycobacteria to NO.

In addition to being more susceptible to ETC-targeting drugs, the Mtb and *M. smegmatis* CbdO mutants displayed increased susceptiblility to cell wall targeting antibiotics. In *M. smegmatis*, a 2.6-fold difference in susceptibility was observed between the mutant and wild type for INH. The mechanism contributing to this susceptibility in the CbdO mutant could either involve cell wall biosynthesis (based on the altered biofilm formation and colony morphology of the mutant, associated with an altered GPL profile), redox balance (based on the altered NAD^+/NADH ratio shown in Appendix G, Table G1), or a combination of both due to the mechanism of action of INH. INH is a prodrug which is activated by KatG and then forms adducts with NAD^+, which then binds to and inhibits the *inhA* encoded enoyl reductase, which is essential for mycolic acid biosynthesis (Rozwarski *et al.*, 1998). We show here that the *M. smegmatis* CbdO mutant has an altered cell wall lipid profile, particularly GPLs. Based on the biofilm defect and colony morphology of Δ*cydA::kan*, it is also possible that the mycolic acid profile of this strain may be altered as observed in other mycobacterial mutants unable to form biofilms (Ojha *et al.*, 2005, Chen *et al.*, 2006), thus leading to an increased susceptibility to INH. Supporting this, increased sensitivity to INH was observed in a mutant strain unable to form mature biofilms (Anand *et al.*, 2015). The Mtb CbdO mutant displays an increase in NAD^+, which may also be true for the *M. smegmatis* strain. In this case, an increased susceptibility could be attributed to an increase in production of INH-NAD adducts, thus leading to increased inhibition of the target, InhA. However, the Mtb mutant did not display an increased sensitivity to INH and exaggerated colony morphology was not observed for this strain, suggesting that the effect of the loss of CbdO on cell wall lipids is more extensive in *M. smegmatis*. The Mtb CbdO mutant did display and increased sensitivity to Ethionamide, which like INH is a prodrug forming adducts with NAD^+ to inhibit InhA when activated by EthA (Vannelli *et al.*, 2002). Perhaps in the Mtb CbdO mutant, the increased NAD^+ alone is sufficient for increased susceptibility to ethionamide but for INH, further disruption of mycolic acid biosynthesis is required to increase sensitivity to the pro-drug.

Meropenem is a β-lactam antibiotic which targets the D,D-carboxypeptidase involved in peptidoglycan synthesis (Kumar *et al.*, 2012). Mycobacteria generally have an inherent

resistance to β-lactam antibiotics in part due to the presence β-lactamases such as BlaC (Flores *et al.*, 2005), therefore the increased sensitivity of Mtb Δ*cydAB* to meropenem without the inclusion of a β-lactamase inhibitor was intriguing. A recent pioneering study on β-lactams in Mtb showed a marked upregulation of *cydAB* upon treatment with Augmentin (AG), which is a combination of the β-lactam- amoxicillin and the β-lactamase inhibitor-clavulanate (Mishra *et al.*, 2017). Mishra *et al*. (2017) described a mechanism for the activity of AG in mycobacteria and identified redox homeostasis as central to the mechanism. They propose that Mtb initiates a specific cascade of events to become tolerant to AG, which includes the redirection of respiratory activity to the energetically less efficient route where CbdO serves as the terminal electron acceptor; this is coupled with the re-routing of carbon metabolism. They further propose that the rerouting or electrons leads to an increase in ROS, which are then detoxified by the mycobacterial redox buffer, mycothiol (MSH). The redox state of MSH then initiates events which lead to either killing of cells or tolerance to AG, via WhiB4, which when increased leads to repression of the β-lactamase BlaC and the regulator BlaR (Mishra *et al.*, 2017). When WhiB4 levels are decreased, BlaC and BlaR are induced thus leading to degradation of the β-lactam and therefore tolerance to the drug. These data point to a global response to antibiotic stress and highlight the importance of the coordination between the ETC and CCM for this. Furthermore, the expression data reported by Mishra and colleagues identify the CbdO as being important for this response. In this context, the increased susceptibility of Δ*cydAB* to meropenem is not surprising and we hypothesize that the inclusion of clavulanate would further potentiate the activity of meropenem in the mutant strain. It is possible that the rerouting of electrons occurs in response to increased oxidative stress induced by AG. Although the authors mention a downregulation of CcO upon treatment with AG, no data supporting this was presented. If CcO expression is not altered, the induction of CbdO is most likely in response to stress, as opposed to being required for energy generation. However, regardless of the mechanism involved, the data presented by Mishra *et al*. (2017) support our hypothesis that the role of CbdO in mycobacteria is not limited to aerobic respiration but rather extends to a number of processes that facilitate adaptation to different conditions.

The increased expression of CbdO-encoding genes during infection (Shi *et al*, 2005), the attenuation of a mutant disrupted in the putative CbdO assembly machinery in mice (Shi *et al*, 2005; Dhar and McKinney, 2010) and the importance of this enzyme complex for

pathogenesis in other organisms (Way *et al.*, 1999, Edwards *et al.*, 2000, Leclerc *et al.*, 2015, Shepherd *et al.*, 2016), suggests the Mtb CbdO mutant would be important for growth *in vivo*. The inability of this mutant to persist in mouse macrophages, as well as during mouse infections confirms this hypothesis. During the compilation of this thesis a study was published demonstrating that the CbdO mutant survived equally as well as wild type during human cell line infections and during mouse infections (Kalia *et al.*, 2017), which was contradictory to what we observed (Figure 2.51B and Appendix G, Figure G1 respectively for macrophage and mouse infection data). With regards to the macrophage experiments, the biggest difference between the two studies were the cell lines used i.e. J774 mouse macrophage cell line in this study and THP-1cell line used by Kalia *et al*. (2017). Therefore, the disparate results could be as a result of differences in the intracellular environment between the two cell lines, with the THP-1 line being more favourable than the J774 mouse cell for growth of Δ*cydAB*. For the mouse infection studies, both experiments carried out aerosol infections, at a low dose in female BALB/c mice. Therefore a reason for the differences is not likely due to host variability. Perhaps the different phenotypes could be attributed to a difference in the Mtb strains used. This study used H37Rv from the ATCC 27294 laboratory collection, and all Mtb mutants were generated in this background. Kalia *et al*. (2017) used an H37Rv strain; however the origin of this strain was not clarified.

Taken together, the data presented herein highlight a role for CbdO in a number of processes, shown in Figure 2.53. We propose that in the absence of a functional CbdO, the oxygen consumption rate decreases, which leads to an increase in activity of NDH thus producing more NAD^+. The increased NAD^+ creates a more reduced environment, which is more prone to oxidative stress (Vilcheze *et al.*, 2017). As a result of the ability of CbdO to scavange oxygen and oxygen radicals, we predict that in the absence of a functional enzyme, increased oxidative stress would be observed. Furthermore, the increased NAD^+ leads to dysregulation of PknG and possibly WhiB4 via BlaI and this causes disruption of cell wall biosynthetic pathways and CCM. As a result, CbdO mutants become more susceptible to cell wall targeting antibiotics, as well as antibiotics which induce oxidative stress. These perturbations in redox balance, cell wall biosynthesis and CCM in the absence of a functional CbdO suggest that targeting this enzyme would be an effective way to simultaneously impair multiple cellular processes that would potentiate the activity of current drugs, particularly

those targeting the cell wall. In this context, this study has provided a foundation for future investigations into the role of CbdO in mycobacterial physiology.

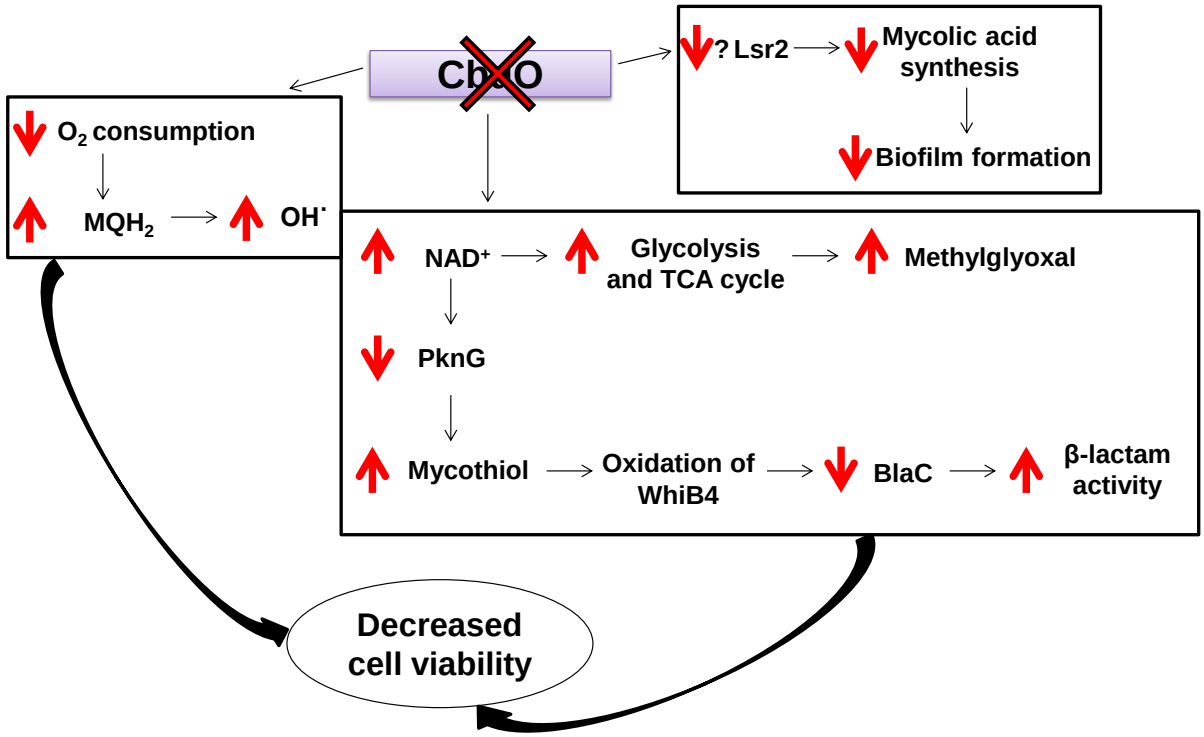
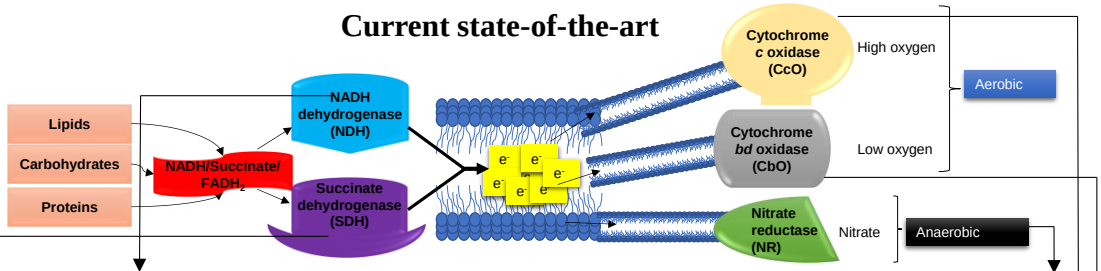


Figure 2.53: Proposed mechanisms for the phenotypes observed in a strain lacking a functional CbdO. We observed reduced oxygen consumption and increased NAD^+ levels in a CbdO mutant. This could lead to increased menaquinol levels, which have been shown to increase oxidative stress in the cell (Vilcheze *et al.*, 2017). Increased NAD^+ levels can increase the activity of glycolysis and the TCA cycle in order to dissipate the cofactor, which could result in the increased production toxic intermediates produced during CCM such as methylglyoxal. Furthermore, disruption of NAD^+ /NADH ratios could lead to a decrease in activity of PknG. This would result in an increase in mycothiol as previously observed (Wolff *et al.*, 2015). Increased mycothiol has been shown to increase the oxidation of WhiB4, resulting in inhibition of BlaC and increased β-lactam activity (Mishra *et al.*, 2017). In addition, the loss of CbdO may interfere with one of its transcriptional regulators, Lsr2 which could lead to a disruption of mycolic acid biosynthesis and thus biofilm formation (Chen*et al.*, 2006, Bartek *et al.*, 2014).

Current state-of-the-art



- NDH-I contributes to apoptosis in the host- Miller *et al.* (2010)
- Both Type II NDH enzymes contribute to ETC activity under different conditions and during infection, with Ndh being essential- Shi *et al.* (2005), Yano *et al.*, (2006), Awasthy *et al* .(2014)
- NDH-II is involved in activity of CFZ- Weinstein *et al.* (2005), Yano *et al.* (2011)

- Contributes to anaerobic survival of Mtb- Sohaskey (2008)
- Protects against RNI and acid stress under hypoxic coniditions- Tan *et al.* (201)

- Essential for aerobic growth- Matsoso *et al.* (2005
- Inhibited by Q203- Pethe *et al.* (2013)
- Mutants disrupted in CcO maturation are attenuated in mice

- Serves as a terminal oxidase that maintains the PMF under hypoxic condtitions- Eoh and Rhee (2013), Hartman *et al.* (2014), Pecsi *et al.* (2014)

- Important for hypoxic growth – Kana *et al.* (2001)
- Compensates for loss of CcO – Matsoso *et al.* (2005), Small *et al.* (2013), Lamprecht *et al.* (2016), Kalia *at al.* (2017)
- CbdO is induced in response to oxidative stress- Boot *et al.* (2017)
- Loss of CbdO potentiates the activity of BDQ, Q203 and CFZ- Lamprecht *et al.* (2016), Kalia *at al.* (2017), Lu *et al.* (2015), Berney *et al.* (2014)
- Mutants unable to assemble CbdO are attenuated and unable to persist following INH treatment- Dhar and McKinney (2010), Shi *et al* (2005)

Key Knowledge Gaps

Does CbdO play a role in ATP generation?

What is the role of CbdO in response to stress?

Is there a role for alternate electron acceptors under aerobic conditions?

What is the role of CbdO in growth on different carbon sources?

Are there other previously undescribed roles for CbdO?

What role does CbdO play in drug tolerance?

Chapter 2- Section I

Chapter 2- Section II

Chapter 2- Section III

What is the role of respiratory and assimilatory NRs in Msm?

Key Findings

Chapter 3

- Yes for both Msm and Mtb
- Associated with reduced oxygen consumption

- Yes, nitrate rescues CcO defect in Msm
- Nitrate reduced growth of CbdO mutant

- Yes, CbdO is involved in biofilm maturation in Msm and Mtb
- Biofilm defects can be rescued by addition of nitrate
- Deletion of CbdO results in an altered lipid profile

- Loss of CbdO gives rise to increased susceptibility to ETC inhibitors and cell wall targeting antibiotics

- CbdO is important for growth on proprionate in Mtb
- CbdO mutant has increased optical density in oleic acid
- Msm CbdO mutant seems sensitive to glycerol

Deletion of both narGHI and narB-encoded NRs did not affect respiratory NR activity

- CbdO seems to be important for survival under oxidative stress
- Mutant experienced increased hydroxyl radicles
- CbdO important for mac survival.

3. Nitrate reduction in *Mycobacterium smegmatis* is not governed exclusively by *narB* or *narGHJI*

3.1 Background

Nitrogen is an essential element for all life, being a vital component of proteins and nucleic acids in both eukaryotes and prokaryotes. The Nitrogen cycle (Figure 3.1) is well characterized and involves the cycling of nitrogen from the atmosphere in various forms through the earth and back. The entire cycle involves different processes including fixation, ammonification, nitrification and denitrification (Thamdrup, 2012). The role of bacteria in the nitrogen cycle is crucial as they are the only organisms capable of carrying out a number of the processes required e.g. denitrification (Moreno-Vivian *et al.*, 1999, Richardson and Watmough, 1999, Thamdrup, 2012). Although nitrogen is abundant in the atmosphere as a gas in a diatomic state (N_2), the triple bond between the two nitrogen atoms requires a large amount of energy to be broken for incorporation of nitrogen into other compounds. More readily available sources of nitrogen include inorganic nitrate-containing compounds, urea, ammonia and proteins/amino acids. Nitrate reduction is considered the most important stage of nitrogen turnover in the nitrogen cycle and this reaction is catalysed by nitrate reductase (NR) enzymes (Morozkina and Zvyagilskaya, 2007).

Prokaryotic NR's are mononuclear Molybdenum-containing enzymes and are assigned to one of three classes based on the ultimate purpose of the nitrate being reduced as well as the location within the cell (Moreno-Vivian *et al.*, 1999). Assimilatory NR's found in the cytoplasm are commonly referred to as Nas enzymes and result in the incorporation of nitrogen into cellular material thus directly contributing to growth (Moreno-Vivian *et al.*, 1999, Richardson *et al.*, 2001, Gonzalez *et al.*, 2006). Dissimilatory or periplasmic NR's, known as Nap enzmyes are generally involved in redox balancing via electron transfer without directly contributing to the generation of a proton motive force (PMF), however Nap enzymes can serve as a respiratory enzyme in bacteria which lack the respiratory NR, Nar (Moreno-Vivian and Ferguson, 1998, Moreno-Vivian *et al.*, 1999, Hille *et al.*, 2014). Nar enzymes are similar to their dissimilatory counterparts in that they are involved in electron transfer, however the electron flow through respiratory NR's is coupled with proton translocation and thus the generation of a PMF across the cytoplasmic membrane and energy

production (Gonzalez *et al.*, 2006, Hille *et al.*, 2014). Common to all three NRs is a catalytic site made up of the molybdenum cofactor (MoCo), specifically *bis*-molybdopterin guanine dinucleotide (*bis*-MGD) and iron-sulfur clusters, usually of the type [4Fe-4S] however, a distinct series of steps is followed for nitrate reduction by each enzyme (Gonzalez *et al.*, 2006).

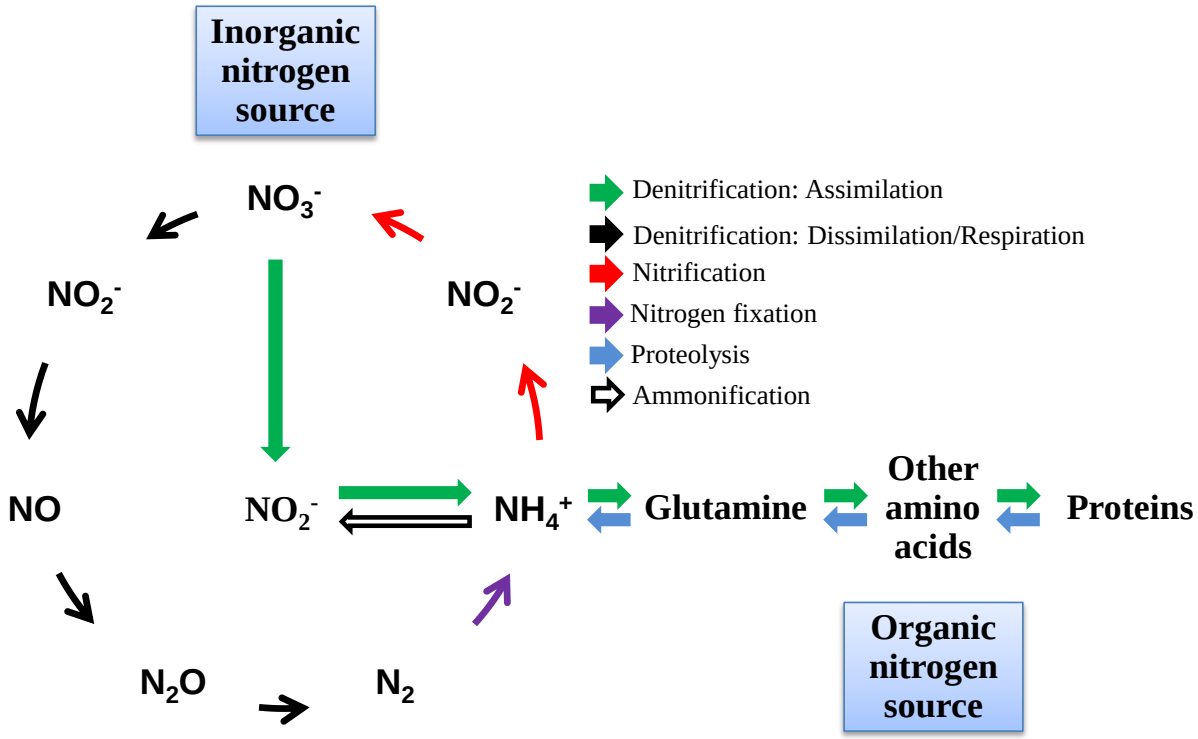


Figure 3.1: A schematic representation of an example of the Nitrogen cycle in prokaryotes. Different prokaryotic organisms are able to catalyse each of the reactions depicted. Figureadapted from Morozkina and Zvyagilskaya (2007).

The respiratory NR is a trimeric enzyme made up of the subunits NarG, NarH and NarI, shown in Figure 3.2A. In *Escherichia coli* during the catalytic reaction electrons are donated to NarI from the menaquinol (MQH_2) pool and this is coupled with the transfer of two protons into the periplasm (Gonzalez *et al.*, 2006). The two electrons are then transferred to *bis*-MGD for the reduction of nitrate to nitrite, in the process consuming two cytoplasmic protons and thus generating a PMF (Gonzalez *et al.*, 2006). An overview of the electron transfer pathway in NarGHI is shown in Figure 3.2A.

There is a large degree of heterogeneity in the gene clusters encoding Nap proteins among different bacteria, with the number of genes involved ranging from five to seven (Richardson *et al.*, 2001, Gonzalez *et al.*, 2006). The catalytic site of Nap is located in the NapA subunit in the periplasm and therefore electrons for nitrate reduction need to be transported from the electron pool in the membrane to NapA. There are two proposed pathways of electron transfer for Nap, depicted in Figure 3.2B (Richardson *et al.*, 2001, Gonzalez *et al.*, 2006, Morozkina and Zvyagilskaya, 2007). The first pathway is used for nitrate respiration in bacteria, which lack Nar. During this pathway electrons are obtained from the ubiquinol pool and are transferred to the catalytic site of the enzyme sequentially via three different proteins with metal centres i.e. NapH, NapG and NapC. NapC transfers electrons to NapB, which then donates the electrons to NapA or in the case of organisms which lack NapB, NapC transfers the electrons directly to NapA (Gonzalez *et al.*, 2006). The alternative pathway is present in bacteria which lack the *napH* and *napG* genes but do encode NapC. In this case, electrons are obtained from MQH_2, as NapC is unable to use UQH_2, and transferred directly to NapA or via NapB. The reduction of nitrate does not contribute to the PMF during this pathway but rather serves as a way to eliminate excess reducing equivalents (Gonzalez *et al.*, 2006).

Similar to the *nap* genes, the assimilatory *nas* genes are found clustered in operons of different compositions (Luque-Almagro *et al.*, 2011). These gene clusters are made up of different combinations of genes encoding a single-subunit or hetero-dimeric assimilatory NR, nitrite reductase genes, nitrate/nitrite transporter genes, genes which encode accessory proteins as well as regulatory genes (Richardson *et al.*, 2001, Gonzalez *et al.*, 2006, Luque-Almagro *et al.*, 2011). There are two classes of assimilatory NR's present in bacteria, which differ according to the electron donor required i.e. either NADH or flavo/ferridoxin (Moreno-Vivian *et al.*, 1999, Gonzalez *et al.*, 2006). Furthermore, although all assimilatory NR's contain *bis*-MGD, they are distinguished in different organisms based on the number and composition of subunits and on electron transfer cofactors bound to the different subunits. For example, the catalytic subunit, NasA from the hetero-dimeric enzyme in *Klebsiella oxytoca* contains one [4Fe-4S] centre and one [2Fe-2S] centre; whereas the catalytic subunit from the hetero-dimer in *Bacillus subtilis* is NasC and contains only a single [4Fe-4S] cluster (Richardson *et al.*, 2001). In contrast, the assimilatory NR from *Azotobacter vinelandii* and the *Cynaobacteria* genus is a monomeric enzyme, referred to as NarB in the latter (Gonzalez *et al.*, 2006). In both cases, only a single [4Fe-4S] centre is present. The *A. vinelandii* enzyme

can only utilize flavodoxin as an electron donor, while C*yanobacteria* are able to use both flavodoxin and ferridoxin (Gonzalez *et al.*, 2006). An example of the electron flow for the single subunit NarB and the heterodimer made up of NasA and NasC are shown in Figure 3.2C. Nitrate assimilation is tightly regulated in bacteria with the reduction of nitrate being closely coupled to nitrite reduction and/or transport, evidenced by the presence of genes encoding proteins for these processes in the the same operon as assimilatory NR encoding genes (Luque-Almagro *et al.*, 2011). The fate of nitrogen from nitrate assimilation generally is to be incorporated into other biomolecules; however, the products of nitrate assimilation could either serve as substrates for further reductive reactions or could be transported out of the cell. The fate of these products depends on the organisms collection of proteins required to perform the reactions as well as the biological needs of the cell at that time.

The physiological role of each NR enzyme is specific, suggesting that the functions of each do not overlap. This is confirmed in the organisms *Paracoccus denitrificans* (Sears *et al.*, 1997) and *Alcaligenes eutrophus* (Siddiqui *et al.*, 1993), which both possess one of each of the three NR enzymes. However, Mtb contains the respiratory NarGHI, which has been shown to fulfil the role of both assimilatory and respiratory NR (Malm *et al.*, 2009). Although a second "fused' respiratory NR, NarX, is annotated in Mtb, no function has been assigned to the protein (Sohaskey and Wayne, 2003). Nitrate reduction is important in Mtb with several lines of evidence implicating NR activity in the virulence and pathogenesis of Mtb (Gouzy *et al.*, 2014) thus highlighting the need for a thorough understanding of nitrogen metabolism in mycobacteria.

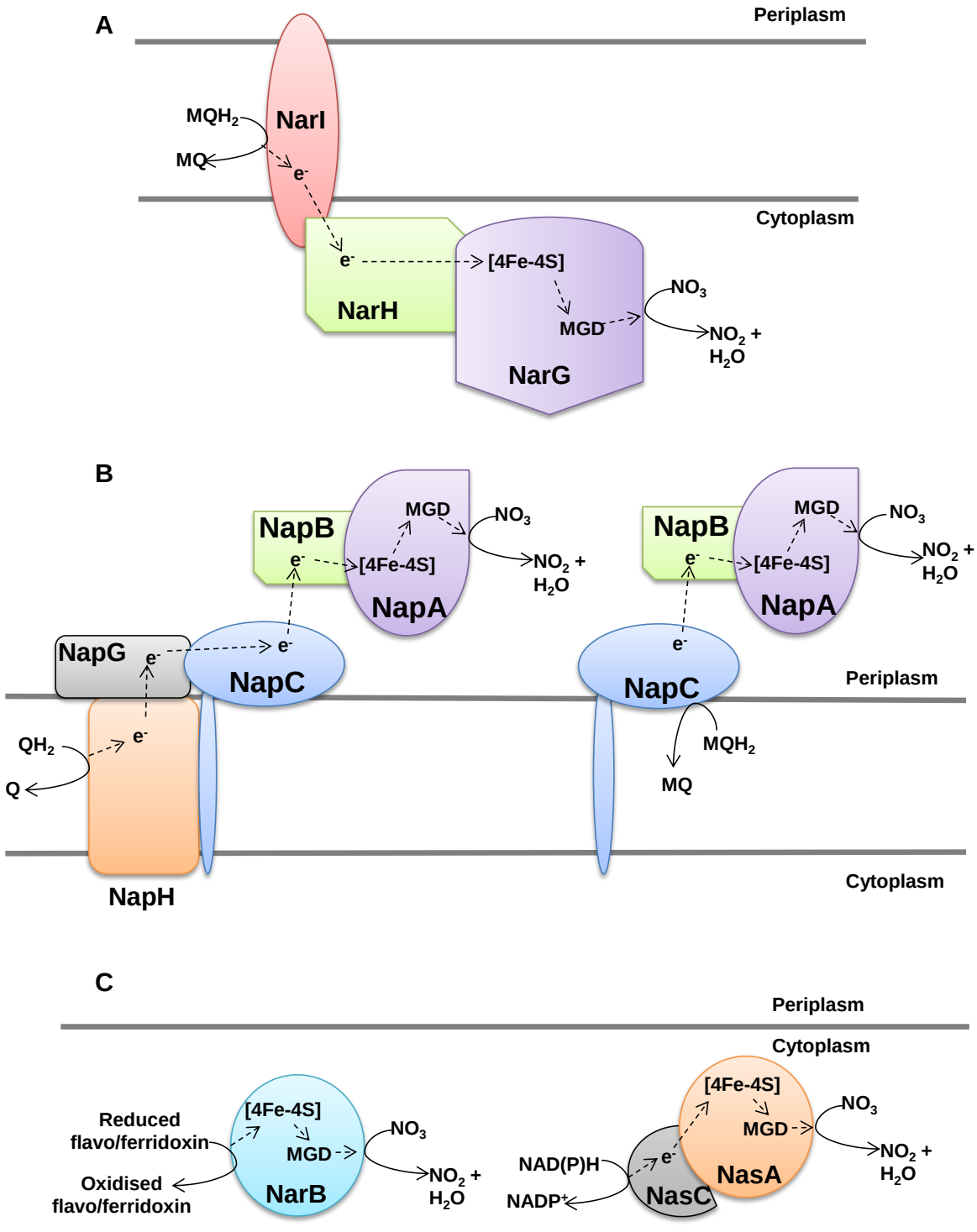


Figure 3.2: A schematic representation of the electron transfer reactions in the different types of NRs. (A) Electron transfer in the respiratory NarGHI NR. **(B)** The two catalytic mechanisms of the dissimilatory NR, Nap **(C)** The catalytic reaction of the single-subunit assimilatory NR, NarB and the two subunit NasA-NasC enzyme. The figure was adapted from Richardson *et al* (2001), Gonzalez *et al* (2006) and Morozkina and Zvyagilskaya (2007)

In contrast to Mtb, *M. smegmatis* possesses two putative NR-encoding genes i.e. the *narGHJI* operon and *narB*, the latter is proposed to encode an assimilatory NR (Khan *et al.*, 2008). NR activity in *M. smegmatis* was first demonstrated by Khan and Sarkar (2006) using inhibitors of NR and the Wayne model. In contrast to previous studies (Weber *et al.*, 2000, Williams *et al.*, 2011), Khan and Sarkar (2006) demonstrate that *M. smegmatis* is able to accumulate nitrite under anaerobic conditions and attributed this to the activity of a respiratory-type NR. In a follow up study, a nitrate assimilation pathway was proposed in *M. smegmatis* (Khan *et al.*, 2008). Once again, the authors used inhibitors of NR together with a specific growth assay wherein the nitrogen source can be defined (Khan *et al.*, 2008). The authors demonstrated that *M .smegmatis* was able to assimilate (as sole nitrogen sources) asparagine, nitrate, nitrite and ammonium under aerobic conditions; while under anaerobic conditions *M. smegmatis* was able to utilize nitrate, nitrite and ammonium (Khan *et al.*, 2008). Furthermore, based on inhibition of growth by sodium azide and $_{L}$-methionine sulfoxamine ($_{L}$-MSO) only in the presence of nitrate, the importance of NR activity in the Wayne model of dormancy was also highlighted (Khan *et al.*, 2008). However, Khan and Sarkar (2012) later alluded to the non-specificity of the inhibitors used and were unable to rule out the presence of an alternative respiratory and/or fermentative pathway which facilitated growth under the conditions tested.

The assimilation of nitrate by *M. smegmatis* was later confirmed by Williams *et al.* (2011) and Narrandes *et al.* (2015), who used the growth assay as a readout for MoCo biosynthesis. The authors demonstrated that *M. smegmatis* strains lacking a functional MoCo biosynthetic pathway were unable to assimilate nitrate, presumably due to the lack of the catalytic MoCo cofactor in a NR enzyme (Williams *et al.*, 2011, Narrandes *et al.*, 2015). Both NarB and NarGHI are annotated as MoCo-dependent enzymes, therefore abrogation of MoCo biosynthesis would disrupt the function of each enzyme, thus making it difficult to determine which is responsible for growth on nitrate as the sole nitrogen source.

3.2 Aims and objectives

Given the results presented in Chapter 2 of this thesis, nitrate reduction seems to contribute to the adaptable nature of the mycobacterial ETC. Given this interplay between aerobic and alternate electron acceptors, we therefore endeavoured to investigate nitrate metabolism further in *M.* smegmatis, wherein this pathway may be different to Mtb. We sought to do this by using the available mutant strains i.e. Δ*narB*, Δ*narGHJI* and Δ*narB* Δ*narGHJI* for which preliminary data already existed suggesting that NR reductase activity is retained in these strains (Narrandes, 2013).

The primary aim of this chapter was to evaluate the contribution of each annotated NR-encoding genes in *M. smegmatis* to nitrate assimilation and respiration.

The specific objectives included:

- The measurement of NR activity under aerobic conditions
- The complementation of the mutant strains with *narB*
- Gene expression analysis of the putative NR-encoding genes in the presence and absence of nitrate
- The evaluation of survival under anaerobic conditions and
- To assess the ability of the mutant strains to form biofilms

3.3 Methods

3.3.1 Nitrate utilisation

Nitrate utilization was measured using the Griess assay, which is based on the production of a red diazonium dye from the reaction of nitrite with naphthylamide under acidic conditions. This assay therefore relies on the availability of nitrite in the sample being tested. As mentioned previously nitrate reduction could lead to the export of nitrite outside the cell, in which case a positive Griess result is observed. Alternatively, nitrite is further assimilated into ammonia or reduced to nitric oxide which leads to a negative Griess result. Therefore, a negative Griess result does not necessarily represent a lack of NR activity. Zinc rapidly reduces nitrate to nitrite (Angeby *et al.*, 2002). A colour change upon the addition of zinc to a sample containing the Griess reagents demonstrates that nitrate is still present and thus a lack of or reduced NR activity can be concluded. The addition of zinc leads to no colour change when all nitrate has been utilized, thus confirming NR activity. This method can be exploited to quantify the amount of nitrite present in a sample by generating a nitrite standard curve with absorbance values at $\lambda_{max530nm}$. In addition, the rate of nitrate utilization can be determined.

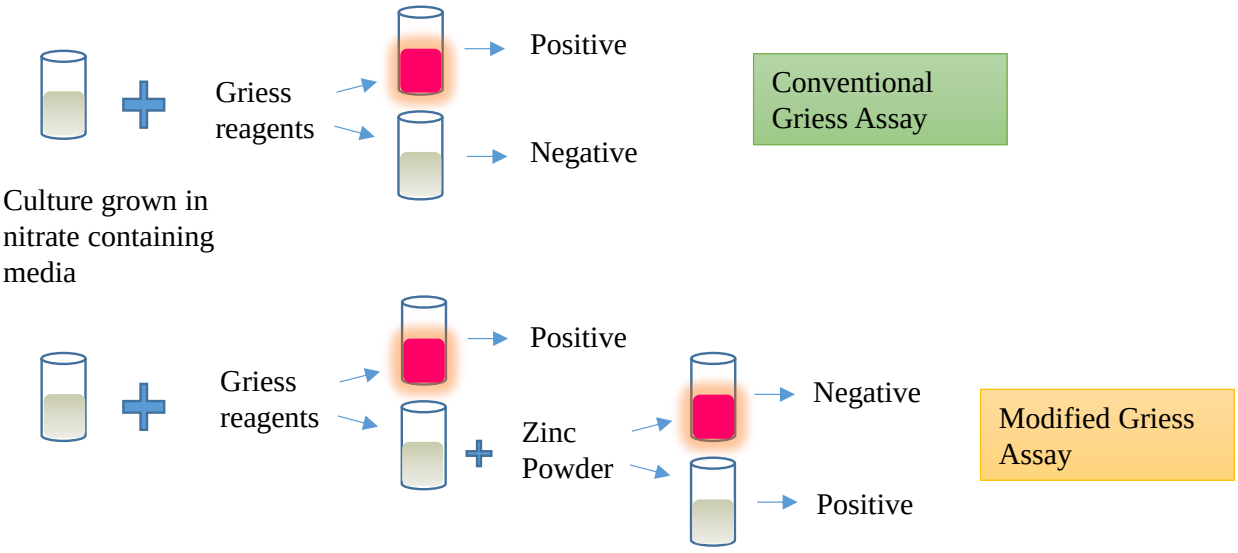


Figure 3.3: A diagram outlining the Conventional and Modified Griess assays used during this study. The conventional Griess assay involves the visualisation of samples following the addition of the Griess reagents. A pink colour represents positivity for nitrate reduction, while no colour change is generally considered negative. In the modified Griess assay, a second step is included for sample the had no colour change during the conventional assay. Upon the addition of zinc, a colour change to pink is indicative of no NR activity and a sample is then classified as NR negative. No colour change after the addition of zinc represents complete nitrate utilisation and thus NR positivity.

To investigate nitrate utilization *M. smegmatis* cultures were inoculated into MPLN and incubated until stationary phase. The Griess assay was performed at the time of inoculation and once cultures had reached the stationary phase, as described by Weber *et al.* (2000) with minor modifications, Figure 3.3. Briefly, 100 µl of 1 % sulfinilic acid and 100 µl of 1 % *N*-(1-Naphthyl) ethylenediamine dihydrochloride (NEDD) were added to 1 ml of culture and mixed thoroughly. In those samples wherein no colour change was observed, a few grains of zinc powder was added, mixed thoroughly and incubated for 5 min at room temperature. As indicated previously, this step was included to ensure that no nitrate remained in the medium. The samples were then clarified by centrifugation at 12 470 x *g* and the absorbance of the supernatants were measured at 530 nm and compared to known standards of nitrite (0.1 nM-1000 nM).

3.3.2 Anaerobic growth

Cultures were grown in MPLN overnight to early-log phase. These cultures were used to inoculate 2 ml MPLN in 10 ml culture tubes to OD 0.05 in duplicate. An aliquot was taken from each tube to determine the starting CFU and one set of tubes was incubated at 37 ºC with no shaking. The other set of tubes were placed in the Oxoid AnaeroGen chamber, which creates an anaerobic environment. Once the indicator showed that the environment was anaerobic, the chamber was incubated at 37 ºC with no shaking. After 7 days an aliquot from each tube was plated to determine CFU.

3.3.3 Construction of *narB* complementing vector

A complementing vector carrying *narB* under the control of the constitutive promoter *hsp60* was constructed. The gene region was amplified using the primers narBF and narBR (listed in Table A3). The PCR product was digested with *Hind*III and *Hpa*I and ligated with the *Hind*III/*Hpa*I linearised vector, pMhsp60. Transformants were selected for on LA plates supplemented with hygromycin. Ten possible clones were selected from the LA plates following an overnight incubation and were screened by restriction digest to confirm the presence of the insert. A single positive clone was then screened further by restriction analysis (Appendix E, Figure E1) and subsequently sent for sequence analysis to ensure that no mutations had been introduced into the promoter or coding region. This vector was then electroporated into the mutant strains, Δ*narB,* Δ*narGHJI* and Δ*narB* Δ*narGHJI* and selected

on 7H10 plates supplemented with hygromycin. Positive clones were confirmed by PCR analysis with the screening primers listed in Table A3 (narScreenF, narScreenoutR, narScreenGR, narBScreenout, narBScreenF anf narBScreenR).

3.3.4 RNA extractions

RNA extractions were performed using the Macherey Nagel NucleoSpin RNA extraction kit following the manufacturer's instructions with slight modifications. Approximately 9 ml of exponential phase cultures were used for RNA extractions. Cultures were pelleted by centrifugation at 2360 ×*g* for 10 mins, the supernatant was removed and the cell pellet re-suspended in 500 µl TE buffer. Lysozyme (10 mg/ml) was then added to the cell suspension and incubated at 37 ˚C for 30-60 mins. This was followed by the addition of buffer RA1 and β-mercaptoethanol and the transfer of the cell suspension to Lysing Matrix B (IEPSA) tubes which contain 0.1 mm silica beads. The mechanical lysis of cells was then performed in the MagnaLyser (Roche) ribolyser with three rounds of ribolysing at 6000 rpm for 30 sec each and a 3 min incubation on ice between each round. Tubes were then centrifuged briefly to pellet the beads and the supernatant was used for extraction following the manufacturer's protocol.

3.3.5 DNase treatment

In addition to an on-column DNase treatment, 1 µg of RNA was treated with Turbo DNase following the protocol from the TURBO DNA-*free*™ Kit (Ambion) to remove trace amounts of DNA in the sample. Briefly, reactions contained 2.5 µl 10× TURBO DNase buffer, 1.5 µl TURBO DNase, 1 µg RNA, and were made up to 25 µl with nuclease-free sdH_2O. Reactions were mixed by gentle flicking of the tubes and incubated at 37 ˚C for 30 mins. This was followed by inactivation of TURBO DNase by the addition of 2.5 µl DNase Inactivation Reagent and incubation at room temperature for 5 mins with intermittent flicking to disperse the inactivation reagent. The inactivation reagent was then pelleted by centrifugation at 10 000 × *g* for 5 min and 23 µl of the supernatant containing RNA was transferred to a clean tube. A reverse primer mix was prepared containing 0.5 µM of each required reverse primer and 2 µl of this mix was added to the DNase-treated RNA. The following protocol was followed to anneal the reverse primers to the treated RNA: 90 sec denaturation at 94 ˚C; 3

min anneal at 65 ˚C and 3 min at 57 ˚C. The RNA with annealed reverse primers was used immediately for cDNA conversion as described below.

3.3.6 cDNA conversion

SuperScript™ III Reverse Transcriptase (Invitrogen) was used to produce cDNA following the manufacturer's instructions. Each reaction contained the following components: 5 µl 5× First-Strand Buffer, 4 µl 25 mM $MgCl_2$, 2 µl 0.1 M DTT, 1 µl dNTP mix (10 mM of each dATP, dCTP, dGTP and dTTP), 0.8 µl SuperScript™ III and 12.5 µl RNA. In parallel, reactions were setup without SuperScript™ III enzyme in order to monitor DNA contamination (RT-free control). Reactions were incubated at 50 ˚C for 60 mins and inactivated by heating at 70 ˚C for 15 mins.

3.3.7 Quantitative Real-Time Polymerase Chain Reaction – q(RT)PCR

PCR reactions were setup with the cDNA prepared as described above. Reactions contained the following components: 10 µl SsoFast™ Evagreen® Supermix (Bio-Rad), 0.75 µl each of 10 mM forward primer and reverse primer, 2 µl cDNA and 6.5 µl sdH_2O. Reactions were run on the Bio-Rad CFX96™ Real-Time PCR Detection System with the following parameters: An initial enzyme activation at 95 ˚C for 30 secs; 40 cycles of 5 secs denaturation at 95 ˚C and 5 secs annealing/extension at 60 ˚C. Melt curves were generated between 65-95 ˚C in 0.5 ˚C increments with 5 secs per step. Gene expression data was analysed with the CFX Manager Software. Standard curves were generated for each target gene in each experiment and the expression of target genes was always normalised to the house-keeping gene *sigA* for both Mtb and *M. smegmatis*.

3.4 Results

3.4.1 Confirmation of strains used

The mutant strains Δ*narB,* Δ*narGHJI* and Δ*narB* Δ*narGHJI* described in this chapter were previously generated. A brief description of how they were constructed and the original Southern blots performed to confirm the genotype of each mutant strain are shown in Appendix D2. The PCR confirmation of each strain used during this study is shown in Appendix E, Figure E2.

3.4.2 *M. smegmatis* NarGHI is dispensable under anaerobic conditions

NarGHI is a respiratory enzyme which serves as the terminal electron acceptor under anaerobic conditions when nitrate is available, thus facilitating growth and/or survival. It has been shown that *M. smegmatis* is able to survive under anaerobic conditions in the presence of nitrate (Khan and Sarkar, 2006). We therefore set out to determine if, like in Mtb (Tan *et al.*, 2010), NarGHI is important for survival under anaerobiosis. No differences in growth were observed between the strains grown under aerobic conditions in MPLN for seven days (Figure 3.4A), consistent with the growth curve results previously reported (Narrandes, 2013). All the *M. smegmatis* strains tested were able to survive equally well under anaerobic conditions in MPLN for seven days, Figure 3.4B. As expected, reduced growth was observed under anaerobic conditions compared to the aerobically grown cultures with CFU fold change ranges between 4.5- 10 and 20- 32 respectively, Figure 3.4C. However, no differences were noted between survival of strains under these conditions. These data provide evidence that the loss of NarB and NarGHI does not attenuate the survival of *M. smegmatis* under aerobic or anaerobic conditions.

3.4.3 NarB and NarGHI are not required for biofilm formation

As described in section 2.15.5, biofilm formation can serve as a model for growth under reduced oxygen tensions. Tovalidate the result presented in Figure 3.4B and rule out that the lack of a phenotype was because of the model used, biofilms were setup for the mutant strains. The images depicted in Figure 3.5A demonstrate that neither mutant had a reduced ability to form biofilms, thus further confirming the results observed in Figure 3.4B. Interestingly, when 7H10 plates were used for CFU determination for the starting inoculum

for the biofilms, we noted that Δ*narB* and Δ*narB* Δ*narGHJI* were more pigmented than the wild type strain, shown in Figure 3.5B.

To confirm that this phenotype was caused by the loss of *narB*, we designed a complementing vector which would express *narB* from the constitutive *hsp60* promoter, which is commonly used for complementation in mycobacteria. The vector was generated as described in section 3.2.3. The resulting vector, pMnarB was first confirmed by restriction analysis (Appendix D, Figure D2) and then by sequencing. Once confirmed, the vector was introduced into Δ*narB* and Δ*narB* Δ*narGHJI* by electroporation to generate the strains, Δ*narB* (pMnarB) and Δ*narB* Δ*narGHJI* (pMnarB) respectively. The set of strains used for

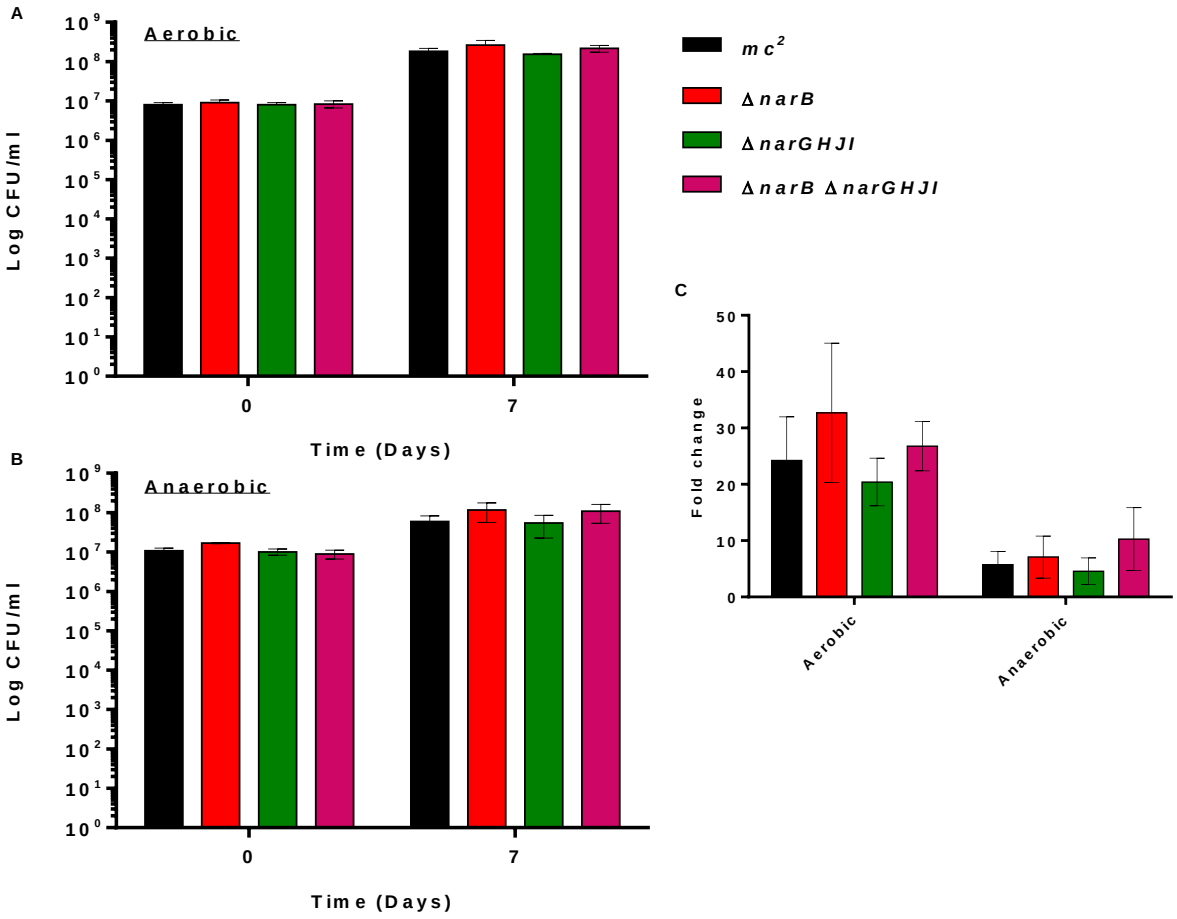


Figure 3.4: Survival of *M. smegmatis* under anaerobic conditions in the presence of nitrate. (A) The increase in biomass of *M. smegmatis* strains grown aerobically in culture tubes for 7 days. **(B)** The increase in biomass of strains incubated anaerobically in an Oxoid chamber for 7 days. **(C)** A comparison of the aerobic versus anaerobic biomass fold change after 7 days. The fold change was determined by dividing the CFU obtained on Day 7 by the CFU obtained on Day 0 for each strain. The averages of three independent experiments are plotted with standard errors depicted.

subsequent experiments was confirmed by PCR analysis, using primers specific for *narB* and *narGHJI*, listed in Table A2. The gels shown in Figure D1A and D1B (Appendix D) confirmed that all the strains used were correct and that the complemented strains were carrying the appropriate vector.

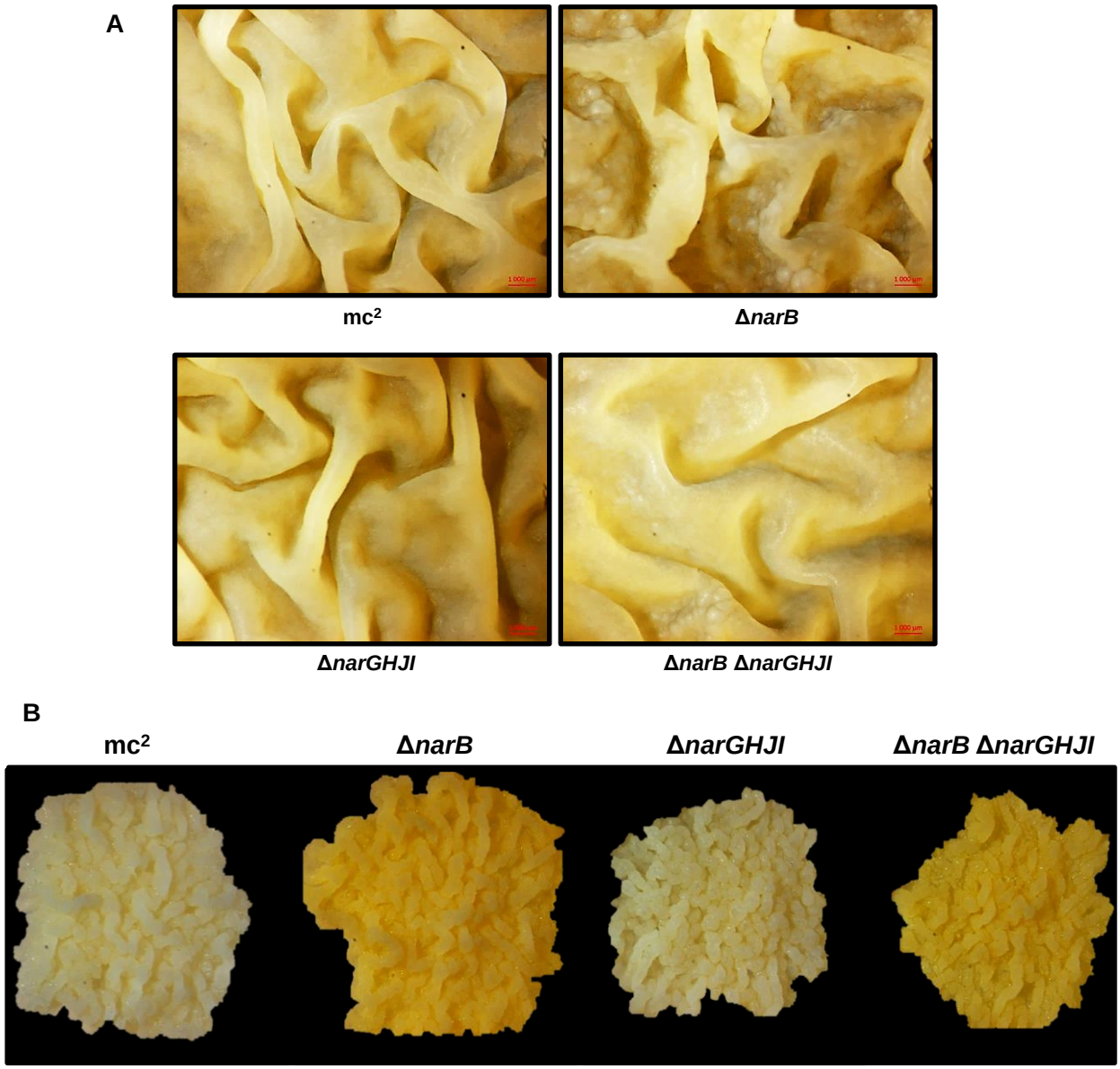


Figure 3.5: Biofilm formation and colony pigmentation of putative NR-deficient strains. (A) Biofilms were setup in Sautons media and incubated at 30˚C for 5 days. Images were captured using the Zeiss dissecting microscope and represent an 8X magnification of the reticulated biofilm surface. **(B)** Colonies were grown on 7H10 solid media and viewed after 7 days with the Zeiss dissecting microscope. The colony images were recorded at 3.25X magnification. Image manipulation included the "remove background" function in Microsoft Powerpoint. Thereafter, individual colony images were placed onto a black background.

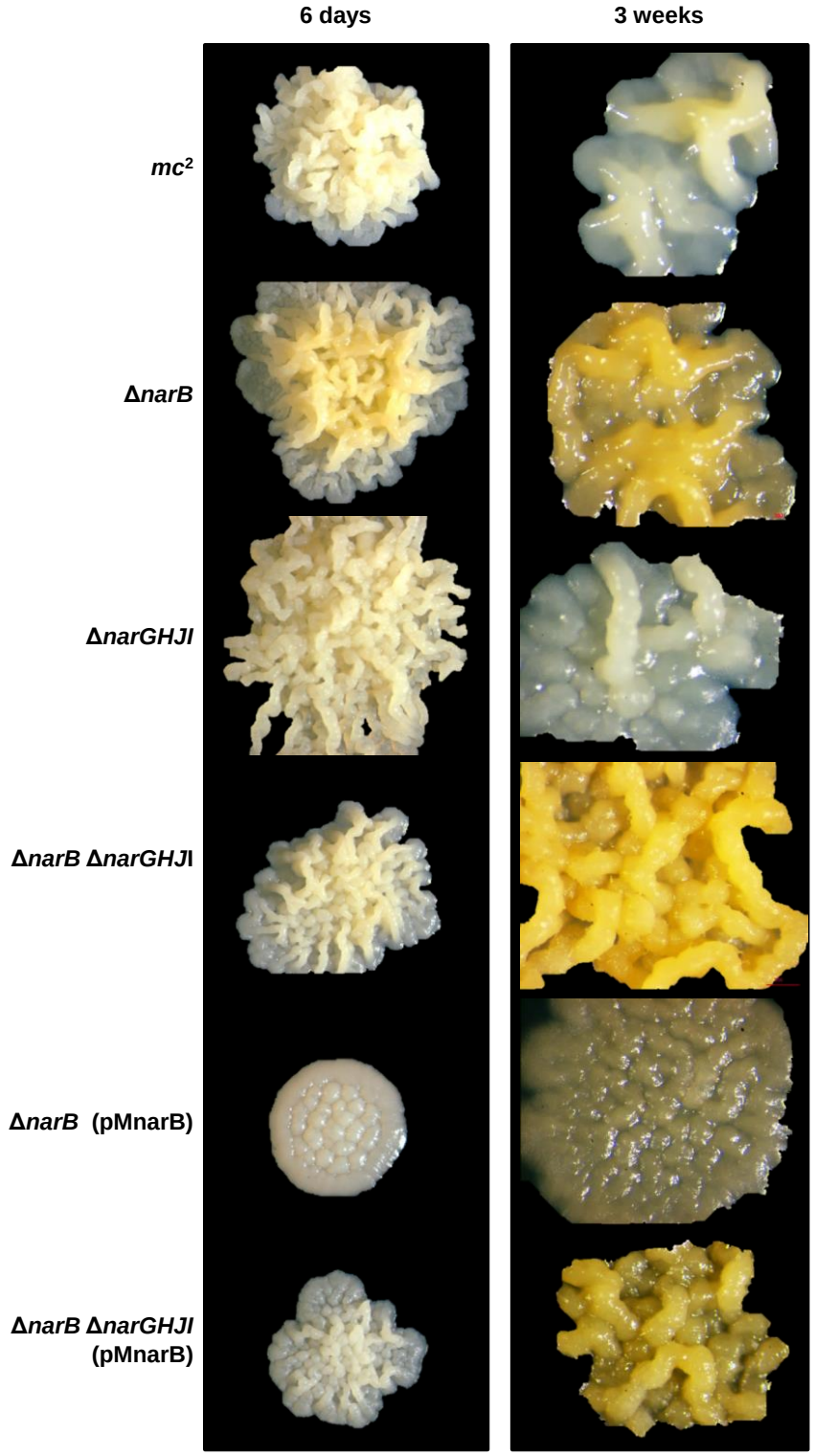


Figure 3.6: The development of colony pigmentation in *M. smegmatis* strains over time. Colonies were grown on 7H10 media and incubated for 6 days at 37 ˚C in an incubator with minimal light exposure, as per normal incubation procedures. Thereafter, the plates were stored at room temperature and exposed to light and images were recorded three weeks after inoculation. Images were captured on the Zeiss dissection microscope and 3.25 X or 5 X magnification was used for day 6 and week three respectively. Image manipulation included the "remove background" function in Microsoft Powerpoint. Thereafter, individual colony images were placed onto a black background.

If the increase in pigmentation observed for Δ*narB* and Δ*narB* Δ*narGHJI* were specific to the loss of *narB*, the reintroduction of an intact gene into the mutant strains should reverse the phenotype. The pigmentation observed in some mycobacterial species has been attributed to the production of carotenoids, the synthesis of which increases upon light exposure (Provvedi *et al.*, 2008). We therefore assessed the development of pigmentation for all the strains grown on 7H10 medium over time and after exposure to light. The images shown in Figure 3.6 confirm the increased pigmentation of Δ*narB* and Δ*narB* Δ*narGHJI*. The pigmentation can be observed slightly in Δ*narB* after 6 days and increases significantly after three weeks. This suggests that this phenomenon is attributable to the increased production of carotenoids. Introduction of pMnarB into Δ*narB* and Δ*narB* Δ*narGHJI* does not appear to reverse the increased pigmentation. This suggests that either the complementation was unsuccessful or that the phenotype was not due to loss of *narB* but rather some second site effect.

3.4.4 Expression of NR-encoding genes in *M. smegmatis*

The ability of Δ*narB*, Δ*narGHJI* and Δ*narB* Δ*narGHJI* to grow in MPLN under aerobic and anaerobic conditions suggests that loss of NarB and NarGHI does not abrogate NR activity in *M. smegmatis*. To investigate this further, the expression pattern of *narB* and *narGHJI* was assessed for the different *M. smegmatis* strains grown in 7H9 and MPLN. When grown to late log phase in 7H9, no *narB* or *narG* transcript was detected in any of the strains, suggesting that these genes are not expressed in *M. smegmatis* under the conditions tested. The lack of expression of *narB* in the genetically complemented strains suggests that genetic complementation was not achieved and provides a reason for the inability to reverse the pigmentation defect in these strains. The inability to detect *narB* and *narG* transcripts in strains grown in 7H9 was not as a result of RNA degradation, as observed by the detection of transcript of the house-keeping gene, *sigA* in equal amounts between strains, Appendix E, Figure E1A. We then assessed the expression of *narB* and *narG* in MPLN to determine if growth in nitrate leads to an induction of these genes. Low levels of *narB* transcript were seen in wild type and Δ*narGHJI*, however quantification was not possible because they were below the limit of accurate detection. Further hampering quantification of *narB* was the detection of a non-specific transcript product that was only observed in reverse transcriptase positive (RT+) reactions for wild type and Δ*narGHJI* but not in the no template control (NTC); thus ruling out contaminating DNA/RNA (Appendix E, Figure E1B). The non-

specific *narB* transcript was also detected in Δ*narB*, but no specific product was detected, confirming the loss of the gene in this strain. In addition, *narG* transcript was detected in wild type and Δ*narB* in equal amounts, shown in Figure 3.8. Although the amount of *narG* transcript was low from samples grown in MPLN, no transcript was detected when these samples were grown in 7H9 (evidenced by the lack of a specific product according to the melt curves). These data thus provide evidence that *narGHJI* expression in *M. smegmatis* is induced in the presence of nitrate, albeit to a low level. This is in contrast to Mtb, in which *narGHJI* expression is constitutive (Sohaskey and Wayne, 2003). The equivalent level of *narG* expression observed in wild type and Δ*narB* strains suggests that the loss of *narB* does not lead to a compensatory increase in *narGHJI*. The lack of detection of *narG* transcript in samples from 7H9 was not due to RNA degradation or disruption of the amplification reaction as *sigA* transcript was detected in comparable amounts for each strain from both 7H9 and MPLN (Appendix E, Figure E1C). As a result of the complete lack of expression of *narB* in the genetically complemented strains, they were not included in subsequent experiments.

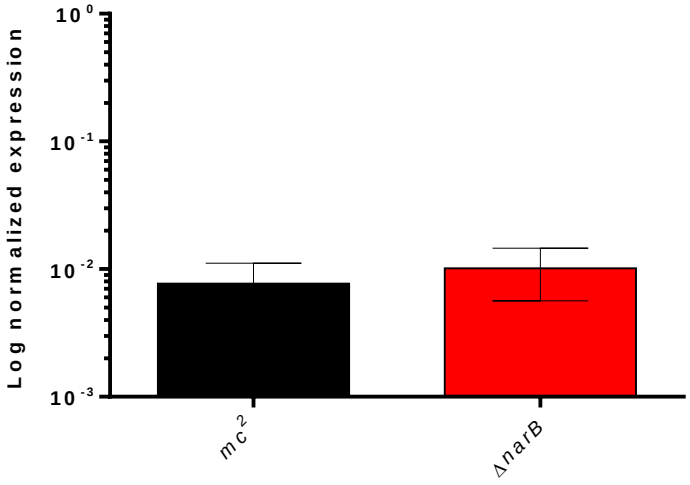


Figure 3.7: The expression of *narG* in the presence of nitrate. Strains were grown to OD_{600} 0,8-1 in MPLN liquid media. Expression was normalized against the house-keeping *sigA* and data from three independent experiments is depicted with standard error bars.

3.4.5 Nitrate utilisation

M. smegmatis is considered to be NR negative, due to the inability to detect nitrite under anaerobic conditions when nitrate is available (Weber *et al.*, 2000). To investigate NR activity in *M. smegmatis*, nitrate utilization was measured using the modified Griess assay as described and shown in Figure 3.3. The MoCo-deficient double mutant, Δ*moaD2* Δ*moaE2* which was previously shown to be defective for nitrate reduction (Williams *et al.*, 2011, Narrandes *et al.*, 2015), was included as a negative as it is unable to assimilate nitrate and would therefore produce a negative Griess result. When the Griess reagents are added to the culture samples taken at Day 0 no colour change was observed (Figure 3.8A, top panel) which was in contrast to the immediate change to pink observed for the nitrite standards (Figure 3.8B). Once zinc was added to the samples taken at the time of inoculation a dark pink colour was produced in all samples (Figure 3.8A, second panel), indicating the presence of nitrate. The intensity of the pink colour decreases after a day's incubation at 37 ˚C (Figure 3.8A, third panel), while no colour change is observed for samples taken after 6 days (Figure 3.8A, fourth panel). As expected, samples from Δ*moaD2* Δ*moaE2,* remained pink over the course of the experiment, confirming the loss of NR activity in this strain. Using the modified Griess assay, nitrate utilisation was quantified, with Figure 3.8C demonstrating the depletion of nitrate in the medium over time. To confirm that the depletion of nitrate from the medium is because of utilisation and not merely transport of nitrate into the cell, the intracellular nitrate levels were also quantified. The intracellular levels of nitrate were approximately 10 fold lower than the extracellular levels on Day 1 and were further depleted by Day 6, confirming that the nitrate is being assimilated and not accumulating intracellularly (Figure 3.8D). Increased intracellular levels of nitrate were detected in Δ*moaD2* Δ*moaE2*, once again confirming the inability of this strain to reduce nitrate. However, no significant differences in the amount of intra- or extracellular nitrate were detected between the wild type, Δ*narB*, Δ*narGHJI* and Δ*narB* Δ*narGHJI* strains. This result confirms that *M. smegmatis* does have NR activity under aerobic conditions and that the lack of NarB and/or NarGHI does not abrogate assimilatory NR activity.

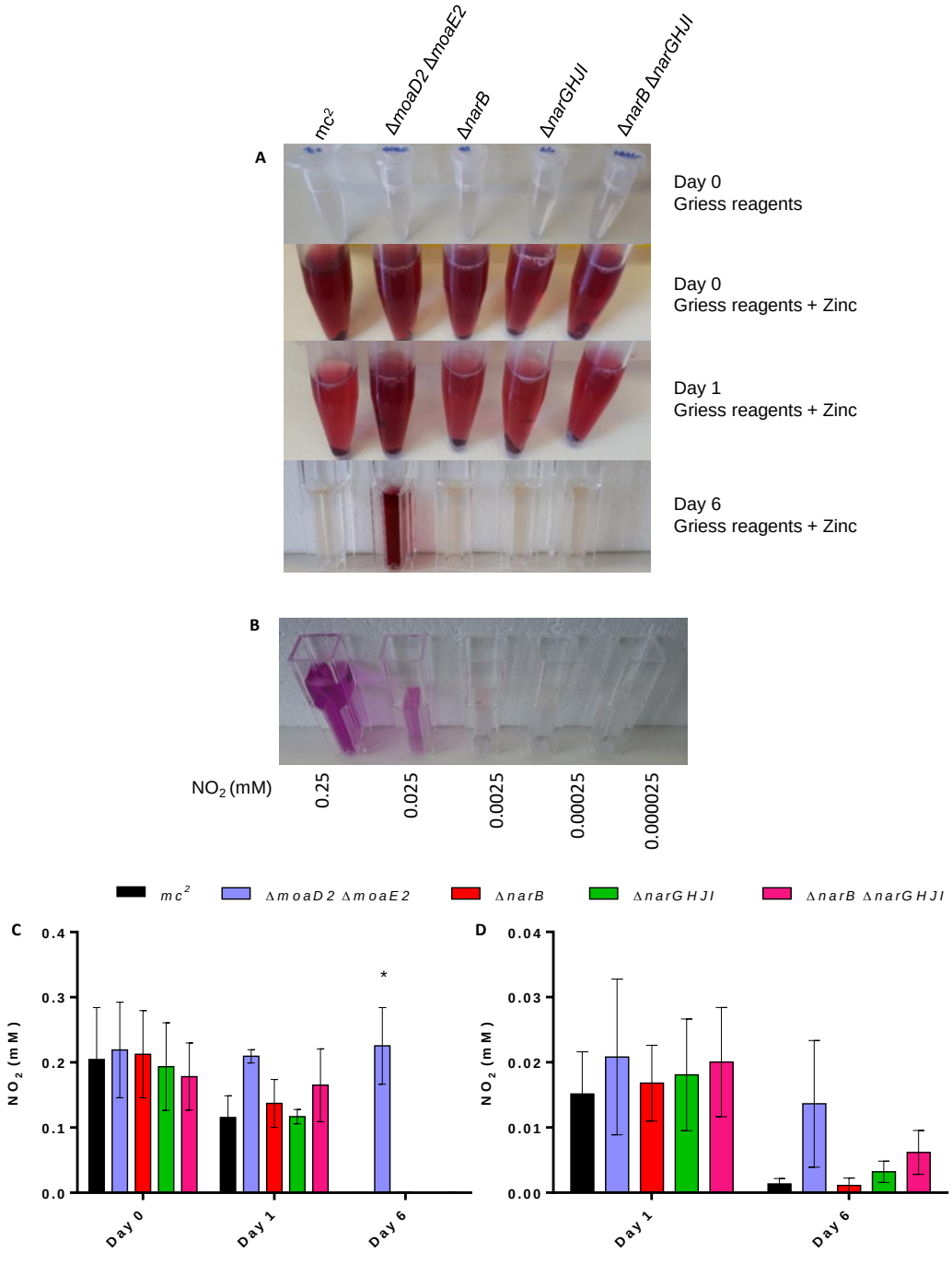


Figure 3.8: Nitrate utilisation in MPLN media. Cultures were grown at 37˚ C with shaking at 115 rpm. The modified Griess assay was performed to determine nitrate utilisationm on Day 0, Day 1 and Day 6. **(A)** Images of samples treated with the Griess reagents and zinc, showing the discolouration over time which represents nitrate depletion. **(B)** Image of nitrite standards treated with the Griess reagents alone. Quantification of extracellular **(C)** and intracellular **(D)** nitrate over time, as a function of nitrite detection using the modified Griess assay. The Students t-test was used to compare between strains. *P=0.01

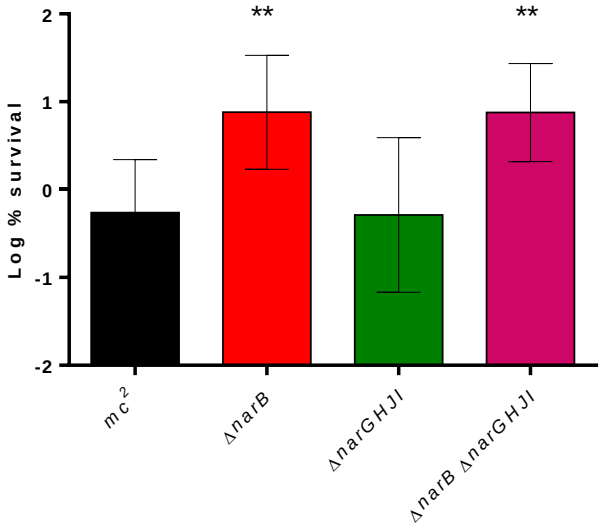


Figure 3.9: *M. smegmatis* Δ*narB* and Δ*narB* Δ*narGHJI* mutants are less susceptible to hydrogen peroxide stress. Cultures were exposed to 5 mM H_2O_2 and percentage survival was determined by comparing the CFU after 30 mins to the inoculum size. The average of two independent experiments is plotted with standard errors. The Student t-test was used for statistical analysis. **P<0.005

3.4.6 NarB plays a role in oxidative stress response and colony pigmentation

The mutants generated in this study displayed no growth defects and equally retained the ability to assimilate nitrate. However, it was observed that the Δ*narB* and Δ*narB* Δ*narGHJI* mutants become more pigmented after prolonged growth on solid 7H10 plates (Figure 3.6). Many mycobacteria are pigmented or become pigmented upon prolonged exposure to light and this pigmentation has been attributed to the production of carotenoids (Provvedi *et al.*, 2008). Carotenoids have free radical scavenging properties and are thus hypothesized to play a role in protection against oxidative stress (Edge *et al.*, 1997). Provvedi *et al.* (2008), showed that a mutant unable to produce carotenoids was hyper-susceptible to hydrogen peroxide stress. We thus hypothesized that the pigmented Δ*narB* mutant maybe more resistant to H_2O_2 stress. This hypothesis was confirmed (Figure 3.9), with the single and double mutants being less susceptible to killing by H_2O_2, suggesting that the amplified colony pigmentation observed in Δ*narB* and Δ*narB* Δ*narGHJI* maybe as a result of increased carotenoid production. To confirm this, the carotenoid content of each strain would need to be quantified. Also, Figure 3.9 reports the results of two biological replicates, further experiments are required to confirm the conclusions.

3.4.7 Bioinformatics analyses of *M. smegmatis* NR proteins

M. smegmatis and Mtb both retain a full repertoire of genes encoding proteins required for each step of the nitrate assimilation pathway (Amon *et al.*, 2009), shown in Figure 3.10. The discrepancies observed between the two organisms include the increased number of nitrate/nitrite transporters present in Mtb and the presence of different additional putative NR-encoding genes in Mtb and *M. smegmatis*, *narX* and *narB* respectively. A large degree of sequence homology is observed between the Mtb and *M. smegmatis narG* genes (76.8%). In addition, the promoter mutation (-215 T>C), strongly associated with differences in NR activity (Stermann *et al.*, 2004), is not present in *M. smegmatis* (Appendix E, Figure E4), suggesting that the expression profile of *narG* in the two organisms could be similar. Furthermore, protein sequence alignments of NarG revealed high sequence homology between different mycobacterial organisms and when compared to the *E. coli* protein, all the catalytic residues are conserved, Appendix E, Figure E5. Pairwise sequence alignments were performed using the EMBOSS Needle tool (Rice *et al.*, 2000).

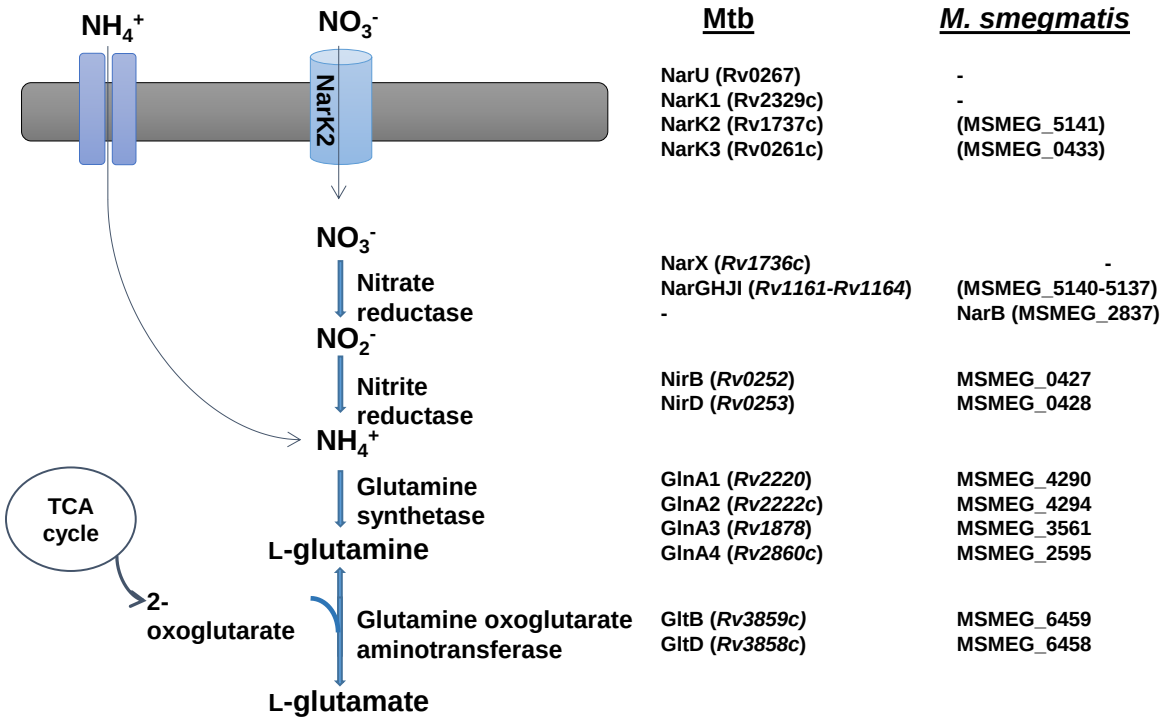


Figure 3.10: Mycobacterial nitrate assimilation pathway. Genes encoding proteins for each step of the pathway are shown for Mtb and *M. smegmatis*. Gene annotations were obtained from Mycobrowser (http://mycobrowser.epfl.ch/) and Amon *et al*. (2009).

These bioinformatics analyses suggest that *M. smegmatis* encodes a functional *narGHJI*-encoded NR.

BLAST (Altschul *et al.*, 1990) analysis revealed that several mycobacterial species harbour a copy of *narB*, including members of the *Mycabacterium avium complex* (MAC), *Mycobacterium fortuitum*, *Mycobacterium yongonense*, *Mycobacterium goodii* and *Mycobacterium kansasii*- all of which are capable of causing disease. However, a *narB* homologue was not identified in any of the organisms belonging to the *M. tuberculosis* Complex. Analysis of the NarB protein sequence (A0QW69) revealed four domains, as shown in Figure 3.11A. This domain architecture is most commonly found in the catalytic subunit of periplasmic nitrate reductases and interestingly, a prediction of the 3D structure of *M. smegmatis* NarB models best to the *Desulfovibrio desulfuricans* periplasmic nitrate reductase (Pdb 2V45) (Najmudin *et al.*, 2008, Zhang, 2008), Figure 3.10B. However, this is likely attributable to the lack of a resolved NarB crystal structure. In addition, using SignalP (Petersen *et al.*, 2011) a signal sequence was not identified in *M. smegmatis* NarB, suggesting that it is most likely located in the cytoplasm. Furthermore, the protein shares homology (31.1%) with the *Synechococcus* sp. PCC 7942 NarB and according to STRING (Szklarczyk *et al.*, 2017) analysis, it could possibly interact with MSMEG_1847, a ferrodoxin which is the predicted physiological electron donor to NarB in *Cyanobacteria* (Rubio *et al.*, 1996).

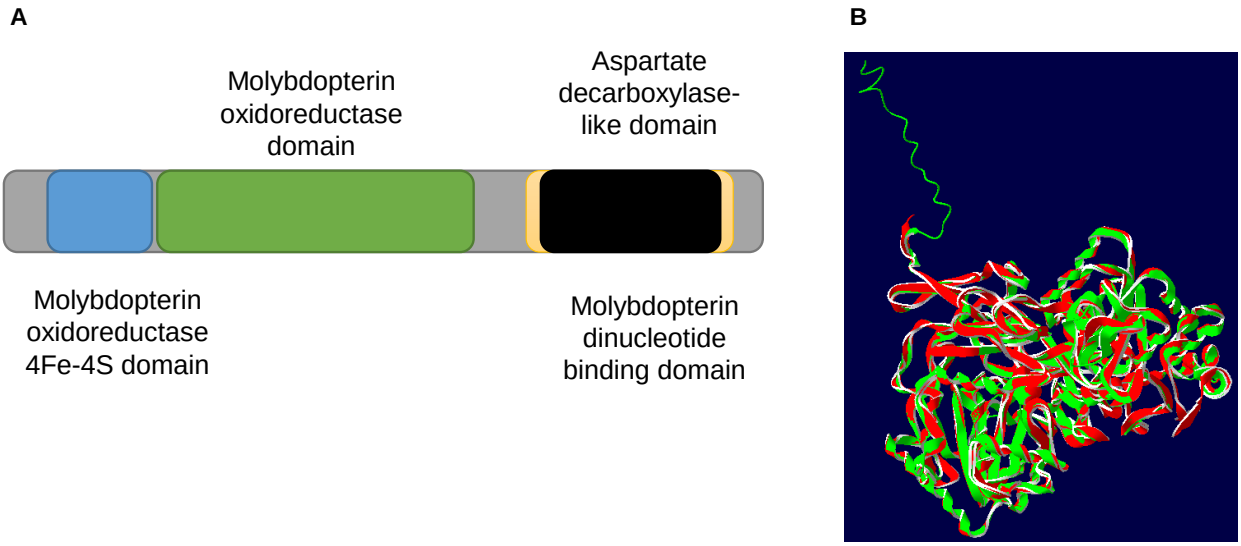


Figure 3.11: NarB domain architecture and predicted 3D structure. (A) NarB domain architecture obtained from InterPro. **(B)** Predicted crystal structure of NarB (Green) overlayed with the best fit template, the periplasmic NR from *Desulfovibrio desulfuricans* (Red). The crystal structure prediction was done using i-TASSER and the NarB amino acid sequence obtained from SmegmaList.

Bioinformatic analyses of the annotated NR-encoding genes and their associated proteins in *M. smegmatis* confirmed that *narB* and *narG* encode enzymes with NR functionality. The retained NR activity in Δ*narB,* Δ*narGHJI* and Δ*narB* Δ*narGHJI* was therefore unexpected. It is possible that an alternate MoCo-dependent NR reductase is present in *M. smegmatis* which is solely responsible for nitrate assimilation or works in combination with other MoCo-dependent NR's for the reduction of nitrate to nitrite. Using the domains shown in Figure 3.11A, the genome of *M. smegmatis* was examined in KEGG (Kanehisa *et al.*, 2016) to identify enzymes with the same architecture which could possibly catalyse the reaction. Seven genes encoding enzymes with the same architecture were identified and are listed in Table 3.1. Of the seven, *narB* and *narG* were two of the hits as expected, while three of the seven genes encoded the MoCo-dependent oxidoreductases formate dehydrogenase and NADH dehydrogenase.

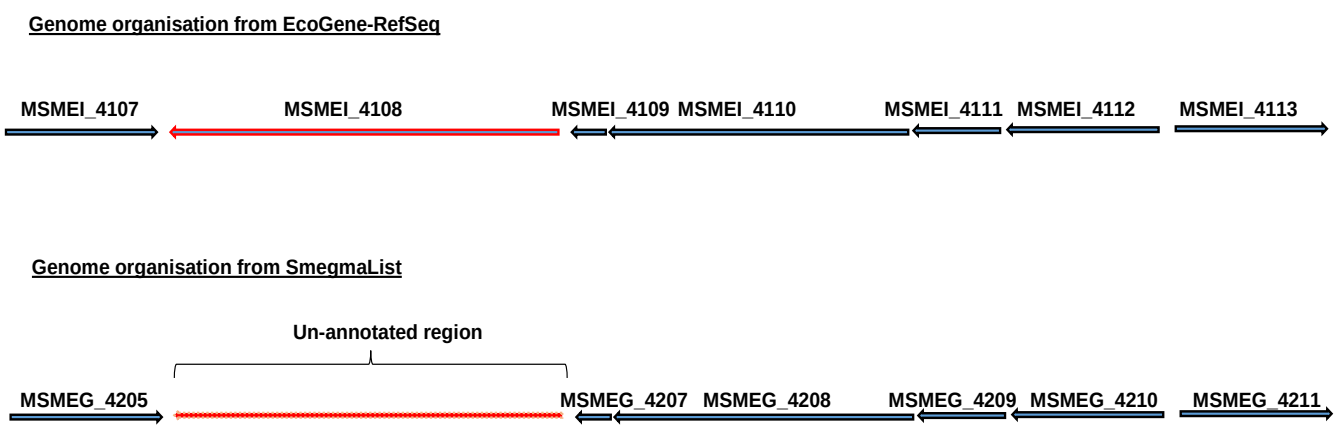
The two remaining hits from the KEGG search were MSMEG_2237 and MSMEG_6816 which are annotated as an anaerobic dehydrogenase and molybdopterin oxidoreductase respectively (Kapopoulou *et al.*, 2011) and could possibly reduce nitrate to nitrite. In addition to the seven genes identified in the *M. smegmatis* genome with the MSMEG annotations, one gene was identified in the *M. smegmatis* genome with the newer MSMEI gene annotations curated by EcoGene-RefSeq (Zhou *et al.*, 2013), MSMEI_4108. MSMEI_4108 is annotated as a putative assimilatory nitrate/sulfite reductase.

Table 3.1: M. smegmatis genes encoding proteins with the same domain architecture as NarB. Alignments were performed using EMBOSS Needle and protein sequences obtained from KEGG.

Gene	Identifier	EC classification	Gene length	Protein length	NarB % homology*
MSMEG_0161	Formate dehydrogenase	1.2.1.2	2820 bp	939 aa	21.6
MSMEG_2057 (*nuoG*)	NADH dehydrogenase subunit G	1.6.5.3	2385 bp	794 aa	17.6
MSMEG_3521	Formate dehydrogenase	1.2.1.2	2250 bp	749 aa	21.6
MSMEG_2837 (*narB*)	Assimilatory nitrate reductase	1.7.7.2	2388 bp	795 aa	-
MSMEG_5140 (*narG*)	Respiratory nitrate reductase	1.7.5.1/1.7.99.4	3675 bp	1224 aa	16.8
MSMEG_2237	Anaerobic dehydrogenase	Not assigned	2283 bp	760 aa	21.2
MSMEG_6816	Molybdopterin oxidoreductase	Not assigned	2163 bp	720 aa	24.4
MSMEI_4108	Putative assimilatory nitrate reductase/sulfite reductase	Not assigned	4056 bp	1351 aa	18.7

In order to identify this gene in SmegmaList (MSMEG gene annotations), a BLAST search was performed using the nucleotide sequence and 100 % homology was detected for an un-annotated region of the SmegmaList genome sequence (Kapopoulou *et al.*, 2011).

A



B

Gene		Coordinates		Annotation
Mycobrowser	**EcoGene-RefSeq**	**Mycobrowser**	**EcoGene-RefSeq**	
MSMEG_4205	MSMEI_4107	4283833-4286454	4585367-4288017	LuxR regulatory protein
-	MSMEI_4108	4288072-4292127	4288072-4292127	Putative assimilatory nitrate/sulfite reductase*
MSMEG_4207	MSMEI_4109	4290634-4291026	4292247-4292639	Universal stress protein
MSMEG_4208	MSMEI_4110	4291023-4292567	4292636-4294177	TctA-Tripartite tricarboxylate transporter
MSMEG_4209	MSMEI_4111	4292564-4293100	4294177-4294713	TctB-Tripartite tricarboxylate transporter
MSMEG_4210	MSMEI_4112	4293097-4294080	4294710-4295657	TctC-Tripartite tricarboxylate transporter
MSMEG_4211	MSMEI_4113	4294185-4295684	4295798-4297477	Histidine kinase regulating citrate/malate biosynthesis

*Annotation only according to EcoGene-RefSeq

C

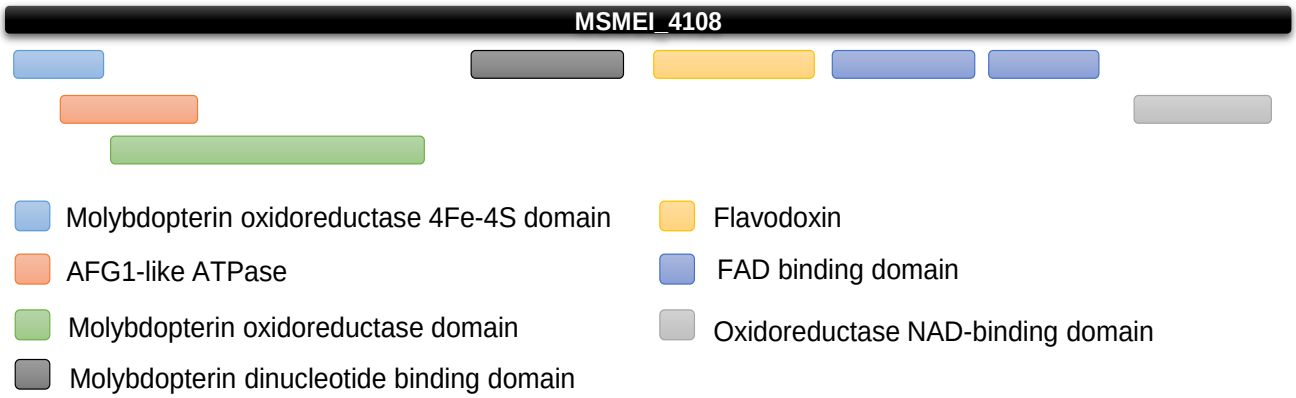


Figure 3.12: Genome organization of MSMEI_4108, an additional putative assimilatory NR in *M. smegmatis*. (A) *M. smegmatis* genome organisations found in two different databases. **(B)** Comparison of the gene coordinates and annotations from the two databases. **(C)** MSMEI_4108 protein domain architecture according to KEGG.

The region was between coordinates 4288072-4292127 and the surrounding gene organisation for both databases was exactly the same, shown in Figure 3.12A and B. No signal sequence or transmembrane domains were detected for MSMEI_4108, suggesting that it is cytoplasmic. In addition, it possesses binding domains for different cytoplasmic electron donors, Figure 3.12C. We thus propose to assign MSMEG_4206 to the coordinates shown in Figure 3.12B and annotate the gene as a putative assimilatory nitrate/sulfite reductase. Further investigation into this gene and its role in nitrate assimilation is currently being conducted.

3.5 Discussion

It has long been accepted that *M. smegmatis* is NR negative, based on the results of the Griess assay (Weber *et al.*, 2000). When performed following the conventional protocol this assay cannot be used to assess NR activity in *M. smegmatis* unless the strain carries a constitutively expressed copy of the Mtb *narGHJI* operon (Weber *et al.*, 2000, Williams *et al.*, 2011), suggesting that *M. smegmatis* is unable to reduce nitrate. However, several studies have shown that *M. smegmatis* is able to use nitrate as the sole nitrogen source (Khan and Sarkar, 2006, Khan *et al.*, 2008, Williams *et al.*, 2011, Khan and Sarkar, 2012, Narrandes *et al.*, 2015). Furthermore, it has been demonstrated NR activity in a strain (Δ*moaD2* Δ*moaE2*) unable to synthesise the *bis*-MGD cofactor was completely abrogated (Williams *et al.*, 2011), providing further evidence that a functional NR is present in *M. smegmatis* and like the Mtb NR, is *bis*-MGD dependent. Using a modified Griess assay we confirm that *M. smegmatis* does indeed reduce nitrate. We show that over time *M. smegmatis* is able to utilize all available nitrate in the medium and that it is completely assimilated. The ability of *M. smegmatis* to reduce nitrate is not surprising as two putative NR-encoding genes are annotated in the genome *i.e. narB* and *narGHJI*. However, the contribution of each to NR activity was unknown. We sought to address this question.

NR activity is a phenotypic characteristic widely accepted to classify and differentiate between mycobacterial species, with Mtb displaying high NR activity while *M. bovis* and *M. bovis* BCG show no distinct NR activity (Khan and Sarkar, 2012). The molecular basis for the difference in NR activity between Mtb and *M. bovis* BCG has been attributed to the lack of a functional *narGHJI*-encoded NR as a result of loss of *narH* expression in the latter (Hutter and Dick, 1999). The reduced NR activity in the pathogenic *M. bovis* has been attributed to a single nucleotide polymorphism in the promoter region of *narG*, although the authors couldn't rule out that other SNPs in the coding region of the *narGHJI* operon also contributed to the differential activity between the two strains (Stermann *et al.*, 2004). *M. smegmatis* retains a fully intact *narGHJI* operon and although there are sequence differences in *narG* between Mtb and *M. smegmatis*, the promoter mutation (-215 T>C) that was strongly associated with differences in NR activity (Stermann *et al.*, 2004) is not present in the latter, suggesting that the enzymes could have similar activities. It has recently been reported that *M. smegmatis* does harbour T>C mutation in *narG*, however the authors were referring to

position -125 instead of -215 (Huang *et al.*, 2015). The different Griess assay results observed in Mtb and *M. smegmatis* could be due to a lack of extracellular nitrite as a result of either (i) more efficient nitrite reductase activity in *M. smegmatis* which leads to the complete reduction of nitrite to ammonia, (ii) reduced nitrite transporter activity in *M. smegmatis* or a combination of both. No intracellular nitrite was detected in *M. smegmatis* during this study, suggesting that it is able to completely assimilate nitrite. The observation that only an *M. smegmatis* strain expressing both its native and the Mtb *narGHJI* is able to produce a positive Griess result (Weber *et al.*, 2000, Williams *et al.*, 2011) could be attributed to an increase in nitrate reduction in the heterologously complemented strain at a rate that the nitrite reductase could not equal, which leads to the detoxification of nitrite by exporting the excess, to yield a positive Griess results. This experiment also suggests that *M. smegmatis* does have nitrite transporter activity. Generating *M. smegmatis* mutant strains lacking a functional nitrite reductase and nitrite transporter, with the subsequent complementation with the Mtb and *M. smegmatis* homologues would allow for a more direct comparison of the activity of these enzymes to be made and would shed more light on the differences in nitrate metabolism between these two organisms. The inherent differences between Mtb and *M. smegmatis* nitrate metabolism could also be due to the difference in their natural environments *i.e.* intracellular for Mtb versus soil for *M. smegmatis.* This is supported by the presence of an additional putative assimilatory NR in *M. smegmatis* as nitrate is more readily available in soil.

M. smegmatis possesses genes encoding two putative nitrate reductase enzymes. NarGHI, encoded by the *narGHJI* operon has been well characterized in *E. coli* and is a respiratory enzyme which serves as the terminal electron acceptor during anaerobic respiration when nitrate is available. The second NR-encoding gene in *M. smegmatis – narB,* is a putative assimilatory NR-encoding gene (Khan *et al.*, 2008). NarB is a cytoplasmic enzyme that has been well characterized in *Cyanobacteria* where it facilitates growth on nitrate (Rubio *et al.*, 1996). Interestingly, similarly to *M. smegmatis,* NarB from the cyanobacterium *Synechococcus* sp. PCC 7942 shares high sequence similarity with a periplasmic NR and it is believed that this is due to a close evolutionary relationship between periplasmic and cytoplasmic assimilatory NR's (Jepson *et al.*, 2004). An additional similarity between the cyanobacterium and *M. smegmatis* is the gene organisation. Assimilatory NR- encoding genes in other organisms are commonly clustered with nitrite reductase and/or transporter

genes, however *narB* in *M. smegmatis* and *Synechococcus* sp. PCC 7942 are not clustered with other genes involved in nitrate metabolism (Rubio *et al.*, 1996, Kapopoulou *et al.*, 2011). Based on the genome organisation, sequence similarities and predicted 3D structure, the *M. smegmatis narB* was expected to encode a functional NR. Although this cannot be ruled out, the inability to detect *narB* transcript in our study and the ability of strains lacking *narB* to assimilate nitrate, as observed during my MSc project when these mutant strains were generated, suggests otherwise. Although *narG* transcript was detected in *M. smegmatis,* the strains lacking *narGHJI* were also able to assimilate nitrate, suggesting that NarGHI is not the only enzyme involved in nitrate assimilation in contrast to the Mtb counterpart (Malm *et al.*, 2009). Furthermore, NarB and NarGHI were dispensable for anaerobic survival in the presence of nitrate, suggesting that either these enzymes are not required for nitrate reduction or that in the absence of each, an alternate enzyme can compensate for the loss.

As *narB* and *narGHJI* are the only genes in the *M. smegmatis* genome hosted on SmegmaList annotated specifically as NR-encoding (Kapopoulou *et al.*, 2011), we sought to further investigate this finding by bioinformatics analysis. Interrogation of the *M. smegmatis* genome revealed three other enzymes with the necessary domains that could possibly serve as NR's i.e. MSMEG_2237, MSMEG_6816 and MSMEI_4108. The first two were identified in the genome sequence curated by SmegmaList and are annotated as an anaerobic dehydrogenase and molybdopterin oxidoreductase respectively (Kapopoulou *et al.*, 2011). The remaining and most promising candidate, MSMEI_4108 is annotated as a putative assimilatory nitrate/sulfite reductase in the *M. smegmatis* genome sequence curated by EcoGene-RefSeq (Zhou *et al.*, 2013). Further analysis of these genes using the tools described herein would allow for a clearer picture of nitrate reduction in *M. smegmatis* to be obtained.

According to the evidence presented, NarB does not appear to be essential for nitrate assimilation. However, the mutant did display a pigmented colony phenotype and preliminary analysis suggested that it was more resistant to oxidative stress. Mycobacterial pigmentation has been attributed to carotenoids, which are known to have oxidative radical scavenging properties. This led to the hypothesis that the mutant strains displaying hyper-pigmentation may be more resistant to oxidative stress as a result of increased carotenoid content. Consistent with this, we demonstrated that these strains are more resistant to oxidative stress as a result of H_2O_2 treatment. However, it cannot be ruled out that the phenotype may be

caused by alternate perturbations in the cell. Measuring the carotenoid content and/or the expression of carotenoid biosynthesis genes would be beneficial. It has been demonstrated that carotenoid biosynthesis is regulated by *sigF* (Provvedi *et al.*, 2008) and interestingly, *narB* has also been shown to be part of the *sigF* regulatory network (Humpel *et al.*, 2010, Singh, 2015). The *sigF* promoter sequence (GTTT-N_{16}-GGGTA) was identified 42 bp upstream of the *narB* start site (Humpel *et al.*, 2010) and it was shown that *narB* is down-regulated in both exponential and stationary phase in a Δ*sigF* mutant (Singh, 2015). A Δ*sigF* mutant strain has reduced pigmentation as a result of reduced expression of *crtI* (a carotenoid biosynthesis gene) and increased sensitivity to H_2O_2 (Provvedi *et al.*, 2008), while we observe increased pigmentation and resistance to H_2O_2 for Δ*narB* and Δ*narB* Δ*narGHJI*. It is possible that in the absence of *narB* there is an accumulation of SigF, which could result in an increase in carotenoid biosynthesis gene expression, thus explaining the pigmentation and oxidative stress resistance observed in Δ*narB* and Δ*narB* Δ*narGHJI* and proposed in Figure 3.13. However, this explanation is largely speculative and requires further confirmation.

A

	ΔnarB	ΔsigF
Pigmentation	↑	↓
H_2O_2 sensitivity	↓	↑
narB expression	↓	↓
sigF expression	?	↓

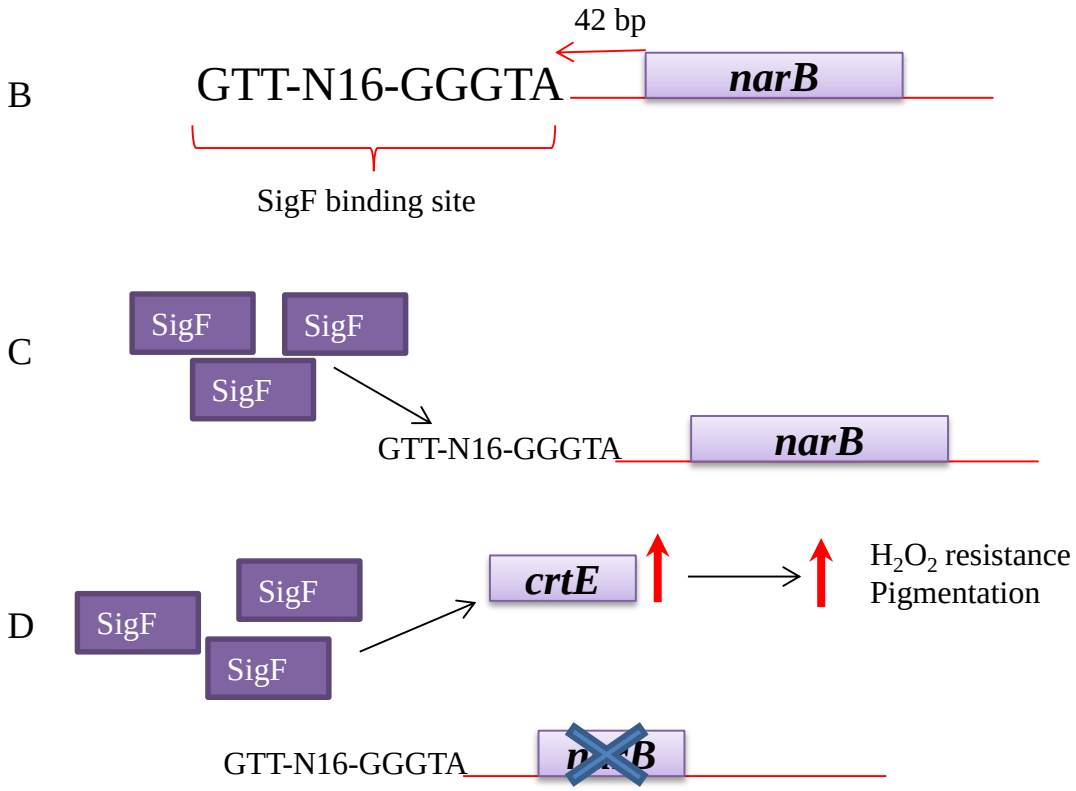


Figure 3.13: A diagram presenting a possible inerplay between *sigF* and *narB*. (A) Comparative phenotypes in a *narB*mutant and *sigF* mutant **(B)** A schematic showing the position and sequence of the SigF binding site 42 bp upstream of the *narB* transcriptional start site. **(C)** Proposed model of *sigf* binding under standard laboratory conditions **(D)** A possible mechanism that mediated increased pigmentation production and resistance to oxidative stress in strains lacking *narB*. Phenotype data was either produced during this study or obtained form the literature (Hümpel *et al*., 2010, Provvedi *et al*., 2008 and Singh *et al*., 2015)

3.6 Conclusions

Herein, we demonstrate that neither *narB* nor *narGHJI* encode proteins which are individually essential for nitrate reduction in *M. smegmatis* under the conditions tested. While *narB* may not be required for nitrate assimilation, it does appear to indirectly be involved in colony pigmentation and the oxidative stress response. Finally, we propose MSMEG_4206 as the putative assimilatory NR in *M. smegmatis*. We demonstrate that NR activity is present in *M. smegmatis*, thus supporting a role for nitrate and possibly a NR enzyme other than NarB or NarGHI in the phenotypes observed in the presence of nitrate in Chapter 2. Once the primary NR enzyme or all the contributors to NR activity in *M. smegmatis* have been identified, they will allow for further investigation of both nitrate assimilation and respiration as well the role of nitrate in aerobic respiration in the absence of aerobic enzymes.

A. Appendix A- General materials and methods

A1. Strains and culture conditions

A1.1. *Escherichia coli* culturing

Escherichia coli DH5α or commercially available OneShot® TOP10 chemically competent cells (Invitrogen) were used for plasmid propagation and grown in Lysogeny Broth liquid medium (LB) or solid medium (LA), supplemented with the appropriate antibiotics at concentrations of 100 µg/ml Ampicilin (Amp), 200 µg/ml Hygromycin (Hyg) and 50 µg/ml Kanamycin (Kan). Strains carrying plasmids < 8 kb were incubated at 37 ºC and those carrying plasmids > 8 kb were propagated at 30º C to minimize plasmid re-arrangements. Liquid cultures were incubated with shaking at 150-250 rpm.

A1.2. *M. smegmatis* culturing

Wild type *M. smegmatis* mc^2 155 and derivative strains were grown in Middlebrook 7H9 liquid medium (Difco) supplemented with either Middlebrook oleic acid-albumin-dextrose-catalase (OADC) enrichment (Difco), albumin-dextrose-saline supplement (ADS) or glucose-NaCl (GN) supplement (0.2% glucose, 0.085% NaCl) as indicated. In addition, 7H9 medium was supplemented with 0.2% glycerol as a carbon source and 0.05% Tyloxapol as detergent to minimize cell clumping. Liquid cultures were incubated at 30-37 ˚C with shaking at 100-115 rpm as indicated. *M. smegmatis* cultures were selected on Middlebrook 7H10 solid medium (Difco) supplemented with 0.085% NaCl, 0.2% glucose and 0.5% glycerol at 30-37 ˚C. Liquid and solid media were supplemented with antibiotics at concentrations of 50 µg/ml Hyg and/or 25 µg/ml Kan where appropriate.

A1.3. Mtb culturing

Mtb was handled in accordance with international biosafety level III (BSL III) laboratory regulations. Wild type Mtb H37Rv and derivative strains were grown in 7H9 liquid medium supplemented with 0.2% glycerol, 0.05% Tyloxapol and either OADC enrichment or ADS, as

indicated. Liquid cultures were grown in tissue culture flasks at 37 ˚C with no agitation. Mtb colonies were selected on Middlebrook 7H11 solid medium (Difco) supplemented with OADC and 0.5% glycerol at 37 ˚C. When required, liquid and solid media were supplemented with the appropriate antibiotics at concentrations of 50 µg/ml Hyg and/or 25 µg/ml Kan.

A2. Bacterial transformations

A2.1. *E. coli* transformations

Chemically competent *E. coli* DH5α cells were prepared as previously described (Sambrook, 1989). A pre-culture of *E. coli* was prepared from a freezer stock and grown overnight at 37 ˚C. A 1 ml aliquot of the pre-culture was used to inoculate 100 ml fresh LB and incubated at 37 ˚C with shaking at 250 rpm for 4 hrs. The exponentially growing cells were then harvested by centrifugation at 1731 × *g* for 6 mins at 4 ˚C (Beckman Coulter Allegra™ X-22R Centrifuge). All subsequent steps were carried out at 4 ˚C. The supernatant was carefully discarded and the cell pellet was gently re-suspended in 10 ml ice cold $CaCl_2$. The cell suspension was then pelleted as before and the pellet re-suspended in 5 ml cold $CaCl_2$, from which 100 µl aliquots were prepared to be used immediately or stored on ice at 4 ˚C overnight before being used for transformations. For transformations, a maximum of 10 µl of DNA (varying concentrations) was added to 100 µl of competent cells and mixed gently by pipetting, followed by 15 min incubation on ice. The DNA-cell mixture was heat shocked for 90 secs at 42 ˚C, incubated on ice for 3 mins, followed by the addition of 800 µl 2×TY and incubated at 37 ˚C to allow for the expression of selective antibiotic resistance genes. Thereafter transformants were selected on solid LA media with the appropriate antibiotics. When using OneShot® TOP10 chemically competent cells, the manufacturer's instructions were followed. Briefly, 5 µl of DNA was added to 50 µl cells and mixed by gentle tapping. The mixture was then incubated on ice for 30 min, followed by heat shock treatment at 42 ˚C for 30 sec and transferred onto ice. Pre-warmed S.O.C medium (250 µl) was then added to the cell suspension and incubated at 37 ˚C for 1hr with shaking. Transformants were selected on solid LA media containing the appropriate antibiotics.

A2.2. *M. smegmatis* electroporations

M. smegmatis cells were transformed by electroporation as previously described (Larsen, 2000). Cells were grown in 50-100 ml of medium to mid-log phase (OD_{600} 0.5-0.8) and harvested at 2360 ×*g* at 4˚ C for 10 min. The bacterial cell pellet was re-suspended in 10 ml of cold 10% glycerol and harvested as before; this wash step was repeated twice more. Cells were harvested and pellets re-suspended in 2 ml of glycerol which was then separated into 400 µl aliquots in Eppendorf tubes. A final wash of the cells was carried out at 12 470 × *g* (Beckman Coulter Microfuge 16) for 1 min and cell pellets were re-suspended in 400µl of 10 % glycerol. These competent cells were used immediately for electroporations. Approximately 1 µg of plasmid DNA was used for electroporations. The DNA was added to 0.2 cm electroporation cuvettes into which 400 µl of electro-competent *M. smegmatis* cells were added and gently mixed. The BIORAD Gene Pulser XCell™ system was used to perform electroporations with the following parameters: 2500 V, 25 µF, 1000 Ω, 0.2 cm. Immediately after the pulse, 800 µl of 2×TY was added and cells were incubated at 37˚ C for 3-16 hr to allow for the phenotypic expression of selectable marker genes. Transformed cells were selected on 7H10 plates containing the appropriate antibiotics and/or selective supplements for 3-7 days.

A2.3. Mtb electroporations

Mtb electroporations were performed following the protocol described for *M .smegmatis* electroporations with minor modifications. Firstly, once Mtb cultures reached an OD_{600} of 0.8-1, glycine was added to a final concentration of 2%. The culture was incubated overnight and electro-competent cells were subsequently prepared as described for *M. smegmatis* except all steps were carried out at room temperature, with 10 % glycerol also at room temperature. In addition, prior to electroporation of Mtb cells, the plasmid DNA was irradiated at 100 mJ/cm^2. Electroporations were incubated overnight at 37 ˚C to allow for the phenotypic expression of selectable marker genes and transformants were subsequently selected on 7H11 plates with the appropriate antibiotics and/or selective supplements following a 3-5 week incubation period.

A3. DNA extractions

A3.1. Small scale plasmid extractions

E. coli cultures carrying the plasmid of interest were grown overnight in 2 ml LB with the appropriate antibiotics, 1 ml of which was used for the extraction procedure. Cultures were spun down at 12 470 × *g* and pellets re-suspended in 100 µl of Solution I (50mM glucose, 25mM Tris-HCl (pH 8), 10 mM EDTA) followed by the addition of 200 µl of Solution II (1% SDS, 0.2 M NaOH) which was mixed by gentle inversion and incubated at room temperature for 5 min. Finally, 150 µl of Solution III (3 M potassium acetate, 11.5% acetic acid) was added and incubated on ice for 5 min. The suspensions were centrifuged for 5 min at 12 470 × *g* after which, the supernatant was decanted into a fresh Eppendorf tube. At this point, 1 µl of RNaseA (10 mg/ml) was added to the supernatant and incubated at 42˚ C for 15 min. Plasmid DNA was then precipitated by the addition of 600 µl of isopropanol, washed with 70% Ethanol and re-suspended in 100 µl of sdH_2O. This was followed by ethanol precipitation of the DNA by addition of 1/10 volume of 3 M sodium acetate (pH 5.3), followed by 3× volume 100% ethanol (-20˚C). DNA was collected by centrifugation at 12 470 × *g* for 20 min, washed with 70% ethanol and dried at 60˚ C for ~10 min in an Eppendorf Concentrator 5301. The dried pellet was then re-suspended in sdH_2O and quantified using the NanoDrop. Alternatively, small scale plasmid extractions were performed using the Qiagen QIAprep Spin Miniprep Kit following the manufacturer's protocol.

A3.2. Large scale plasmid extractions

The bulk extraction of plasmid DNA from *E. coli* cells was carried out with the Machery-Nagel NucleoBond Plasmid DNA Purification kit. The manufacturer's protocol was followed with the addition of an ethanol precipitation step (as described above) after elution.

A3.3. Small scale genomic DNA extractions

The colony boil method was used for the small scale extraction of DNA from *M. smegmatis* and Mtb. Briefly, a colony (~10 mm diameter) was re-suspended in 100 µl of sdH_2O and 10

µl was spotted onto fresh solid medium to maintain a viable stock of the colony. An equal volume (90 µl) of chloroform was then added to the remaining cell suspension, mixed thoroughly and boiled at 95˚ C for 5 min. Thereafter, the mixture was centrifuged at 12 470 × *g* for 5 min. The aqueous suspension above the cell debris interface was carefully decanted into a fresh Eppendorf tube and was used as a DNA template in PCR reactions or for transformations.

A3.4. Large scale genomic DNA extractions

The cetyltrimethylammonium bromide (CTAB) method was used for the bulk extraction of chromosomal DNA from *M. smegmatis* and Mtb. Cells were grown to a lawn on 7H10 plates (with the appropriate antibiotics where necessary) from which four loopfuls of the culture were re-suspended in 500 µl of TE buffer. Alternatively, ~ 5 ml of a stationary phase culture was harvested by centrifugation and the cell pellet re-suspended in 500 µl TE buffer. *M. smegmatis* cells were killed by heating the suspension at 65˚C for 20 min, while Mtb cells were killed at 80 ˚C for an hour. Thereafter the same protocol was followed for both Mtb and *M. smegmatis.* Following the heat-killing step, 80 µl of lysozyme (10 mg/ml) was added to the cell suspension and incubated at 37˚C for an hour. Thereafter, 6 µl of proteinase K and 70 µl of 10% SDS were mixed into the suspension and the mixture was incubated at 65˚C for 2 hours. This was followed by the addition of 100 µl of NaCl (5M) and 80 µl of pre-warmed CTAB/NaCl with mixing. This suspension was then incubated at 65˚C for 10 min. DNA was purified from this mixture by adding an equal volume of chloroform: isoamyl alcohol (24:1 v/v), mixing vigorously and centrifuging at 12 470 × *g* for 5 min. The top aqueous layer was decanted into a fresh Eppendorf tube, to which 600 µl of isopropanol was added to precipitate the DNA by centrifugation at 12 470 × *g* for 20 min. The pellet was washed with 70% ethanol followed by an ethanol precipitation (as described previously), drying and re-suspension in sdH_2O.

A4. DNA quantification

DNA was quantified on the Nanodrop ND-1000 Spectrophotometer (Thermo Scientific), which allowed for the purity of the sample to be measured by assessing the 260/280 ratio (RNA contamination) and the 230/260 ratio (organic salts contamination). Agarose gel

electrophoresis was also used to estimate DNA concentrations based on the intensity of the DNA bands observed and comparing to the intensity of the molecular weight marker bands (Roche and Fermentas) of known concentrations. The molecular weight markers used throughout this study were λIII, λIV and λVI.

A5. Agarose gel electrophoresis

Agarose gel electrophoresis, which allows for the separation of DNA fragments based on their size, was used to view DNA. Agarose gels (0.8-2 %) were prepared in TAE buffer with ethidium bromide at a final concentration of 0.5 µg/ml. DNA was mixed with loading dye prior to being loaded onto the gel and separated in TAE buffer at 80-100 V. Molecular weight markers were always included on the gels to determine the size of the DNA fragments being separated. Gels were viewed and images captured under UV light using the Vacutec G:Box SYNGENE system and software (GeneSnap).

A6. DNA manipulation

A6.1. DNA amplification

Primers for DNA amplification by Polymerase chain reaction (PCR) were designed using the online program Primer3 (http://frodo.wi.mit.edu/), which identifies the most appropriate primer sequences from the input region based on the selection criteria stipulated in Table A1.

Table A 4: Criteria used for the selection of oligonucleotide sequences on Primer3

	Size	**Tm**	**GC %**
Minimum	18	55	55
Optimum	23	60	62
Maximum	25	63	70

Routine PCR reactions for screening were performed with FastStart Taq DNA Polymerase (Roche), following the manufacturer's instructions. PCR reactions were set up in 25 µl with

the following components: 1× PCR Reaction buffer with $MgCl_2$, 1× GC Rich, dNTPs to a final concentration of 0.2 mM each, forward and reverse primers to a final concentration of 1 µM each, DNA template between 10-100 ng/µl and 2U enzyme. Reactions were always made up to volume with sterile distilled nuclease free water. Cycling conditions were carried out as follows: one cycle of an initial denaturation at 94° ˚C for 4 min; 30-35 cycles of 30 sec denaturation at 94 ˚C, 30 sec annealing at 55-65 ˚C and 30-90 sec elongation at 72 ˚C, which was followed by a final elongation step at 72 ˚C for 7 min.

PCR products to be used for cloning were amplified with the high-fidelity, proof reading enzyme, Q5® High-Fidelity DNA Polymerase (New England Biolabs). Each reaction contained the following components: 1× Q5 Reaction Buffer, 200 µM dNTPs, forward and reverse primers at a final concentration of 0.5 µM each, 1× Q5 High GC Enhancer, DNA template between 50-500 ng/µl and 0.5-2U enzyme. Cycling conditions were as follows: an initial denaturation at 98 ˚C for 30 secs; 30-40 cycles of 10 sec denaturation at 98 ˚C, 30 sec annealing at the calculated annealing temperature and 30-90 sec elongation at 72 ˚C, which was followed by a 2 min final elongation step at 72 ˚C.

A6.2. Restriction digestion

Restriction enzymes used were purchased either from New England Biolabs (NEB) or Roche. Restriction digests were carried out as per the manufacturer's instructions with the recommended buffers. Double digests were either carried out simultaneously in a compatible buffer or sequentially with inactivation of the first enzyme at 65 ˚C, followed by the addition of fresh buffer and the second enzyme when the buffers were incompatible. For plasmid screening approximately 0.5-1 µg of DNA was digested in a reaction volume of 10-20 µl and incubated at 37 ˚C for 1 hour, unless otherwise recommended. Bulk digests were carried out for plasmid DNA and PCR products with 1-3 µg of DNA in reaction volumes of 15-30 µl and incubated at the recommended temperature for 1 hour. Approximately 2-5 µg of genomic DNA was digested in reaction volumes of 20-50 µl and incubated at the recommended temperature overnight (no more than 16 hours) for Southern blot analysis.

A6.3. Modification of DNA overhangs

Restriction digest fragments with 3' and/or 5' overhangs, which were incompatible for cloning were required to be blunted prior to ligation. These fragments were blunted either by removing overhangs, filling in gaps or a combination of both. T4 DNA Polymerase (NEB) or DNA Polymerase I, Large (Klenow) Fragment (NEB) were used for blunting of DNA fragments with unwanted overhangs. Both enzymes catalyse the synthesis of DNA in the 5'→ 3' direction and possess 3'→5' exonuclease activity. As per the manufacturer's instructions, reactions with T4 DNA Polymerase were carried out at ~12 ˚C in the presence of 100 µM dNTPs for 15 min and were inactivated by the addition of 10 mM EDTA and heating at 75° C for 20 min. Reactions setup with DNA Polymerase I, Large (Klenow) Fragment were supplemented with 33 µM dNTPs, carried out at room temperature for 15 min and inactivated by the addition of 10 mM EDTA and boiling at 75 ˚C for 20 mins. Prior to being used in ligation reactions, blunted fragments were purified using the NucleoSpin PCR/Gel Extraction kit following the manufacturer's instructions.

A6.4. DNA dephosphorylation

Phosphate groups from the termini of linearized vector DNA fragments need to be removed in order to prevent self-ligation and thus reduce the production of transformants carrying an empty vector during cloning. Antarctic phosphatase (NEB) catalyses the removal of 5' phosphate groups from DNA and was used for this reaction. The reaction volume varied according to the amount of DNA used but the supplied buffer was always used at 1/10 the final reaction volume with 1U of enzyme per microgram of DNA. Reactions were incubated at 37 °C for 1 hour and the enzyme was inactivated by heating at 65° C for 20 minutes. Dephosphorylated DNA fragments were purified using the NucleoSpin PCR/Gel Extraction kit, following manufacturer's instructions, prior to being used in ligation reactions.

A6.5. DNA ligation

DNA fragments were ligated together using T4 DNA Ligase (NEB). An optimum ratio of vector DNA to insert DNA needs to be used in order for the ligation reaction to be successful.

A constant of 50 ng was always used for the vector DNA and the amount of insert DNA required for a 1:5 (vector: insert) reaction was calculated using the equation:

$$Amount\ of\ insert\ DNA\ (ng) = \frac{50\ ng \text{ x size of insert (bp)}}{size\ of\ vector\ (bp)} \times 5$$

Ligation reactions were setup according to the manufacturer's instructions and contained the appropriate volume of DNA, 1 µl of enzyme, 1.5 µl of the supplied buffer (with ATP) and were made up to 15 µl with sdH_2O. The reactions were incubated at room temperature for 30 minutes for cohesive-end ligations and 2 hrs for blunt-end ligations. This was followed by heat inactivation at 65 ˚C for 10 mins prior to transformation and viewing on a gel. To assess the extent of ligation, observed as a decrease in the amount of individual fragments and an increase in the amount of circular DNA, 5 µl of the reaction was run on a 1% agarose gel.

Table A 5: A list of strains used and generated during this study

Strain	Description	Reference
Mtb		
H37Rv	Laboratory strain (ATCC 27294)	Laboratory collection
Δ*cydAB*	Derivative of H37Rv carrying a deletion in the *cydAB* genes (unmarked)	B. D. Kana, unpublished
Δ*cydAB*::pHINTcyd	Derivative of Δ*cydAB* carrying the *cydABCD* gene cluster integrated at the *attB* locus	B. D. Kana, unpublished
Δ*cydAB*Δ*narGHJI*	Derivative of Δ*cydAB* carrying the above mentioned deletion in the *narGHJI* operon (unmarked)	B. D. Kana, unpublished
M. smegmatis		
mc^2 155	High frequency transformation mutant of ATCC 607	Snapper *et al*., 1990
Δ*qcrCAB::hyg*	*qcrCAB* deletion-insertion mutant of mc^2 155; Hyg^R	Matsoso *et al*., 2005
Δ*cydA::aph*	*cydA* knockout mutant of mc^2 155; Kan^R	Kana *et al*., 2001
Δ*cydA::aph*(pOTBCYD)	Δ*cydA::aph* carrying *Mtb cydABDC* gene cluster on pOTBCYD; Kan^R, Hyg^R	Kana *et al*., 2001
Δ*narB*	Derivative of $mc^2$155 carrying an unmarked deletion in *M. smegmatis narB*	N.C. Narrandes, MSc dissertation 2013
Δ*narGHJI*	Derivative of $mc^2$155 carrying an unmarked deletion in *M. smegmatis narGHJI* operon	N.C. Narrandes, MSc dissertation 2013
Δ*narB* Δ*narGHJI*	Derivative of Δ*narB* carrying an unmarked deletion in *M. smegmatis narGHJI* operon	N.C. Narrandes, MSc dissertation 2013
Δ*narB* (pMnarB)	Derivative of Δ*narB* carrying *narB* expressed constitutively from the *hsp60* promoter	This work
Δ*narB* Δ*narGHJI* (pMnarB)	Derivative of Δ*narB* Δ*narGHJI* carrying *narB* expressed constitutively from the *hsp60* promoter	This work
Δ*qcrCAB*	Derivative of $mc^2$155 carrying an unmarked deletion in *M. smegmatis qcrCAB*	This work
Plasmids		
p2NIL	Cloning vector; Km^r	Parish *et al.*, 2000
pGOAL19	Plasmid carrying *hyg, lacZ, and sacB* genes as a *Pac*I cassette; Amp^r, Hyg^r	Parish *et al.*, 2000
pMhsp60	A mycobacterial expression vector carrying the *hsp60* promoter. Hyg^r	Williams *et al*., 2011
pMnarB	A derivative of pMhsp60 carrying the full length *narB* under the control of *hsp60*. Hyg^r	This study
p2nilqcrKO	A derivative of p2NIL carrying the unmarked mutant allele for *M. smegmatis qcrCAB*. Kan^R	This study
pqcrKO	A derivative of p2nilqcrKO carrying the *hyg*, *lacZ* and *sacB* genes from pGOAL19. Amp^r, Hyg^r, Kan^R	This study

Table A 6: A list of the primers used during this study

Primer name	Primers sequence
Screening primers	
narScreenF	GGACGTGTGGAAGAACTGCT
narScreen out R	GATCCGCACGAAATGGTC
narScreenG R	GTAGTCGGTCTCCTGGGTCTC
narBScreen out	GGTCATGATCGGCCCTCT
narBScreenF	GATGCGTCCGTCCTTGAC
narBScreenR	TCGTAGCTCAGTGGGAGAGC
Qcr ScreenR	CGCCGTGAGCGACTTGTG
qcrseq4	GCCTTCGTCCTTCTGTTG
qcrInt ScreenR	CCCTTACCGGTGAAGTTG
KanF	ATGAGCCATATTCAACGGG
KanR	TTAGAAAAACTCATCGAGC
Mtb cydScrF	CCA CCG TGC TGA GTA GAT AG
Mtb cydScrR	CGG TAT CAC CAC CGT CTA
Mtb cydScrI	GAC CGT CAG GAC AGA GAA G
cydUSF	gcgcGAATTCGACGGTCAAATCCAGCACG
cydDSR	gcgcACGCGTGAAGTAGATCGGCCAGCGATA
Complementation	
narB F	AAGCTTTCATGGCTCGCACAGACCGGATC (*Hind*III)
narB R	GTTAACCTCTCAGAGGTGTTCGTCGGCGA (*Hpa*I)
RT PCR primers	
narG RTF	CAACGGGGTCCTGGTATGTC
narG RTR	TTGATCAACAGCCGGGTCAG
SSF	GGGCGTGATGTCCATCTCCT
SSR	GTATCCCGGTGCATGGTC
narB RTF3	TTCCACACCCGCACCAAG
narB RTR3	AACGGCAGGAACACCACC

B. Appendix B-Bioinformatics tools

B1. BLAST

(http://blast.ncbi.nlm.nih.gov/Blast.cgi)

The Basic Local Alignment Search Tool (BLAST) allows for the comparison of nucleotide and protein sequences to sequenced genomes contained in a database. This tool facilitates the identification of similar DNA regions and proteins among different organisms based on sequence alignments and aids in assigning characteristics to genes and proteins of unknown function.

B2. Mycobrowser

(http://mycobrowser.epfl.ch)

Mycobrowser is a database containing genomic and proteomic data of various mycobacterial organisms, importantly *M. tuberculosis* H37Rv and *M. smegmatis*. The database is manually curated and allows for the retrieval of gene and protein sequences and also provides links to functional information associated with the annotations.

B3. EcoGene-RefSeq

(www.ecogene.org/refseq)

This database houses more than 2700 genome sequences of prokaryotic organisms. It allows for the retrival of gene and protein sequences and facilitates sequences comparison between multiple organisms.

B4. KEGG Pathway Database

(http://www.genome.jp/kegg/pathway.html)

Kyoto Encyclopedia of Genes and Genomes (KEGG) is a database containing a collection of manually drawn pathway maps of several cellular processes from copious organisms. It aids in the global understanding of biological systems from the gene to the organisms environment. This tool allows for the study of specific metabolic pathways.

B5. i-TASSER

(https://zhanglab.ccmb.med.umich.edu/I-TASSER/)

i-TASSER (Iterative Threading ASSEmbly Refinement) is a database which allows for the prediction of protein structures and function based on the sequence queried.

B6. Sequence alignments

Sequence alignment tools allow for the alignment of protein or nucleotide sequences to identify homology from which structural and functional similarities or evolutionary relationships can be inferred.

B6.1. ClustalW2

(http://www.ebi.ac.uk/Tools/msa/clustalw2/)

ClustalW2, a program developed by the European Bioinformatics Institute is a multiple sequence alignment (MSA) tool used to identify similarities and/or differences among three or more protein or nucleotide sequences of the same length at a time. This tool allows for the identification of conserved residues within sequences and for evolutionary relationships to be studied between the sequences.

B6.2. Needle

(http://www.ebi.ac.uk/Tools/psa/emboss_needle/) - protein

(http://www.ebi.ac.uk/Tools/psa/emboss_needle/nucleotide.html) – nucleotide

Needle is a pairwise alignment tool that differs from ClustalW2 in that it only allows for the alignment of two sequences of any length at a time and identifies regions of similarity within the sequences which could point to structural, functional and/or evolutionary relationships shared.

C. Appendix C

C1. Media components

7H9

Monosodium phosphate	2g	Magnesium sulfate	0.05
Disodium phosphate	1.g	Zinc sulfate	0.001
Monosodium glutamate	0.5g	Copper sulfate	0.001
Sodium citrate	0.1g	Biotin	0.5mg
Ammonium sulfate	0.5g	Calcium chloride	0.5mg
Pyridoxine	0.001g	Glycerol	0.2%
Ferric ammonium citrate	0.04g		

7H10

Monosodium phosphate	1.5g	Zinc sulfate	0.001
Disodium phosphate	1.5g	Copper sulfate	0.001
Monosodium glutamate	0.5g	Biotin	0.5mg
Sodium citrate	0.4g	Calcium chloride	0.5mg
Ammonium sulfate	0.5g	Malachite green	0.25mg
Pyridoxine	0.001g	Agar	17g
Ferric ammonium citrate	0.04g	Glycerol	0.5%
Magnesium sulfate	0.025g		

7H11

Monosodium phosphate	1.5g	Zinc sulfate	1mg
Disodium phosphate	1.5g	Copper sulfate	1mg
Monosodium glutamate	0.5g	Biotin	0.5mg
Sodium citrate	0.4g	Calcium chloride	0.5mg
Ammonium sulfate	0.5g	Pancreatic digest of casein	1g
Pyridoxine	0.001g	Malachite green	0.25mg
Ferric ammonium citrate	0.05g	Agar	13.5g
Magnesium sulfate	0.05g	Glycerol	0.5%

MB

Magnesium chloride	0.5 mM	Potassium nitrate	10 mM
Calcium chloride	0.5 mM	Monopotassium dihydrogen phosphate	2 mg

Disodium monohydrogen phosphate	5 mg	Manganese chloride	0.02 mg
Potassium sulfate	4 mg	Sodium borate	0.02 mg
Zinc chloride	0.08 mg	Ammonium molybdate	0.02 mg
Iron chloride	0.4 mg	Glycerol	0.2%
Copper chloride	0.02 mg		

Sautons (SM)

Asparagine	4 g	Monopotassium dihydrogen phosphate	0.5 g
Magnesium sulfate	0.5 g	Ammonium ferric citrate	0.05 g
Citric acid	2 g	Glycerol	6%
Zinc chloride	0.0001%		

MPLN

Monosodium dihydrogen phosphate	5 g
Sodium citrate	2 g
Magnesium sulfate	0.6 g
Sodium nitrate	10 mM
Glycerol	2%

PCB (pH 4.5)

Sodium citrate	200 mM
Citric acid	100 mM

LA

Tryptone	1%
Sodium chloride	0.5%
Yeats extract	0.5%

LB

Tryptone	1%
Sodium chloride	0.5%
Yeats extract	0.5%
Agar	1.5%

2xTY

Tryptone	2%
Sodium chloride	0.5%
Yeast extract	1%

SOC

Yeast extract	0.5%
Tryptone	2%
Sodium chloride	10 mM
Potassium chloride	2.5 mM
Magnesium chloride	10 mM
Magnesium sulfate	10 mM
Glucose	20 mM

C2. Media supplement stocks

OADC (10X)

Bovine serum albumin fraction V (BSA)	0.5%
Dextrose	0.2%
Catalase	0.004%
Oleic acid	0.005%
Sodium chloride	0.085%

ADS (10X)

BSA	0.5%
Glucose	0.2%
Sodium chloride	0.085%

GN (100X)

Glucose	0.2%
Sodium chloride	0.085%

Tween80 (25%)

10 ml Tween80 in 40 ml dH_2O

Tyloxapol (10%)

5 ml tyloxapol in 45 ml dH_2O

Sucrose (75 %)

75 g sucrose in 100 ml dH_2O

X-gal (2%)

1 g X-gal in 50 ml deionised DMF

D. Cloning and strain generation

D1. Strains used in Chapter 2

The generation of *M. smegmatis* strains used in Chapter 2 was previously described by Kana *et al*. (2001) [Δ*cydA::kan* and Δ*cydA::kan* (pOTBCYD)] and Matsoso *et al*. (2005) for Δ*qcrCAB::hyg*. Each of the mutant strains was a deletion-insertion mutant. The *M. smegmatis* Δ*cydA::kan* was complemented with pOTBCYD which was an episomal vector carrying the Mtb genes under the control of the native promoter, therefore Δ*cydA::kan* (pOTBCYD) was heterologously complemented. Mtb Δ*cydAB* was a knockout mutant previously generated by Kana, B.D by homologous recombination (unpublished). The mutant retained only 245 bp of the 5' region of *cydA* and 157 bp of the 3' region of *cydB*. The complemented strain of Mtb carried an integrating vector which harboured a region of the chromosome that contained the *cydAB* and the *cydDC* operons, therefore Δ*cydAB::*pHINTCYD carried two functional copies of *cydD* and *cydC*.

D2. Strains used in Chapter 3

Briefly, each of the strains was generated by homologous recombination with Δ*narB* missing 2368 bp of the gene and Δ*narGHJI* retaining only 15 bp of the 5' end of *narG* and 10 bp of the 3' end of *narI*. The double mutant Δ*narB* Δ*narGHJI* was generated by knocking out *narGHJI* in the Δ*narB* background. The genomic maps and Southern blots which were performed during my MSc for each mutant strain are shown in Figure D1 and D2 to provide clarity on the genotype of the mutants generated. Each blot produced the correct bands, thus confirming the genotype of each strain.

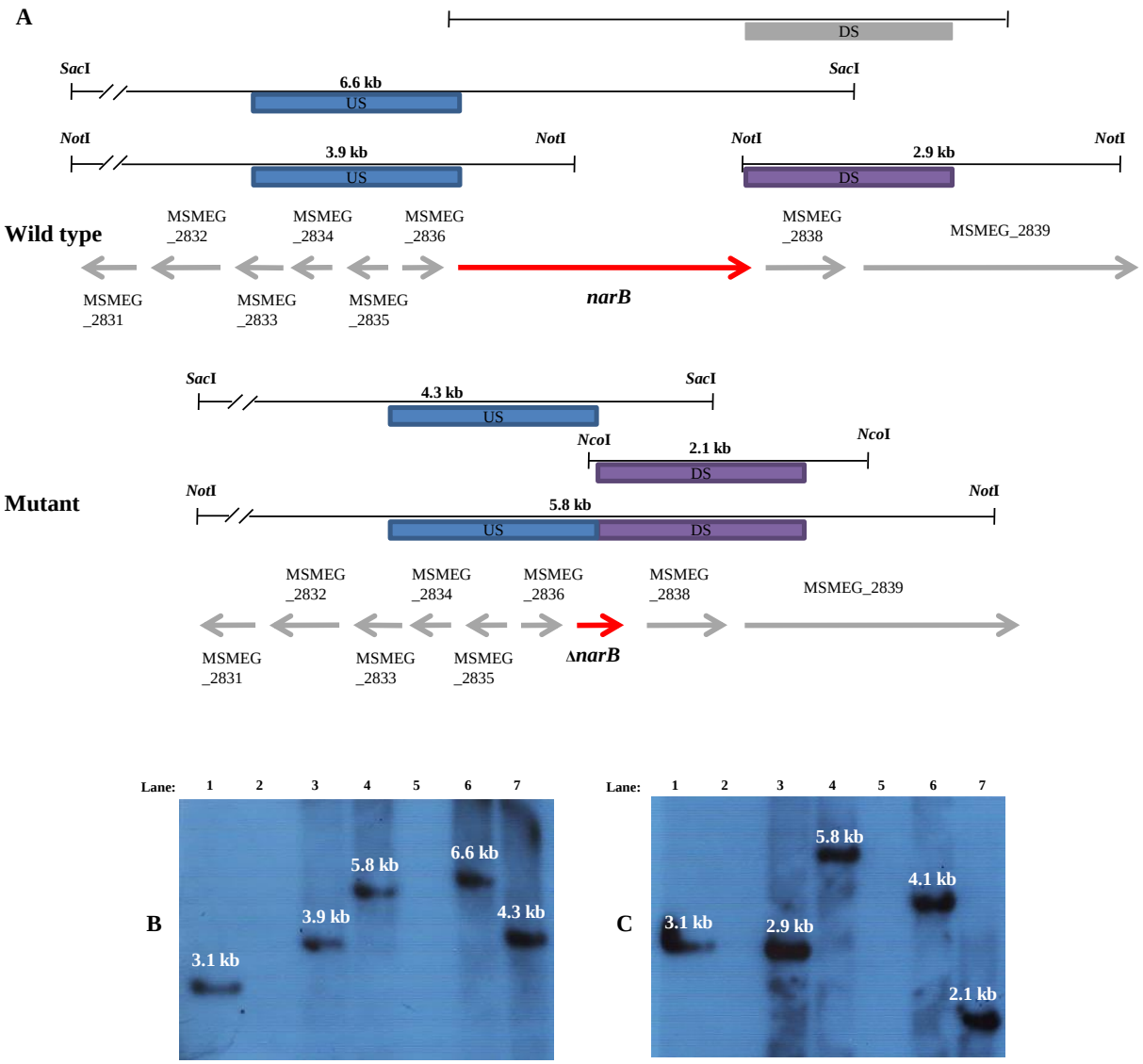


Figure D 1: Genotypic confirmation of Δ*narB*. (A) Schematic representation of genomic maps of wild type and mutant *narB* regions. Restriction enzymes, probes and expected fragment sizes for southern blot confirmation are depicted. **(B)** Southern blot with upstream probe (US). Lane 1: Marker λIV, Lane 2: Empty, Lane 3: *Not*I digested wild type DNA, Lane 4: *Not*I digested Δ*narB* DNA, Lane 5: Empty, Lane 6: *Sac*I digested wild type DNA, Lane 7: *Sac*I digested Δ*narB* DNA. **(C)** Southern blot with downstream probe (DS). Lane 1: Marker λIV, Lane 2: Empty, Lane 3: *Not*I digested wild type DNA, Lane 4: *Not*I digested Δ*narB* DNA, Lane 5: Empty, Lane 6: *Nco*I digested wild type DNA, Lane 7: *Nco*I digested Δ*narB* DNA.

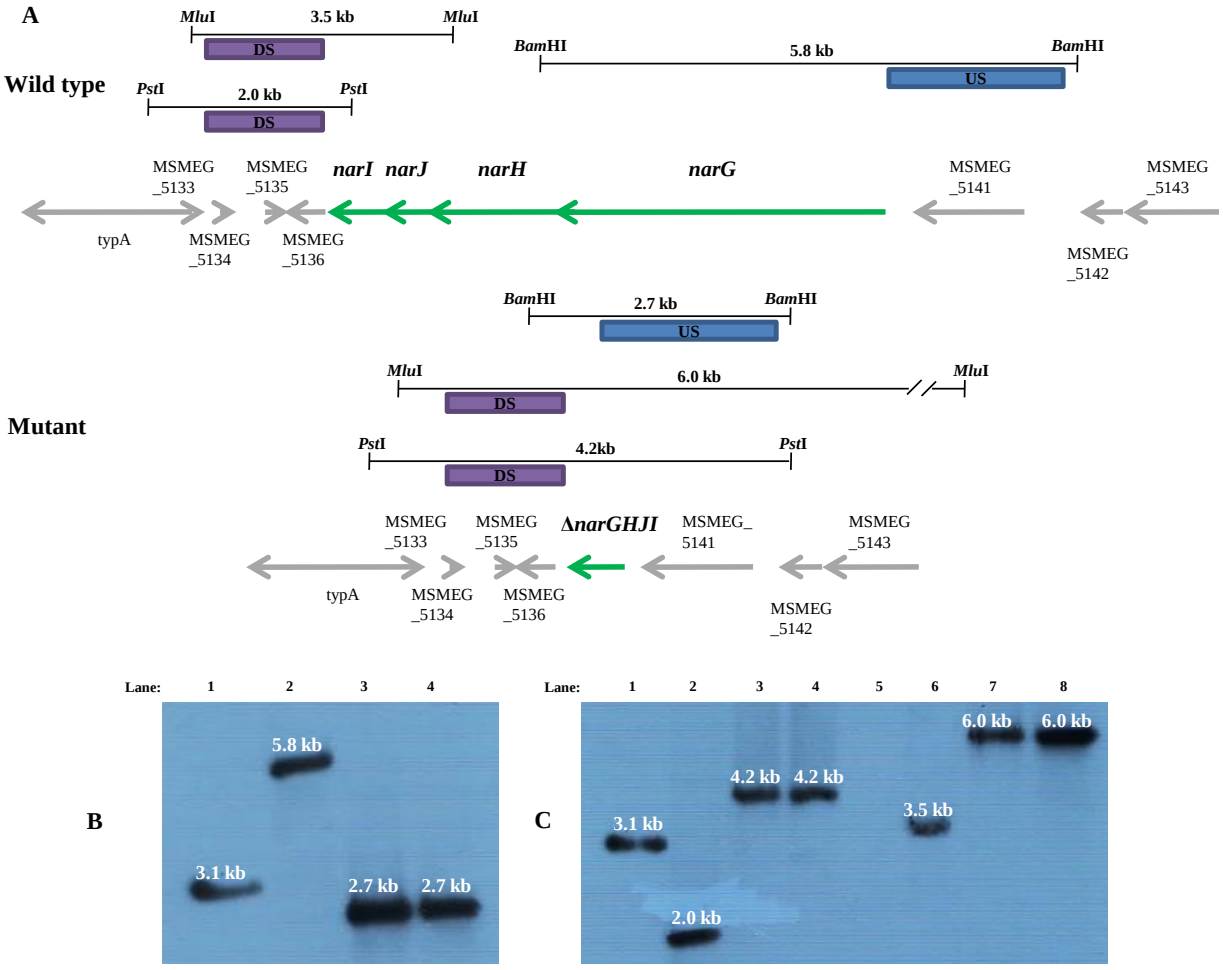


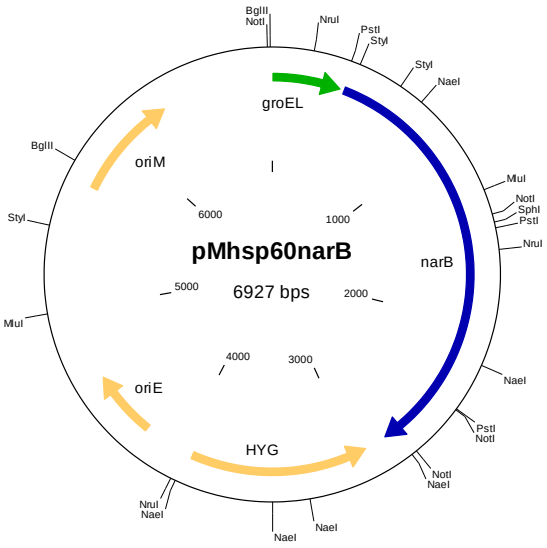
Figure D 2: Genotypic confirmation of *Δ*narGHJI *and* Δ*narB* Δ*narGHJI*. (A) Schematic representation of genomic maps of wild type and mutant *narGHJI* regions. Restriction enzymes, probes and expected fragment sizes for southern blot confirmation are depicted. **(B)** Southern blot with upstream probe (US). Lane 1: Marker λIV, Lane 2: *Bam*HI digested wild type DNA, Lane 3: *Bam*HI digested Δ*narGHJI* DNA, Lane 4: *Bam*HI digested Δ*narB* Δ*narGHJI* DNA. **(C)** Southern blot with downstream probe (DS). Lane 1: Marker λIV, Lane 2: *Pst*I digested wild type DNA, Lane 3: *Pst*I digested Δ*narGHJI* DNA, Lane 4: *Pst*I digested Δ*narB* Δ*narGHJI* DNA, Lane 5: Empty, Lane 6: MuI digested wild type DNA, Lane 7: *Mlu*I digested Δ*narGHJI* DNA, Lane 8: *Mlu*I digested Δ*narB* Δ*narGHJI* DNA.

E. Supplementary results for Chapter 3

E1. Complementing vector generation

The complementing vector, pMnarB was constructed as described in section 3.3.3 and confirmed by restriction mapping shown in Figure E1. Restriction enzyme star activity was observed for *Bgl*II, *Sph*I and *Nae*I, however the predominat correct bands were observed in each case and sequence analysis revealed that no mutations ha dbeen incorporated into the promoter or coding sequence of the gene. This vector was then introduced into Δ*narB* and Δ*narB* Δ*narGHJI* and all the strains used were confirmed by PCR analysis.

Enzyme	Expected sizes
*Bgl*II	1142, 5785
*Nru*I	1406, 2362, 3159
*Not*I	276, 999, 1459, 4193
*Sph*I	Linear
*Mlu*I	3235, 3692
*Nae*I	182, 486, 543, 552, 1400, 3764
*Sty*I	223, 1927, 4777



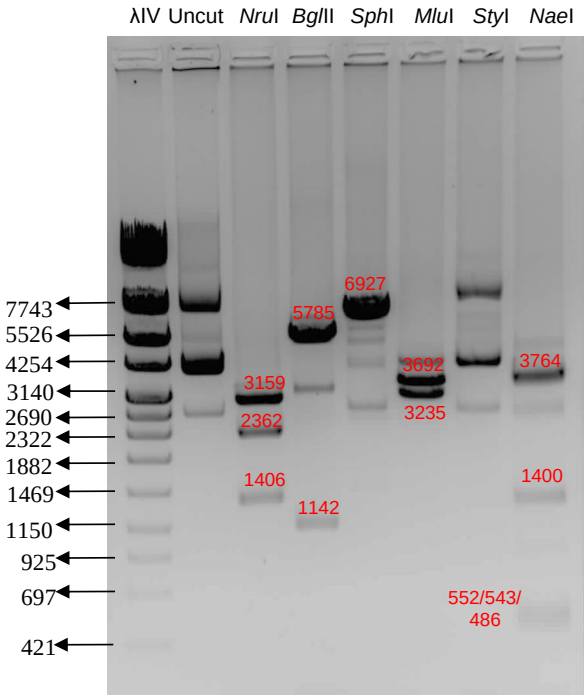


Figure E 1: Confirmation of the *narB* complementing vector, pMnarB. The expected fragment sizes for each restriction enzyme used are listed in the table. The vector map shows the distribution of the restriction sites and the gel shows the pattern obtained for each restriction digest.

E2. PCR confirmation of strains

A schematic representation of the genomic region of each mutant compared to the wild type region is shown in Figure E2 along with the PCR confirmations of each strain. In each case the

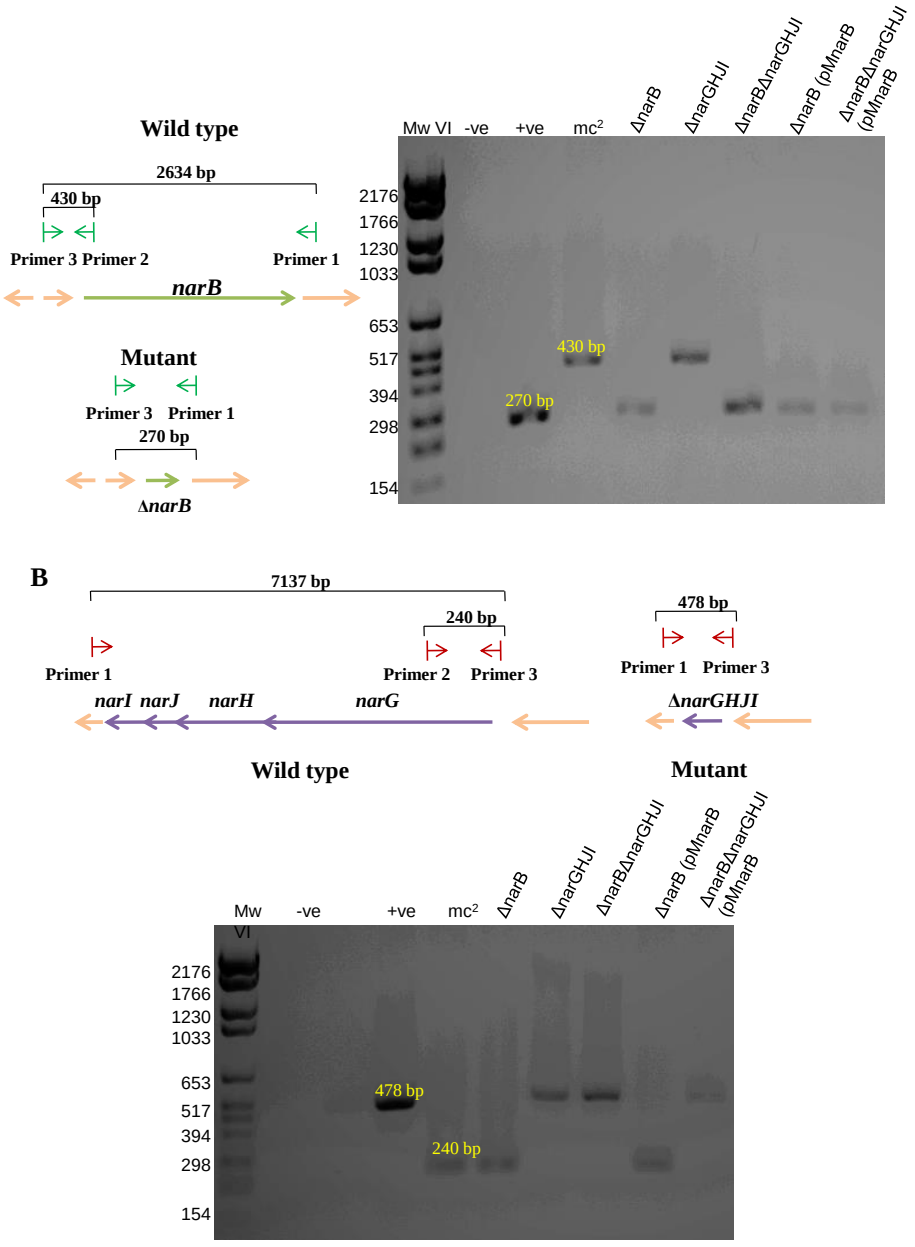


Figure E 2: The genotypic confirmation of mutant strains previously generated. (A) Genome organisation of the wild type and mutant narB region. The gel shows the PCR products obtained for screening with the *narB* screening primers. Primer 1- narBScreen out R, primer 2- narBScreenR , primer 3- narBScreenF . **(B)** Genome organisation of the wild type and mutant region for narGHJI. The gel image depicts the PCR products obtained from PCR reactions with the *narGHJI* screening primers. Primer 1- narScreenout, primer 2- narScreenF, primer 3- narScreenR.

correct amplicon was observed, thus confirming that all the strains were correct.

E3. Expression of *sigA*

The expression analysis of *narB* and *narG* revealed that the specific transcript products for both genes could not be detected from cultures grown in 7H9 while increased detection of the non-specific product was detected for samples grown in MPLN. As evidence that the lack of transcript detection was not because of degradation of the RNA sample, expression of the housekeeping gene *sigA* is shown in Figure E3A and C for samples grown in 7H9 and MPLN respectively. Figure E3B highlights the non-specific product detected in samples wherein *narB*

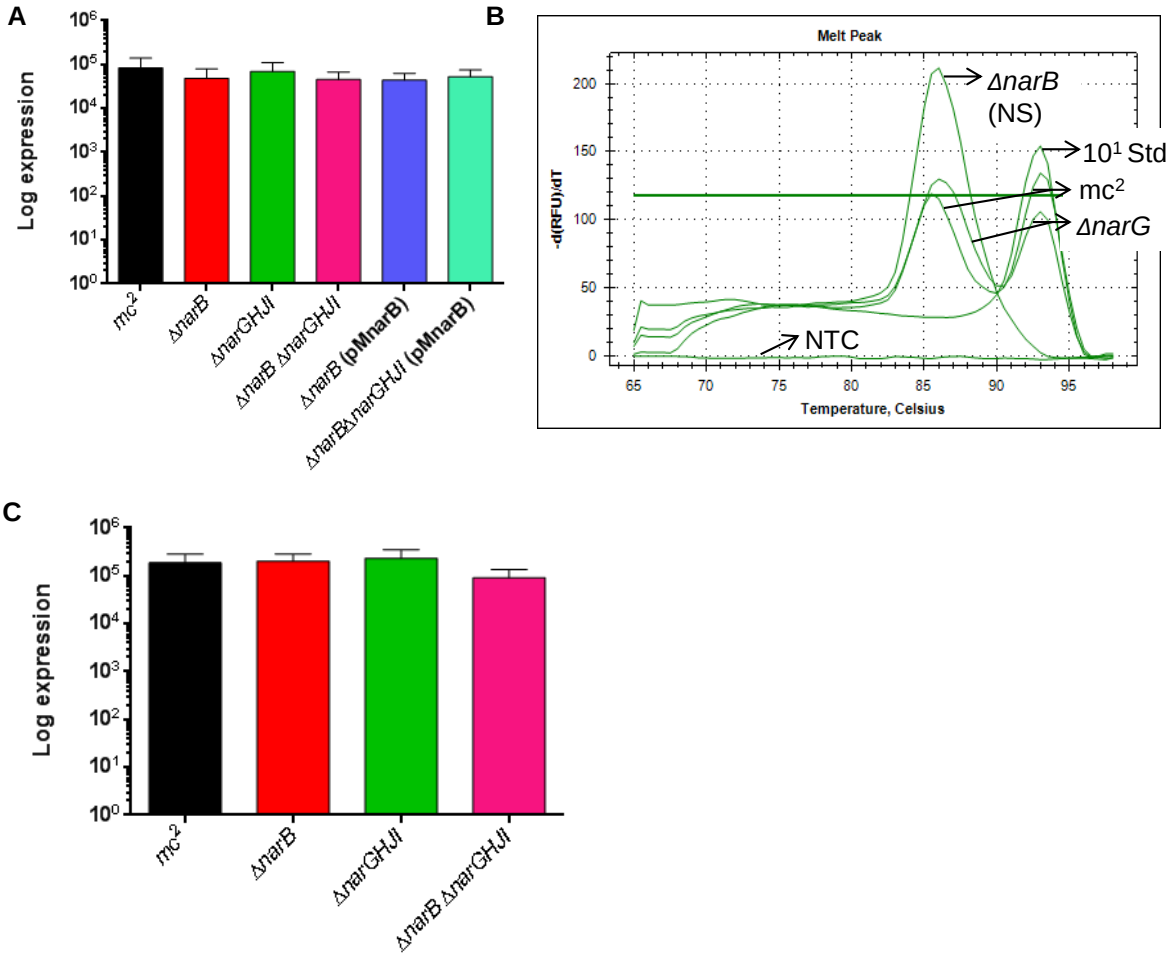


Figure E 3: The expresssion of *sigA* in strains grown in 7H9 or MPLN. (A) Expression in 7H9. **(B)** An example of a melt curve obtained for *narB* primers highlighting the non-specific product detected in the different strains when grown in MPLN.

primers were used. The non-specific product is seen in wild type and Δ *narGHJI* along with some of the specific product. However, only the non-specific product was detected in Δ*narB*. The control showing the position of the specific *narB* transcript product is one of the samples used for the standard, which was a dilution of genomic DNA labelled as "Std 10^1". The absence of any product in the no-template-control (NTC) confirms that the non-specific product is not a result of DNA/RNA contamination.

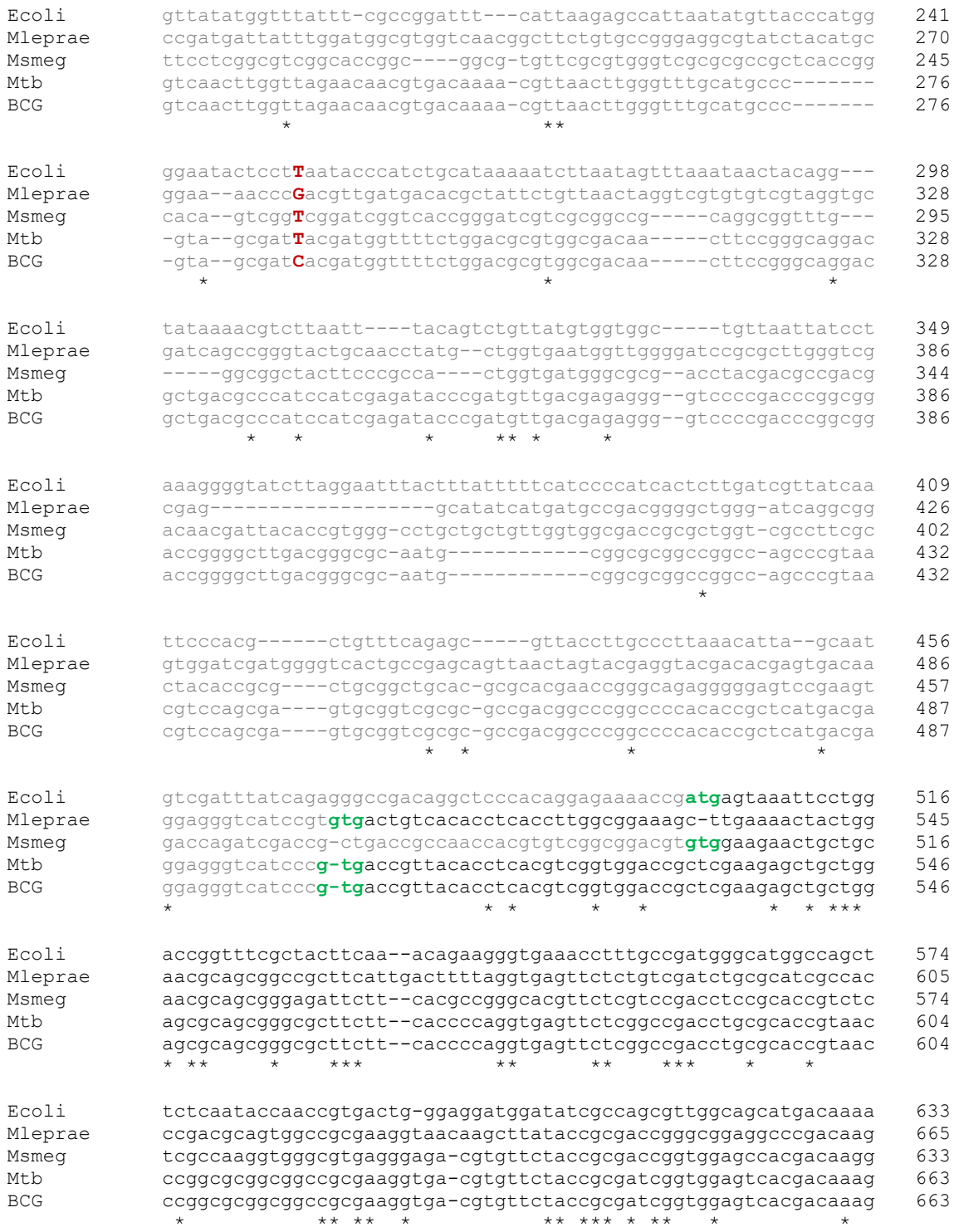


Figure E 4: Sequence alignments of narG promoter regions. Grey text shows the narG upstream promoter region. Black text depicts nucleotides of the narG gene sequence. Green text represents the start codon of each homologue while the red uppercase text depicts the promoter mutation site with which differing NR activity is associated. Ecoli: *Escherichia coli*, Mleprae: *Mycobacterium leprae*, Msmeg: *Mycobacterium smegmatis*, Mtb: *Mycobacterium tuberculosis*, BCG: *Mycobacterium bovis* BCG.

```
Ecoli              ----------MSKFLDRFRYFKQKGETFADGHGQLLNTNRDWEDGYRQRWQHDKIVRSTH    50
MSMEG_5140         ----------MEELLQRSGRFFTPGTFSSDLRTVSRQGGREGDVFYRDRWSHDKVVRSTH    50
M.canettii         MTITPHVGGPLEELLERSGRFFTPGEFSADLRTVTRRGGREGDVFYRDRWSHDKVVRSTH    60
M.bovis            MTVTPHVGGPLEELLERSGRFFTPGEFSADLRTVTRRGGREGDVFYRDRWSHDKVVRSTH    60
M.africanum        MTVTPHVGGPLEELLERSGRFFTPGEFSADLRTVTRRGGREGDVFYRDRWSHDKVVRSTH    60
MTBC               MTVTPHVGGPLEELLERSGRFFTPGEFSADLRTVTRRGGREGDVFYRDRWSHDKVVRSTH    60
M.tuberculosis     MTVTPHVGGPLEELLERSGRFFTPGEFSADLRTVTRRGGREGDVFYRDRWSHDKVVRSTH    60
                             :.::*:*   *   *   :* :    .  *: :  **:**.***:*****

Ecoli              GVNCTGSCSWKIYVKNGLVTWETQQTDYPRTRPDLPNHEPRGCPRGASYSWYLYSANRLK    110
MSMEG_5140         GVNCTGSCSWKIYVKDGIITWETQETDYPSVGPDRPEYEPRGCPRGAAFSWYTYSPTRVR    110
M.canettii         GVNCTGSCSWKIYVKDGIITWETQQTDYPSVGPDRPEYEPRGCPRGASFSWYSYSPTRVR    120
M.bovis            GVNCTGSCSWKIYVKDGIITWETQQTDYPSVGPDRPEYEPRGCPRGASFSWYSYSPTRVR    120
M.africanum        GVNCTGSCSWKIYVKDGIITWETQQTDYPSVGPDRPEYEPRGCPRGASFSWYSYSPTRVR    120
MTBC               GVNCTGSCSWKIYVKDGIITWETQQTDYPSVGPDRPEYEPRGCPRGASFSWYSYSPTRVR    120
M.tuberculosis     GVNCTGSCSWKIYVKDGIITWETQQTDYPSVGPDRPEYEPRGCPRGASFSWYSYSPTRVR    120
                   ***************:*::*****:**** . ** *::**********::*** ** .*::

Ecoli              YPMMRKRLMKMWREAKALHSDPVEAWASIIEDADKAKSFKQARGRGGFVRSSWQEVNELI    170
MSMEG_5140         YPYARGVLVEMYREARARLGDPVLAWADIQADPERRRRYQSARGKGGLVRVSWAEATEMI    170
M.canettii         YPYARGVLVEMYREAKTRLGDPVLAWADIQADPERRRRYQQARGKGGLVRVSWAEASEMI    180
M.bovis            YPYARGVLVEMYREAKTRLGDPVLAWADIQADPERRRRYQQARGKGGLVRVSWAEASEMV    180
M.africanum        YPYARGVLVEMYREAKTRLGDPVLAWADIQADPERRRRYQQARGKGGLVRVSWAEASEMV    180
MTBC               YPYARGVLVEMYREAKTRLGDPVLAWADIQADPERRRRYQQARGKGGLVRVSWAEASEMV    180
M.tuberculosis     YPYARGVLVEMYREAKTRLGDPVLAWADIQADPERRRRYQQARGKGGLVRVSWAEASEMV    180
                   **  *  *::*:***::  .*** ***.*  * :: : ::.***:**:** ** *..*::

Ecoli              AASNVYTIKNYGPDRVAGFSPIPAMSMVSYASGARYLSLIGGTCLSFYDWYCDLPPASPQ    230
MSMEG_5140         AAAHVHTIKTYGPDRIAGFSPIPAMSMVSHAAGSRFVELIGGVMTSFYDWYADLPVASPQ    230
M.canettii         AAAHVHTIKTYGPDRVAGFSPIPAMSMVSHAAGSRFVELIGGVMTSFYDWYADLPVASPQ    240
M.bovis            AAAHVHTIKTYGPDRVAGFSPIPAMSMVSHAAGSRFVELIGGVMTSFYDWYADLPVASPQ    240
M.africanum        AAAHVHTIKTYGPDRVAGFSPIPAMSMVSHAAGSRFVELIGGVMTSFYDWYADLPVASPQ    240
MTBC               AAAHVHTIKTYGPDRVAGFSPIPAMSMVSHAAGSRFVELIGGVMTSFYDWYADLPVASPQ    240
M.tuberculosis     AAAHVHTIKTYGPDRVAGFSPIPAMSMVSHAAGSRFVELIGGVMTSFYDWYADLPVASPQ    240
                   **:.*:***.*****:**************:*:*:*::.****.  ******.*** ****

Ecoli              TWGEQTDVPESADWYNSSYIIAWGSNVPQTRTPDAHFFTEVRYKGTKTVAVTPDYAEIAK    290
MSMEG_5140         VFGDQTDVPESGDWWDAAYLMMWGSNVPVTRTPDAHWMAEVRYRGTKVVSVSPDYADNTK    290
M.canettii         VFGDQTDVPESGDWWDASYLVMWGSNVPITRTPDAHWMAEARYRGAKVVVVSPDYADNTK    300
M.bovis            VFGDQTDVPESGDWWDASYLVMWGSNVPITRTPDAHWMAEARYRGAKVVVVSPDYADNTK    300
M.africanum        VFGDQTDVPESGDWWDASYLVMWGSNVPITRTPDAHWMAEARYRGAKVVVVSPDYADNTK    300
MTBC               VFGDQTDVPESGDWWDASYLVMWGSNVPITRTPDAHWMAEARYRGAKVVVVSPDYADNTK    300
M.tuberculosis     VFGDQTDVPESGDWWDASYLVMWGSNVPITRTPDAHWMAEARYRGAKVVVVSPDYADNTK    300
                   .:*:*******.**::::*:: ****** *******:::*.**:*:*.* *:****: :*

Ecoli              LCDLWLAPKQGTDAAMALAMGHVMLREFHLDNPSQYFTDYVRRYTDMPMLVMLEERDGYY    350
MSMEG_5140         FADEWMPCAAGTDGALAMAMGHVILSECFVQNEVPYFTDFARRFTDLPFLAKLEERDGAL    350
M.canettii         FADEWVRCAAGTDTALAMAMGHVILSECYVRNQVPFFVDYVRRYTDLPFLIKLEKRGEVL    360
M.bovis            FADEWVRCAAGTDTALAMAMGHVILSECYVRNQVPFFVDYVRRYTDLPFLIKLEKRGDLL    360
M.africanum        FADEWVRCAAGTDTALAMAMGHVILSECYVRNQVPFFVDYVRRYTDLPFLIKLEKRGDLL    360
MTBC               FADEWVRCAAGTDTALAMAMGHVILSECYVRNQVPFFVDYVRRYTDLPFLIKLEKRGDLL    360
M.tuberculosis     FADEWVRCAAGTDTALAMAMGHVILSECYVRNQVPFFVDYVRRYTDLPFLIKLEKRGDLL    360
                   :.* *:    *** *:*:*****:* * .: *   :*.*:.**:**:*:*  **:*
```

```
Ecoli              AAGRMLRAADLVDALGQENNPEWKTVAFN-TNGEMVAPNGSIGFRWGEKG--KWNLEQRD    407
MSMEG_5140         VPGKNLTAADLTPDVAAQENAAFKPALLDSASDSIAIPQGSLGFRFGESGLGNWNLDLEN    410
M.canettii         VPGKFLTAADIDEEI---ENAAFKPALLDELTNTVVVPQGSLGFRFGEDGVGKWNLDLGS    417
M.bovis            VPGKFLTAADIGEES---ENAAFKPALLDELTNTVVVPQGSLGFRFGEDGVGKWNLDLGS    417
M.africanum        VPGKFLTAADIGEES---ENAAFKPALLDELTNTVVVPQGSLGFRFGEDGVGKWNLDLGS    417
MTBC               VPGKFLTAADIGEES---ENAAFKPALLDELTNTVVVPQGSLGFRFGEDGVGKWNLDLGS    417
M.tuberculosis     VPGKFLTAADIGEES---ENAAFKPALLDELTNTVVVPQGSLGFRFGEDGVGKWNLDLGS    417
                   . *: * ***:       :*  :* . ::  .  :. *:**:***:**.*  :***:  .

Ecoli              GKTGEETELQLSLLGSQ--DEIAEVGFPYFGGDGTEHFNKVELENVLLHKLPVKRLQLAD    465
MSMEG_5140         LAPALTVAADTGETAE-----VTLPRFDTLDGHGDT----------MVRGVPVR-----R    450
M.canettii         VVPALSVEMDHAVNGDRSAELVTLPSFDTIDGHGET----------VSRGVPVR-----R    462
M.bovis            VVPALSVEMDKAVNGDRSAELVTLPSFDTIDGHGET----------VSRGVPVR-----R    462
M.africanum        VVPALSVEMDKAVNGDRSAELVTLPSFDTIDGHGET----------VSRGVPVR-----R    462
MTBC               VVPALSVEMDKAVNGDRSAELVTLPSFDTIDGHGET----------VSRGVPVR-----R    462
M.tuberculosis     VVPALSVEMDKAVNGDRSAELVTLPSFDTIDGHGET----------VSRGVPVR-----R    462
                      .  .  : .  ..     ::   *  : *.*            : : :**:

Ecoli              GSTALVTTVYDLTLANYGLERGLNDVNCATSYDD-VKAYTPAWAEQITGVSRSQIIRIAR    524
MSMEG_5140         VGEHLVCTVFDLMLAQYGVARPGLPGDWPTGFDDATRPYTPAWQEPITGVAAAQAIRVAR    510
M.canettii         VGKHLVCTVFDLMLAHYGVKRAGLPGEWPTGYHDRTQQNTPAWQESITGVPAAQAIRFAK    522
M.bovis            AGKHLVCTVFDLMLAHYGVARAGLPGEWPTGYHDRTQQNTPAWQESITGVPAAQAIRFAK    522
M.africanum        AGKHLVCTVFDLMLAHYGVARAGLPGEWPTGYHDRTQQNTPAWQESITGVPAAQAIRFAK    522
MTBC               AGKHLVCTVFDLMLAHYGVARAGLPGEWPTGYHDRTQQNTPAWQESITGVPAAQAIRFAK    522
M.tuberculosis     AGKHLVCTVFDLMLAHYGVARAGLPGEWPTGYHDRTQQNTPAWQESITGVPAAQAIRFAK    522
                    .  ** **:** **.**: *     :  *.:.* .:  **** * ****  :* **.*:

Ecoli              EFADNADKTHGRSMIIVGAGLNHWYHLDMNYRGLINMLIFCGCVGQSGGGWAHYVGQEKL    584
MSMEG_5140         EFARNAEETRGRSMIIMGAGICQWFHGDATYRAVLALLLLTGSMGRNGGGWAHYVGQEKC    570
M.canettii         EFARNATESGGRSMIIMGGGICHWFHSDVMYRSVLALLMLTGSMGRNGGGWAHYVGQEKV    582
M.bovis            EFARNATESGGRSMIIMGGGICHWFHSDVMYRSVLALLMLTGSMGRNGGGWAHYVGQEKV    582
M.africanum        EFARNATESGGRSMIIMGGGICHWFHSDVMYRSVLALLMLTGSMGRNGGGWAHYVGQEKV    582
MTBC               EFARNATESGGRSMIIMGGGICHWFHSDVMYRSVLALLMLTGSMGRNGGGWAHYVGQEKV    582
M.tuberculosis     EFARNATESGGRSMIIMGGGICHWFHSDVMYRSVLALLMLTGSMGRNGGGWAHYVGQEKV    582
                   *** ** :: ******:*.*: :*:* *  **.:: :*:: *.:*:.************

Ecoli              RPQTGWQPLAFALDWQRPARHMNSTSYFYNHSSQWRYETVTAEELLSPMADKSRYTGHLI    644
MSMEG_5140         RPVTGWATMAMATDWSRPPRQMAGTSYWYAHTDQWRYDGYQADALSSPVGRGRFRGRHTM    630
M.canettii         RPLTGWQTMAMATDWSRPPRQVPGASYWYAHTDQWRYDGYGADKLASPVGRGRFAGKHTM    642
M.bovis            RPLTGWQTMAMATDWSRPPRQVPGASYWYAHTDQWRYDGYGADKLARPVGRGRFAGKHTM    642
M.africanum        RPLTGWQTMAMATDWSRPPRQVPGASYWYAHTDQWRYDGYGADKLASPVGRGRFAGKHTM    642
MTBC               RPLTGWQTMAMATDWSRPPRQVPGASYWYAHTDQWRYDGYGADKLASPVGRGRFAGKHTM    642
M.tuberculosis     RPLTGWQTMAMATDWSRPPRQVPGASYWYAHTDQWRYDGYGADKLASPVGRGRFAGKHTM    642
                   ** ***  :*:* **.** *:: .:**:* *:.****:   *: *  *:.       * :

Ecoli              DFNVRAERMGWLPSAPQLGTNPLTIAGEAEKAGMNPVDYTVKSLKEGSIRFAAEQPENGK    704
MSMEG_5140         DVLASAAAMGWSPFFPQFDRSSLDVADEARAADQEIPAYVTAKLADGSLKLAVTDPDNPA    690
M.canettii         DLLTSATAMGWSPFYPQFDRSSLDVADEARAAGRDIGDYVTEQLAQHKLKLSITDPDNPV    702
M.bovis            DLLTSATAMGWSPFYPQFDRSSLDVADEARAAGRDVGDYVAEQLAQHKLKLSITDPDNPV    702
M.africanum        DLLTSATAMGWSPFYPQFDRSSLDVADEARAAGRDVGDYVAEQLAQHKLKLSITDPDNPV    702
MTBC               DLLTSATAMGWSPFYPQFDRSSLDVADEARAAGRDVGDYVAEQLAQHKLKLSITDPDNPV    702
M.tuberculosis     DLLTSATAMGWSPFYPQFDRSSLDVADEARAAGRDVGDYVAEQLAQHKLKLSITDPDNPV    702
                   *. . *  *** *  **:  . * :* **. *  :   *.. .* : .::::  :*:*

Ecoli              NHPRNLFIWRSNLLGSSGKGHEFMLKYLLGTEHGIQGKDLGQQGGVKPEEVDWQDNGLEG    764
MSMEG_5140         NWPRVLDVWRANLLGSSSKGNEYFLRHLLGTTSNLQAAP----NGVRPSSVTCTDDIPEG    746
M.canettii         NWPRVLTVWRANLIGSSGKGGEYFLRHLLGTDSNAQSEP--AADAVRPRNVVWDNEIPEG    760
```

```
M.bovis             NWPRVLTVWRANLIGSSGKGGEYFLRHLLGTDSNVQSDP--PTDGVHPRDVVWDSDIPEG    760
M.africanum         NWPRVLTVWRANLIGSSGKGGEYFLRHLLGTDSNVQSDP--PTDGVHPRDVVWDSDIPEG    760
MTBC                NWPRVLTVWRANLIGSSGKGGEYFLRHLLGTDSNVQSDP--PTDGVHPRDVVWDSDIPEG    760
M.tuberculosis      NWPRVLTVWRANLIGSSGKGGEYFLRHLLGTDSNVQSDP--PSDGVHPRDVVWDSDIPEG    760
                    * ** * :**:**:***.** *::*::****    *.       .*:* .*   .:  **

Ecoli               KLDLVVTLDFRLSSTCLYSDIILPTATWYEKDDMNTSDMHPFIHPLSAAVDPAWEAKSDW    824
MSMEG_5140          KLDLLMSIDFRMTSTTLLSDVVLPAATWYEKADLSSTDMHPYVHAFSPAVDPPWETRSDF    806
M.canettii          KLDLMMSIDFRMTSTTLVSDVVLPAATWYEKSDLSSTDMHPYVHSFSPAIDPPWETRSDF    820
M.bovis             KLDLIMSIDFRMTSTTLVSDVVLPAATWYEKSDLSSTDMHPYVHSFSPAIDPPWETRSDF    820
M.africanum         KLDLIMSIDFRMTSTTLVSDVVLPAATWYEKSDLSSTDMHPYVHSFSPAIDPPWETRSDF    820
MTBC                KLDLIMSIDFRMTSTTLVSDVVLPAATWYEKSDLSSTDMHPYVHSFSPAIDPPWETRSDF    820
M.tuberculosis      KLDLIMSIDFRMTSTTLVSDVVLPAATWYEKSDLSSTDMHPYVHSFSPAIDPPWETRSDF    820
                    ****:::***::** * **::**:****** *:.::****::* :* *:** **::**:

Ecoli               EIYKAIAKKFSEVCVGHLGKETDIVTLPIQHDSAAELAQPLD-VKDWKKGECDLIPGKTA    883
MSMEG_5140          EAFGAIARAFSTLAARHLGVRTDVVLGTLQHDTLGAMAYPSGTEHDWRVTGETPVPGRTM    866
M.canettii          DAFAAIARAFSALAKRHLGTRTDVVLTALQHDTPDAMAYPDGTERDWLATGEVPVPGRTM    880
M.bovis             DAFAAIARAFSALAKRHLGTRTDVVLTALQHDTPDEMAYPDGTERDWLATGEVPVPGRTM    880
M.africanum         DAFAAIARAFSALAKRHLGTRTDVVLTALQHDTPDEMAYPDGTERDWLATGEVPVPGRTM    880
MTBC                DAFAAIARAFSALAKRHLGTRTDVVLTALQHDTPDEMAYPDGTERDWLATGEVPVPGRTM    880
M.tuberculosis      DAFAAIARAFSALAKRHLGTRTDVVLTALQHDTPDEMAYPDGTERDWLATGEVPVPGRTM    880
                    : : ***: ** :.  *** .**:*   :***:   :* *    :**       :**:*

Ecoli               PHIMVVERDYPATYERFTSIGPLMEKIGNGGKGIAWNTQSEMDLLRKLNYTKAEGPAKGQ    943
MSMEG_5140          GPLAVVERDYGAIAQKWAALGPLVEGLGVTTKGLTTHPTREVAELGAKFGVMDSGAAQGR    926
M.canettii          SKLTVVERDYTAIYDKWLTLGPLIDQFGMTTKGYTVHPFREVSELAANFGVMNSGVAVGR    940
M.bovis             SKLTVVERDYTAIYDKWLTLGPLIDQFGMTTKGYTVHPFREVSELAANFGVMNSGVAVGR    940
M.africanum         SKLTVVERDYTAIYDKWLTLGPLIDQFGMTTKGYTVHPFREVSELAANFGVMNSGVAVGR    940
MTBC                SKLTVVERDYTAIYDKWLTLGPLIDQFGMTTKGYTVHPFREVSELAANFGVMNSGVAVGR    940
M.tuberculosis      SKLTVVERDYTAIYDKWLTLGPLIDQFGMTTKGYTVHPFREVSELAANFGVMNSGVAVGR    940
                      : ****** *  ::: ::***:: :*   ** : .   *:  *     .  .* * *:

Ecoli               PMLNTAIDAAEMILTLAPETNGQVAVKAWAALSEFTGRDHTHLALNKEDEKIRFRDIQAQ   1003
MSMEG_5140          PAITTGERMADVILALSGTSNGRLAVEGFAELERRTGRKLVHLALGSEERRITYADAQAR    986
M.canettii          PAITTAKRMADVILALSGTCNGRLAVEGFLELEKRTGQRLAHLAEGSEERRITYADTQAR   1000
M.bovis             PAITTAKRMADVILALSGTCNGRLAVEGFLELEKRTGQRLAHLAEGSEERRITYADTQAR   1000
M.africanum         PAITTAKRMADVILALSGTCNGQLAVEGFLELEKRTGQRLAHLAEGSEERRITYADTQAR   1000
MTBC                PAITTAKRMADVILALSGTCNGRLAVEGFLELEKRTGQRLAHLAEGSEERRITYADTQAR   1000
M.tuberculosis      PAITTAKRMADVILALSGTCNGRLAVEGFLELEKRTGQRLAHLAEGSEERRITYADTQAR   1000
                    * :.*.   *::**:*:   **::**:.:  *.. **:  .***  .*:.:* : * **:

Ecoli               PRKIISSPTWSGLEDEHVSYNAGYTNVHELIPWRTLSGRQQLYQDHQWMRDFGESLLVYR   1063
MSMEG_5140          PVPVITSPEWSGSETGGRRYAPFTVNIEELKPFHTLTGRMHFYVDHDWLEELGEQLPVYR   1046
M.canettii          PVPVITSPEWSGSESGGRRYAPFTINIEHLKPFHTLTGRMHFYLAHDWVEELGEQLPVYR   1060
M.bovis             PVPVITSPEWSGSESGGRRYAPFTINIEHLKPFHTLTGRMHFYLAHDWVEELGEQLPVYR   1060
M.africanum         PVPVITSPEWSGSESGGRRYAPFTINIEHLKPFHTLTGRMHFYLAHDWVEELGEQLPVYR   1060
MTBC                PVPVITSPEWSGSESGGRRYAPFTINIEHLKPFHTLTGRMHFYLAHDWVEELGEQLPVYR   1060
M.tuberculosis      PVPVITSPEWSGSESGGRRYAPFTINIEHLKPFHTLTGRMHFYLAHDWVEELGEQLPVYR   1060
                    *  :*:** *** *     *     *:..* *::**:** ::*  *:*:.::**.* ***

Ecoli               PPIDTRSVKEV------IGQKSNGNQEKALNFLTPHQKWGIHSTYSDNLLMLTLGRGGPV   1117
MSMEG_5140          PPLDMARLFGESRLGAGPGADGAGGVGLTVRYLTPHSKWSIHSEYQDNLFMLSLSRGGPT   1106
M.canettii          PPLDMARLFNQPEL--GPTDD---GLGLTVRYLTPHSKWSFHSTYQDNLYMLSLSRGGPT   1115
M.bovis             PPLDMARLFNQPEL--GPTDD---GLGLTVRYLTPHSKWSFHSTYQDNLYMLSLSRGGPT   1115
M.africanum         PPLDMARLFNQPEL--GPTDD---GLGLTVRYLTPHSKWSFHSTYQDNLYMLSLSRGGPT   1115
MTBC                PPLDMARLFNQPEL--GPTDD---GLGLTVRYLTPHSKWSFHSTYQDNLYMLSLSRGGPT   1115
M.tuberculosis      PPLDMARLFNQPEL--GPTDD---GLGLTVRYLTPHSKWSFHSTYQDNLYMLSLSRGGPT   1115
                    **:*   :            .       ::.:****.**.:** *.*** **:*.****.
```

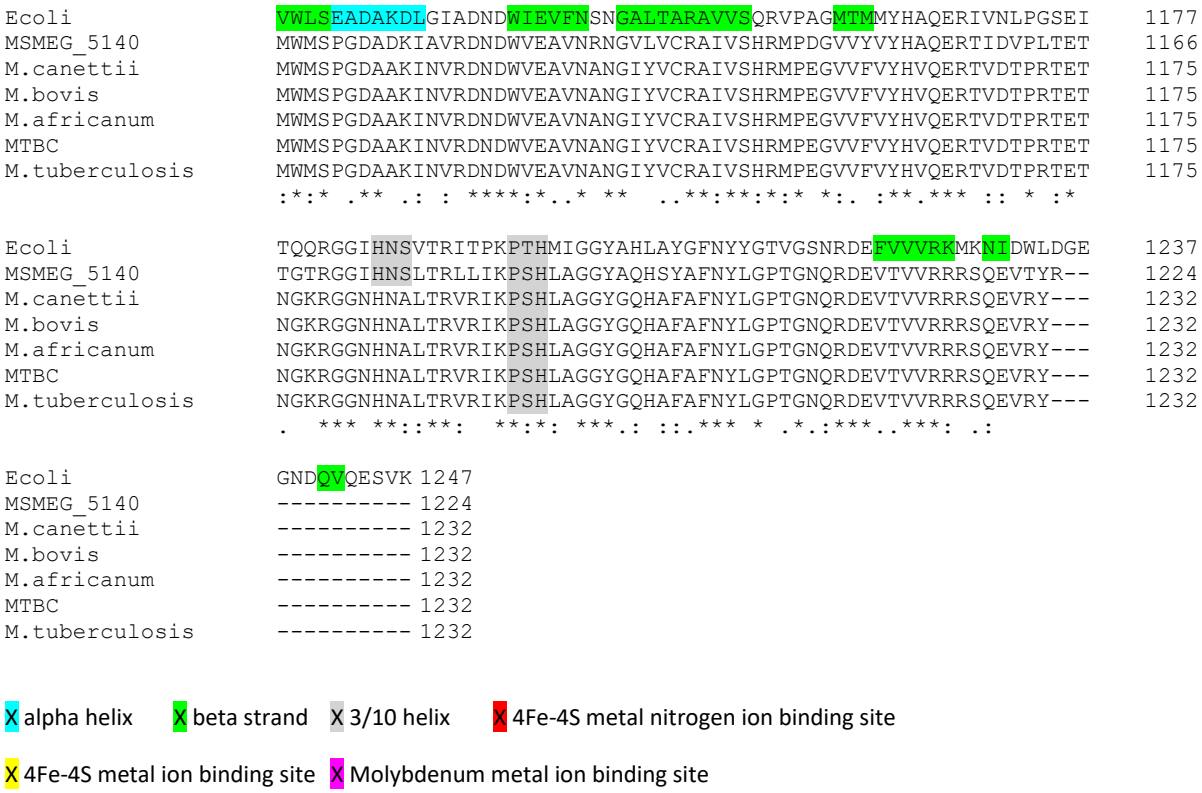


Figure E 5: Sequence alignments of NarG from different organisms. The amino acids shaded in different colours represent different secondary structures and ligand binding sites. Ecoli: *Escherichia coli*, MSMEG: *Mycobacterium smegmatis*, M.tuberculosis: *Mycobacterium tuberculosis*, M. africanum: *Mycobacterium africanum*, MTBC: *Mycobacterium tuberculosis* complex, M. canetti: *Mycobacterium canettii*, M. bovis: *Mycobacterium bovis* BCG.

F. Appendix F-Anaerobic model in *M. smegmatis*

A preliminary anaerobic model was setup in wild type *M. smegmatis* to test the model, with and without nitrate. The data shown in Figure F1 demonstrate that the model is functional, i.e. anaerobic incubation leads to a loss in viability of the culture. Furthermore, the presence of the anaerobic terminal electron acceptor, nitrate, did not enhance the capability of *M. smegmatis* to survive in a model of gradual oxygen depletion and was thus excluded from further experiments.

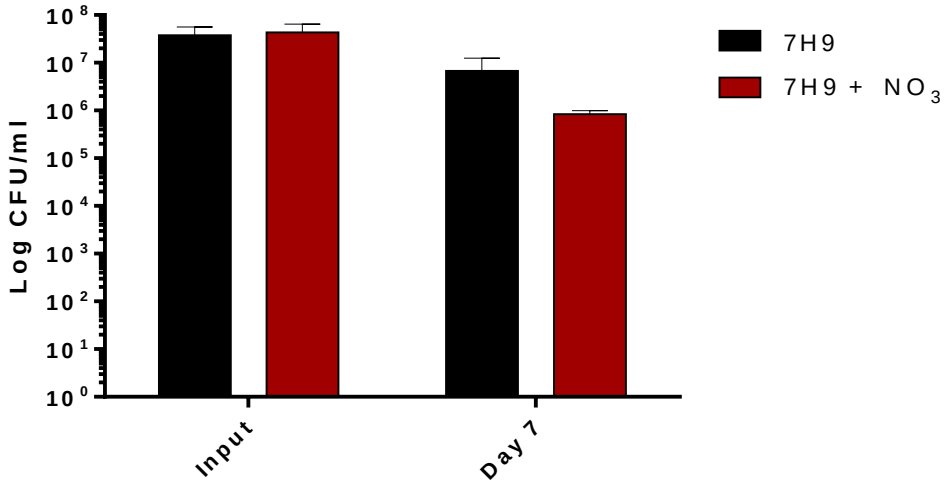


Figure F 1: An anaerobic shift-down model tested for wild type *M. smegmatis* in the presence and absence of nitrate. The 24-well plate was incubated at 37 ˚C in a sealed container which was made anaerobic by the inclusion of the Anaerogen gas pack.

G. Appendix G- Previously generated, unpublished data on the Mtb CbdO mutant

As mentioned in Appendix D, the Mtb CbdO mutant was previously generated in our laboratory by Kana, B. D (unpublished). In addition to generating the strain, Kana, B. D also performed a set of experiments to evaluate the redox state of the cell and the survival of this mutant in a mouse infection model. The redox state of the cell was determined by measuring the NAD^+/NADH ratio of the cell with the cycling assay as described by Bernofsky and Swan (1973). The results shown in Table G1 provide evidence that the redox state of the Mtb CbdO is disrupted, with an increased level of NAD^+ observed. This result suggests that the Mtb CbdO mutant is in a more reduced state than the wild type.

Table G 1: A comparison of the NAD+/NADH ratios in Mtb strains

Strain	NAD^+/NADH
H37Rv	1.1
Δ*cydAB*	2.3
Δ*cydAB* (pHINTCYD)	0.8

The amount of each cofactor was determined by the cycling assay described by Bernofsky and Swan (1973) from Mtb cultures grown under standard aerobic conditions.

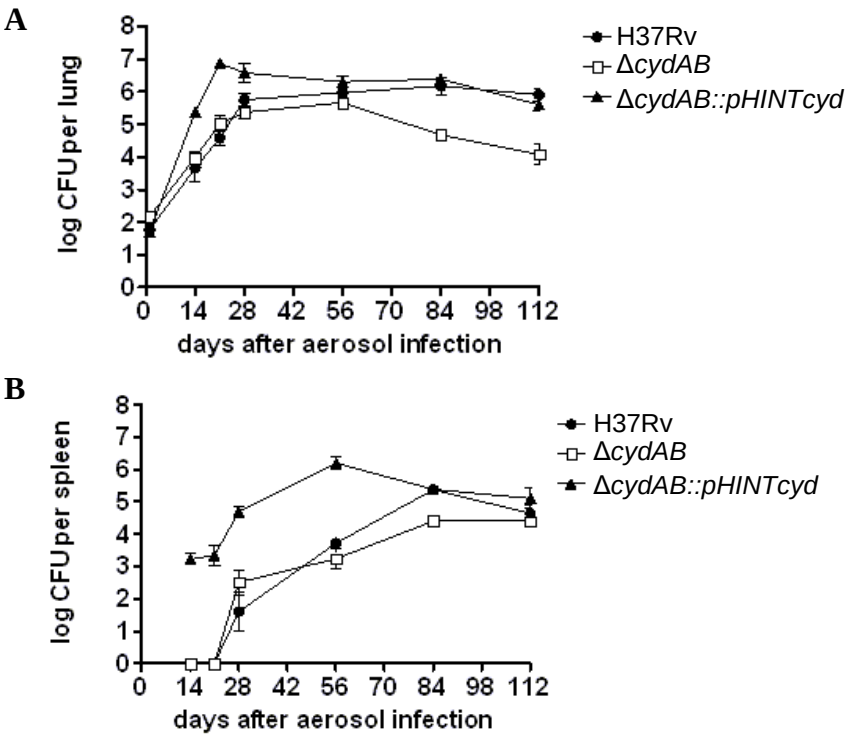


Figure G 1: An asseement of the virulence of the Mtb CbdO mutant in a mouse infection model. **(A)** The bacterial load measured in lungs over the course of the experiment. **(B)** The bacterial load measured in spleens over the course of the experiment. For each time point 4-5 mice were sacrificed per strain for CFU determination.

The mouse infection experiment with wild type, Δ*cydAB* and Δ*cydAB::pHINTCYD* was performed by TARGET. The virulence of the Mtb Δ*cydAB* mutant was evaluated in a mouse infection model using 4-5 week old mice at a low dose of aerosol infection (~ 100 CFU). For each time point, 4-5 mice were sacrificed per strain to determine the lung and spleen CFU. From this experiment it was observed that the CbdO mutant was unable to persist as well as the wild type during mouse infections, shown in Figure G1. These data highlight a role for CbdO in Mtb virulence.

H. Appendix H-CCM entry points for different carbon sources

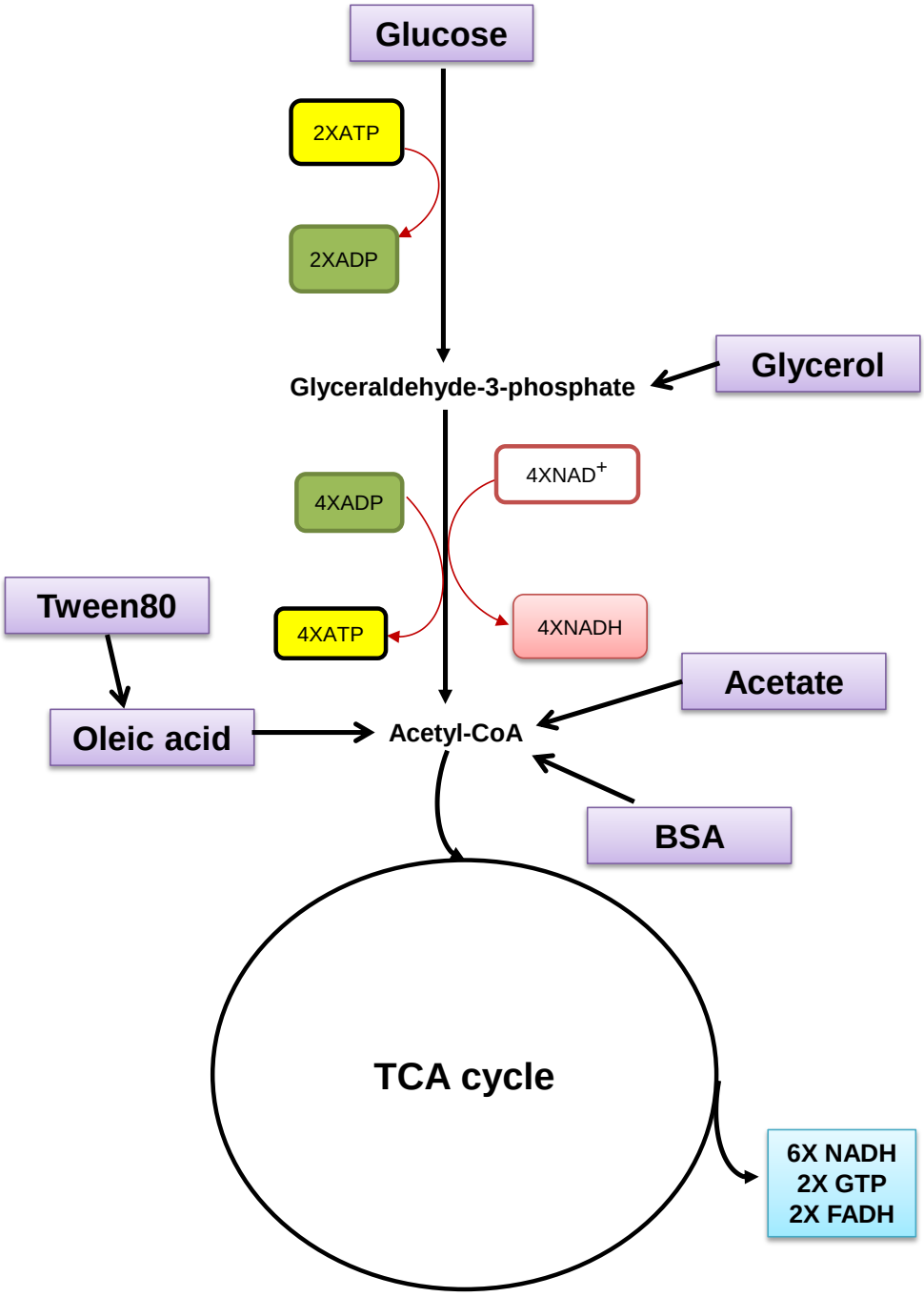


Figure H 1: A schematic representation of the TCA cycle and glycolysis higlighting the point of entry for the different carbon sources used during this study. The number of ATP and NADH molecules shown are based on the number theoretically produced when glucose is the carbon source

4. References

Abrahams, K. A., Cox, J. A., Spivey, V. L., *et al.* (2012). Identification of novel imidazo[1,2-a]pyridine inhibitors targeting *M. tuberculosis* QcrB. *PLoS One,* 7**,** e52951.

Abubakar, I., Pimpin, L., Ariti, C., *et al.* (2013). Systematic review and meta-analysis of the current evidence on the duration of protection by bacillus Calmette-Guerin vaccination against tuberculosis. *Health Technol Assess,* 17**,** 1-372, v-vi.

Akhtar, S., Khan, A., Sohaskey, C. D., *et al.* (2013). Nitrite reductase NirBD is induced and plays an important role during in vitro dormancy of *Mycobacterium tuberculosis*. *J Bacteriol,* 195**,** 4592-9.

Altschul, S. F., Gish, W., Miller, W., *et al.* (1990). Basic local alignment search tool. *J Mol Biol,* 215**,** 403-10.

Aly, S., Wagner, K., Keller, C., *et al.* (2006). Oxygen status of lung granulomas in *Mycobacterium tuberculosis*-infected mice. *J Pathol,* 210**,** 298-305.

Amon, J., Titgemeyer, F. & Burkovski, A. (2009). A genomic view on nitrogen metabolism and nitrogen control in mycobacteria. *J Mol Microbiol Biotechnol,* 17**,** 20-9.

Anand, A., Verma, P., Singh, A. K., *et al.* (2015). Polyketide Quinones Are Alternate Intermediate Electron Carriers during Mycobacterial Respiration in Oxygen-Deficient Niches. *Mol Cell,* 60**,** 637-50.

Andries, K., Verhasselt, P., Guillemont, J., *et al.* (2005). A diarylquinoline drug active on the ATP synthase of *Mycobacterium tuberculosis*. *Science,* 307**,** 223-7.

Andries, K., Villellas, C., Coeck, N., *et al.* (2014). Acquired resistance of *Mycobacterium tuberculosis* to bedaquiline. *PLoS One,* 9**,** e102135.

Angeby, K. A., Klintz, L. & Hoffner, S. E. (2002). Rapid and inexpensive drug susceptibility testing of *Mycobacterium tuberculosis* with a nitrate reductase assay. *J Clin Microbiol,* 40**,** 553-5.

Arora, K., Ochoa-Montano, B., Tsang, P. S., *et al.* (2014). Respiratory flexibility in response to inhibition of cytochrome C oxidase in *Mycobacterium tuberculosis*. *Antimicrob Agents Chemother,* 58**,** 6962-5.

Arora, K., Ochoa-Montano, B., Tsang, P. S., *et al.* (2017). Correction for Arora et al., "Respiratory Flexibility in Response to Inhibition of Cytochrome c Oxidase in *Mycobacterium tuberculosis*". *Antimicrob Agents Chemother,* 61.

Aung, H. L., Berney, M. & Cook, G. M. (2014). Hypoxia-activated *cytochrome bd* expression in *Mycobacterium smegmatis* is cyclic AMP receptor protein dependent. *J Bacteriol,* 196**,** 3091-7.

Awasthy, D., Ambady, A., Narayana, A., *et al.* (2014). Roles of the two type II NADH dehydrogenases in the survival of *Mycobacterium tuberculosis* in vitro. *Gene,* 550**,** 110-6.

Bader, M., Muse, W., Ballou, D. P., *et al.* (1999). Oxidative protein folding is driven by the electron transport system. *Cell,* 98**,** 217-27.

Barry, C. E., 3rd, Boshoff, H. I., Dartois, V., *et al.* (2009). The spectrum of latent tuberculosis: rethinking the biology and intervention strategies. *Nat Rev Microbiol,* 7**,** 845-55.

Bartek, I. L., Woolhiser, L. K., Baughn, A. D., *et al.* (2014). *Mycobacterium tuberculosis* Lsr2 is a global transcriptional regulator required for adaptation to changing oxygen levels and virulence. *MBio,* 5**,** e01106-14.

Berg, J. M., Tymoczko, J. L. & Stryer, L. (2002). *Biochemistry, Fifth Edition*, W.H. Freeman.

Berney, M. & Cook, G. M. (2010). Unique flexibility in energy metabolism allows mycobacteria to combat starvation and hypoxia. *PLoS One,* 5**,** e8614.

Berney, M., Greening, C., Conrad, R., *et al.* (2014a). An obligately aerobic soil bacterium activates fermentative hydrogen production to survive reductive stress during hypoxia. *Proc Natl Acad Sci U S A,* 111**,** 11479-84.

Berney, M., Greening, C., Hards, K., *et al.* (2014b). Three different [NiFe] hydrogenases confer metabolic flexibility in the obligate aerobe *Mycobacterium smegmatis*. *Environ Microbiol,* 16**,** 318-30.

Berney, M., Hartman, T. E. & Jacobs, W. R., Jr. (2014c). A *Mycobacterium tuberculosis* cytochrome bd oxidase mutant is hypersensitive to bedaquiline. *MBio,* 5**,** e01275-14.

Berney, M., Weimar, M. R., Heikal, A., *et al.* (2012). Regulation of proline metabolism in mycobacteria and its role in carbon metabolism under hypoxia. *Mol Microbiol,* 84**,** 664-81.

Bernofsky, C. & Swan, M. (1973). An improved cycling assay for nicotinamide adenine dinucleotide. *Anal Biochem,* 53**,** 452-8.

Berube, B. J. & Parish, T. (2018). Combinations of Respiratory Chain Inhibitors Have Enhanced Bactericidal Activity against *Mycobacterium tuberculosis*. *Antimicrob Agents Chemother,* 62.

Bhatt, K. & Salgame, P. (2007). Host innate immune response to *Mycobacterium tuberculosis*. *J Clin Immunol,* 27**,** 347-62.

Billig, S., Schneefeld, M., Huber, C., *et al.* (2017). Lactate oxidation facilitates growth of *Mycobacterium tuberculosis* in human macrophages. *Sci Rep,* 7**,** 6484.

Bloch, D., Belevich, I., Jasaitis, A., *et al.* (2004). The catalytic cycle of cytochrome *c* oxidase is not the sum of its two halves. *Proc Natl Acad Sci U S A,* 101**,** 529-33.

Bloch, H. & Segal, W. (1956). Biochemical differentiation of *Mycobacterium tuberculosis* grown in vivo and in vitro. *J Bacteriol,* 72**,** 132-41.

Boot, M., Jim, K. K., Liu, T., *et al.* (2017). A fluorescence-based reporter for monitoring expression of mycobacterial cytochrome bd in response to antibacterials and during infection. *Sci Rep,* 7**,** 10665.

Borisov, V. B., Davletshin, A. I. & Konstantinov, A. A. (2010). Peroxidase activity of cytochrome *bd* from *Escherichia coli*. *Biochemistry (Mosc),* 75**,** 428-36.

Borisov, V. B., Forte, E., Davletshin, A., *et al.* (2013). Cytochrome *bd* oxidase from *Escherichia coli* displays high catalase activity: an additional defense against oxidative stress. *FEBS Lett,* 587**,** 2214-8.

Borisov, V. B., Forte, E., Siletsky, S. A., *et al.* (2015). Cytochrome *bd* from *Escherichia coli* catalyzes peroxynitrite decomposition. *Biochim Biophys Acta,* 1847**,** 182-8.

Borisov, V. B., Gennis, R. B., Hemp, J., *et al.* (2011a). The cytochrome *bd* respiratory oxygen reductases. *Biochim Biophys Acta,* 1807**,** 1398-413.

Borisov, V. B. & Verkhovsky, M. I. (2009). Oxygen as Acceptor. *EcoSal Plus,* 3.

Borriello, G., Werner, E., Roe, F., *et al.* (2004). Oxygen limitation contributes to antibiotic tolerance of *Pseudomonas aeruginosa* in biofilms. *Antimicrob Agents Chemother,* 48**,** 2659-64.

Boshoff, H. I., Myers, T. G., Copp, B. R., *et al.* (2004). The transcriptional responses of *Mycobacterium tuberculosis* to inhibitors of metabolism: novel insights into drug mechanisms of action. *J Biol Chem,* 279**,** 40174-84.

Brock, M. & Buckel, W. (2004). On the mechanism of action of the antifungal agent propionate. *Eur J Biochem,* 271**,** 3227-41.

Brosch, R., Gordon, S. V., Marmiesse, M., *et al.* (2002). A new evolutionary scenario for the *Mycobacterium tuberculosis* complex. *Proc Natl Acad Sci U S A,* 99**,** 3684-9.

Bryk, R., Lima, C. D., Erdjument-Bromage, H., *et al.* (2002). Metabolic enzymes of mycobacteria linked to antioxidant defense by a thioredoxin-like protein. *Science,* 295**,** 1073-7.

Cave, A. J. E. D., A (1939). The evidence for the incidence of tuberculosis in ancient Egypt. *British Journl of Tuberculosis,* 33**,** 142-152.

Chen, J. M., German, G. J., Alexander, D. C., *et al.* (2006). Roles of Lsr2 in colony morphology and biofilm formation of *Mycobacterium smegmatis*. *J Bacteriol,* 188**,** 633-41.

Cole, S. T., Brosch, R., Parkhill, J., *et al.* (1998). Deciphering the biology of *Mycobacterium tuberculosis* from the complete genome sequence. *Nature,* 393**,** 537-44.

Collins, L. & Franzblau, S. G. (1997). Microplate alamar blue assay versus BACTEC 460 system for high-throughput screening of compounds against *Mycobacterium tuberculosis* and *Mycobacterium avium*. *Antimicrob Agents Chemother,* 41**,** 1004-9.

Cook, G. M., Greening, C., Hards, K., *et al.* (2014a). Energetics of pathogenic bacteria and opportunities for drug development. *Adv Microb Physiol,* 65**,** 1-62.

Cook, G. M., Hards, K., Dunn, E., *et al.* (2017). Oxidative Phosphorylation as a Target Space for Tuberculosis: Success, Caution, and Future Directions. *Microbiol Spectr,* 5.

Cook, G. M., Hards, K., Vilcheze, C., *et al.* (2014b). Energetics of Respiration and Oxidative Phosphorylation in Mycobacteria. *Microbiol Spectr,* 2.

Crofts, A. R. (2004). The cytochrome *bc1* complex: function in the context of structure. *Annu Rev Physiol,* 66**,** 689-733.

Cunningham-Bussel, A., Bange, F. C. & Nathan, C. F. (2013a). Nitrite impacts the survival of *Mycobacterium tuberculosis* in response to isoniazid and hydrogen peroxide. *Microbiologyopen.*

Cunningham-Bussel, A., Zhang, T. & Nathan, C. F. (2013b). Nitrite produced by *Mycobacterium tuberculosis* in human macrophages in physiologic oxygen impacts bacterial ATP consumption and gene expression. *Proc Natl Acad Sci U S A,* 110**,** E4256-65.

Daniel, T. M. (2006). The history of tuberculosis. *Respir Med,* 100**,** 1862-70.

Dartois, V. & Barry, C. E., 3rd (2013). A medicinal chemists' guide to the unique difficulties of lead optimization for tuberculosis. *Bioorg Med Chem Lett,* 23**,** 4741-50.

De Carvalho, L. P., Fischer, S. M., Marrero, J., *et al.* (2010a). Metabolomics of *Mycobacterium tuberculosis* reveals compartmentalized co-catabolism of carbon substrates. *Chem Biol,* 17**,** 1122-31.

De Carvalho, L. P., Zhao, H., Dickinson, C. E., *et al.* (2010b). Activity-based metabolomic profiling of enzymatic function: identification of *Rv1248c* as a mycobacterial 2-hydroxy-3-oxoadipate synthase. *Chem Biol,* 17**,** 323-32.

De Jonge, M. R., Koymans, L. H., Guillemont, J. E., *et al.* (2007). A computational model of the inhibition of *Mycobacterium tuberculosis* ATPase by a new drug candidate R207910. *Proteins,* 67**,** 971-80.

Delogu, G., Sali, M. & Fadda, G. (2013). The biology of mycobacterium tuberculosis infection. *Mediterr J Hematol Infect Dis,* 5**,** e2013070.

Dhar, N. & Mckinney, J. D. (2010). *Mycobacterium tuberculosis* persistence mutants identified by screening in isoniazid-treated mice. *Proc Natl Acad Sci U S A,* 107**,** 12275-80.

Dhiman, R. K., Mahapatra, S., Slayden, R. A., *et al.* (2009). Menaquinone synthesis is critical for maintaining mycobacterial viability during exponential growth and recovery from non-replicating persistence. *Mol Microbiol,* 72**,** 85-97.

Donoghue, H. D., Lee, O. Y., Minnikin, D. E., *et al.* (2010). Tuberculosis in Dr Granville's mummy: a molecular re-examination of the earliest known Egyptian mummy to be scientifically examined and given a medical diagnosis. *Proc Biol Sci,* 277**,** 51-6.

Edge, R., Mcgarvey, D. J. & Truscott, T. G. (1997). The carotenoids as anti-oxidants--a review. *J Photochem Photobiol B,* 41**,** 189-200.

Edwards, S. E., Loder, C. S., Wu, G., *et al.* (2000). Mutation of cytochrome *bd* quinol oxidase results in reduced stationary phase survival, iron deprivation, metal toxicity and oxidative stress in *Azotobacter vinelandii*. *FEMS Microbiol Lett,* 185**,** 71-7.

Ehrt, S. & Schnappinger, D. (2009). Mycobacterial survival strategies in the phagosome: defence against host stresses. *Cell Microbiol,* 11**,** 1170-8.

Endley, S., Mcmurray, D. & Ficht, T. A. (2001). Interruption of the *cydB* locus in *Brucella abortus* attenuates intracellular survival and virulence in the mouse model of infection. *J Bacteriol,* 183**,** 2454-62.

Eoh, H. & Rhee, K. Y. (2013). Multifunctional essentiality of succinate metabolism in adaptation to hypoxia in *Mycobacterium tuberculosis*. *Proc Natl Acad Sci U S A,* 110**,** 6554-9.

Eoh, H. & Rhee, K. Y. (2014). Methylcitrate cycle defines the bactericidal essentiality of isocitrate lyase for survival of *Mycobacterium tuberculosis* on fatty acids. *Proc Natl Acad Sci U S A,* 111**,** 4976-81.

Ernst, J. D. (2012). The immunological life cycle of tuberculosis. *Nat Rev Immunol,* 12**,** 581-91.

Ferguson-Miller, S. & Babcock, G. T. (1996). Heme/Copper Terminal Oxidases. *Chem Rev,* 96**,** 2889-2908.

Firmani, M. A. & Riley, L. W. (2002). Reactive nitrogen intermediates have a bacteriostatic effect on *Mycobacterium tuberculosis* in vitro. *J Clin Microbiol,* 40**,** 3162-6.

Flores, A. R., Parsons, L. M. & Pavelka, M. S., Jr. (2005). Characterization of novel *Mycobacterium tuberculosis* and *Mycobacterium smegmatis* mutants hypersusceptible to beta-lactam antibiotics. *J Bacteriol,* 187**,** 1892-900.

Formicola, V., Milanesi, Q. & Scarsini, C. (1987). Evidence of spinal tuberculosis at the beginning of the fourth millennium BC from Arene Candide cave (Liguria, Italy). *Am J Phys Anthropol,* 72**,** 1-6.

Forte, E., Borisov, V. B., Davletshin, A., *et al.* (2013). Cytochrome *bd* oxidase and hydrogen peroxide resistance in *Mycobacterium tuberculosis*. *MBio,* 4**,** e01006-13.

Forte, E., Borisov, V. B., Falabella, M., *et al.* (2016). The Terminal Oxidase Cytochrome *bd* Promotes Sulfide-resistant Bacterial Respiration and Growth. *Sci Rep,* 6**,** 23788.

Freedberg, W. B., Kistler, W. S. & Lin, E. C. (1971). Lethal synthesis of methylglyoxal by *Escherichia coli* during unregulated glycerol metabolism. *J Bacteriol,* 108**,** 137-44.

Gao, X., Wen, X., Esser, L., *et al.* (2003). Structural basis for the quinone reduction in the *bc1* complex: a comparative analysis of crystal structures of mitochondrial cytochrome *bc1* with bound substrate and inhibitors at the Qi site. *Biochemistry,* 42**,** 9067-80.

Garcia-Horsman, J. A., Barquera, B., Rumbley, J., *et al.* (1994). The superfamily of heme-copper respiratory oxidases. *J Bacteriol,* 176**,** 5587-600.

Gengenbacher, M. & Kaufmann, S. H. (2012). *Mycobacterium tuberculosis*: success through dormancy. *FEMS Microbiol Rev,* 36**,** 514-32.

Gideon, H. P. & Flynn, J. L. (2011). Latent tuberculosis: what the host "sees"? *Immunol Res,* 50**,** 202-12.

Gonzalez, P. J., Correia, C., Moura, I., *et al.* (2006). Bacterial nitrate reductases: Molecular and biological aspects of nitrate reduction. *J Inorg Biochem,* 100**,** 1015-23.

Gorke, B. & Stulke, J. (2008). Carbon catabolite repression in bacteria: many ways to make the most out of nutrients. *Nat Rev Microbiol,* 6**,** 613-24.

Gould, T. A., Van De Langemheen, H., Munoz-Elias, E. J., *et al.* (2006). Dual role of *isocitrate lyase 1* in the glyoxylate and methylcitrate cycles in *Mycobacterium tuberculosis*. *Mol Microbiol,* 61**,** 940-7.

Gouzy, A., Poquet, Y. & Neyrolles, O. (2014). Nitrogen metabolism in *Mycobacterium tuberculosis* physiology and virulence. *Nat Rev Microbiol,* 12**,** 729-37.

Graf, S., Fedotovskaya, O., Kao, W. C., *et al.* (2016). Rapid Electron Transfer within the III-IV Supercomplex in *Corynebacterium glutamicum*. *Sci Rep,* 6**,** 34098.

Griffin, J. E., Gawronski, J. D., Dejesus, M. A., *et al.* (2011). High-resolution phenotypic profiling defines genes essential for mycobacterial growth and cholesterol catabolism. *PLoS Pathog,* 7**,** e1002251.

Gupta, P., Sarkar, S., Das, B., *et al.* (2016). Biofilm, pathogenesis and prevention--a journey to break the wall: a review. *Arch Microbiol,* 198**,** 1-15.

Haagsma, A. C., Driessen, N. N., Hahn, M. M., *et al.* (2010). ATP synthase in slow- and fast-growing mycobacteria is active in ATP synthesis and blocked in ATP hydrolysis direction. *FEMS Microbiol Lett,* 313**,** 68-74.

Hards, K., Robson, J. R., Berney, M., *et al.* (2015). Bactericidal mode of action of bedaquiline. *J Antimicrob Chemother,* 70**,** 2028-37.

Hartman, T., Weinrick, B., Vilcheze, C., *et al.* (2014). Succinate dehydrogenase is the regulator of respiration in *Mycobacterium tuberculosis*. *PLoS Pathog,* 10**,** e1004510.

Heikal, A., Hards, K., Cheung, C. Y., *et al.* (2016). Activation of type II NADH dehydrogenase by quinolinequinones mediates antitubercular cell death. *J Antimicrob Chemother,* 71**,** 2840-7.

Hershkovitz, I., Donoghue, H. D., Minnikin, D. E., *et al.* (2008). Detection and molecular characterization of 9,000-year-old *Mycobacterium tuberculosis* from a Neolithic settlement in the Eastern Mediterranean. *PLoS One,* 3**,** e3426.

Hesseling, A. C., Rabie, H., Marais, B. J., *et al.* (2006). Bacille Calmette-Guerin vaccine-induced disease in HIV-infected and HIV-uninfected children. *Clin Infect Dis,* 42**,** 548-58.

Hille, R., Hall, J. & Basu, P. (2014). The mononuclear molybdenum enzymes. *Chem Rev,* 114**,** 3963-4038.

Hoeser, J., Hong, S., Gehmann, G., *et al.* (2014). Subunit CydX of *Escherichia coli* cytochrome *bd* ubiquinol oxidase is essential for assembly and stability of the di-heme active site. *FEBS Lett,* 588**,** 1537-41.

Homolka, S., Projahn, M., Feuerriegel, S., *et al.* (2012). High resolution discrimination of clinical *Mycobacterium tuberculosis* complex strains based on single nucleotide polymorphisms. *PLoS One,* 7**,** e39855.

Huang, Q., Abdalla, A. E. & Xie, J. (2015). Phylogenomics of Mycobacterium Nitrate Reductase Operon. *Curr Microbiol,* 71**,** 121-8.

Humpel, A., Gebhard, S., Cook, G. M., *et al.* (2010). The SigF Regulon in *Mycobacterium smegmatis* Reveals Roles in Adaptation to Stationary Phase, Heat, and Oxidative Stress. *Journal of Bacteriology,* 192**,** 2491-2502.

Hutter, B. & Dick, T. (1999). Up-regulation of *narX*, encoding a putative 'fused nitrate reductase' in anaerobic dormant *Mycobacterium bovis* BCG. *FEMS Microbiol Lett,* 178**,** 63-9.

Iverson, T. M. (2013). Catalytic mechanisms of complex II enzymes: a structural perspective. *Biochim Biophys Acta,* 1827**,** 648-57.

Jang, J., Kim, R., Woo, M., *et al.* (2017). Efflux Attenuates the Antibacterial Activity of Q203 in *Mycobacterium tuberculosis*. *Antimicrob Agents Chemother,* 61.

Jepson, B. J., Anderson, L. J., Rubio, L. M., *et al.* (2004). Tuning a nitrate reductase for function. The first spectropotentiometric characterization of a bacterial assimilatory nitrate reductase reveals novel redox properties. *J Biol Chem,* 279**,** 32212-8.

Jones-Carson, J., Husain, M., Liu, L., *et al.* (2016). Cytochrome *bd*-Dependent Bioenergetics and Antinitrosative Defenses in Salmonella Pathogenesis. *MBio,* 7.

Junemann, S., Butterworth, P. J. & Wrigglesworth, J. M. (1995). A suggested mechanism for the catalytic cycle of cytochrome *bd* terminal oxidase based on kinetic analysis. *Biochemistry,* 34**,** 14861-7.

Jung, J. Y., Madan-Lala, R., Georgieva, M., *et al.* (2013). The intracellular environment of human macrophages that produce nitric oxide promotes growth of mycobacteria. *Infect Immun,* 81**,** 3198-209.

Kadenbach, B. & Huttemann, M. (2015). The subunit composition and function of mammalian cytochrome c oxidase. *Mitochondrion,* 24**,** 64-76.

Kalia, N. P., Hasenoehrl, E. J., Ab Rahman, N. B., *et al.* (2017). Exploiting the synthetic lethality between terminal respiratory oxidases to kill *Mycobacterium tuberculosis* and clear host infection. *Proc Natl Acad Sci U S A,* 114**,** 7426-7431.

Kana, B. D., Machowski, E. E., Schechter, N., Teh, J. S., Rubin, H., Mizrahi, V. 2009. Electron transport and respiration in mycobacteria. *In:* PARISH, T., BROWN, A. (ed.) *Mycobacterium: Genomics and Molecular Biology* London: Caister Academic Press.

Kana, B. D., Weinstein, E. A., Avarbock, D., *et al.* (2001). Characterization of the *cydAB*-encoded cytochrome *bd* oxidase from *Mycobacterium smegmatis*. *J Bacteriol,* 183**,** 7076-86.

Kanehisa, M., Sato, Y., Kawashima, M., *et al.* (2016). KEGG as a reference resource for gene and protein annotation. *Nucleic Acids Res,* 44**,** D457-62.

Kang, S., Kim, R. Y., Seo, M. J., *et al.* (2014). Lead optimization of a novel series of imidazo[1,2-a]pyridine amides leading to a clinical candidate (Q203) as a multi- and extensively-drug-resistant anti-tuberculosis agent. *J Med Chem,* 57**,** 5293-305.

Kapopoulou, A., Lew, J. M. & Cole, S. T. (2011). The MycoBrowser portal: a comprehensive annotated resource for mycobacterial genomes. *Tuberculosis (Edinb),* 91**,** 8-13.

Kappelman, J., Alcicek, M. C., Kazanci, N., *et al.* (2008). First *Homo erectus* from Turkey and implications for migrations into temperate Eurasia. *Am J Phys Anthropol,* 135**,** 110-6.

Khan, A., Akhtar, S., Ahmad, J. N., *et al.* (2008). Presence of functional nitrate assimilation pathway in *Mycobacterium smegmatis*. *Microbial Pathogenesis,* 44**,** 71-77.

Khan, A. & Sarkar, D. (2006). Identification of a respiratory-type nitrate reductase and its role for survival of *Mycobacterium smegmatis* in Wayne model. *Microbial Pathogenesis,* 41**,** 90-95.

Khan, A. & Sarkar, D. (2012). Nitrate reduction pathways in mycobacteria and their implications during latency. *Microbiology,* 158**,** 301-7.

Kim, B. H. & Gadd, G. M. (2008). *Bacterial physiology and metabolism,* Cambridge university press.

Kim, M. S., Jang, J., Ab Rahman, N. B., *et al.* (2015). Isolation and Characterization of a Hybrid Respiratory Supercomplex Consisting of *Mycobacterium tuberculosis Cytochrome bcc* and *Mycobacterium smegmatis Cytochrome aa3*. *J Biol Chem,* 290**,** 14350-60.

Korshunov, S., Imlay, K. R. & Imlay, J. A. (2016). The cytochrome *bd* oxidase of *Escherichia coli* prevents respiratory inhibition by endogenous and exogenous hydrogen sulfide. *Mol Microbiol,* 101**,** 62-77.

Koul, A., Arnoult, E., Lounis, N., *et al.* (2011). The challenge of new drug discovery for tuberculosis. *Nature,* 469**,** 483-90.

Koul, A., Dendouga, N., Vergauwen, K., *et al.* (2007). Diarylquinolines target subunit c of mycobacterial ATP synthase. *Nat Chem Biol,* 3**,** 323-4.

Koul, A., Vranckx, L., Dendouga, N., *et al.* (2008). Diarylquinolines are bactericidal for dormant mycobacteria as a result of disturbed ATP homeostasis. *J Biol Chem,* 283**,** 25273-80.

Koul, A., Vranckx, L., Dhar, N., *et al.* (2014). Delayed bactericidal response of *Mycobacterium tuberculosis* to bedaquiline involves remodelling of bacterial metabolism. *Nat Commun,* 5**,** 3369.

Kumar, P., Arora, K., Lloyd, J. R., *et al.* (2012). Meropenem inhibits D,D-carboxypeptidase activity in *Mycobacterium tuberculosis*. *Mol Microbiol,* 86**,** 367-81.

Lamprecht, D. A., Finin, P. M., Rahman, M. A., *et al.* (2016). Turning the respiratory flexibility of *Mycobacterium tuberculosis* against itself. *Nat Commun,* 7**,** 12393.

Larsen, M. H. 2000. Appendix 1. *In:* HATFUL, G. F., JACOBS, W. R., JR. (ed.) *Molecular genetics of mycobacteria.* Washington, D.C.: ASM Press.

Lechartier, B. & Cole, S. T. (2015). Mode of Action of Clofazimine and Combination Therapy with Benzothiazinones against *Mycobacterium tuberculosis*. *Antimicrob Agents Chemother,* 59**,** 4457-63.

Leclerc, J., Rosenfeld, E., Trainini, M., *et al.* (2015). The Cytochrome *bd* Oxidase of *Porphyromonas gingivalis* Contributes to Oxidative Stress Resistance and Dioxygen Tolerance. *PLoS One,* 10**,** e0143808.

Lenaerts, A. J., Hoff, D., Aly, S., *et al.* (2007). Location of persisting mycobacteria in a Guinea pig model of tuberculosis revealed by r207910. *Antimicrob Agents Chemother,* 51**,** 3338-45.

Liu, J., Chakraborty, S., Hosseinzadeh, P., *et al.* (2014). Metalloproteins containing cytochrome, iron-sulfur, or copper redox centers. *Chem Rev,* 114**,** 4366-469.

Lo, T. W., Westwood, M. E., Mclellan, A. C., *et al.* (1994). Binding and modification of proteins by methylglyoxal under physiological conditions. A kinetic and mechanistic study with N alpha-acetylarginine, N alpha-acetylcysteine, and N alpha-acetyllysine, and bovine serum albumin. *J Biol Chem,* 269**,** 32299-305.

Lu, P., Heineke, M. H., Koul, A., *et al.* (2015). The cytochrome *bd*-type quinol oxidase is important for survival of *Mycobacterium smegmatis* under peroxide and antibiotic-induced stress. *Sci Rep,* 5**,** 10333.

Luque-Almagro, V. M., Gates, A. J., Moreno-Vivian, C., *et al.* (2011). Bacterial nitrate assimilation: gene distribution and regulation. *Biochem Soc Trans,* 39**,** 1838-43.

Lynn, M., Wilson, A. R. & Solotorovsky, M. (1979). Role of bovine serum albumin in the nutrition of *Mycobacterium tuberculosis*. *Appl Environ Microbiol,* 38**,** 806-10.

Madkour, M. M. (2003). *Textbook of tuberculosis,* New York, Springer.

Maklashina, E., Cecchini, G. & Dikanov, S. A. (2013). Defining a direction: electron transfer and catalysis in *Escherichia coli* complex II enzymes. *Biochim Biophys Acta,* 1827**,** 668-78.

Maksymiuk, C., Balakrishnan, A., Bryk, R., *et al.* (2015). E1 of alpha-ketoglutarate dehydrogenase defends *Mycobacterium tuberculosis* against glutamate anaplerosis and nitroxidative stress. *Proc Natl Acad Sci U S A,* 112**,** E5834-43.

Malm, S., Tiffert, Y., Micklinghoff, J., *et al.* (2009). The roles of the nitrate reductase NarGHJI, the nitrite reductase NirBD and the response regulator GlnR in nitrate assimilation of *Mycobacterium tuberculosis*. *Microbiology,* 155**,** 1332-9.

Mason, M. G., Shepherd, M., Nicholls, P., *et al.* (2009). Cytochrome *bd* confers nitric oxide resistance to *Escherichia coli*. *Nat Chem Biol,* 5**,** 94-6.

Matsoso, L. G., Kana, B. D., Crellin, P. K., *et al.* (2005). Function of the cytochrome *bc1-aa3* branch of the respiratory network in mycobacteria and network adaptation occurring in response to its disruption. *J Bacteriol,* 187**,** 6300-8.

Matsumoto, Y., Muneyuki, E., Fujita, D., *et al.* (2006). Kinetic mechanism of quinol oxidation by cytochrome *bd* studied with ubiquinone-2 analogs. *J Biochem,* 139**,** 779-88.

Mckinney, J. D., Honer Zu Bentrup, K., Munoz-Elias, E. J., *et al.* (2000). Persistence of *Mycobacterium tuberculosis* in macrophages and mice requires the glyoxylate shunt enzyme isocitrate lyase. *Nature,* 406**,** 735-8.

Megehee, J. A., Hosler, J. P. & Lundrigan, M. D. (2006). Evidence for a cytochrome *bcc-aa3* interaction in the respiratory chain of *Mycobacterium smegmatis*. *Microbiology,* 152**,** 823-9.

Miesel, L., Weisbrod, T. R., Marcinkeviciene, J. A., *et al.* (1998). NADH dehydrogenase defects confer isoniazid resistance and conditional lethality in *Mycobacterium smegmatis*. *J Bacteriol,* 180**,** 2459-67.

Miller, J. L., Velmurugan, K., Cowan, M. J., *et al.* (2010). The type I NADH dehydrogenase of *Mycobacterium tuberculosis* counters phagosomal NOX2 activity to inhibit TNF-alpha-mediated host cell apoptosis. *PLoS Pathog,* 6**,** e1000864.

Miller, M. J., Hermodson, M. & Gennis, R. B. (1988). The active form of the cytochrome *d* terminal oxidase complex of *Escherichia coli* is a heterodimer containing one copy of each of the two subunits. *J Biol Chem,* 263**,** 5235-40.

Mishra, S., Shukla, P., Bhaskar, A., *et al.* (2017). Efficacy of beta-lactam/beta-lactamase inhibitor combination is linked to WhiB4-mediated changes in redox physiology of *Mycobacterium tuberculosis*. *Elife,* 6.

Mobius, K., Arias-Cartin, R., Breckau, D., *et al.* (2010). Heme biosynthesis is coupled to electron transport chains for energy generation. *Proc Natl Acad Sci U S A,* 107**,** 10436-41.

Moosa, A., Lamprecht, D. A., Arora, K., *et al.* (2017). Susceptibility of Mycobacterium tuberculosis Cytochrome bd Oxidase Mutants to Compounds Targeting the Terminal Respiratory Oxidase, Cytochrome c. *Antimicrob Agents Chemother,* 61.

Moreno-Vivian, C., Cabello, P., Martinez-Luque, M., *et al.* (1999). Prokaryotic nitrate reduction: molecular properties and functional distinction among bacterial nitrate reductases. *J Bacteriol,* 181**,** 6573-84.

Moreno-Vivian, C. & Ferguson, S. J. (1998). Definition and distinction between assimilatory, dissimilatory and respiratory pathways. *Mol Microbiol,* 29**,** 664-6.

Morozkina, E. V. & Zvyagilskaya, R. A. (2007). Nitrate reductases: structure, functions, and effect of stress factors. *Biochemistry (Mosc),* 72**,** 1151-60.

Moseki, M. R. 2017. *Functional analysis of the cydDC encoded ABC-type transporter in Mycobacterium smegmatis.* Master of Science in Medicine, University of the Witwatersrand.

Mowa, M. B., Warner, D. F., Kaplan, G., *et al.* (2009). Function and regulation of class I ribonucleotide reductase-encoding genes in mycobacteria. *J Bacteriol,* 191**,** 985-95.

Munoz-Elias, E. J. & Mckinney, J. D. (2005). *Mycobacterium tuberculosis isocitrate lyases 1* and *2* are jointly required for *in vivo* growth and virulence. *Nat Med,* 11**,** 638-44.

Munoz-Elias, E. J., Upton, A. M., Cherian, J., *et al.* (2006). Role of the methylcitrate cycle in *Mycobacterium tuberculosis* metabolism, intracellular growth, and virulence. *Mol Microbiol,* 60**,** 1109-22.

Najmudin, S., Gonzalez, P. J., Trincao, J., *et al.* (2008). Periplasmic nitrate reductase revisited: a sulfur atom completes the sixth coordination of the catalytic molybdenum. *J Biol Inorg Chem,* 13**,** 737-53.

Narrandes, N. C. 2013. *Functional characterisation of molybdopterin synthase-encoding genes in mycobacteria.* Master of Science in Medicine, University of the Witwatersrand.

Narrandes, N. C., Machowski, E. E., Mizrahi, V., *et al.* (2015). Cleavage of the *moaX*-encoded fused molybdopterin synthase from *Mycobacterium tuberculosis* is necessary for activity. *BMC Microbiol,* 15**,** 22.

Nerlich, A. G. & Losch, S. (2009). Paleopathology of human tuberculosis and the potential role of climate. *Interdiscip Perspect Infect Dis,* 2009**,** 437187.

Niebisch, A. & Bott, M. (2003). Purification of a cytochrome *bc-aa3* supercomplex with quinol oxidase activity from *Corynebacterium glutamicum*. Identification of a fourth subunity of cytochrome *aa3* oxidase and mutational analysis of diheme cytochrome *c1*. *J Biol Chem,* 278**,** 4339-46.

Noy, T., Vergnolle, O., Hartman, T. E., *et al.* (2016). Central Role of Pyruvate Kinase in Carbon Co-catabolism of *Mycobacterium tuberculosis*. *J Biol Chem,* 291**,** 7060-9.

Ojha, A., Anand, M., Bhatt, A., *et al.* (2005). GroEL1: a dedicated chaperone involved in mycolic acid biosynthesis during biofilm formation in mycobacteria. *Cell,* 123**,** 861-73.

Ojha, A. & Hatfull, G. F. (2007). The role of iron in *Mycobacterium smegmatis* biofilm formation: the exochelin siderophore is essential in limiting iron conditions for biofilm formation but not for planktonic growth. *Mol Microbiol,* 66**,** 468-83.

Ojha, A. K., Baughn, A. D., Sambandan, D., *et al.* (2008). Growth of *Mycobacterium tuberculosis* biofilms containing free mycolic acids and harbouring drug-tolerant bacteria. *Mol Microbiol,* 69**,** 164-74.

Ojha, A. K., Varma, S. & Chatterji, D. (2002). Synthesis of an unusual polar glycopeptidolipid in glucose-limited culture of *Mycobacterium smegmatis*. *Microbiology,* 148**,** 3039-48.

Orme, I. M. & Basaraba, R. J. (2014). The formation of the granuloma in tuberculosis infection. *Semin Immunol,* 26**,** 601-9.

Ortner, D. J. (1979). Disease and mortality in the Early Bronze Age people of Bab edh-Dhra, Jordan. *Am J Phys Anthropol,* 51**,** 589-97.

Osborne, J. P. & Gennis, R. B. (1999). Sequence analysis of cytochrome *bd* oxidase suggests a revised topology for subunit I. *Biochim Biophys Acta,* 1410**,** 32-50.

Pai, M., Behr, M. A., Dowdy, D., *et al.* (2016). Tuberculosis. *Nat Rev Dis Primers,* 2**,** 16076.

Parish, T. & Stoker, N. G. (2000). Use of a flexible cassette method to generate a double unmarked *Mycobacterium tuberculosis tlyA plcABC* mutant by gene replacement. *Microbiology,* 146 (Pt 8)**,** 1969-75.

Park, H. D., Guinn, K. M., Harrell, M. I., *et al.* (2003). *Rv3133c/dosR* is a transcription factor that mediates the hypoxic response of *Mycobacterium tuberculosis*. *Mol Microbiol,* 48**,** 833-43.

Pecsi, I., Hards, K., Ekanayaka, N., *et al.* (2014). Essentiality of succinate dehydrogenase in *Mycobacterium smegmatis* and its role in the generation of the membrane potential under hypoxia. *MBio,* 5.

Petersen, T. N., Brunak, S., Von Heijne, G., *et al.* (2011). SignalP 4.0: discriminating signal peptides from transmembrane regions. *Nat Methods,* 8**,** 785-6.

Pethe, K., Bifani, P., Jang, J., *et al.* (2013). Discovery of Q203, a potent clinical candidate for the treatment of tuberculosis. *Nat Med,* 19**,** 1157-60.

Pethe, K., Sequeira, P. C., Agarwalla, S., *et al.* (2010). A chemical genetic screen in *Mycobacterium tuberculosis* identifies carbon-source-dependent growth inhibitors devoid of in vivo efficacy. *Nat Commun,* 1**,** 57.

Provvedi, R., Kocincova, D., Dona, V., *et al.* (2008). SigF controls carotenoid pigment production and affects transformation efficiency and hydrogen peroxide sensitivity in *Mycobacterium smegmatis*. *J Bacteriol,* 190**,** 7859-63.

Puckett, S., Trujillo, C., Wang, Z., *et al.* (2017). Glyoxylate detoxification is an essential function of malate synthase required for carbon assimilation in *Mycobacterium tuberculosis*. *Proc Natl Acad Sci U S A,* 114**,** E2225-E2232.

Ramakrishnan, L. (2012). Revisiting the role of the granuloma in tuberculosis. *Nat Rev Immunol,* 12**,** 352-66.

Rao, S. P., Alonso, S., Rand, L., *et al.* (2008). The protonmotive force is required for maintaining ATP homeostasis and viability of hypoxic, nonreplicating *Mycobacterium tuberculosis*. *Proc Natl Acad Sci U S A,* 105**,** 11945-50.

Recht, J. & Kolter, R. (2001). Glycopeptidolipid acetylation affects sliding motility and biofilm formation in *Mycobacterium smegmatis*. *J Bacteriol,* 183**,** 5718-24.

Rice, P., Longden, I. & Bleasby, A. (2000). EMBOSS: the European Molecular Biology Open Software Suite. *Trends Genet,* 16**,** 276-7.

Rich, P. R. & Marechal, A. (2010). The mitochondrial respiratory chain. *Essays Biochem,* 47**,** 1-23.

Richards, J. P. & Ojha, A. K. (2014). Mycobacterial Biofilms. *Microbiol Spectr,* 2.

Richardson, D. J. (2000). Bacterial respiration: a flexible process for a changing environment. *Microbiology,* 146 (Pt 3)**,** 551-71.

Richardson, D. J., Berks, B. C., Russell, D. A., *et al.* (2001). Functional, biochemical and genetic diversity of prokaryotic nitrate reductases. *Cell Mol Life Sci,* 58**,** 165-78.

Richardson, D. J. & Watmough, N. J. (1999). Inorganic nitrogen metabolism in bacteria. *Curr Opin Chem Biol,* 3**,** 207-19.

Rickman, L., Scott, C., Hunt, D. M., *et al.* (2005). A member of the cAMP receptor protein family of transcription regulators in *Mycobacterium tuberculosis* is required for virulence in mice and controls transcription of the *rpfA* gene coding for a resuscitation promoting factor. *Mol Microbiol,* 56**,** 1274-86.

Roberts, G., Vadrevu, I. S., Madiraju, M. V., *et al.* (2011). Control of CydB and GltA1 expression by the SenX3 RegX3 two component regulatory system of *Mycobacterium tuberculosis*. *PLoS One,* 6**,** e21090.

Rozwarski, D. A., Grant, G. A., Barton, D. H., *et al.* (1998). Modification of the NADH of the isoniazid target (InhA) from *Mycobacterium tuberculosis*. *Science,* 279**,** 98-102.

Rubio, L. M., Herrero, A. & Flores, E. (1996). A cyanobacterial *narB* gene encodes a ferredoxin-dependent nitrate reductase. *Plant Mol Biol,* 30**,** 845-50.

Ryan, G. J., Hoff, D. R., Driver, E. R., *et al.* (2010). Multiple *M. tuberculosis* phenotypes in mouse and guinea pig lung tissue revealed by a dual-staining approach. *PLoS One,* 5**,** e11108.

Rybniker, J., Vocat, A., Sala, C., *et al.* (2015). Lansoprazole is an antituberculous prodrug targeting cytochrome *bc1*. *Nat Commun,* 6**,** 7659.

Safarian, S., Rajendran, C., Muller, H., *et al.* (2016). Structure of a *bd* oxidase indicates similar mechanisms for membrane-integrated oxygen reductases. *Science,* 352**,** 583-6.

Sala, C., Haouz, A., Saul, F. A., *et al.* (2009). Genome-wide regulon and crystal structure of BlaI (Rv1846c) from *Mycobacterium tuberculosis*. *Mol Microbiol,* 71**,** 1102-16.

Salo, W. L., Aufderheide, A. C., Buikstra, J., *et al.* (1994). Identification of *Mycobacterium tuberculosis* DNA in a pre-Columbian Peruvian mummy. *Proc Natl Acad Sci U S A,* 91**,** 2091-4.

Sambrook, J., Fritsch, E. F., Maniatis, T. 1989. Molecular Cloning. A laboratory manual.

. Second ed. Cold Spring Harbour, New York.: Cold Spring Harbour Laboratory Press.

Sassetti, C. M., Boyd, D. H. & Rubin, E. J. (2003). Genes required for mycobacterial growth defined by high density mutagenesis. *Mol Microbiol,* 48**,** 77-84.

Savvi, S., Warner, D. F., Kana, B. D., *et al.* (2008). Functional characterization of a vitamin B12-dependent methylmalonyl pathway in *Mycobacterium tuberculosis*: implications for propionate metabolism during growth on fatty acids. *J Bacteriol,* 190**,** 3886-95.

Sazanov, L. A. (2015). A giant molecular proton pump: structure and mechanism of respiratory complex I. *Nat Rev Mol Cell Biol,* 16**,** 375-88.

Schaefer, W. B. & Lewis, C. W., Jr. (1965). Effect of oleic acid on growth and cell structure of mycobacteria. *J Bacteriol,* 90**,** 1438-47.

Sears, H. J., Little, P. J., Richardson, D. J., *et al.* (1997). Identification of an assimilatory nitrate reductase in mutants of *Paracoccus denitrificans* GB17 deficient in nitrate respiration. *Arch Microbiol,* 167**,** 61-6.

Shepherd, M., Achard, M. E., Idris, A., *et al.* (2016). The cytochrome *bd-I* respiratory oxidase augments survival of multidrug-resistant *Escherichia coli* during infection. *Sci Rep,* 6**,** 35285.

Sherman, D. R., Voskuil, M., Schnappinger, D., *et al.* (2001). Regulation of the *Mycobacterium tuberculosis* hypoxic response gene encoding alpha -crystallin. *Proc Natl Acad Sci U S A,* 98**,** 7534-9.

Shi, L., Sohaskey, C. D., Kana, B. D., *et al.* (2005). Changes in energy metabolism of *Mycobacterium tuberculosis* in mouse lung and under in vitro conditions affecting aerobic respiration. *Proc Natl Acad Sci U S A,* 102**,** 15629-34.

Shirude, P. S., Paul, B., Roy Choudhury, N., *et al.* (2012). Quinolinyl Pyrimidines: Potent Inhibitors of NDH-2 as a Novel Class of Anti-TB Agents. *ACS Med Chem Lett,* 3**,** 736-40.

Siddiqui, R. A., Warnecke-Eberz, U., Hengsberger, A., *et al.* (1993). Structure and function of a periplasmic nitrate reductase in Alcaligenes eutrophus H16. *J Bacteriol,* 175**,** 5867-76.

Siegele, D. A., Imlay, K. R. & Imlay, J. A. (1996). The stationary-phase-exit defect of *cydC* (*surB*) mutants is due to the lack of a functional terminal cytochrome oxidase. *J Bacteriol,* 178**,** 6091-6.

Siegele, D. A. & Kolter, R. (1993). Isolation and characterization of an *Escherichia coli* mutant defective in resuming growth after starvation. *Genes Dev,* 7**,** 2629-40.

Singh, A. K. D., D. Singh,V. Srivastava,V. Biswas,R.K. Singh,B.N. (2015). Characterization of *Mycobacterium smegmatis sigF* mutant and its regulon: overexpression of SigF antagonist (MSMEG_1803) in *M. smegmatis* mimics *sigF* mutant phenotype, loss of pigmentation, and sensitivity to oxidative stress. *MicorbiologyOpen,* 4**,** 896-916.

Small, J. L., Park, S. W., Kana, B. D., *et al.* (2013). Perturbation of cytochrome *c* maturation reveals adaptability of the respiratory chain in *Mycobacterium tuberculosis*. *MBio,* 4**,** e00475-13.

Sohaskey, C. D. (2005). Regulation of nitrate reductase activity in *Mycobacterium tuberculosis* by oxygen and nitric oxide. *Microbiology,* 151**,** 3803-10.

Sohaskey, C. D. (2008). Nitrate enhances the survival of *Mycobacterium tuberculosis* during inhibition of respiration. *J Bacteriol,* 190**,** 2981-6.

Sohaskey, C. D. & Wayne, L. G. (2003). Role of *narK2X* and *narGHJI* in hypoxic upregulation of nitrate reduction by *Mycobacterium tuberculosis*. *J Bacteriol,* 185**,** 7247-56.

Sone, N., Nagata, K., Kojima, H., *et al.* (2001). A novel hydrophobic diheme *c*-type cytochrome. Purification from *Corynebacterium glutamicum* and analysis of the QcrCBA operon encoding

three subunit proteins of a putative cytochrome reductase complex. *Biochim Biophys Acta,* 1503**,** 279-90.

Sreevatsan, S., Pan, X., Stockbauer, K. E., *et al.* (1997). Restricted structural gene polymorphism in the *Mycobacterium tuberculosis* complex indicates evolutionarily recent global dissemination. *Proc Natl Acad Sci U S A,* 94**,** 9869-74.

Stermann, M., Sedlacek, L., Maass, S., *et al.* (2004). A promoter mutation causes differential nitrate reductase activity of *Mycobacterium tuberculosis* and *Mycobacterium bovis*. *J Bacteriol,* 186**,** 2856-61.

Sukheja, P., Kumar, P., Mittal, N., *et al.* (2017). A Novel Small-Molecule Inhibitor of the *Mycobacterium tuberculosis* Demethylmenaquinone Methyltransferase MenG Is Bactericidal to Both Growing and Nutritionally Deprived Persister Cells. *MBio,* 8.

Szklarczyk, D., Morris, J. H., Cook, H., *et al.* (2017). The STRING database in 2017: quality-controlled protein-protein association networks, made broadly accessible. 45**,** D362-d368.

Tan, M. P., Sequeira, P., Lin, W. W., *et al.* (2010). Nitrate respiration protects hypoxic *Mycobacterium tuberculosis* against acid- and reactive nitrogen species stresses. *PLoS ONE,* 5**,** e13356.

Taylor, G. M., Young, D. B. & Mays, S. A. (2005). Genotypic analysis of the earliest known prehistoric case of tuberculosis in Britain. *J Clin Microbiol,* 43**,** 2236-40.

Thamdrup, B. (2012). New Pathways and Processes in the Global Nitrogen Cycle. *Annual Review of Ecology, Evolution, and Systematics,* 43**,** 407-428.

Thony-Meyer, L. (1997). Biogenesis of respiratory cytochromes in bacteria. *Microbiol Mol Biol Rev,* 61**,** 337-76.

Tian, J., Bryk, R., Itoh, M., *et al.* (2005a). Variant tricarboxylic acid cycle in *Mycobacterium tuberculosis*: identification of alpha-ketoglutarate decarboxylase. *Proc Natl Acad Sci U S A,* 102**,** 10670-5.

Tian, J., Bryk, R., Shi, S., *et al.* (2005b). *Mycobacterium tuberculosis* appears to lack alpha-ketoglutarate dehydrogenase and encodes pyruvate dehydrogenase in widely separated genes. *Mol Microbiol,* 57**,** 859-68.

Tran, S. L. & Cook, G. M. (2005). The F1Fo-ATP synthase of *Mycobacterium smegmatis* is essential for growth. *J Bacteriol,* 187**,** 5023-8.

Trunz, B. B., Fine, P. & Dye, C. (2006). Effect of BCG vaccination on childhood tuberculous meningitis and miliary tuberculosis worldwide: a meta-analysis and assessment of cost-effectiveness. *Lancet,* 367**,** 1173-80.

Upton, A. M. & Mckinney, J. D. (2007). Role of the methylcitrate cycle in propionate metabolism and detoxification in *Mycobacterium smegmatis*. *Microbiology,* 153**,** 3973-82.

Vandal, O. H., Pierini, L. M., Schnappinger, D., *et al.* (2008). A membrane protein preserves intrabacterial pH in intraphagosomal *Mycobacterium tuberculosis*. *Nat Med,* 14**,** 849-54.

Vannelli, T. A., Dykman, A. & Ortiz De Montellano, P. R. (2002). The antituberculosis drug ethionamide is activated by a flavoprotein monooxygenase. *J Biol Chem,* 277**,** 12824-9.

Vanorsdel, C. E., Bhatt, S., Allen, R. J., *et al.* (2013). The *Escherichia coli* CydX protein is a member of the CydAB cytochrome bd oxidase complex and is required for cytochrome *bd* oxidase activity. *J Bacteriol,* 195**,** 3640-50.

Velmurugan, K., Chen, B., Miller, J. L., *et al.* (2007). *Mycobacterium tuberculosis nuoG* is a virulence gene that inhibits apoptosis of infected host cells. *PLoS Pathog,* 3**,** e110.

Via, L. E., Lin, P. L., Ray, S. M., *et al.* (2008). Tuberculous granulomas are hypoxic in guinea pigs, rabbits, and nonhuman primates. *Infect Immun,* 76**,** 2333-40.

Vilcheze, C., Hartman, T., Weinrick, B., *et al.* (2017). Enhanced respiration prevents drug tolerance and drug resistance in *Mycobacterium tuberculosis*. *Proc Natl Acad Sci U S A,* 114**,** 4495-4500.

Vilcheze, C., Weisbrod, T. R., Chen, B., *et al.* (2005). Altered NADH/NAD+ ratio mediates coresistance to isoniazid and ethionamide in mycobacteria. *Antimicrob Agents Chemother,* 49**,** 708-20.

Voskuil, M. I., Schnappinger, D., Visconti, K. C., *et al.* (2003). Inhibition of respiration by nitric oxide induces a *Mycobacterium tuberculosis* dormancy program. *J Exp Med,* 198**,** 705-13.

Wall, D., Delaney, J. M., Fayet, O., *et al.* (1992). *arc*-dependent thermal regulation and extragenic suppression of the *Escherichia coli* cytochrome *d* operon. *J Bacteriol,* 174**,** 6554-62.

Watanabe, S., Zimmermann, M., Goodwin, M. B., *et al.* (2011). Fumarate reductase activity maintains an energized membrane in anaerobic *Mycobacterium tuberculosis*. *PLoS Pathog,* 7**,** e1002287.

Way, S. S., Sallustio, S., Magliozzo, R. S., *et al.* (1999). Impact of either elevated or decreased levels of cytochrome *bd* expression on *Shigella flexneri* virulence. *J Bacteriol,* 181**,** 1229-37.

Wayne, L. G., Hayes, L. G. (1996). An In Vitro Model for Sequential Study of Shiftdown of *Mycobacterium tuberculosis* through Two Stages of Nonreplicating Persistence. *Infection and Immunity,* 64**,** 2062-2069.

Weber, I., Fritz, C., Ruttkowski, S., *et al.* (2000). Anaerobic nitrate reductase (*narGHJI*) activity of *Mycobacterium bovis* BCG *in vitro* and its contribution to virulence in immunodeficient mice. *Mol Microbiol,* 35**,** 1017-25.

Weinstein, E. A., Yano, T., Li, L. S., *et al.* (2005). Inhibitors of type II NADH:menaquinone oxidoreductase represent a class of antitubercular drugs. *Proc Natl Acad Sci U S A,* 102**,** 4548-53.

Weiss, R. A. & Mcmichael, A. J. (2004). Social and environmental risk factors in the emergence of infectious diseases. *Nat Med,* 10**,** S70-6.

Who 2012a. Global Tuberculosis Report 2012.

Who 2012b. Recommendations for investigating contacts of persons with infectious tuberculosis in low- and middle-income countries.

Who (2014). Companion handbook to the WHO guidlines for the programmatic management of drug-resistant tuberculosis.

Who (2015). Guidlines on the management of latent tuberculosis infection.

Who 2016. WHO Global Tuberculosis Report 2016.

Who (2017). Global tuberculosis report 2017.

Wikstrom, M. (2004). Cytochrome c oxidase: 25 years of the elusive proton pump. *Biochim Biophys Acta,* 1655**,** 241-7.

Williams, M. J., Kana, B. D. & Mizrahi, V. (2011). Functional analysis of molybdopterin biosynthesis in mycobacteria identifies a fused molybdopterin synthase in *Mycobacterium tuberculosis*. *J Bacteriol,* 193**,** 98-106.

Wolf, A. J., Desvignes, L., Linas, B., *et al.* (2008). Initiation of the adaptive immune response to *Mycobacterium tuberculosis* depends on antigen production in the local lymph node, not the lungs. *J Exp Med,* 205**,** 105-15.

Wolff, K. A., De La Pena, A. H., Nguyen, H. T., *et al.* (2015). A redox regulatory system critical for mycobacterial survival in macrophages and biofilm development. *PLoS Pathog,* 11**,** e1004839.

Yano, T., Kassovska-Bratinova, S., Teh, J. S., *et al.* (2011). Reduction of clofazimine by mycobacterial type 2 NADH:quinone oxidoreductase: a pathway for the generation of bactericidal levels of reactive oxygen species. *J Biol Chem,* 286**,** 10276-87.

Yano, T., Li, L. S., Weinstein, E., *et al.* (2006). Steady-state kinetics and inhibitory action of antitubercular phenothiazines on *Mycobacterium tuberculosis* type-II NADH-menaquinone oxidoreductase (NDH-2). *J Biol Chem,* 281**,** 11456-63.

Yano, T., Rahimian, M., Aneja, K. K., *et al.* (2014). *Mycobacterium tuberculosi*s type II NADH-menaquinone oxidoreductase catalyzes electron transfer through a two-site ping-pong mechanism and has two quinone-binding sites. *Biochemistry,* 53**,** 1179-90.

Yoshida, M., Muneyuki, E. & Hisabori, T. (2001). ATP synthase--a marvellous rotary engine of the cell. *Nat Rev Mol Cell Biol,* 2**,** 669-77.

Yoshikawa, S. & Shimada, A. (2015). Reaction mechanism of cytochrome *c* oxidase. *Chem Rev,* 115**,** 1936-89.

Zhang, Y. (2008). I-TASSER server for protein 3D structure prediction. *BMC Bioinformatics,* 9**,** 40.

Zhou, J., Richardson, A. J. & Rudd, K. E. 2013. EcoGene-RefSeq:EcoGene tools applied to the RefSeq Prokaryote genomes.

Zink, A., Haas, C. J., Reischl, U., *et al.* (2001). Molecular analysis of skeletal tuberculosis in an ancient Egyptian population. *J Med Microbiol,* 50**,** 355-66.